(NASA-CP-2297) NONLINEAR STRUCTURAL ANALYSIS (NASA) 168 p HC A08/MF A01 CSCL 20K

N84-31688 THRU N84-31700 Unclas G3/39 20486

*NASA Conference Publication 2297*

# Nonlinear Structural Analysis

*Proceedings of a workshop*
*held at NASA Lewis Research Center*
*Cleveland, Ohio*
*April 19 and 20, 1983*

NASA
National Aeronautics
and Space Administration
Scientific and Technical
Information Branch
1984

# PREFACE

NASA Lewis Research Center developed and has been conducting research on an enlarged engine structures program since 1979. Development of advanced methods of nonlinear structural analysis of engine components is a significant part this enlarged engine structures program and is an integrated research effort involving Lewis, industry, and the university community.

A two-day workshop was held at Lewis Research Center on April 19 and 20, 1983, to report recent progress in nonlinear structural analysis for engine structures. The workshop was organized into three sessions as follows: Session I - New Concepts/Formulations, Session II - Algorithms/Convergence, and Session III - Inelastic Analysis and Interactive Elements.

New concepts/formulations include (1) the slave finite-element formulation for space and time where interpolation polynomials (amenable to explicit integration) are used to express all variables entering the formulation over the element domain, (2) new variational principles leading to new formulations for hybrid stress finite elements that possess ideal characteristics, such as minimum sensitivity to geometric distortion, minimum number of independent stress parameters, and rank sufficiency, (3) shear-deformed shell finite elements for laminated composites based on the total Lagrangian description accounting for anisotropic material behavior, dynamic response, arbitrary laminate configuration, and arbitrary ply properties, and (4) large-aspect-ratio finite elements for nonlinear shell-type structures analysis based on a higher order "degenerated: shell element with nine nodes and accounting for elastic-plastic behavior.

Algorithms/convergence include (1) self-adaptive solution strategies focusing on alternative formulations for developing algorithms that avoid the need for global updating and inversion, (2) element-by-element solution procedures where approximate factorization is considered for solving the large finite-element equation systems that arise in nonlinear structural analyses, (3) automatic finite-element generators, where the use of VAXIMA (MACSIMA in VAX) is used to generate the equations that describe the finite-element formulation, and (4) convergence criteria considering the effects of underintegration on the element approximations.

Inelastic analysis and interactive elements include (1) inelastic and dynamic fracture, focusing on large, dynamic crack propagation by developing methods for new path-independent integrals, for generalized inelastic constitutive relations, and for new complementary energy approaches, (2) interactive finite elements where novel methods are developed to describe the bearing/-support interaction for general engine structural dynamics analysis, (3) nonlinear composite structures analysis applicable to high-temperature composite material behavior, and (4) three-dimensional inelastic analysis via boundary integral, concentrating on the development of discrete element analysis based on boundary integral concepts having the potential for substantial computational efficiency for local concentrations compared with traditional finite-element analysis.

 PRECEDING PAGE BLANK NOT FILMED

Collectively, the papers included in these proceedings are representative of cutting-edge methodology in all three disciplines. The authors of the papers are nationally and internationally recognized experts in their respective areas. The reader should bear in mind that the papers describe research in progress. Results and conclusions reported are subject to revision as additional results become available. In any event, these results and conclusions are those of the respective authors and not of the U.S. Government.

As workshop coordinator, I would like to thank all the authors for preparing their papers on time as well as the attendees whose extensive contributions to the workshop discussions helped make the workshop a very successful technical information exchange forum. Finally, I thank all those who helped with the mechanics of organizing and conducting the workshop.

C. C. Chamis
Lewis Research Center
Cleveland, Ohio

CONTENTS


Page

SESSION I - NEW CONCEPTS/FORMULATIONS

Slave Finite Elements: The Temporal Element Approach to Nonlinear Analysis
Slade Gellen, Bell Aerospace Textron . . . . . 1 D1

New Variational Formulations of Hybrid Stress Elements
T. H. H. Pian, K. Sumihara, and D. Kang, Massachusetts Institute of Technology . . . . . 17 D2

A Shear Deformable Shell Element for Laminated Composites
W. C. Chao and J. N. Reddy, Virginia Polytechnic Institute and State University . . . . . 31 D3

Nonlinear Finite Element Analysis of Shells with Large Aspect Ratio
T. Y. Chang and K. Sawamiphakdi, The Univeristy of Akron . . . . . 45 D4

SESSION II - ALGORITHMS/CONVERGENCE

Self-Adaptive Solution Strategies
Joseph Padovan, University of Akron . . . . . 55 D5

Element-by-Element Solution Procedures for Nonlinear Structural Analysis
Thomas J. R. Hughes, James Winget, and Itzhak Levit, Stanford University . . . . . 65 D6

Automatic Finite Element Generators
Paul S. Wang, Kent State University . . . . . 85 D7

Stability and Convergence of Underintegrated Finite Element Approximations
J. Tinsley Oden, The University of Texas . . . . . 99 D8

SESSION III - INELASTIC ANALYSIS AND INTERACTIVE ELEMENTS

Inelastic and Dynamic Fracture, and Stress Analyses
Satya N. Atluri, Georgia Institute of Technology . . . . . 105 D9

Interactive Finite Elements for General Engine Dynamics Analysis
Maurice L. Adams, Case Western Reserve University, Joseph Podovan and Demeter G. Fertis, The University of Akron . . . . . 119 D10

Nonlinear Analysis for High-Temperature Composites - Turbine Blades/Vanes
Dale A. Hopkins and Christos C. Chamis, Lewis Research Center . . . . 131 D11

Three-Dimensional Stress Analysis Using the Boundary Element Method
Raymond B. Wilson, Pratt & Whitney Aircraft, Prasanta K. Banerjee, State University of New York . . . . . 149 D12

Summary
Christos C. Chamis, Lewis Research Center . . . . . 161 omit

N84
31689

UNCLAS

N84 31689 D1

# SLAVE FINITE ELEMENTS: THE TEMPORAL ELEMENT APPROACH TO NONLINEAR ANALYSIS*

Slade Gellin
Bell Aerospace Textron

## SUMMARY

A formulation method for finite elements in space and time incorporating nonlinear geometric and material behavior is presented. The method uses interpolation polynomials for approximating the behavior of various quantities over the element domain, and only explicit integration over space and time. While applications are general, the plate and shell elements that are currently being programmed will be used to model turbine blades, vanes and cumbustor liners.

## INTRODUCTION

The extension of the finite element method to the solution of transient field problems by discretizing in time as well as in space has been investigated in the last fifteen years. The works most often cited are those by Argyris and Scharpf (Ref. 1) and Fried (Ref. 2). The starting point of their work was Hamilton's principle. Generally, sample problems consisted of axial thrust members, and only linear geometric and material properties were assumed. There were some arbitrary decisions made concerning the proper use of the initial conditions in the global system in order to derive the correct set of equations for the given problem. Many of the theoretical fine points were explained by Simkins (Ref. 3), who demonstrated his findings using point mass structures. His results indicated that very high levels of accuracy can be obtained with only a very small number of elements. He notes that the temporal elements are well suited to handle sudden changes in load function, extending the interval of solution indefinitely without restart, and providing great detail to the solution in any subinterval. Furthermore, conventional step-by-step integration algorithms may call for a large number of time steps, particularly for the hyperbolic equations of structural dynamics should the excitation or material properties change rapidly in time. It is within this spirit that this research was undertaken.

During the course of this work it was found that many theoretical questions needed to be answered. Some of these questions have deep physical and mathematical importance, others are exercises in intellectual gamesmanship. Hopefully, they will be addressed in forth-coming papers. The focus here will be on incorporating nonlinear geometric and material behavior into the temporal element approach, within the framework of the ground rules discussed in the following paragraphs.

*This work was performed under NASA Contract No. NAS3-23279.

First, the elements will be of what will be referred to as the "prismatic" type. The space time domain is thought of as a long, prismatic, member in four dimensions, with the "length" dimension corresponding to time. The three dimensional "cross-section" is the spatial model of the structure. A prismatic element consists of the space-time domain occupied by a spatial finite element from $t=t_i$ to $t=t_j$. Geometrically, this is a well defined set of "longitudinal fibers" over a certain "length". A set of local coordinates is chosen with the time direction the same as global time, but translated so that the time interval goes from 0 to $T=t_j-t_i$. See Figure 1.

Second, all field quantities will either be derived from the displacement field directly or calculated at grid points and then interpolated with their own shape functions over the space-time domain. This will facilitate the explicit integration that also will be required for the procedure. Note that certain spatial geometries for the element may require special handling. Isoparametric representation of elements may not be desirable as only numerical integration schemes will generally be feasible.

Finally, it will be assumed that the constitutive laws will be linear between the time derivatives of the appropriate kinematical and dynamical quantities. Some linearization must be available in order for the matrix techniques of finite element analysis to be applicable.

The non-linear algorithm is derived in the following section. In the subsequent section, a simple, but purposely poorly constructed example conducive to hand computation is presented. Finally, some brief comments about the current research being done using the temporal element concept will be given.

## Non-Linear Algorithm

Like most non-linear algorithms, the one presented here is based on an iterative procedure involving quasi-linearization. The difference in philosophy between the method presented here and the conventional step-by-step methods, such as the tangent modulus or residual force methods, is demonstrated graphically in Figure 2. In both Figures 2(a) and 2(b), the heavily drawn curve represents the "exact" time history of quantity A, which may be thought of as the displacement of a certain point, or a stress at a point, etc. In Figure 2(a), the step-by-step method has calculated the path OA, representing the history up to that point. At A, the procedure generates successive approximations $AB_i$ until convergence to the path AB is achieved. The procedure is now repeated at B. For the algorithm presented here, Figure 2(b) indicates that successive iterations generate an entire load history. This load history allows for determining loading and unloading paths for the entire time interval of interest, eliminating the guesswork or subinterval changes usually associated with the step-by-step methods. Iterations converge until the curve OC is obtained.

The theoretical basis for the algorithm is Hamilton's law of varying action. Essentially, it is the principle of virtual work integrated over time. It is expressed mathematically as

$$\int_{t_1}^{T} \int_{V} (\delta\vec{\varepsilon} \cdot \vec{\sigma} - \delta\vec{v} \cdot \vec{p})\, dV dt \; - \; \{\delta u\}^T \{F^*\} = 0 \qquad (1)$$

where $\vec{\varepsilon}$, $\vec{\sigma}$, $\vec{v}$ and $\vec{p}$ are the strain, stress, velocity and momentum fields, respectively, and $\{u\}$ is the set of element degrees of freedom (d.o.f.). Note that each element of $\{u\}$ represents a displacement measure at a certain point in place and time. The vector $\{F^*\}$ represents the equivalent point impulse-momentum difference due to known body forces and tractions applied over $S_\sigma$, the portion of the surface S where tractions are specified and thermal loading as well as "known momenta" applied over the time boundaries and equivalent loads exerted on the element by its contiguous neighbors. The variations in (1) are taken with respect to the displacement field $\vec{u}$, which is expressed in terms of shape functions $[N(\vec{x},t)]$ as

$$\vec{u} = [N]\{u\} \tag{2}$$

The displacement $\vec{u}$ is assumed to be admissible. In this case, that means the shape functions [N] are interelement continuous, as well as continuously differentiable in the space-time domain. The strain-displacement law may be written formally as

$$\vec{\varepsilon} = \vec{f}(\vec{u}) \tag{3}$$

where $\vec{f}$ is a function of $\vec{u}$ and its spatial partial derivatives, and, in general, is non-linear. Taking variations of (3) yields

$$\delta\vec{\varepsilon} = \vec{f}'(\vec{u})\delta\vec{u} \tag{4}$$

where the prime has a general meaning relating to derivatives with respect to $\vec{u}$ and its partial derivatives. In a similar manner, the velocity-displacement relations may be expressed as

$$\vec{v} = \vec{g}(\vec{u}) \tag{5}$$

where $\vec{g}$, like $\vec{f}$, is a (non-linear) function of $\vec{u}$ and its spatial and temporal first derivatives. Taking the variation of (5) yields

$$\delta\vec{v} = \vec{g}'(\vec{u})\delta\vec{u} \tag{6}$$

It is also interesting to note the time derivatives of (3) and (5):

$$\overset{o}{\vec{\varepsilon}} = \vec{f}'(\vec{u})\ \overset{o}{\vec{u}} \tag{7a}$$

$$\overset{o}{\vec{v}} = \vec{g}'(\vec{u})\ \overset{o}{\vec{u}} \tag{7b}$$

Constitutive laws between $\vec{\varepsilon}$ and $\vec{\sigma}$, and $\vec{v}$ and $\vec{p}$ may be formulated, according to the groundrules specified above, as

$$\overset{o}{\vec{\sigma}} = [E(\vec{\sigma},\vec{\varepsilon},\vec{\theta},\vec{x},t,\ldots)]\overset{o}{\vec{\varepsilon}} + \overset{o}{\vec{\tau}}\ (\vec{\sigma},\vec{\varepsilon},\vec{\theta},\vec{x},t,\ldots) \tag{8a}$$

$$\overset{o}{\vec{p}} = [\rho(\vec{\sigma},\vec{\varepsilon},\vec{\theta},\vec{x},t,\ldots)]\overset{o}{\vec{v}} + \overset{o}{\vec{\pi}}\ (\vec{\sigma},\vec{\varepsilon},\vec{\theta},\vec{x},t,\ldots) \tag{8b}$$

ORIGINAL PAGE IS
OF POOR QUALITY

where $\vec{\theta}$ is the temperature field. Equations (8) are integrated from 0 to t; thus,

$$\vec{\sigma} = \int_0^t \overset{o}{\vec{\sigma}}\, dt' + \vec{\sigma}_o \tag{9a}$$

$$\vec{p} = \int_0^t \overset{o}{\vec{p}}\, dt' + \vec{p}_o \tag{9b}$$

where $\vec{\sigma}_o$ and $\vec{p}_o$ are the values of the stress and momentum at local time t=0. These may be approximated by

$$\vec{\sigma}_o = [N_\sigma(\vec{x})]\{\sigma_o\} \tag{10a}$$

$$\vec{p}_o = [N_p(\vec{x})]\{p_o\} \tag{10b}$$

where the number of parameters in $\{\sigma_o\}$ and $\{p_o\}$ is arbitrary. Ideally, $[N_p]$ is interelement continuous, and both $[N_\sigma]$ and $[N_p]$ are as sophisticated as the stress and momentum fields derived from [N] in the linear theory, though neither requirement is really mandatory.

In the iterative procedure to be used, "current" values of displacement, stress, strain, etc., for the entire load history are in hand. These values are used to evaluate $\vec{f}'$, $\vec{g}'$, [E], $\overset{o}{\vec{\tau}}$, [ρ] and $\overset{o}{\vec{\pi}}$. The quantities $\delta\vec{u}$ and $\overset{o}{\vec{u}}$ are calculated from (2) where the set {u} are unknown, representing the "updated" solution. Similarly, $\{\sigma_o\}$ and $\{p_o\}$ are unknowns.

Equations (3)-(7) may be re-expressed as

$$\delta\vec{\varepsilon} = [f'][N]\{\delta u\} \tag{11a}$$

$$\overset{o}{\vec{\varepsilon}} = [f'][\overset{o}{N}]\{u\} \tag{11b}$$

$$\delta\vec{v} = [g'][N]\{\delta u\} \tag{11c}$$

$$\overset{o}{\vec{v}} = [g'][\overset{o}{N}]\{u\} \tag{11d}$$

where [f′] and [g′] are 6x3 and 3x3 operator matrices, respectively. Stress and momentum matrices are defined by

$$[S] = \int_{o_t}^{t} [E][f'][\overset{o}{N}]\, dt' \tag{12a}$$

$$[M] = \int_0^t [\rho][g'][\overset{o}{N}]\, dt' \tag{12b}$$

and stress and momentum vectors are defined as

$$\vec{\tau} = \int_0^t \overset{o}{\vec{\tau}}\, dt' \tag{13a}$$

$$\vec{\pi} = \int_0^t \overset{o}{\vec{\pi}}\, dt' \tag{13b}$$

ORIGINAL PAGE IS
OF POOR QUALITY

Using (10), (12) and (13) in (9) yields

$$\vec{\sigma} = [S]\{u\} + \vec{\tau} + [N_\sigma]\{\sigma_o\} \tag{14a}$$

$$\vec{p} = [M]\{u\} + \vec{\pi} + [N_p]\{p_o\} \tag{14b}$$

Equations (14) may be evaluated at t=T. (Quantities evaluated at this time are given a T subscript.) Assuming that $[N_\sigma]$ and $[N_p]$ can also approximate $\bar{\sigma}_T$ and $\bar{p}_T$, equations (14) take on the form

$$[S_T]\{u\} + \vec{\tau}_T + [N_\sigma]\{\sigma_o - \sigma_T\} = \{0\} \tag{15a}$$

$$[M_T]\{u\} + \vec{\pi}_T + [N_p]\{p_o - p_T\} = \{0\} \tag{15b}$$

at t=T. Equations (15) are used as subsidiary conditions to the problem. They are added to (1) with the use of lagrange multiplier fields. In particular, the choices for the stress and momentum fields, respectively, is given as

$$\vec{\lambda}_\sigma = [N_\sigma]\{\lambda_\sigma\} \tag{16a}$$

$$\vec{\lambda}_p = [N_p]\{\lambda_p\} \tag{16b}$$

These fields are used with (15) and integrated over the volume. These conditions, as well as equations (11a), (11c), and (14) are used in (1) to give

$$\{\delta u\}^T([K_e]\{u\} - \{F^*\} - \{F^e_\tau\} - \{F^e_\pi\} + [A^e_\sigma]\{\sigma_o\} - [A^e_p]\{p_o\})$$

$$+ \delta(\{\lambda_\sigma\}^T([B^e_\sigma]\{u\} + [C^e_\sigma]\{\sigma_o - \sigma_T\} - \{q^e_\tau\}))$$

$$+ \{\lambda_p\}^T([B^e_p]\{u\} + [C^e_p]\{p_o - p_T\} - \{q^e_\pi\}) = 0 \tag{17}$$

where

$$[K_e] = \int_0^T \int_V ([N]^T[f']^T[S] - [N]^T[g']^T[M])\, dV dt \tag{18a}$$

$$[A^e_\sigma] = \int_0^T \int_V [N]^T[f']^T[N_\sigma] dV dt \tag{18b}$$

$$[A^e_p] = \int_0^T \int_V [N]^T[g']^T[N_p] dV dt \tag{18c}$$

$$[B^e_\sigma] = \int_V [N_\sigma]^T[S_T] dV \tag{18d}$$

ORIGINAL PAGE IS
OF POOR QUALITY

$$[B_p^e] = \int_v [N_p]^T [M_T] dV \tag{18e}$$

$$[C_\sigma^e] = \int_v [N_\sigma]^T [N_\sigma] dV \tag{18f}$$

$$[C_p^e] = \int_v [N_p]^T [N_p] dV \tag{18g}$$

$$\{F_\tau^e\} = -\int_0^T \int_v [N]^T [f']^T \vec{\tau}\, dV dt \tag{18h}$$

$$\{F_\pi^e\} = \int_0^T \int_v [N]^T [g']^T \vec{\pi} dV dt \tag{18i}$$

$$\{q_\tau^e\} = -\int_v [N_\sigma]^T \vec{\tau}_T dV \tag{18j}$$

$$\{q_\pi^e\} = -\int_v [N_p]^T \vec{\pi}_T dV \tag{18k}$$

The set of equations generated by (17) when variations are taken on $\{u\}$, $\{\sigma_o\}$, $\{p_o\}$, $\{\lambda_\sigma\}$ and $\{\lambda_p\}$ are

$$[K_e]\{u\} + [A_\sigma^e]\{\sigma_o\} - [A_p^e]\{p_o\} + [B_\sigma^e]^T\{\lambda_\sigma\} + [B_p^e]^T\{\lambda_p\}$$

$$= \{F^*\} + \{F_\tau^e\} + \{F_\pi^e\} \tag{19a}$$

$$[C_\sigma^e]\{\lambda_\sigma\} = \{0\} \tag{19b}$$

$$[C_p^e]\{\lambda_p\} = \{0\} \tag{19c}$$

$$[B_\sigma^e]\{u\} + [C_\sigma^e]\{\sigma_o - \sigma_T\} = \{q_\tau^e\} \tag{19d}$$

$$[B_p^e]\{u\} + [C_p^e]\{p_o - p_T\} = \{q_\pi^e\} \tag{19e}$$

Note that the matrices $[C_\sigma^e]$ and $[C_p^e]$ will be square and invertible, thus making the mulipliers identically zero. They may then be omitted from equation (19a). Equations (19a, d, e) are assembled into the systems

$$[K]\{u\} + [A_\sigma]\{\sigma\} - [A_p]\{p\} = \{\tilde{P}\} \tag{20a}$$

$$[B_\sigma]\{u\} + [C_\sigma]\{\sigma\} = \{q_\tau\} \tag{20b}$$

$$[B_p]\{u\} + [C_p]\{p_o\} = \{q_\pi\} \tag{20c}$$

ORIGINAL PAGE IS
OF POOR QUALITY

where the assembly enforces the conditions of continuity across a time boundary for stress and continuity of momentum across a time boundary to the extent that no impulses per unit volume are applied, and, if such impulses are implied, an appropriate discontinuity is maintained. The results should leave $[C_\sigma]$ and $[C_p]$ square and invertible. Thus, equations (20b,c) are solved for $\{\sigma\}$ and $\{p\}$ and used in (20a) to derive the global stiffness equations

$$[\hat{K}]\{u\} = \{\hat{P}\} \tag{21}$$

where

$$[\hat{K}] = [K] - [A_\sigma][C_\sigma]^{-1}[B_\sigma] + [A_p][C_p]^{-1}[B_p] \tag{22a}$$

$$[\hat{P}] = [\bar{P}] - [A_\sigma][C_\sigma]^{-1}[q_\tau] + [A_p][C_p]^{-1}[q_\pi] \tag{22b}$$

Equations (21) are solved for $\{u\}$ and then back-substituted into all the pertinent equations to calculate the important quantities to be used in the next iteration.

## A Simple Numerical Example

To demonstrate some of the procedures developed, a numerical example will be worked out. A rod of length L, and cross-sectional area A built in at both ends, is loaded at its midpoint by a continuously time varying load P(t) given as

$$P(t) = 2\sigma_Y A\left(\frac{t}{T}\right) \tag{23}$$

where T is the time interval of interest and $\sigma_Y$ is the nominal yield stress of the material satisfying the uniaxial stress strain law of the Ramberg-Osgood type (Reference 4)

$$\epsilon = \frac{\sigma}{E}\left[1 + \frac{3}{7}\left(\frac{\sigma}{\sigma_Y}\right)^8\right] \tag{24}$$

where E is the elastic modulus of the material. The loading is assumed quasistatic and thus dynamic effects may be ignored. (Note that if P(t) is discontinuous, dynamic effects must be introduced in order to maintain continuity of displacement and stress across a time boundary.) The rod is initially in the undeformed state; thus, not only is $u(x,0)=0$, but $\sigma(x,0)=0$. See Figure 3.

The problem is discretized using four elements, each of dimensions L/2 by T/2, as seen in Figure 4. Each element is of the type shown in Figure 5. The displacement field for this element is modeled using the bilinear shape functions

$$u(x,t) = u^e_{11}(1-x/L')(1-t/T') + u^e_{21}(1-x/L')(t/T') + u^e_{12}(x/L')(1-t/T') + u^e_{22}(x/L')(t/T') \tag{25}$$

ORIGINAL PAGE IS
OF POOR QUALITY

where the e superscript is a reminder that the quantities in (25) refer to local numbering and local axes. It can be shown, using methods derived in (Ref. 3), that the element statics equations for a linear elastic rod are

$$\frac{AET'}{L'}\begin{bmatrix} 1/3 & 1/6 & -1/3 & -1/6 \\ 1/6 & 1/3 & -1/6 & -1/3 \\ -1/3 & -1/6 & 1/3 & 1/6 \\ -1/6 & -1/3 & 1/6 & 1/3 \end{bmatrix} \begin{Bmatrix} u^e_{11} \\ u^e_{21} \\ u^e_{12} \\ u^e_{22} \end{Bmatrix} = \begin{Bmatrix} F^e_{11} \\ F^e_{21} \\ F^e_{12} \\ F^e_{22} \end{Bmatrix} \tag{26}$$

For the structure being studied here, $L' = L/2$ and $T' = T/2$; furthermore, only $u_{22}$ and $u_{32}$ are non-zero. The global stiffness equations for the linear elastic system are thus

$$\frac{AET}{L}\begin{bmatrix} 4/3 & 1/3 \\ 1/3 & 2/3 \end{bmatrix} \begin{Bmatrix} u_{22} \\ u_{32} \end{Bmatrix} = \sigma_Y AT \begin{Bmatrix} 1/2 \\ 5/12 \end{Bmatrix} \tag{27}$$

The solution is $u_{22} = 1/4\ \sigma_Y L/E$, $u_{32} = 1/2\ \sigma_Y L/E$. The stress state is $\sigma_2 = \sigma(T/2) = 1/2\sigma_Y$ and $\sigma_3 = \sigma(T) = \sigma_Y$, where the values are in tension on the left half of the rod and in compression for those on the right. The results are exact.

When the non-linear behavior is incorporated, the formulation described herein is used. The non-trivial matrices to be found are $[K_e]$, $[A^e_\sigma]$, $[B^e_\sigma]$ and $[C^e_\sigma]$.

The rate dependent form of (24) is

$$\overset{o}{\sigma} = E\,\alpha\,\overset{o}{\varepsilon} \tag{28}$$

where

$$\alpha(t) = \left[\, 1 + \frac{27}{7}\left(\frac{\sigma(t)}{\sigma_Y}\right)^8 \,\right]^{-1} \tag{29}$$

For the problem at hand, the stress state is assumed (for each element) to be a function of time only. Thus,

$$[N_\sigma] = 1 \tag{30}$$

The matrix [E] is approximated as a linear function in time by interpolating through the end points of the time interval; specifically,

$$[E] = E\alpha(0)\,[1 - t/T'] + E\alpha(T')(t/T') \tag{31}$$

Note how extremely poor this approximation is for the desired time step used in this example.

For the bilinear shape functions,

$$[f'][\overset{o}{N}] = \frac{1}{L'T'}\,[1 \quad -1 \quad -1 \quad 1] \tag{32}$$

ORIGINAL PAGE IS
OF POOR QUALITY

Incorporating (31) and (32) into (12a) yields

$$[S] = \frac{E}{L'}\left\{\alpha(0)\left[\left(\frac{t}{T'}\right) - \frac{1}{2}\left(\frac{t}{T'}\right)^2\right] + \frac{\alpha(T')}{2}\left(\frac{t}{T'}\right)^2\right\}[1 \quad -1 \quad -1 \quad 1] \tag{33}$$

Evaluating (33) at t=T , noting (30), and integrating over the volume yields

$$[B_\sigma^e] = EA\left[\frac{\alpha(0) + \alpha(T')}{2}\right][1 \quad -1 \quad -1 \quad 1] \tag{34a}$$

$$[C_\sigma^e] = AL' \tag{34b}$$

Using (33) in (18a) gives

$$[K_e] = \frac{AET'}{L'}\begin{bmatrix} -\left(\frac{\alpha_0}{8}+\frac{\alpha_1}{24}\right) & \frac{\alpha_0}{8}+\frac{\alpha_1}{24} & \frac{\alpha_0}{8}+\frac{\alpha_1}{24} & -\left(\frac{\alpha_0}{8}+\frac{\alpha_1}{24}\right) \\ -\left(\frac{5\alpha_0}{24}+\frac{\alpha_1}{8}\right) & \frac{5\alpha_0}{24}+\frac{\alpha_1}{8} & \frac{5\alpha_0}{24}+\frac{\alpha_1}{8} & -\left(\frac{5\alpha_0}{24}+\frac{\alpha_1}{8}\right) \\ \frac{\alpha_0}{8}+\frac{\alpha_1}{24} & -\left(\frac{\alpha_0}{8}+\frac{\alpha_1}{24}\right) & -\left(\frac{\alpha_0}{8}+\frac{\alpha_1}{24}\right) & \frac{\alpha_0}{8}+\frac{\alpha_1}{24} \\ \frac{5\alpha_0}{24}+\frac{\alpha_1}{8} & -\left(\frac{5\alpha_0}{24}+\frac{\alpha_1}{8}\right) & -\left(\frac{5\alpha_0}{24}+\frac{\alpha_1}{8}\right) & \frac{5\alpha_0}{24}+\frac{\alpha_1}{8} \end{bmatrix} \tag{35}$$

where $\alpha_o = \alpha(0)$ and $\alpha_1 = \alpha(T')$, and using (30) in (18b) yields

$$[A_\sigma^e] = AT'\begin{bmatrix} -1/2 \\ -1/2 \\ 1/2 \\ 1/2 \end{bmatrix} \tag{36}$$

Global assembly is now performed. First, it is remembered that only $u_{22}$ and $u_{32}$ are non-trivial; secondly, it is known that $\sigma(0) = \sigma_1 = 0$ and thus $\alpha(0) = \alpha_1 = 1$. Let a 2 subscript be used for quantities associated with t=T/2, and a 3 subscript be associated with quantities evaluated at t=T. Furhter, by symmetry, the value of the tension in an element on the left hand side of the structure would equal the value of compression in the corresponding element on the righ-hand side of the structure, so $\alpha^{Left} = \alpha^{Right}$ at a given time t. Finally, it is to be remembered that for the current discretization T' = T/2 and L' = L/2. All these imply that (20a) and (20b) may be written as

$$\frac{AET}{L}\begin{bmatrix} \frac{5}{12} - \frac{\alpha_3}{12} & \frac{\alpha_2}{4} + \frac{\alpha_3}{12} \\ -\frac{5\alpha_2}{12} - \frac{\alpha_3}{4} & \frac{5\alpha_2}{12} + \frac{\alpha_3}{4} \end{bmatrix}\begin{Bmatrix} u_{22} \\ u_{32} \end{Bmatrix} + AT\begin{bmatrix} 1/2 \\ 1/2 \end{bmatrix}\sigma_2 = \sigma_Y AT\begin{Bmatrix} 1/2 \\ 5/12 \end{Bmatrix} \tag{37a}$$

ORIGINAL PAGE IS
OF POOR QUALITY

$$\frac{EA(1+\alpha_2)}{2}\begin{bmatrix}1 & 0\end{bmatrix}\begin{Bmatrix}u_{22}\\u_{32}\end{Bmatrix} - \frac{AL}{2}\sigma_2 = 0 \qquad (37b)$$

Solving (37b) for $\sigma_2$ and using the results in (37a) yields the global stiffness equations

$$\frac{AET}{L}\begin{bmatrix}\frac{11}{12}+\frac{\alpha_2}{2}-\frac{\alpha_3}{12} & \frac{\alpha_2}{4}+\frac{\alpha_3}{12}\\ \frac{1}{2}+\frac{\alpha_2}{12}-\frac{\alpha_3}{4} & \frac{5\alpha_2}{12}+\frac{\alpha_3}{4}\end{bmatrix}\begin{Bmatrix}u_{22}\\u_{32}\end{Bmatrix} = \sigma_Y AT\begin{Bmatrix}1/2\\5/12\end{Bmatrix} \qquad (38)$$

Note that if the structure is considered linear elastic that $\alpha_2 = \alpha_3 = 1$, and equations (38) become identical to the elastic global equations (27).

Equations (38) were solved iteratively for $u_{22}$, $u_{32}$, $\sigma_2$ and $\sigma_3$ using a hand-held calculator maintaining four-place accuracy in the coefficients of the stiffness matrix. Table 1 lists the results of each iteration where the elastic case is taken as the initial condition. It should be noted that the trend indicated by the table implies that greater accuracy must be retained to achieve convergence; however, three place accuracy is reached rather quickly. The results are not bad when considering the absolutely horrendous approximations used in the example. It is concluded that the general method is viable.

## Related Research

As noted in the introduction, there were many theoretical questions which were needed to be answered that arose during the course of this study. Many of the questions concerning the incorporation of the initial conditions to the transient problem into a formulation that is inherently suited to boundary type conditions were answered both independently and through (ref. 3). There were other questions concerning non-prismatic or semi-prismatic discretizations, and their possible use in both formulating elements and in modeling specific problems in space and time. Several modified or hybrid variational formulations were developed to model elements possessing certain qualities, such as an embedded hole or non-rectangular geometry for grid elements, where interelement continuity would be more difficult to maintain. A search for a four-dimensional, unified theory for elastic dynamic solid mechanics was undertaken in order to better understand the parallel conditions that must exist between the spatial and temporal properties of a structure. Not to be overlooked are the various computer programming difficulties, particularly the large numbers of d.o.f. per element that could be generated for elements of this type, and the adaptability of element modules with a solution procedure provided by another host program.

## CONCLUDING REMARKS

The Slave Finite Element approach to non-linear analysis has been presented. Despite the large number of dof in the system for any given problem, the anticipated

reduced number of calculations, the ease in changing time steps by using various grid options, the increased detail within any subinterval, and the accuracy demonstrated in elastic problems demonstrates the viability of the method. Continued research is necessary to fully understand and exploit the potential of the method.

## REFERENCES


1. Argyris, J.H. and Scharpf, D. W.: Finite Elements in Time and Space. Nuc. Eng. Design, 10, 1969, pp. 456-464.

2. Fried, I.: Finite Element Analysis of Time Dependent Phenomena. AIAA J., 7, 1969, pp. 1170-1172.

3. Simkins, T.E.: Finite Elements for Initial Value Problems in Dynamics. AIAA J., 19, 1981, pp. 1357-1362.

4. Ramberg, W., and Osgood, W. R.: Description of Stress-Strain Curves by Three Parameters. NACA TN 902, 1943.

TABLE 1: NUMERICAL COMPUTATIONS FOR SAMPLE PROBLEM

| Iteration # | $u_{22}E/\sigma_Y L$ | $u_{32}E/\sigma_Y L$ | $\sigma_2/\sigma_Y$ | $\sigma_3/\sigma_Y$ | $\alpha_2$ | $\alpha_3$ |
|---|---|---|---|---|---|---|
| 0 | .2500 | .5000 | .5000 | 1.0000 | .9852 | .2059 |
| 1 | .2409 | .6252 | .4782 | .9359 | .9896 | .3058 |
| 2 | .2423 | .6016 | .4821 | .9475 | .9889 | .2853 |
| 3 | .2420 | .6061 | .4813 | .9452 | .9890 | .2892 |
| 4 | .2420 | .6053 | .4813 | .9457 | .9890 | .2884 |
| 5 | .2420 | .6054 | .4813 | .9457 | .9890 | .2887 |
| (no further change in stiffness matrix) | | | | | | |
| EXACT | .2504 | .7143 | .5000 | 1.0000 | | |
| % ERROR | 3.4 | 15.3 | 3.7 | 5.5 | | |

ORIGINAL PAGE IS
OF POOR QUALITY

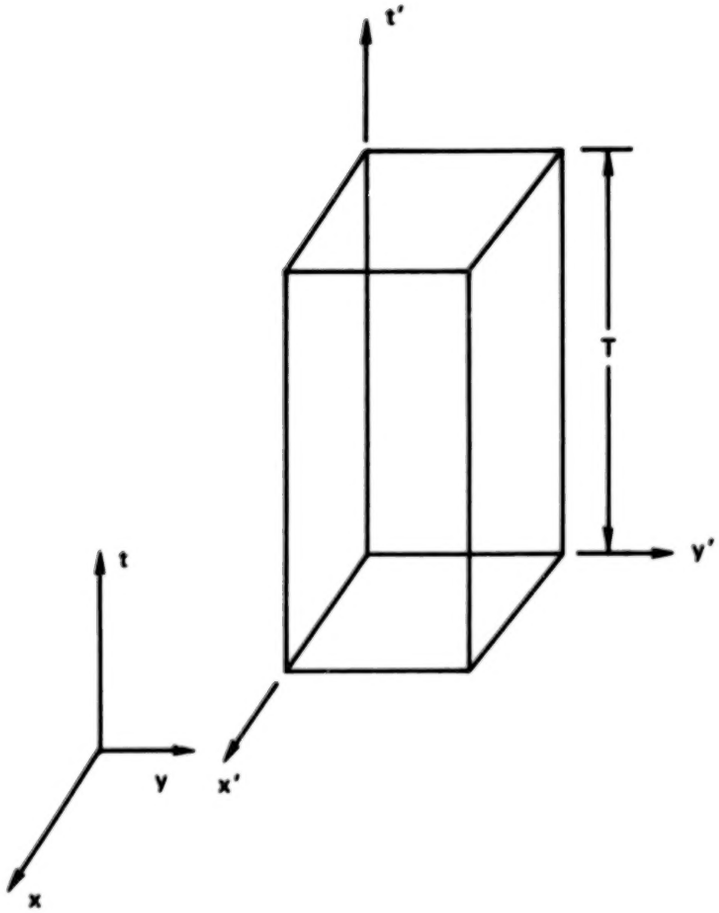


Figure 1. Two Dimensional Prismatic Element

ORIGINAL PAGE IS
OF POOR QUALITY

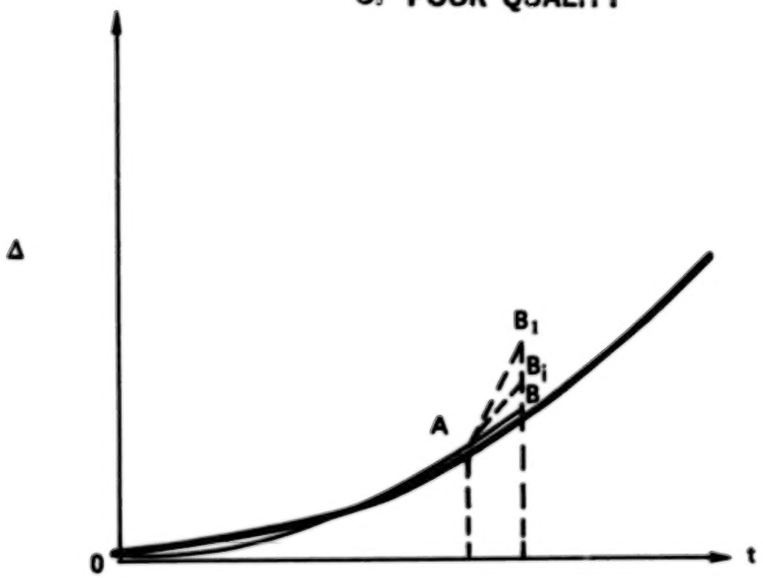


(a)

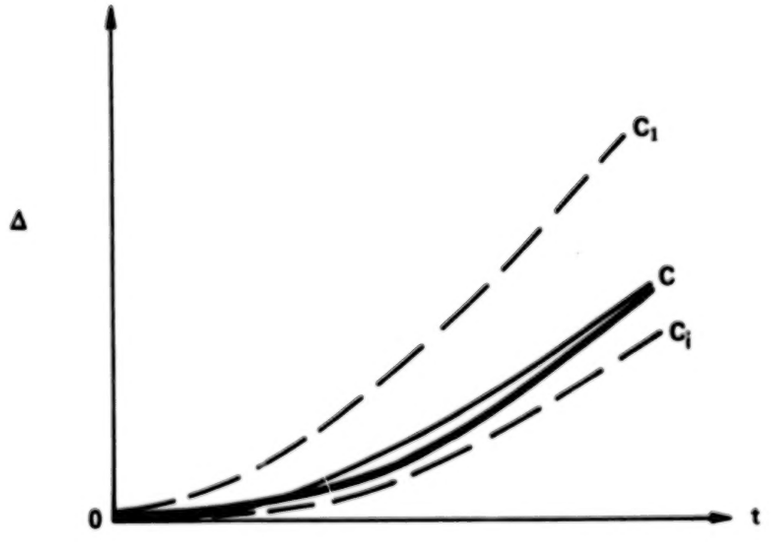


(b)

Figure 2. Comparison of Non-Linear Algorithms (a) Step-By-Step Method
(b) Slave Finite Element Method

ORIGINAL PAGE IS
OF POOR QUALITY

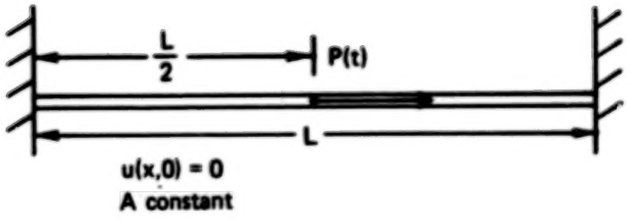


Figure 3. Sample Problem

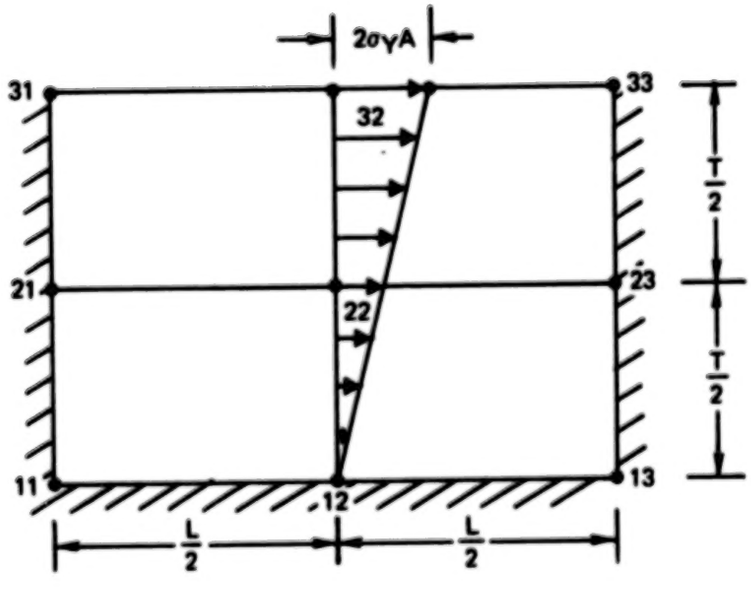


Figure 4. Discretization

ORIGINAL PAGE IS
OF POOR QUALITY

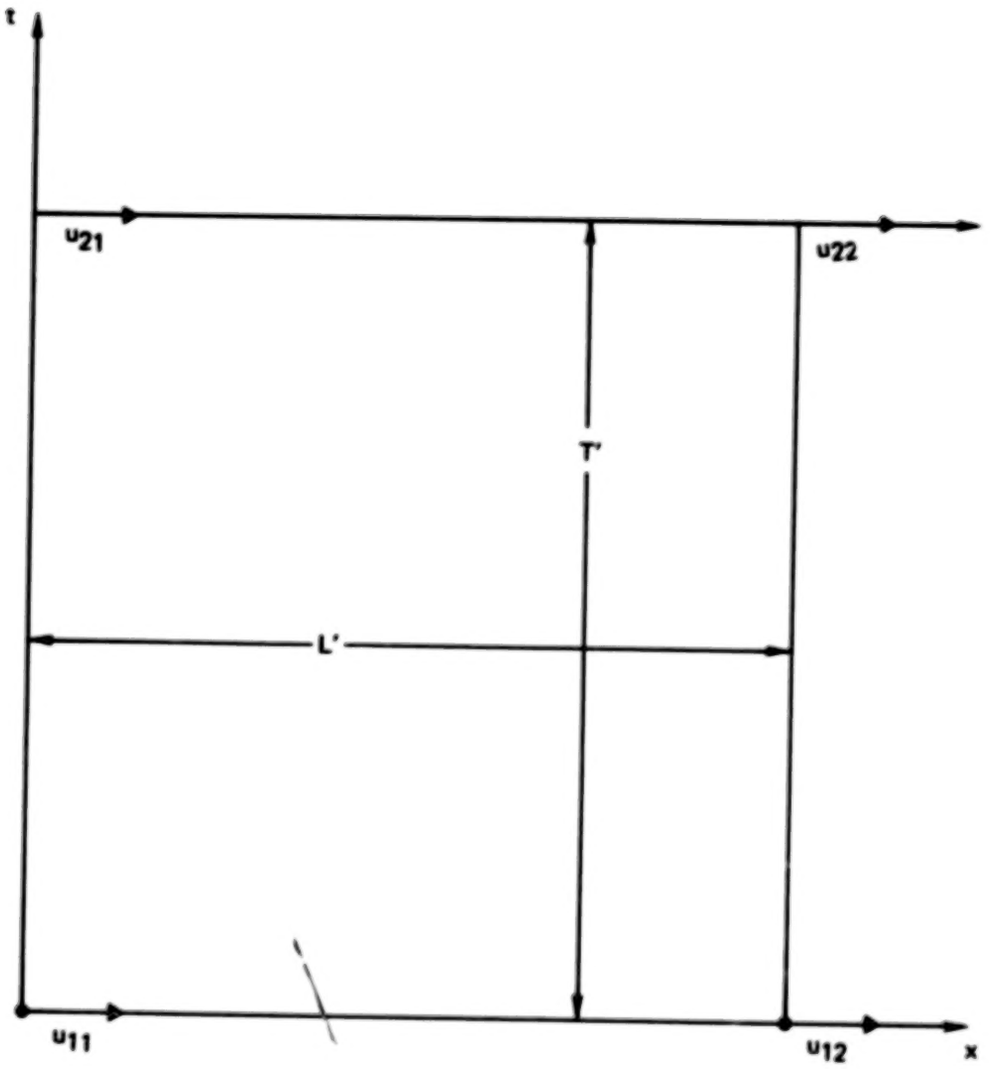


Figure 5. Prismatic Rod Element

N84
31690

UNCLAS

N84 31690

D2

# NEW VARIATIONAL FORMULATIONS OF HYBRID STRESS ELEMENTS*

T.H.H. Pian,† K. Sumihara†† and D. Kang††
Massachusetts Institute of Technology

## SUMMARY

In the variational formulations of finite elements by the Hu-Washizu and Hellinger-Reissner principles the stress equilibrium condition can be maintained by the inclusion of internal displacements which function as the Lagrange multipliers for the constraints. These new versions permit the use of natural coordinates and the relaxation of the equilibrium conditions and, render considerable improvements in the assumed stress hybrid elements. These include the derivation of invariant hybrid elements which possess the ideal qualities such as minimum sensitivity to geometric distortions, minimum number of independent stress parameters, rank sufficient and ability to represent constant strain-states and bending moments. Another application is the formulation of semiLoof thin shell elements which can yield excellent results for many severe test cases because the rigid body nodes, the momentless membrane strains and the inextensional bending modes can all be represented.

## INTRODUCTION

In the original formulation of the assumed stress hybrid elements by the modified complementary energy principle (ref. 1) and the later extension using the Hellinger-Reissner (ref. 2) the assumed stress are made to satisfy the equilibrium equations a priori. This restricts the derivation to the use of physical coordinates such as Cartesian coordinates and shell surface coordinates, etc. and to the coupling of the various stress components by the equilibrium equations. Such restrictions are the chief obstacles for the construction of shell elements by the hybrid method and the main reasons why the element properties often deteriorate rapidly when unfavorable reference coordinates are used for stresses and/or when the element geometry is distorted.

Recently new versions of the Hellinger-Reissner and the Hu-Washizu principles have been suggested for more efficient formulations of hybrid stress elements (refs. 3 and 4). This paper presents two specific applications of these principles: (1) the formulation of invariant hybrid stress elements by the Hellinger-Reissner principle and (2) the derivation of semiLoof shell elements by the Hu-Washizu principle.

The research reported here is one part of a program the objective of which is to advance the numerical tools for analyzing engine structures which needs to be modelled by 3-D solids and/or shell structures.

---

*The work was sponsored by the NASA Lewis Research Center under NASA Grant No. NAG 3-33.

†Professor of Aeronautics and Astronautics

††Graduate Student

## FORMULATION OF INVARIANT HYBRID STRESS ELEMENTS

The modified version of the Hellinger-Reissner principle for the formulation of the element stiffness matrix may be stated as

$$\pi_R = \int_V [-\frac{1}{2} \underset{\sim}{\sigma}^T \underset{\sim}{S} \underset{\sim}{\sigma} + \underset{\sim}{\sigma}^T (\underset{\sim}{D}\, \underset{\sim}{u}_q) - (\underset{\sim}{D}^T \underset{\sim}{\sigma})^T \underset{\sim}{u}_\lambda] dV = \text{Stationary} \qquad (1)$$

where $\sigma$ = stress, $S$ = elastic compliance, $V$ = element volume, $\underset{\sim}{u}_q$ = element displacements that are interpolated compatibly in terms of nodal displacements $q$ and $\underset{\sim}{u}_\lambda$ = additional internal displacements which are expressed in terms of parameters $\underset{\sim}{\lambda}$ that can be statically condensed. Here

$$(\underset{\sim}{D}^T \underset{\sim}{\sigma}) = 0 \qquad (2)$$

is the equation of equilibrium. Hence the last term in the functional plays the role of conditions of constraint with the corresponding Lagrange multipliers. Thus, the assumed stresses $\underset{\sim}{\sigma}$ need not be coupled initially and the introduction of displacement parameters $\underset{\sim}{\lambda}$ will reduce the number of independent stress parameters.

As an example, the derivation of the quadrilateral membrane element is presented. Here, for the $\sigma$ stresses, the nine terms are complete in linear terms in the natural or isoparametric coordinates $\xi$, $\eta$,

$$\underset{\sim}{\sigma} = \begin{Bmatrix} \sigma_x \\ \sigma_y \\ \tau_{xy} \end{Bmatrix} = \begin{bmatrix} 1 & \xi & \eta & & & & & & \\ & & & 1 & \xi & \eta & & & \\ & & & & & & 1 & \xi & \eta \end{bmatrix} \begin{Bmatrix} \beta_1 \\ \vdots \\ \beta_9 \end{Bmatrix} \qquad (3)$$

The element displacements are interpolated by bilinear polynomials in the natural coordinates. Here it is expected that in the limiting case of rectangular elements the present formulation should yield the 5-$\beta$ hybrid stress element (ref. 5) that is known to have excellent properties.

Thus, four internal displacement terms are need. They are, indeed, the same ones used by Wilson et al. (ref. 6) in their incompatible elements, i.e.

$$\begin{aligned} u_\lambda &= \lambda_1(1-\xi^2) + \lambda_2(1-\eta^2) \\ v_\lambda &= \lambda_3(1-\xi^2) + \lambda_4(1-\eta^2) \end{aligned} \qquad (4)$$

It is noted that these additional displacement terms are essential because they now make the displacements $\underset{\sim}{u}$ complete in quadratic terms.

In the actual formulation it turns out that the four $\lambda$ terms yield only two independent equations of constraints for the $\beta$'s. It was found necessary to consider the element geometry with a small perturbation as shown in Figure 1. With the x and y components of the perturbation represented by $\pm\Delta x$ and $\pm\Delta y$ the Jacobian is

ORIGINAL PAGE IS
OF POOR QUALITY

$$|J| = \begin{bmatrix} a_1 + a_2\eta + \Delta x(1-\eta^2) & b_1 + b_2\eta + \Delta y(1-\eta^2) \\ a_3 + a_2\xi - 2\Delta x\xi\eta & b_3 + b_2\xi - 2\Delta y\xi\eta \end{bmatrix} \tag{5}$$

where $a_1 = \frac{1}{4}(-x_1 + x_2 + x_3 - x_4)$; $b_1 = \frac{1}{4}(-y_1 + y_2 + y_3 - y_4)$

$a_2 = \frac{1}{4}(x_1 - x_2 + x_3 - x_4)$; $b_2 = \frac{1}{4}(y_1 - y_2 + y_3 - y_4)$

$a_3 = \frac{1}{4}(-x_1 - x_2 + x_3 + x_4)$; $b_3 = \frac{1}{4}(-y_1 - y_2 + y_3 + y_4)$ (6)

Here $x_i, y_i$ are the coordinates of the corner nodes and the ratio $\Delta y/\Delta x$ is equal to $b_1/a_1$.

In this case the four $\lambda$-terms yield four equations of constraints and $\beta_2$, $\beta_6$, $\beta_8$ and $\beta_9$ can be expressed in terms of $\beta_3$ and $\beta_5$. The assumed stresses can be rearranged in matrix form as

$$\begin{Bmatrix} \sigma_x \\ \sigma_y \\ \tau_{xy} \end{Bmatrix} \equiv \begin{bmatrix} 0 & 1 & 0 & a_1^2\eta & a_3^2\xi \\ 0 & 1 & 0 & b_1^2\eta & b_3^2\xi \\ 0 & 0 & 1 & a_1b_1\eta & a_3b_3\xi \end{bmatrix} \begin{Bmatrix} \beta_1 \\ \vdots \\ \beta_5 \end{Bmatrix} \tag{7}$$

In the case of a rectangular element with $\xi$ and $\eta$ in parallel with x and y, $b_1$ and $a_3$ vanish and the 5 $\beta$-terms of reference 5 is obtained. For hybrid stress elements, particularly of higher orders, there exist many possible choices for the assumed stress. The new variational principle, thus, provides a rational procedure to establish the appropriate stress terms for hybrid elements both of regular shape and with geometrical distortions. Because the present formulation is based on natural coordinates the resultant element stiffness matrix is always an invariant. It can also be shown that it always has sufficient rank. The element, of course, can also pass the constant strain patch test.

It turns out that the same result can be obtained when the stresses based upon the basis vectors of the natural coordinates $\xi$ and $\eta$ are expressed as

$$\underset{\sim}{\tau} = \begin{Bmatrix} \tau^{11} \\ \tau^{22} \\ \tau^{12} \end{Bmatrix} = \begin{bmatrix} 1 & 0 & 0 & \eta & 0 \\ 0 & 1 & 0 & 0 & \xi \\ 0 & 0 & 1 & 0 & 0 \end{bmatrix} \begin{Bmatrix} \beta_1 \\ \vdots \\ \beta_5 \end{Bmatrix} \tag{8}$$

and in converting the tensor stress $\tau^{ij}$ to the physical component $\sigma^{ij}$ by

$$\sigma^{ij} = J^i_k \, J^j_\ell \, \tau^{k\ell} \tag{9}$$

the value of the Jacobian at $(\xi,\eta) = (0,0)$ is used. By such a step the constant stress state can be maintained hence the resulting element can pass the patch test.

A tapered and swept panel with one edge clamped and the opposite edge acted by a distributed shear load was used bt Cook (ref. 7) for testing the sensitivities of finite elements to geometric distortions. The resulting normal stress distributions along the mid-span section are determined by the following four elements using the same 4x4 mesh as shown in figure 2:

(1) Element Q-4 by bi-linear assumed displacements.

(2) Element HG by original 5-β assumed stress method with the global x-y axes as reference.

(3) Element HL by original 5-β assumed stress method with the reference x'-y' axes located at equal angles with the natural ξ-η axes.

(4) Present invariant hybrid stress element.

A solution obtained by element HL using 16x16 mesh is used as a reference. It is seen by the result by the present element is already very close to the reference solution while the solutions by the other elements all have much larger errors. The assumed stress given by eq. (8) is thus the optimal choice for assumed stress hybrid elements.

Eight-node solid elements have also been constructed by the same approach. It is used to analyze the bending of a rectangular bar with two elements which are distorted. The effect of the element distortion on the tip deflection and normal stress is shown in figures 3 and 4. Also included for comparison are the results obtained by the assumed displacement method and by the original hybrid stress method using the beam axis as reference. It is seen that under large distortions the original hybrid stress element may become almost as rigid as the assumed displacement element, but the present invariant element is much less sensitive to distortions.

## THIN SHELL ANALYSES BY SEMILOOF ELEMENTS

Thin shell elements are formulated by the Hu-Washizu principle with additional internal displacements for enforcing the stress equilibrium conditions and with relaxed continuity conditions along the interelement boundaries. The principle is expressed as

$$\pi_{HW} = \int_V \left[ \frac{1}{2} \underset{\sim}{\varepsilon}^T \underset{\sim}{c}\, \underset{\sim}{\varepsilon} - \underset{\sim}{\sigma}^T \underset{\sim}{\varepsilon} + \underset{\sim}{\sigma}^T (\underset{\sim}{D}\, \underset{\sim}{u}_q) - (\underset{\sim}{D}^T \underset{\sim}{\sigma})^T \underset{\sim}{u}_\lambda \right] dV - \int_{\partial V} \underset{\sim}{T}^T (\underset{\sim}{u}_q - \underset{\sim}{\bar{u}}) dS = \text{stationary} \qquad (10)$$

where strains $\varepsilon$, stresses $\sigma$ and element displacements $u_q$ and $u_\lambda$ and boundary displacement $\bar{u}$ are independent. The key step in the finite element formulation is that both $\sigma$ and $\varepsilon$ are approximated by the same function, i.e.

$$\underset{\sim}{\varepsilon} = \underset{\sim\sim}{P}\underset{\sim}{\alpha} \quad \text{and} \quad \underset{\sim}{\sigma} = \underset{\sim\sim}{P}\underset{\sim}{\beta} \qquad (11)$$

where P are not coupled among different components. The displacements $u_q$, $u_\lambda$ and $\bar{u}$ are interpolated by

ORIGINAL PAGE IS
OF POOR QUALITY

$$\underset{\sim}{u}_q = \underset{\sim}{N}\underset{\sim}{q} \; ; \quad \underset{\sim}{u}_\lambda = \underset{\sim}{M}\underset{\sim}{\lambda} \; ; \quad \text{and} \quad \underset{\sim}{\tilde{u}} = \underset{\sim}{L}\underset{\sim}{q} \tag{12}$$

and the functional $\pi_{HW}$ is reduced to

$$\pi_{HW} = \frac{1}{2}\underset{\sim}{\alpha}^T\underset{\sim}{J}\underset{\sim}{\alpha} - \underset{\sim}{\beta}^T\underset{\sim}{H}\underset{\sim}{\alpha} + \underset{\sim}{\beta}^T\underset{\sim}{G}\underset{\sim}{q} - \underset{\sim}{\beta}^T\underset{\sim}{R}\underset{\sim}{\lambda} \tag{13}$$

where $\underset{\sim}{J} = \int_V \underset{\sim}{P}^T\underset{\sim}{C}\underset{\sim}{P}\, dV \; ; \quad \underset{\sim}{H} = \int_V \underset{\sim}{P}^T\underset{\sim}{P}\, dV$

$$\underset{\sim}{G} = \int_V \underset{\sim}{P}^T(\underset{\sim}{D}\underset{\sim}{N})dV \; ; \quad \underset{\sim}{R} = \int_V (\underset{\sim}{D}^T\underset{\sim}{P})^T\underset{\sim}{M}\, dV \tag{14}$$

Here $\underset{\sim}{H}$ is a symmetric and positive definite matrix which can be partitioned with submatrics located only along the diagonal. Thus, the inversion of $\underset{\sim}{H}$ reduces to that of the individual submatrices.

Variation of $\pi_{HW}$ with respect to $\beta$, $\alpha$ and $\lambda$ in the element level will enable the solutions of these variables in terms of $\underset{\sim}{q}$ and the following expression can be obtained for the element stiffness.

$$\underset{\sim}{k} = \underset{\sim}{G}^T\underset{\sim}{W}\underset{\sim}{G} - \underset{\sim}{G}^T\underset{\sim}{W}\underset{\sim}{R}\,(\underset{\sim}{R}^T\underset{\sim}{W}\underset{\sim}{R})^{-1}\,\underset{\sim}{R}^T\underset{\sim}{W}\underset{\sim}{G} \tag{15}$$

where

$$\underset{\sim}{W} = \underset{\sim}{H}^{-1}\underset{\sim}{J}\underset{\sim}{H}^{-1} \tag{16}$$

and the order of $\underset{\sim}{R}^T\underset{\sim}{W}\underset{\sim}{R}$ is the same as the number of equilibrium constraint equations obtained by $\underset{\sim}{\lambda}$.

To maintain good qualities a thin shell element must be able to represent (1) the rigid body modes, (2) the momentless membrane strains and (3) the inextensional bending modes. By using the Hu-Washizu principle for which the assumed strain and stress components are uncoupled the last two deformation modes can be easily included and by satisfying the equilibrium conditions in the element level the rigid body displacements can be guaranteed.

Another condition that is desirable for the formulation of thin shell elements is for the three displacement components u, v, and w to be of the same order. For ordinary shell elements for which the nodal displacements w and $w_{,\alpha}$ and $w_{,\beta}$ are needed to interpolate the lateral displacements while only u and v are used for the assumed inplane displacements, these displacement components will naturally be unbalanced. In a semiLoof element, however, all the displacement components are interpolated in terms of their own nodal values hence are automatically of identical orders. By the assumed stress hybrid method the continuation of the normal rotations $w_{,n}$ along the boundary are imposed through the boundary displacements $\tilde{u}$. Thus, in addition to the advantage of expressing equilibrium equations at the boundary nodes with only three degrees of freedom, a semiLoof element is also most natural for the balanced assumed displacements.

Hybrid semiLoof elements for triangular and quadrilateral planform with

24 and 32 DOF respectively were constructed based on the shallow shell theory of Marguerre and the optimal number of $\beta$'s and $\lambda$'s were determined. The nodal displacements are u, v and w at each corner node and each mid-side node and $w_{,n}$ at 1/3 way points of all edges.

The semiLoof approach has also been used to construct two hybrid quadrilateral elements of 32-DOF based on the cylindrical shell theory using 36 and 38 $\beta$-parameters respectively. The stresses are later constrained by using 7$\lambda$'s. For the 36-$\beta$ element the in-plane and moment components are complete in quadratic terms. The element has two kinematic deformation modes, hence a 38-$\beta$ element is also developed by adding cubic terms for the in-plane stresses components $\ell^{11}$ and $\ell^{22}$. For the internal displacements the $\hat{u_1}$ and $\hat{u_2}$ components each contains 3 terms while the w component contains only a single term.

Figures 5 and 6 present comparisons of vertical deflections at the edge of a cylindrical shell roof under gravity loads by three 32 DOF semiLoof quadrilateral elements, one which is based on the shallow shell theory and the other two, by the deep shell theory. Also included for comparison are the solutions by the assumed displacement methods. The result by Dawe's (ref. 8) is by 54-DOF triangular elements based on the deep shallow theory. Dawe's element is known to be an excellent element although it is not easily adopted because of its use of higher derivatives as nodal displacements and its difficulty for handling the intersection of shells. The result by Cowper et al. (ref. 9) is again obtained by the triangular elements based on the shallow shell theory. That element as well as the degenerated solid element with reduced integration (ref. 10) all coverge to that by the shallow shell theory. On the other hand, the solutions by the hybrid semiLoof elements based on the cylindrical shell theory, converge to the solution obtained by the deep shell theory. This is a clear indication that the appropriate shell theory must be incorporated in the construction of shell elements. Figure 7 shows stress distributions obtained by the semiLoof element with 38$\beta$ using 3x3 and 4x4 meshes.

Morley (ref. 11) has proposed a challenging test example which consists of a thin circular cylinder with reciprocal shear tractions applied along a cut in the axial direction resulting in a state of uniform torsion (fig. 8). This problem is very sensitive to the assumed displacement fields in the finite element. Another severe test case is a thin cylindrical shell under internal pressure for which the element used must be able to represent momentless membrane stresses. It has been found that the present semiLoof cylindrical shell element with 36$\beta$ and 7$\lambda$ can pass these tests successfully.

## CONCLUSIONS

The new versions of the Hellinger-Reissner and Hu-Washizu principles using additional internal displacements open up the options for constructing hybrid stress elements. A new hybrid stress element developed by the present method has invariant properties and has been demonstrated to be much less sensitive to geometric distortions. Several semiLoof shell elements have been constructed and proved to be successful even for very severe test examples. Introduction of the new variational principles, thus, represents a significant advancement in the finite element development.

## REFERENCES


1. Pian, T.H.H; and Tong, P.: Basis of Finite Element Methods for Solid Continua. Int. J. Num. Meth. Engng, vol. 1, 1968, pp. 3-28.

2. Pian, T.H.H.: Finite Element Methods by Variational Principles with Relaxed Continuity Requirements. Variational Methods in Engineering, C.A. Brebbia and H. Tottenham (Ed.), Southampton Univ. Press, 1973, pp. 3/1-3/24.

3. Pian, T.H.H.; and Chen, D.P.: Alternative Ways for Formulation of Hybrid Stress Elements. Int. J. Num. Meth. Engng., vol. 18, 1982, pp. 1679-1684.

4. Pian, T.H.H.; Chen, D.P.; and Kang, D.: A New Formulation of Hybrid/Mixed Finite Elements. Computers and Structures, vol. 16, 1983, pp. 81-87.

5. Pian, T.H.H.: Derivation of Element Stiffness Matrices by Assumed Stress Distributions. AIAA J., vol. 2, 1964, pp. 1333-1336.

6. Wilson, E.L.; Taylor, R.L.; Doherty, W.; and Ghaboussi, J.: Imcompatible Displacement Models. Numerical and Computer Methods in Structural Mechanics, (Eds. S.J. Fenves et al.), Academic Press, 1973, pp. 43-57.

7. Cook, R.D.: Improved Two-Dimensional Finite Element. ASCE J. Structural Div., ST9, Sept. 1974, pp. 1851-1863.

8. Dawe, D.J.: High-Order Triangular Finite Element for Shell Analysis. Int. J. Solids Structures, vol. 11, 1975, pp. 1097-1110.

9. Cowper, G.R.; Lindberg, G.M.; and Olson, M.D.: A Shallow Shell Finite Element Triangular Shape. Int. J. Solids Structures, vol. 6, 1970, pp. 1133-1156.

10. Zienkiewicz, O.C.; Taylor, R.L.; and Too, T.M.: Reduced Integration Technique in General Analysis of Plates and Shells. Int. J. Num. Meth. Engng., vol. 3, 1971, pp. 275-290.

11. Morley, L.S.D.: Analysis of Developable Shells with Special Reference to the Finite Element Method and Circular Cylinders. Phil. Trans. Roy. Soc. London, vol. 281, no. 1300, 1976, pp. 113-170.

ORIGINAL PAGE IS
OF POOR QUALITY

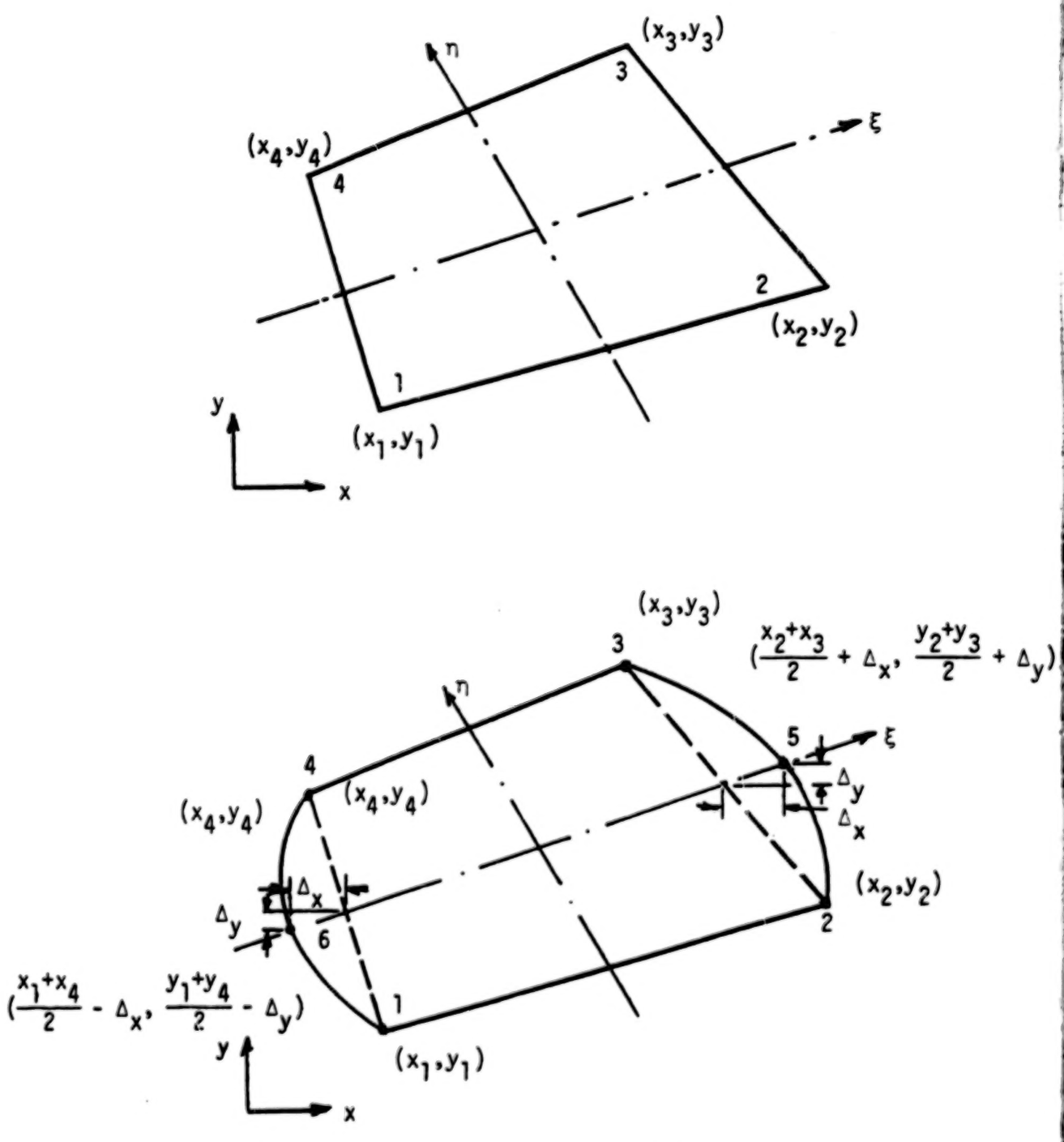


Fig. 1 Quadrilateral Element with Small Perturbation

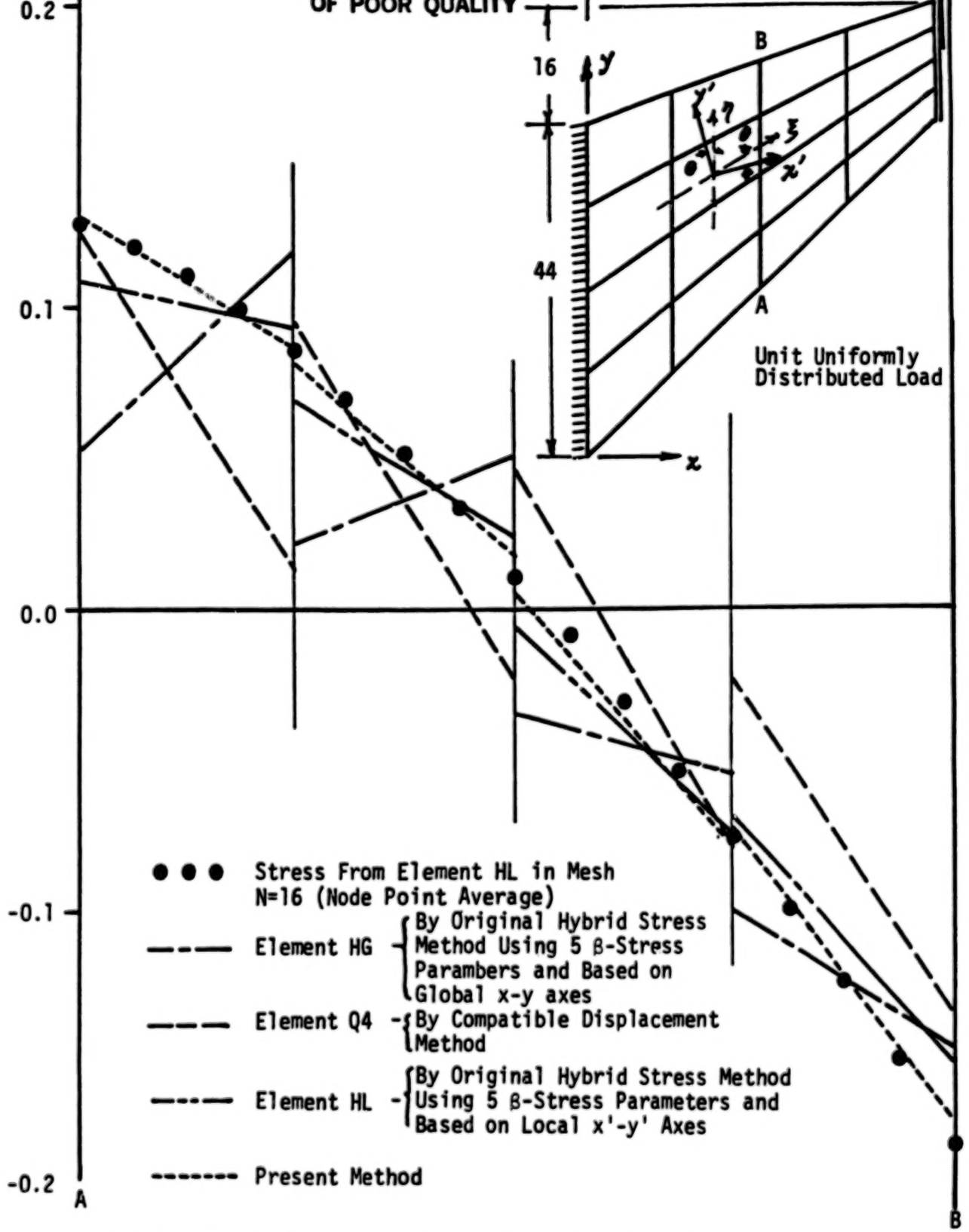


Fig. 2 Normal Stress $\sigma_x$ Along Line AB for Mesh N=4

ORIGINAL PAGE IS
OF POOR QUALITY

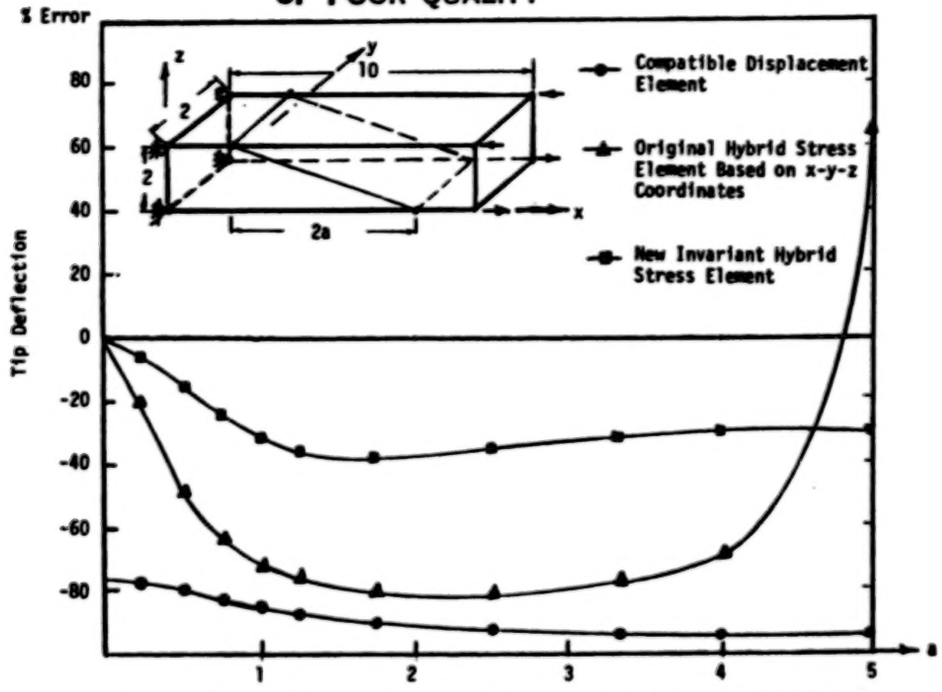


Fig. 3 Effect of Element Distortion on Tip Deflection of Cantilever Rectangular Beams Under Pure Bending

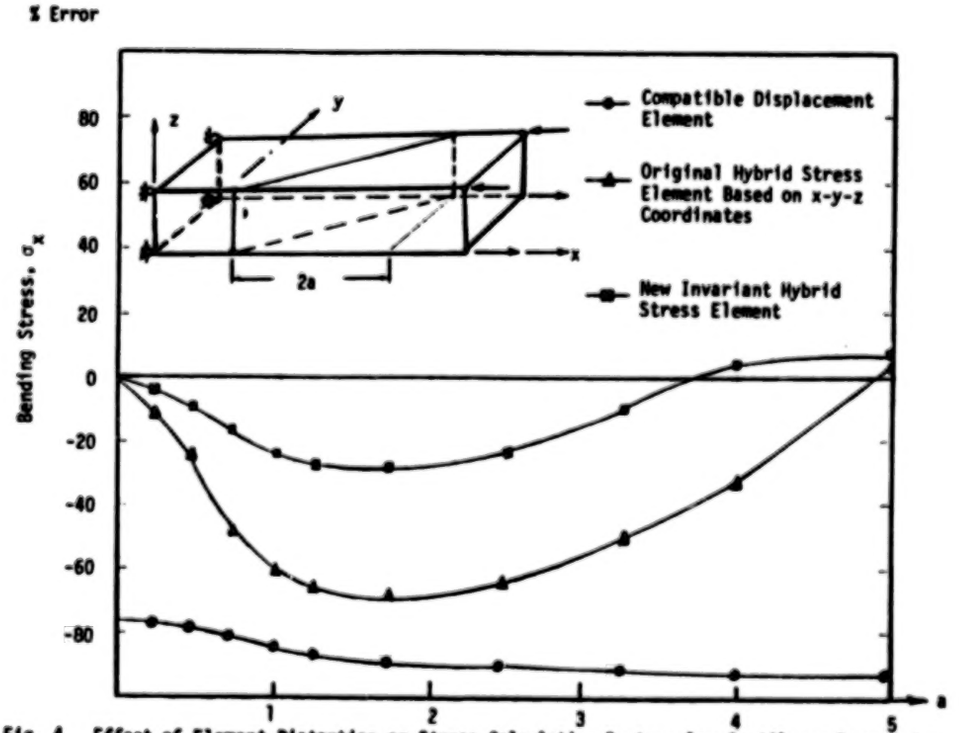


Fig. 4 Effect of Element Distortion on Stress Calculation Rectangular Cantilever Beam Under Pure Bending $\sigma_x$ at $\xi=\eta=\zeta=0.577$ of the Element at the Root

ORIGINAL PAGE IS
OF POOR QUALITY

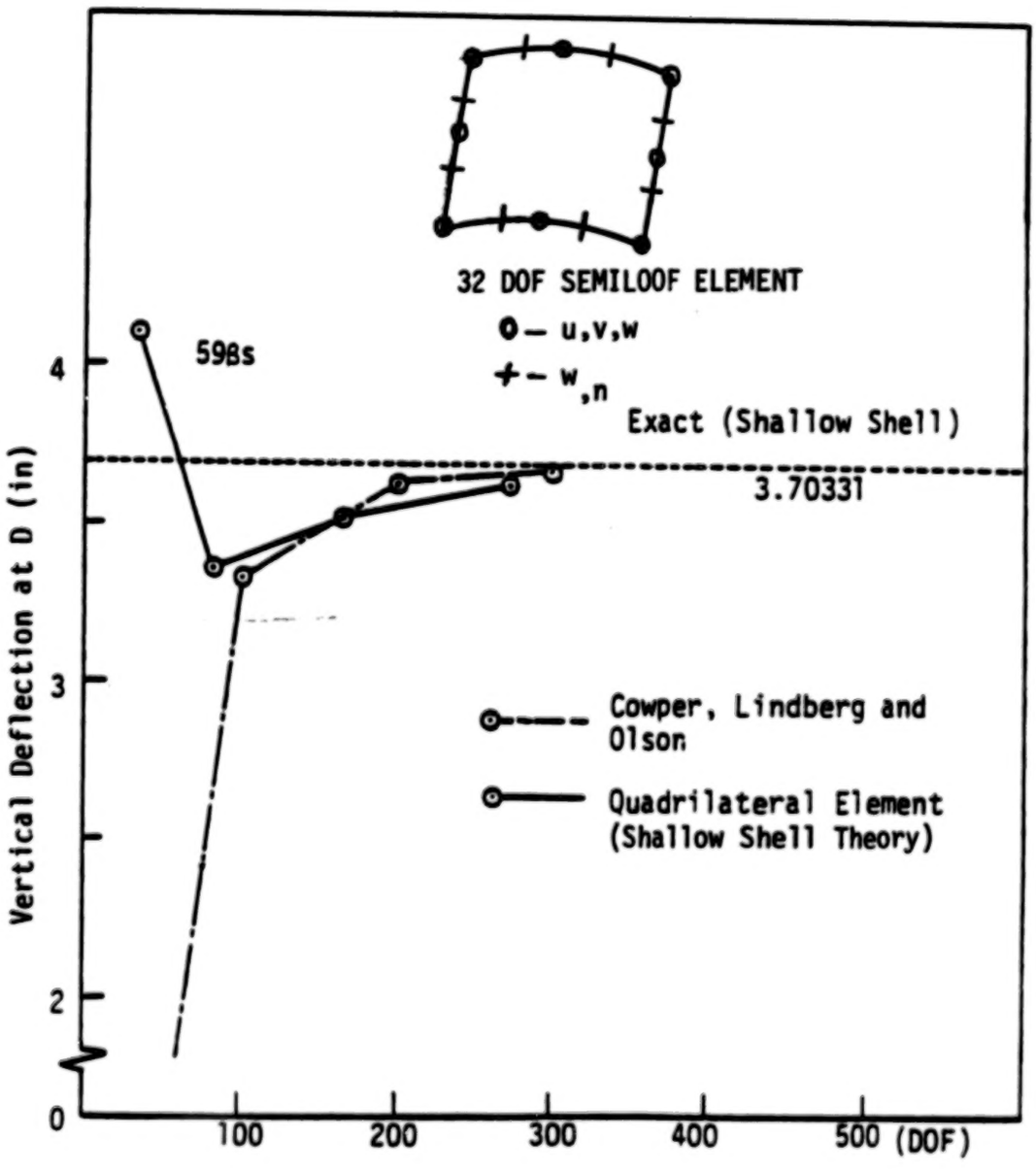


Fig. 5 Convergence of Vertical Deflection at D for Cylindrical Shell Roof Problem

ORIGINAL PAGE IS
OF POOR QUALITY

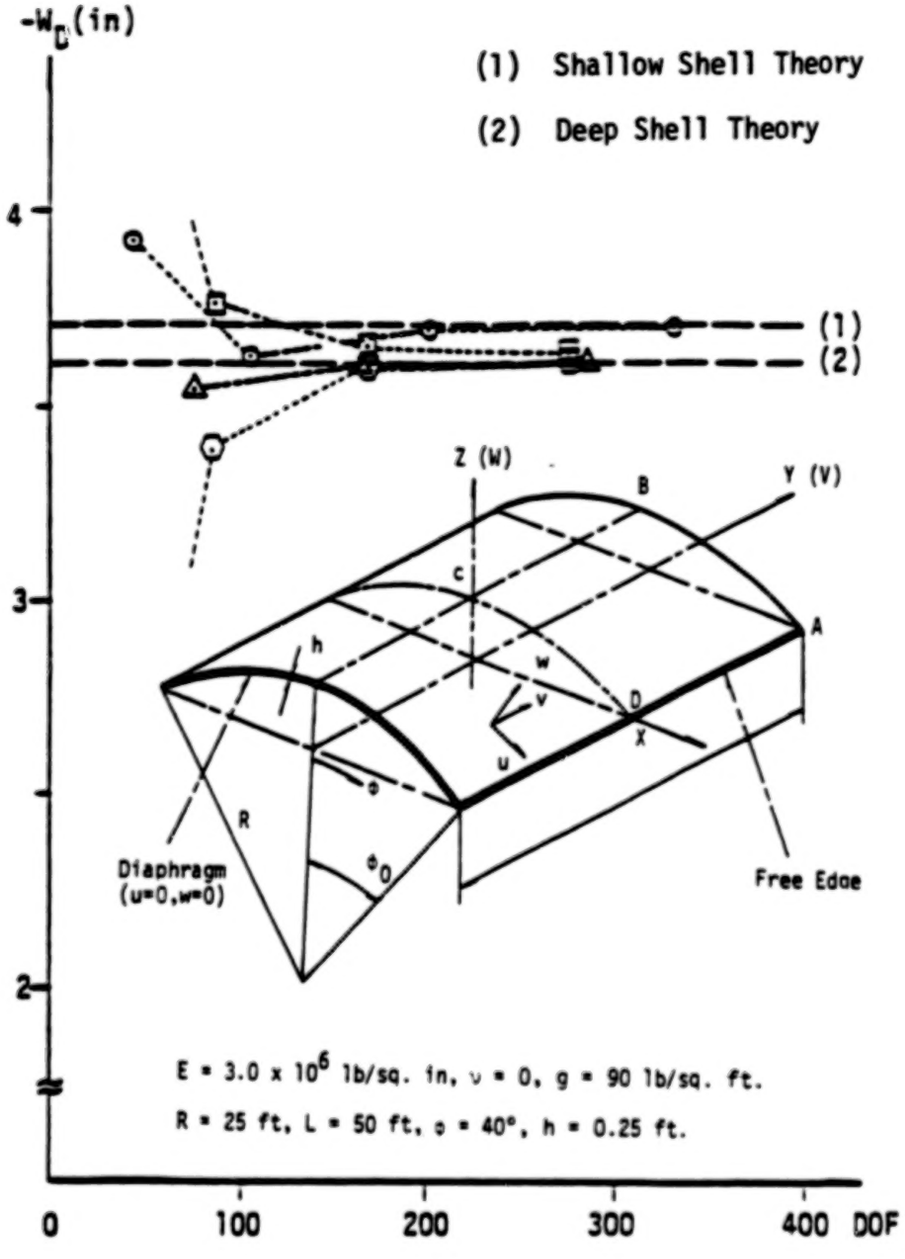


⊙ Degenerated Shell with Reduced Integration

△ Dawe's 54 DOF Triangular Element

⊡ Hybrid SemiLoof 32 DOF 36β 7λ } General Shallow Shell Theory

⊙ Hybrid SemiLoof 32 DOF 38β 7λ } General Shallow Shell Theory

Fig. 6 Convergence of Deflection at D in Cylindrical Shell Roof Problem

ORIGINAL PAGE IS
OF POOR QUALITY

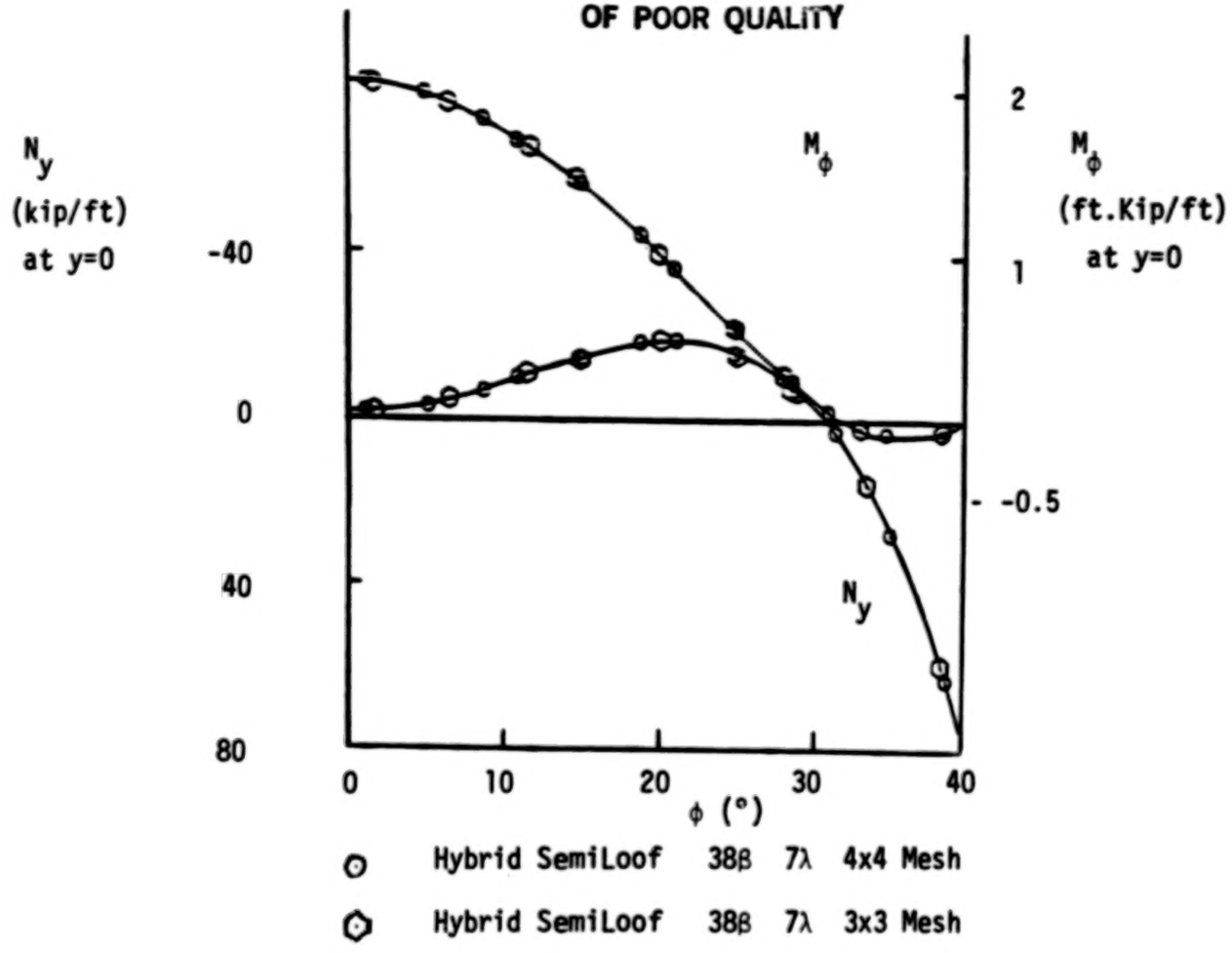


Fig. 7 Stress Distribution in Cylindrical Shell Roof Problem

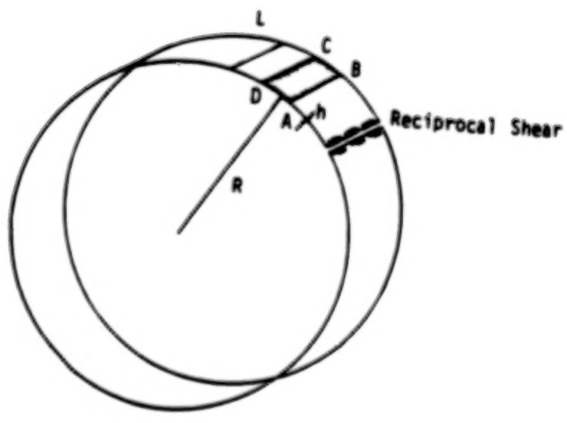


Fig. 8 Shear Load on a Slit Cylinder

N84
31691

UNCLAS

N84 31691

D3

# A SHEAR DEFORMABLE SHELL ELEMENT FOR LAMINATED COMPOSITES†

W. C. Chao and J. N. Reddy

Department of Engineering Science and Mechanics
Virginia Polytechnic Institute and State University
Blacksburg, VA 24061

## SUMMARY

A three-dimensional element based on the total Lagrangian description of the motion of a layered anisotropic composite medium is developed, validated, and used to analyze layered composite shells. The element contains the following features: geometric nonlinearity, dynamic (transient) behavior, and arbitrary lamination scheme and lamina properties. Numerical results of nonlinear bending, natural vibration, and transient response are presented to illustrate the capabilities of the element.

## INTRODUCTION

Composite materials and reinforced plastics are increasingly used in automobiles, aircrafts, space vehicles, and pressure vessels. With the increased use of fiber-reinforced composites as structural elements, studies involving the thermomechanical behavior of shell components made of composites are receiving considerable attention. Functional requirements and economic considerations of design have forced designers to use accurate but economical methods of determining stresses, natural frequencies, buckling loads, etc. The majority of the research papers in the open literature on shells is concerned with bending, vibration, and buckling of isotropic shells. As composite materials are making their way into many engineering structures, analyses of shells made of such materials become important. The application of advanced fiber composites in jet engine fan or compressor blades and high performance aircraft require studies involving transient response of composite shell structures to assess the capability of these materials under dynamic loads.

A review of the literature indicates that first, there does not exist any finite-element analysis of geometrically nonlinear transient response of laminated anisotropic shells, and second, the 3-D degenerated element is not exploited for geometrically nonlinear analysis of laminated anisotropic shells. The present study was undertaken to develop a finite-element analysis capability for the static and dynamic analysis of geometrically nonlinear theory of layered anisotropic shells. A

† A more detailed account of this paper can be found in NASA CR-168182.



PRECEDING PAGE BLANK NOT FILMED

ORIGINAL PAGE IS
OF POOR QUALITY

3-D degenerated element with total Lagrangian description is developed and used to analyze various shell problems.

## INCREMENTAL, TOTAL-LAGRANGIAN FORMULATION OF A CONTINUOUS MEDIUM

The primary objective of this section is to review the formulation of equations governing geometrically nonlinear motion of a continuous medium. In the interest of brevity only necessary equations are presented (see [1-5]).

We describe the motion of a continuous body in a Cartesian coordinate system. The simultaneous position of all material points (i.e., the configuration) of the body at time t is denoted by $C_t$, and $C_o$ and $C_{t+\delta t}$ denote the configurations at reference time t = 0 and time t + $\delta$t, respectively. In the total Lagrangian description all dependent variables are referred to the reference configuration. The coordinates of a typical point in $C_t$ is denoted by ${}^t\underset{\sim}{x} = ({}^tx_1, {}^tx_2, {}^tx_3)$. The displacement of a particle at time t is given by

$$ {}^t\underset{\sim}{u} = {}^t\underset{\sim}{x} - {}^o\underset{\sim}{x} \text{ or } {}^tu_i = {}^tx_i - {}^ox_i \tag{1} $$

The increment of displacement during time t to t + $\delta$t is defined by

$$ u_i = {}^{t+\delta t}u_i - {}^tu_i \tag{2} $$

The principle of virtual displacements can be employed to write the equilibrium equations at any fixed time t. The principle, applied to the large-displacements case, can be expressed mathematically as

$$ \int_{V_o} \rho_o \, {}^{t+\delta t}\ddot{u}_i \, \delta u_i \, dV_o + \int_{V_o} {}^{t+\delta t}S_{ij} \, \delta({}^{t+\delta t}\varepsilon_{ij}) dV_o $$
$$ = \int_{A_o} {}^{t+\delta t}T_i \, \delta u_i \, dA_o + \int_{V_o} {}^{t+\delta t}F_i \, \delta u_i \, dV_o \tag{3} $$

where summation on repeated indices is implied; $V_o$, $A_o$, and $\rho_o$ denote, respectively, a volume element, area element, and density in the initial configuration, $S_{ij}$ are the components of second the Piola-Kirchhoff stress tensor, $\varepsilon_{ij}$ the components of the Green-Lagrangian stran tensor, $T_i$ the components of boundary stresses, and $F_i$ are the components of the body force vector. The superposed dots on $u_i$ denote differentiation with respect to time, and $\delta$ denotes the variational symbol. In writing Eq. (3) it is assumed that $\varepsilon_{ij}$ is related to the displacement components by the kinematic relations

$$ {}^{t+\delta t}\varepsilon_{ij} = \frac{1}{2}({}^{t+\delta t}u_{i,j} + {}^{t+\delta t}u_{j,i} + {}^{t+\delta t}u_{m,i} \, {}^{t+\delta t}u_{m,j}) \tag{4} $$

where $u_{i,j} = \partial u_i / \partial x_j$.

ORIGINAL PAGE IS
OF POOR QUALITY

The stress components ${}^{t+\delta t}S_{ij}$ can be decomposed into two parts:

$$ {}^{t+\delta t}S_{ij} = {}^{t}S_{ij} + S_{ij} \tag{5} $$

where $S_{ij}$ is the incremental stress tensor. The incremental stress components $S_{ij}$ are related to the incremental Green-Lagrange strain components, $\varepsilon_{ij} = e_{ij} + \eta_{ij}$, by the generalized Hooke's law:

$$ S_{ij} = C_{ijkl}\varepsilon_{kl}, \tag{6} $$

where $C_{ijkl}$ are the components of the elasticity tensor. Using Eqs. (4)-(6), one can be express Eq. (3) in the alternate form

$$ \int_{V_o} \rho_o \, {}^{t+\delta t}\ddot{u}_i \delta u_i \, dV_o + \int_{V_o} C_{ijkl}(e_{kl}\delta\eta_{ij} + \eta_{kl}\delta e_{ij})dV_o $$
$$ + \int_{V_o} {}^{t}S_{ij} \, \delta e_{ij} \, dV_o = \delta W - \int_{V_o} {}^{t}S_{ij} \, \delta\eta_{ij} \, dV_o \tag{7} $$

where $\delta W$ is the virtual work due to external loads.

## FINITE-ELEMENT MODEL

The coordinates of a typical point in the element can be written as (see Fig. 1)

$$ x_i = \sum_{j=1}^{n} \phi_j(\xi_1,\xi_2) \frac{1+\zeta}{2} (x_i^j)_{top} + \sum_{j=1}^{n} \phi_j(\xi_1,\xi_2) \frac{1-\zeta}{2} (x_i^j)_{bottom} \tag{8} $$

where n is the number of nodes, $\phi_i(\xi_1,\xi_2)$ are the finite-element interpolation (or shape) functions, which, in the element take the value of unity at node i and zero at all other nodes, $\xi_1$ and $\xi_2$ are the normalized curvilinear coordinates in the middle plane of the shell, and $\zeta$ is a linear coordinate in the thickness direction and $x_1^i$, $x_2^i$, and $x_3^i$ are the global coordinates at node i.

In the present study the current coordinates ${}^{t}x_i$ are interpolated by the expression

$$ {}^{t}x_i = \sum_{j=1}^{n} \phi_j({}^{t}x_i^j + \frac{1}{2}\zeta h_j \, {}^{t}\hat{e}_{3i}^j) \tag{9} $$

and the displacements by

$$ {}^{t}u_i = \sum_{j=1}^{n} \phi_j [{}^{t}u_i^j + \frac{1}{2}\zeta h_j ({}^{t}\hat{e}_{3i}^j - {}^{0}\hat{e}_{3i}^j)] \tag{10} $$

$$ u_i = \sum_{j=1}^{n} \phi_j [u_i^j + \frac{1}{2}\zeta h_j ({}^{t+\Delta t}\hat{e}_{3i}^j - {}^{t}\hat{e}_{3i}^j)] \tag{11} $$

ORIGINAL PAGE IS
OF POOR QUALITY

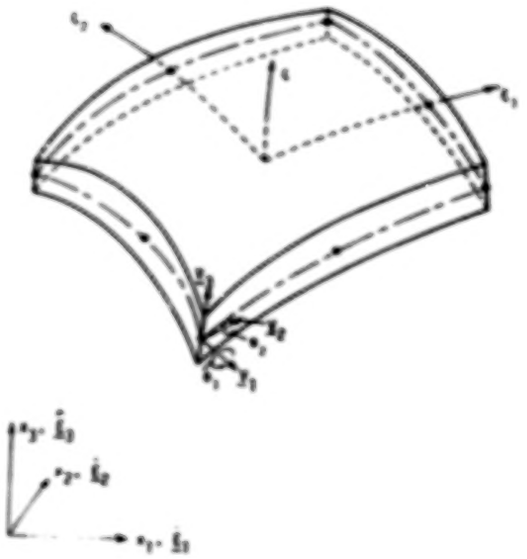

Figure 1. Geometry of the degenerated three-dimensional element

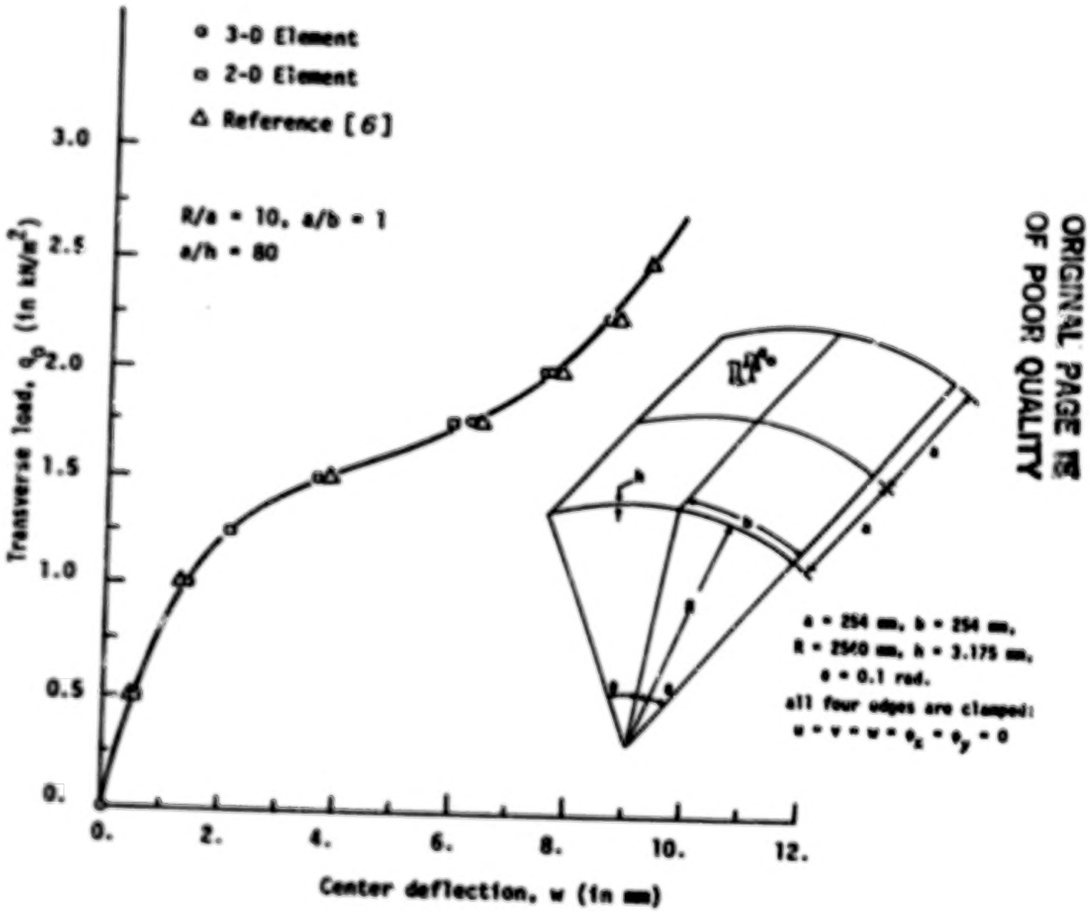


Figure 2. Load-deflection curve for a clamped cylindrical shell under uniform load

ORIGINAL PAGE IS
OF POOR QUALITY

Here ${}^t u_i^j$ and $u_i^j$ denote, respectively, the displacement and incremental displacement components in the $x_i$-direction at the j-th node.

Substitution of Eqs. (4)-(6) and (9)-(11) into Eq. (7) yields

$$\int_{V_o} \rho_o [T]^t\{\ddot{u}\} dV_o + ({}^t[K_L] + {}^t[K_{NL}])\{\Delta\} = {}^{t+\delta t}\{R\} - {}^{t+\delta t}\{F\} \tag{12}$$

where ${}^t[K_L]$, ${}^t[K_{NL}]$, $\{R\}$, and $\{F\}$ are the linear and nonlinear stiffness matrices, force vector, and unbalanced force vectors

Application of the Newmark direct integration scheme (see [2]) for the approximation of the time derivatives in Eq. (12) leads to

$$[\hat{K}]\{\Delta\} = {}^{t+\delta t}\{\hat{R}\} - {}^{t+\delta t}\{F\}^{(k-1)} \tag{13}$$

where

$$[\hat{K}] = a_o \, {}^t[M] + {}^t[K]$$

$${}^{t+\delta t}\{\hat{R}\} = {}^{t+\delta t}\{R\} + a_2 \left[{}^t\{P_1\} - \frac{1}{\delta t}({}^t\{P_2\} - {}^t\{P_3\})\right] + a_3 \{P_4\} \tag{14}$$

and $a_o$, $a_2$, etc. are the parameters in the Newmark integration scheme.

## DISCUSSION OF THE NUMERICAL RESULTS

The results to be discussed are grouped into three major categories: (1) static bending, (2) natural vibration, and (3) transient response. All results, except for the vibrations, are presented in a graphical form. All of the results presented here were obtained on an IBM 370/3081 computer with double precision arithmatic.

### Static Analysis

1. Cylindrical Shell Subjected to Radial Pressure Consider a circular cylindrical panel, clamped along all four edges and subjected to uniform radial inward pressure. The geometric and material properties are

$$R = 2540 \text{ mm}, \; a = b = 254 \text{ mm}, \; h = 3.175 \text{ mm},$$

$$\theta = 0.1 \text{ rad}, \; E = 3.10275 \text{ kN/mm}^2, \; \nu = 0.3$$

Due to the symmetry of the geometry and deformation, only one quarter of the panel is analyzed. A load step of 0.5 KN/m$^2$ was used in order to get a close representation of the deformation path. Figure 2 shows the central deflection versus the pressure for the panel dimensions a = 254 mm and b = 254 mm. The solution for agrees very closely with that obtained by Dhatt [6] and the shell element of Reddy [7].

2. Nine-Layer Cross-Ply (0°/90°/0°/...) Spherical Shell Subjected to Uniform Loading Consider a spherical shell laminated of nine layers of graphite-epoxy material ($E_1/E_2 = 40$, $G_{12}/E_2 = 0.6$, $G_{13} = G_{12} = G_{23}$, $\nu_{12} = 0.3$), subjected to uniformly distributed loading, and simply supported on all its edges (i.e., transverse deflection and tangential rotations are zero). A comparison of the load-deflection curves obtained by the present element with those obtained by Noor [8] is presented (for the parameters $h/a = 0.01$ and $R/a = 10$) in Fig. 3. The results agree very well with each other, the present 2-D results being closer to Noor's solution. This is expected because Noor's element is based on a shell theory.

3. Two-Layer Cross-Ply and Angle-Ply (45°/-45°) Shells Under Uniform Loading The geometry of the cylindrical shell used here is the same as that considered in Problem 1. The shell is assumed to be simply supported on all edges. The material properties of individual lamina are the same as those used in Problem 2. A mesh of 2x2 nine-node elements in a quarter shell is used to model the problem. The results of the analysis are presented in the form of load-deflection curves in Fig. 4. From the results, one can conclude that the angle-ply shell is more stiffer than the cross-ply shell. The geometry and boundary conditions used for the spherical shells are the same as those used in Problem 2. The geometric parameters used are: $R/a = 10$, $a/h = 100$. The load-deflection curves for the cross-ply and angle-ply shells are shown in Fig. 5. From the plots it is apparent that, for the load range considered, the angle-ply shell, being stiffer, does not exhibit much geometric nonlinearity. The load-deflection curve of the cross-ply shell exhibits varying degree of nonlinearity with the load. For load values between 100 and 150, the shell becomes relatively more flexible.

## Natural Vibration of Twisted Plates

4. Natural vibration of cantilevered twisted plates Here we discuss the results obtained for natural frequencies of various twisted plates. This analysis was motivated by their relevance to natural vibrations of turbine blades. Consider an isotropic cylindrical panel with a twist angle $\theta$ at the free end. Table 1 contains the natural frequencies of a square plate for various values of the twist angle $\theta$ and ratios of side to thickness. A 2x2 mesh and 4x4 mesh of 9-node elements are employed to study the convergence trend. The results of the refined mesh are included in the parentheses. The results agree with many others published in a recent NASA report.

## Transient Analysis

5. Spherical Cap Under Axisymmetric Pressure Loading Consider a spherical cap, clamped on the boundary and subjected to axisymmetric pressure loading, $p_o$. The geometric and material properties are

$$R = 22.27 \text{ in.}, \; h = 0.41 \text{ in.}, \; E = 10.5 \times 10^6 \text{ psi}, \; \nu = 0.3,$$

$$\rho = 0.095 \text{ lb/in}^3, \; \theta = 26.67°, \; p_o = 100 \text{ ksi}, \; \delta t = 10^{-5} \text{ sec.}$$

This problem has been analyzed by Stricklin, et al. [9] using an axisymmetric shell element. In the present study the spherical cap is discretized into five nine-node 2-D or 3-D elements. Figure 6 shows the deflection of the center as a function of time. The present solutions are in excellent agreement in most places with that of

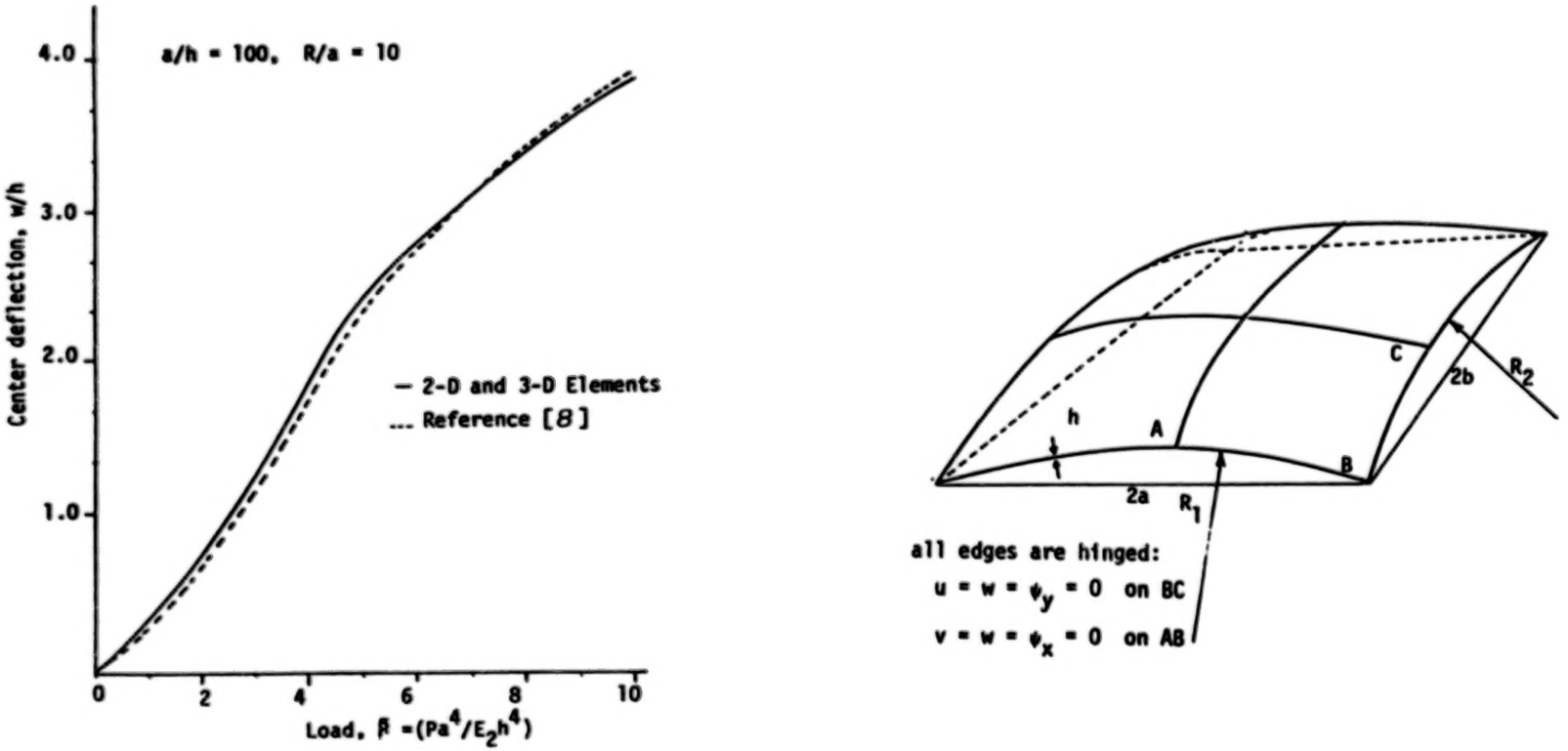


Figure 3. Center deflection versus load parameter for nine-layer cross-ply spherical shell under uniform load



ORIGINAL PAGE IS
OF POOR QUALITY

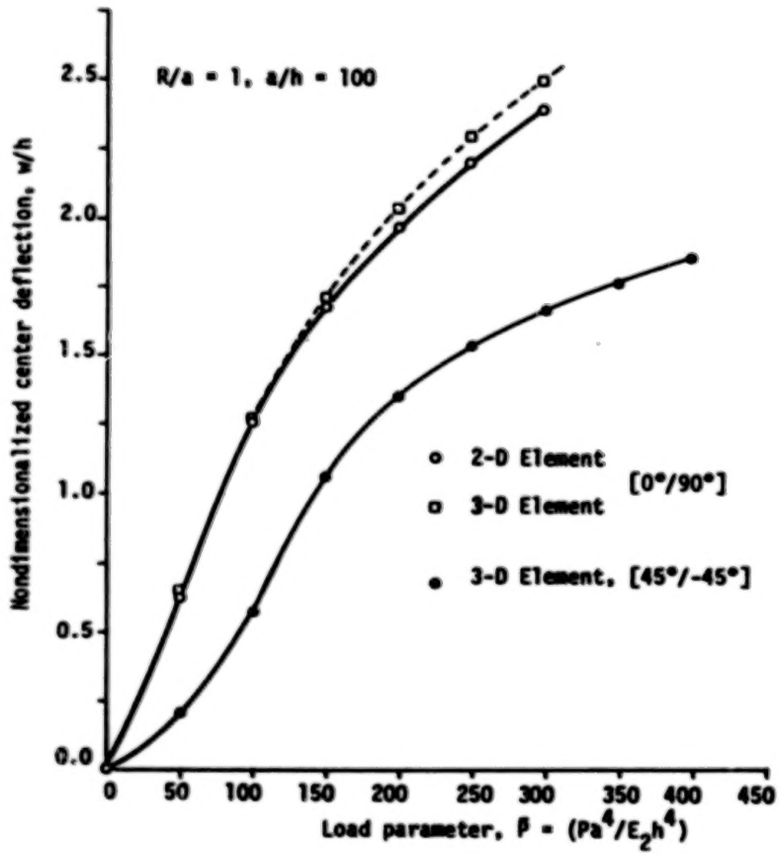


Figure 4. Center deflection versus load parameter for two-layer composite cylindrical shell

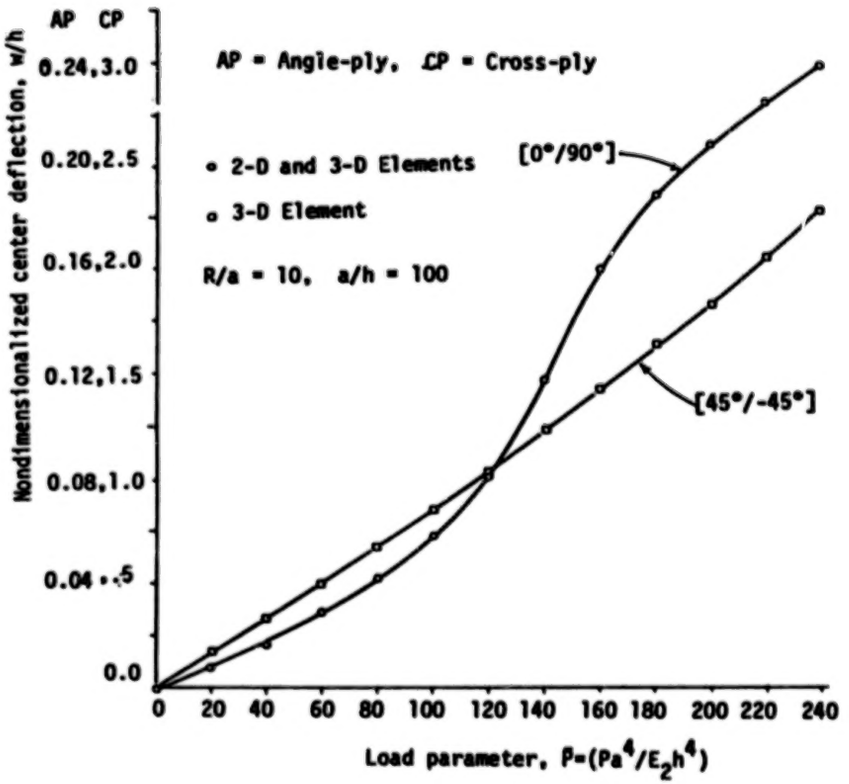


Figure 5. Center deflection versus load parameter for composite spherical shell

ORIGINAL PAGE IS
OF POOR QUALITY

Table 1 Natural Frequencies of Twisted Square Plates

$$\bar{\omega} = \omega a^2\sqrt{\rho h/D}\ , \quad D = \frac{Eh^3}{12(1-\nu^2)}\ , \quad \nu = 0.3$$

| a/h | Twist Angle | Mode 1 | 2 | 3 | 4 | 5 | 6 |
|---|---|---|---|---|---|---|---|
| 20 | 0° | * 3.4556<br>† (3.4583) | 8.4110<br>(8.3353) | 22.0999<br>(21.0238) | 28.2089<br>(26.7465) | 31.9740<br>(30.1454) | 55.1625<br>(52.0784) |
| | 15° | 3.4359 | 10.2920 | 21.5199 | 27.2054 | 32.7430 | 44.5375 |
| | 30° | 3.3790<br>(3.3694) | 13.7014<br>(14.2222) | 19.9840<br>(18.9795) | 25.0943<br>(26.8104) | 34.3341<br>(34.4591) | 45.8987<br>(45.7547) |
| | 45° | 3.2908 | 18.1009 | 15.9097 | 23.5680 | 35.5332 | 45.7013 |
| | 60° | 6.1800 | 17.8319 | 15.5635 | 24.1842 | 36.1466 | 44.9152 |
| 5 | 0° | * 3.33916<br>**(3.3390) | 7.3948<br>(7.3559) | 10.8083<br>(10.883) | 18.4930<br>(17.757) | 23.7907<br>(22.769) | 26.0552<br>(24.125) |
| | 15° | 3.31713<br>(3.3170) | 7.4816<br>(7.4504 | 10.8053<br>(10.774) | 18.4043<br>(17.771) | 23.6767<br>(22.694) | 24.9474<br>(24.083) |
| | 30° | 3.2538<br>(3.2538) | 7.7593<br>(7.7089) | 10.5248<br>(10.478) | 18.4091<br>(17.795) | 23.3734<br>(22.471) | 24.6116<br>(23.943) |
| | 45° | 3.1570<br>(3.1569) | 8.1435<br>(8.0728) | 10.1270<br>(10.062) | 18.3843<br>(17.79) | 22.9126<br>(22.117) | 24.0566<br>(23.651) |
| | 60° | 3.0370<br>(3.0366) | 8.5855<br>(8.4814) | 9.67198<br>(8.5911) | 18.3089<br>(17.730) | 22.3670<br>(21.684) | 23.3533<br>(23.160) |

* 2x2, 9-node mesh
**3x3, 9-node mesh
† 4x4, 9-node mesh

Stricklin et al [9]. The difference between the solutions is mostly in the regions of local minimum and maximum.

6. Two-Layer Cross-Ply Cylindrical Shell Under Uniform Load A cylindrical shell with a = b = 5", R = 10", h = 0.1" is simply-supported on the four edges. The deep shell is laminated by 2 layers (0°/90°) and exerted by a uniform step load $\hat{P} = (a^4 P/E_2 h^4)$ Figure 7 contains a plot of the center deflection versus time for 2-D and 3-D elements. The time step used is $\delta t = 0.1 \times 10^{-4}$ sec. The solutions obtained 2-D shell element and 3-D degenerate element are in good agreement.

7. Four-Layer Angle Ply (45°/-45°/45°/-45°) Cylindrical Shell Under Uniform Load Here we present result for a cylindrical shell which has the same geometry as in Problem 3 above. The shell is subjected to a uniform step load $\hat{P} = 50$. Figure 4.8 contains a plot of the center deflection versus time for 2-D and 3-D elements. The two elements yield solutions that agree very well in the beginning of the cycle, and the 2-D element gives negative values of the deflection at the end of the cycle. The discrepency is due to the fact that the 2-D element does not account for geometric changes from one time step to next.

8. Two-Layer Angle-Ply (45°/-45°) Spherical Shell Under Uniform Loading Consider a spherical shell with a = b = 10", R = 20" and h = 0.1", simply supported at four edges and is exerted by a uniform step load. The shell consists of two layers, (45°/-45°). Figure 9 shows the center deflection versus time for P = 50 and $\hat{P} = 500$ with time step $0.2 \times 10^{-5}$ sec. For the small load the curve is relatively smooth compared to that of the larger load. This is due to the fact that the geometric nonlinearity exhibited at $\hat{P} = 50$ is smaller compared to that at $\hat{P} = 500$.

The results of Problems 3, 4, 6, 7, and 8 should serve as references for future investigations. For additional results the reader is referred to Reference 10. This completes the discussion of the results.

## CONCLUSIONS

The present 3-D degenerated element has computational simplicity over a fully three-dimensional element and the element accounts for full geometric nonlinearities in contrast to 2-D elements based on shell theories. As demonstrated via numerical examples, the deflections obtained by the 2-D shell element deviate from those obtained by the 3-D element for deep shells. Further, the 3-D element can be used to model general shells that are not necessarily doubly-curved. For example, the vibration of twisted plates cannot be studied using the 2-D shell element discussed in [7]. Of course, the 3-D degenerated element is computationally more demanding than the 2-D shell theory element for a given problem. In summary, the present 3-D element is an efficient element for the analysis of layered composite plates and shells undergoing large displacements and transient motion.

The 3-D element presented herein can be modified to include thermal stress analysis capability and material nonlinearities. While the inclusion of thermal stresses is a simple exercise, the inclusion of nonlinear material effects is a difficult task. An acceptable material model should be a generalization of Ramberg-Osgood relation to a layered anisotropic medium. Another area that requires further

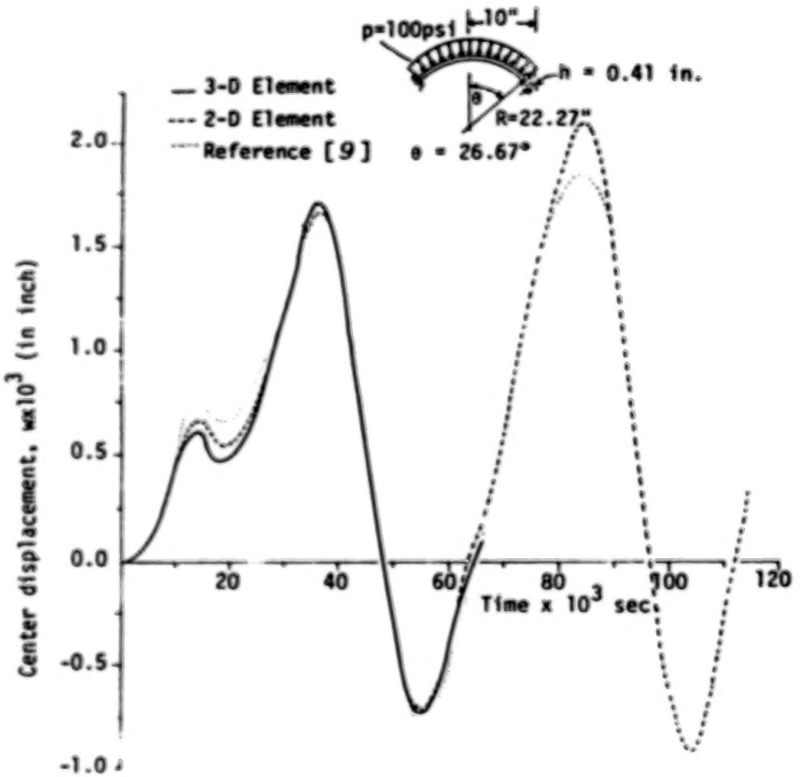


Figure 6. Center deflection versus time for a spherical cap under axisymmetric dynamic load ($p_o$ = 100 psi)

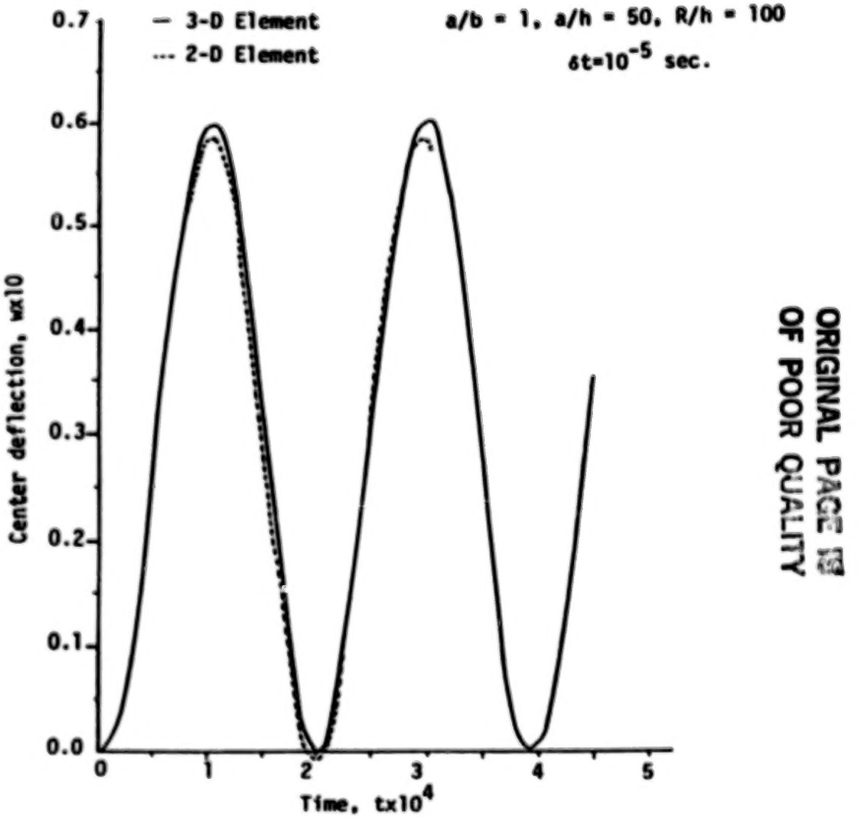


Figure 7. Center deflection versus time for a two-layer cross-ply cylindrical shell under uniform step load

ORIGINAL PAGE IS
OF POOR QUALITY

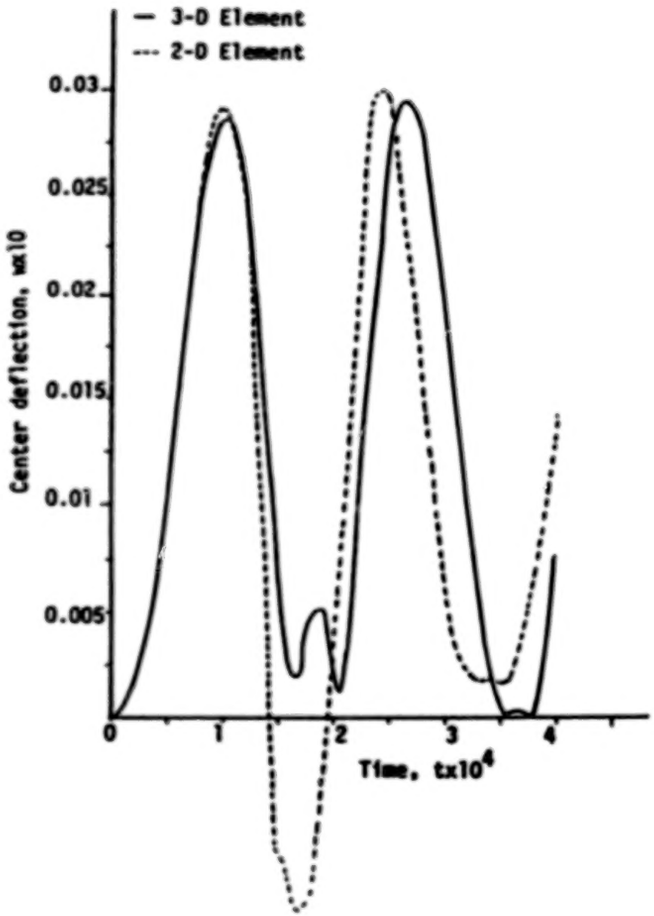


Figure 8. Center deflection versus time for four-layer angle-ply [45°/-45°/45°/-45°] cylindrical shell under uniform load

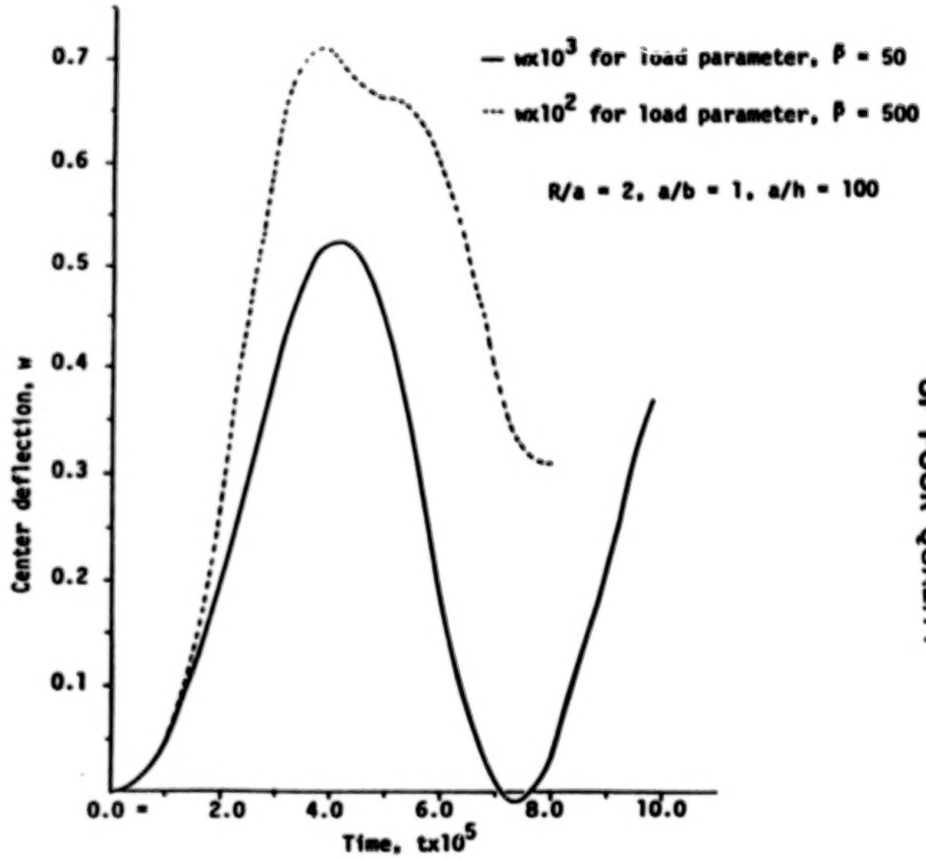


Figure 9. Center deflection versus time for two-layer angle-ply [45°/-45°] spherical shell under uniform load

ORIGINAL PAGE IS
OF POOR QUALITY

study is the inclusion of damping effects, which are more significant than the shear deformation effects.

Acknowledgments

The present study was conducted under a research grant from the Structures Research Section of NASA Lewis Research Center. The authors are very grateful for the support and encouragement by Dr. C. C. Chamis of NASA/Lewis. It is also a pleasure to acknowledge the typing of the manuscript by Mrs. Vanessa McCoy.

## REFERENCES

1. B. Krakeland, "Nonlinear Analysis of Shells Using Degenerate Isoparametric Elements," Finite Elements in Nonlinear Mechanics, International Conference on Finite Elements in Nonlinear Solid and Structural Mechanics, At Geilo, Norway, Aug. 1977, pp. 265-284.

2. K. J. Bathe, E. Ramm and E. L. Wilson, "Finite Element Formulations for Large Deformation Dynamic Analysis," International Journal for Numerical Methods in Engineering, Vol. 9, 1975, pp. 353-386.

3. G. A. Dupuris, H. D. Hibbit, S. F. McNamara and P. V. Marcal, "Nonlinear Material and Geometric Behavior of Shell Structures," Computers and Structures, Vol. 1, 1971, pp. 223-239.

4. G. Horrigmoe and P. G. Bergan, "Nonlinear Analysis of Free-Form Shells by Flat Finite Elements," Computer Methods in Applied Mechanics and Engineering, 16, 1978, pp. 11-35.

5. S. Ahmad, B. M. Irons and O. C. Zienkiewicz, "Analysis of Thick and Thin Shell Structures by Curved Finite Elements," International Journal for Numerical Methods in Engineering, 2, 1970, pp. 419-451.

6. G. S. Dhatt, "Instability of Thin Shells by the Finite Element Method," IASS Symposium for Folded Plates and Prismatic Structures, Vienna, 1970.

7. J. N. Reddy, "Bending of Laminated Anisotropic Shells by a Shear Deformable Finite Element," Fibre Science and Technology, Vol. 17, pp. 9-24, 1982.

8. A. K. Noor and S. J. Hartley, "Nonlinear Shell Analysis Via Mixed Isoparametric Elements," Computers and Structures, Vol. 7, 1977, pp. 615-626.

9. J. A. Stricklin, J. E. Martinez, J. R. Tillerson, J. H. Hong, and W. E. Haisler, "Nonlinear Dynamic Analysis of Shells of Revolution by Matrix Displacement Method," AIAA, Vol. 9, No. 4, April 1974, pp. 629-636.

10. W. C. Chao and J. N. Reddy, "Geometrically Nonlinear Analysis of Layered Composite Plates and Shells," NACA CR-168182, Virginia Polytechnic Institute,, Blacksburg, VA 24061, 1983.

N84
31692

UNCLAS

N84 31692

D4

# NONLINEAR FINITE ELEMENT ANALYSIS OF SHELLS WITH LARGE ASPECT RATIO*

T. Y. Chang and K. Sawamiphakdi
The University of Akron

## SUMMARY

A higher order 'degenerated' shell element with 9-nodes was selected for large deformation and post-buckling analysis of thick or thin shells. Elastic-plastic material properties may also be included. A description on the post-buckling analysis algorithm is given. Using a square plate, it was demonstrated that the 9-node element does not have shear locking effect even if its aspect ratio was increased to the order $10^8$. Two sample problems are given to show the analysis capability of the shell element.

## INTRODUCTION

Research work in finite element analysis applied to plates and shells has endured for more than twenty years due to the complexity of the problems involved. Continuing progress is still being made on topics relating to nonlinear shell analysis. In particular, recent interest has been focused on large deformation and post-buckling behavior of shells. Applications of such analysis problems can be found in turbine blades, nuclear vessels and offshore tubular members, etc.

Development of a finite element procedure for plate or shell analysis can be achieved by two distinct approaches: i) using classical shell theories or ii) deriving finite element equations directly from the three dimensional continuum theory. Although there are several shell theories of different approximations [1] which are useful for linear analysis, they cannot be readily extended to nonlinear cases with sufficient generality. Consequently, most of the recent nonlinear shell research was concentrated in the latter approach.

Based on the three-dimensional continuum theory, several different directions can be pursued to formulate a shell element. One approach is to deduce a shell element from a 3/D isoparametric solid by imposing necessary kinematic assumptions in connection with the small dimension of the shell thickness. Adoption of isoparametric formulation offers two immediate advantages: i) the requirement of rigid body modes is satisfied, and ii) element properties are invariant with reference coordinates. Several variations of isoparametric-base shell elements have appeared in the literature. One class of elements is the so-called 'degenerated' shell family with 4 to 16 nodes, which was originally proposed by Ahmad, Iron and Zienkiewicz [2] for linear shells. Although these elements are quite versatile for extension to nonlinear analysis, several numerical difficulties were experienced. The most notorious problem is that the lower order elements exhibit shear-locking phenomenon as the thickness of the shell becomes small (or large aspect ratio-element size vs. thickness). One way to circumvent this problem is to adopt a reduced integration tech-

*Work supported by NASA Grant NASG3-317.

 PRECEDING PAGE BLANK NOT FILMED

nique for evaluation of element stiffness. An alternate solution is to use higher order elements, such as 9- or 16-node Lagrange element.

In this paper, some of the recent nonlinear analysis results for a 9-node 'degenerated' shell element are reported. Nonlinearities considered in our work include large deformations, post-buckling behavior and elastic-plastic materials.

## DEGENERATED SHELL ELEMENT

Detailed description of this element can be found in [3,4] and therefore will not be repeated herein. We will only briefly outline this element for the sake of completeness. The geometry of the element is circumscribed by its middle surface which consists of 9-nodes as shown in Fig. 1. Each node has five degrees of freedom, three translations in the direction of global axes and two rotations about a local system. Displacement patterns in the surface of the shell are represented by quadratic polynomials. Whereas in the thickness direction, displacements are approximated by Mindlin's plate assumptions. If the center node of the element is removed, it reduces to an 8-node serendipity element. Otherwise, the element is called a 9-node Lagrange element.

## SOLUTION METHOD

The nonlinear shell equations are solved by an incremental tangent stiffness approach. For each load increment, either the full or modified Newton-Raphson algorithm can be optioned in conjunction with secant accelerated iterations. For shells exhibiting softening behavior, the modified Newton-Raphson with or without accelerated iterations was found most effective. On the other hand, for shells exhibiting stiffening effect or near instability, the full Newton-Raphson algorithm is necessary for obtaining convergent solutions. However, if one is to follow the structural response of a shell beyond its instability point (post-buckling behavior), any of the aforementioned algorithms fails to apply due to the singularity of tangent stiffness matrix. For this purpose, a different algorithm must be employed.

There are at least four different methods available for post-buckling analysis: i) Artificial spring, ii) specified displacements at nodes, iii) use of current stiffness, and iv) constrained arc length. A comprehensive review of these methods was given by Ramm [5] and Riks [6]. Of all the methods that have been applied to post-buckling analysis of shells, the constrained arc length is most effective due to its generality. Actually, in concept this method is equivalent to a displacement control analysis, in which numerical instability of a system is circumvented by specified boundary displacements.

There are several ways of defining constrained arc length [7-9,4], but the most general definition is as follows. For the i-th iteration of a load increment, we calculate an arc length ds by

$$ds^2 = \alpha \{q^{i+1}(\lambda_{i+1})\}^T \{q^{i+1}(\lambda_{i+1})\} + \beta\lambda_{i+1}^2 \{\Delta R\}^T \{\Delta R\}$$

$$= \alpha \{q^i(\lambda_i)\}^T \{q^i(\lambda_i)\} + \beta\lambda_i^2 \{\Delta R\}^T \{\Delta R\} \quad (1)$$

and ds must be kept constant, where ds is the arc length at the beginning of the load step. In Eq. (1), the following definitions are given:

$q^i$ = Incremental displacement vector from time t to t+Δt after i-th iteration.

$\lambda_i$ = A load factor after i-th iteration.

$\alpha,\beta$ = Scaling factors, $0 \leq \alpha,\beta \geq 1$.

For a given problem, the analysis will proceed incrementally with the standard load control and the determinant ratio of tangent stiffness is monitored. When the determinant ratio reaches a small value, i.e. $|\det K_T/\det K_0| \leq$ tol., the structure is considered to be near unstable. Then the analysis procedure is switched to a constrained arc length method. Thus, the post-buckling behavior of a shell structure can be traced without encountering any numerical difficulty.

## ASPECT RATIO

It is known that the use of 'degenerated' shell elements for thin plate or thin shell analysis may give unsatisfactory results due to the so-called shear locking phenomenon. This phenomenon was demonstrated for 4- and 8-node elements. One way to alleviate this problem is to use a reduced integration scheme [10,11]. However, this approach can, at best, postpone the problem and it breaks down when the shell thickness is further reduced. An alternate solution to the shear locking problem is to adopt higher order Lagrange elements with 9 or 16 nodes. From our study, we found that the 9-node element gives very satisfactory results. For discussion purpose, we define.

Aspect Ratio $R_a$ = (Largest Element Dimension)/Thickness

To determine how thin a shell can be modeled by the 9-node elements, a clamped plate subjected to uniform load was analyzed by varying the aspect ratio ranging from 10 to $10^8$. The following cases were considered:

Case 1. 8-node elements with 2 x 2 integration order
Case 2. 8-node elements with 3 x 3 integration order
Case 3. 9-node elements with 2 x 2 integration order
Case 4. 9-node elements with 3 x 3 integration order

Using symmetry condition, one quarter of the plate was sufficiently modeled by a 4 x 4 mesh. The plate was loaded well into the large deformation range and the results are compared at a load factor $(qa^4/Eh^4) = 200$. The finite element results for all four cases in conjunction with an exact solution are shown in Fig. 2. It is clearly seen that the 9-node Lagrange element does not show any shear locking up to a ridiculus value of aspect ratio $10^8$. The problem was also analyzed for a simply-supported condition and the same results were obtained.

## NUMERICAL EXAMPLES

Two sample problems are presented herein to demonstrate the analysis capability of the 9-node Lagrange element together with the post-buckling algorithm described in the previous section.

### 1. Large Deflection of an Elastic-Plastic Sandwich Cap

A sandwich spherical cap, shown in Fig. 3, was made of two identical aluminum face sheets and a honeycomb core. The face sheets were assumed to be bilinear elastic-plastic, whereas the core was elastic. The cap was subjected to pressure with two variations. i) pressure with constant direction, and ii) pressure always normal to the deformed surface (follower pressure). This problem was previously analyzed by Sharifi and Popov [12] using two-dimensional axisymmetric elements and the experimental results were obtained by Lin and Popov [13]. The pressure load was applied incrementally in fifteen steps up to 0.8 Pu, where Pu = ultimate pressure of the cap. Then the load increment was reduced in half to complete the analysis. As the pressure was approaching to the ultimate value, the load control analysis was switched to constrained displacement method. Throughout the analysis, the modified Newton-Raphson iterations with secant acceleration was exercised. It is noted that the secant acceleration for iteration is activated only if the number of iterations required is greater than two (2). On the average, 4-5 iterations per load step were used when the cap was becoming structurally unstable. For the case of constant-direction pressure, our calculated ultimate pressure was found to be 30.15 psi, which is fairly close to the buckling load 30.6 psi predicted by Plantema [14] and 29.3 psi reported in [12]. For the follower pressure, our calculated ultimate pressure is somewhat lower than the constant direction case, i.e. Pu = 27.6 psi. This value is compared favorably with the experimental results 27. psi in [13]. The plastic hinge was found at a location of 0.8 a from the center of the cap (a = half span of the spherical cap). This location is identical to that given in [12].

### 2. Post-Buckling of a Spherical Shell

A spherical shallow shell, subjected to a concentrated force at the apex and supported by fixed hinges, was considered. Two different cases of material properties were included: i) linearly elastic material, ii) elastic-perfectly plastic material. This problem was previously analyzed by Argyris et al. [15] using triangular shell elements and Parisch [16] using 4-node 'degenerated' shell elements.

In the case of elastic material, a load increment $\Delta p = 0.1$ Pu, Pu = ultimate load, was imposed to the shell. Since this structure exhibits prolonged softening behavior, the use of modified Newton-Raphson iterations gave considerable difficulty in obtaining convergent solution, the full Newton algorithm with 3-5 iterations had to be employed. When the load was increased to about 0.9 Pu, the constrained arc length method was exercised. From our analysis, the ultimate load was found to be Pu = 53.5 lb., slightly higher than the values 51.5 lb. in [16].

For elastic-plastic material, our analysis was conducted in four stages in accordance with the structural behavior:

1. Stable region with small deformation (OA in Fig. 4). In this region, nonlinearity of shell is merely caused by elastic-plastic deformation and no numerical dif-

ficulty was experienced. With the use of full-Newton-Raphson, only two iterations were needed per load step.

2. Materially unstable, pre-buckling stage (AB). The structure became mildly unstable due to the progression of plastic zone. After the plasticity had spread to some extent, internal plastic unloading was taking place as a result of geometric change of the shell surface (i.e. large deformation effect). Therefore, there was an actual stiffening phenomenon shown in Fig. 4. In this loading range, the determinant ratio of the shell stiffness was less than 0.1, and consequently convergence was difficult to obtain. Analysis was conducted by using the constrained arc length method.

3. Post-buckling stage (BC). The structure is highly unstable and the corresponding structural stiffness became negative, but still definite. The constrained arc length method together with full Newton-Raphson algorithm must be used in order to obtain convergent solution. The external load was gradually reduced until a minimum value was reached (at C). The number of iterations per load step required for this region is about 4-5. It is noted that the curvature of the shell surface, as a result of large deformation, was changed from convex to concave shape.

4. Membrane action (CD). After the shell was completely turned upside down, only membrane action was present. In this case, the structure has much greater stiffness, and hence resumed its stable condition. Correspondingly, the analysis was switched back to load control with either modified or full Newton-Raphson iterations.

The load vs deflection responses for both elastic and elastic-plastic materials are compared with those by Argyris [15] and Parisch [16]. Our results correlate quite closely with Parisch's solutions, but differ substantially with Argyris' solution, especially the post-buckling response of elastic-plastic analysis.

## CONCLUSION

Applications of a 9-node Lagrange shell element to large deformation and post-buckling analysis of elastic-plastic shells have been demonstrated in this paper. Based on our study, this element does not exhibit any shear locking effect for a square plate problem even though the aspect ratio of the element was increased to as much as $10^8$. Obviously, this value is way beyond the range of any real-world shell structures. Nevertheless, several additional topics need further attentions. Those include the study of its applications to dynamic and creep buckling analysis, more efficient ways of evaluating element stiffness to reduce computational effort. The latter point may be improved by using a symbolic mathematical manipulation package to perform close-form integrations.

## REFERENCES

1. Kraus, H.: Thin Elastic Shells, John Wiley and Sons, New York 1967.

2. Ahmad, S.; Iron, B. M.; and Zienkiewicz, O. C.: Analysis of Thick and Thin Shell Structures by Curved Finite Element. Int. J. Numer. Meths. Engrg., 2, 1970, pp. 419-451.

3. Chang, T. Y.; and Sawamiphakdi, K.: Large Deformation Analysis of Shells by Finite Element Method. Comput. & Structures, 13, 1981, pp. 331-340.

4. Chang, T. Y.; and Sawamiphakdi, K.: Large Deflection and Post-Buckling Analysis of Shell Structures. Comput. Meths. in Appl. Mech. and Engrg., 32, 1982, pp. 311-326.

5. Ramm, E.: Strategies for Tracing the Nonlinear Response Near Limit Points. In Nonlinear Finite Element Analysis in Structural Mechanics (Edited by W. Wunderlich, E. Stein and K. J. Bathe) Ruhr-Universitat Bochum, Germany, 1980, pp. 63-89.

6. Riks, E.: Some Computational Aspects of the Stability Analysis of Nonlinear Structures, presented at Fenomech '81 Conf., Institut fur Statik and Dynamik der Luft-und Raumfahrtkonstruktionen, Universitat Stuttgat, Germany, 1981.

7. Crisfield, M.A." A Fast Incremental/Iterative Solution Procedure that Handles 'Snap-Through'. Comput. & Structures, 13, 1981, pp. 55-62.

8. Riks, E.: An Incremental Approach to the Solution of Snapping and Buckling Problems, Int. J. Solids and Structures, 15, 1979, pp. 529-551.

9. Wempner, G.: Discrete Approximations Related to Nonlinear Theories of Solids. Int. J. Solids and Structures, 7, 1971, pp. 1581-1599.

10. Zienkiewicz, O.C., Taylor, R. L.; and Too, J. M.: Reduced Integration Technique in General Analysis of Plates and Shells. Int. J. Numer. Meths. Engrg., 2, 1970, pp. 419-451.

11. Hughes, T. J. R.; Cohen, M.; and Haroun, M.: Reduced and Selective Integration Techniques in the Finite Element Analysis of Plates. Nucl. Engrg. Des., 46, 1978, pp. 203-222.

12. Sharifi, P.; and Popov, E. P.: Nonlinear Finite Element Analysis of Sandwich Shells of Revolution. AIAA J., 11, 1973, pp. 715-722.

13. Lin, M. S.; and Popov, E. P.: Buckling of Spherical Sandwich Shells. Experimental Mechanics, 8, 1968, pp. 433-440.

14. Plantema, F. J.: Sandwich Construction, John Wiley and Sons, New York, 1966.

15. Argyris, J. H.; and Doltsinis, J. S.: On the Large Strain Inelastic Analysis in Natural Formulation, Part I. Quasistatic Problems. Comp. Meths. Appl. Mech. Engrg., 20, 1979, pp. 213-251.

16. Parisch, H.: Large Displacements of Shells Including Material Nonlinearities. Comp. Meths. Appl. Mech. Engrg., 27, 1981, pp. 183-214.

ORIGINAL PAGE IS
OF POOR QUALITY

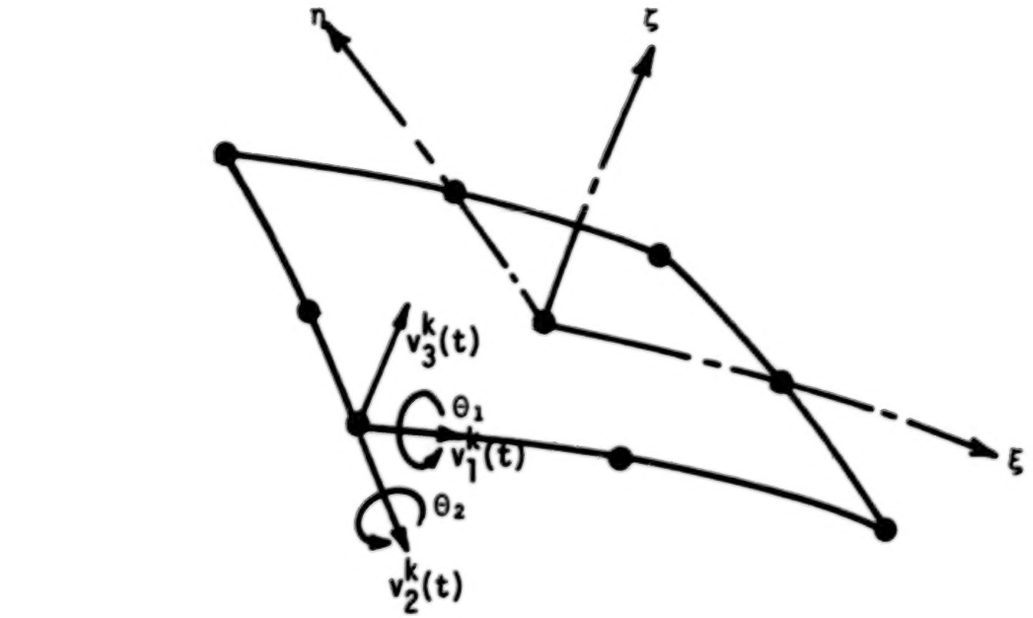


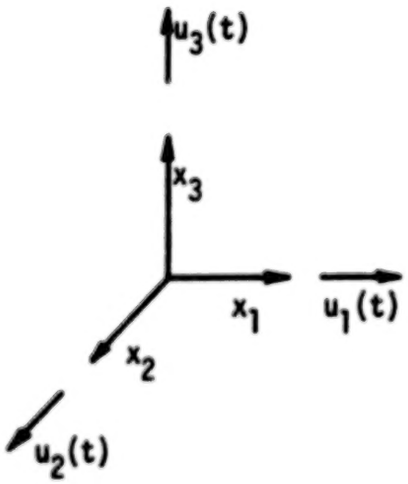


Fig. 1 A 9-Node Shell Element

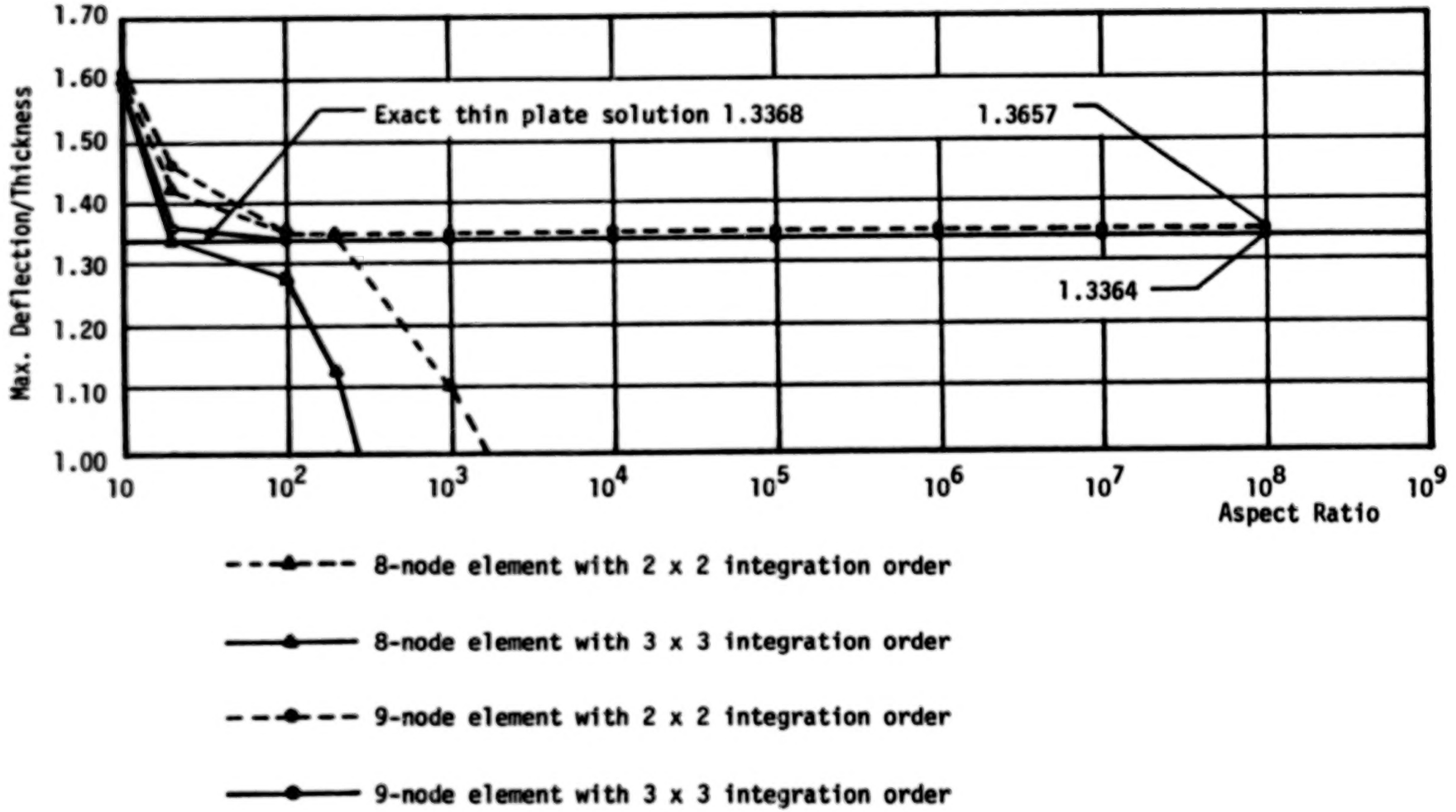


Fig. 2 Max. Deflection of a Square Plate vs. Different Aspect Ratios

ORIGINAL PAGE IS
OF POOR QUALITY

ORIGINAL PAGE IS
OF POOR QUALITY

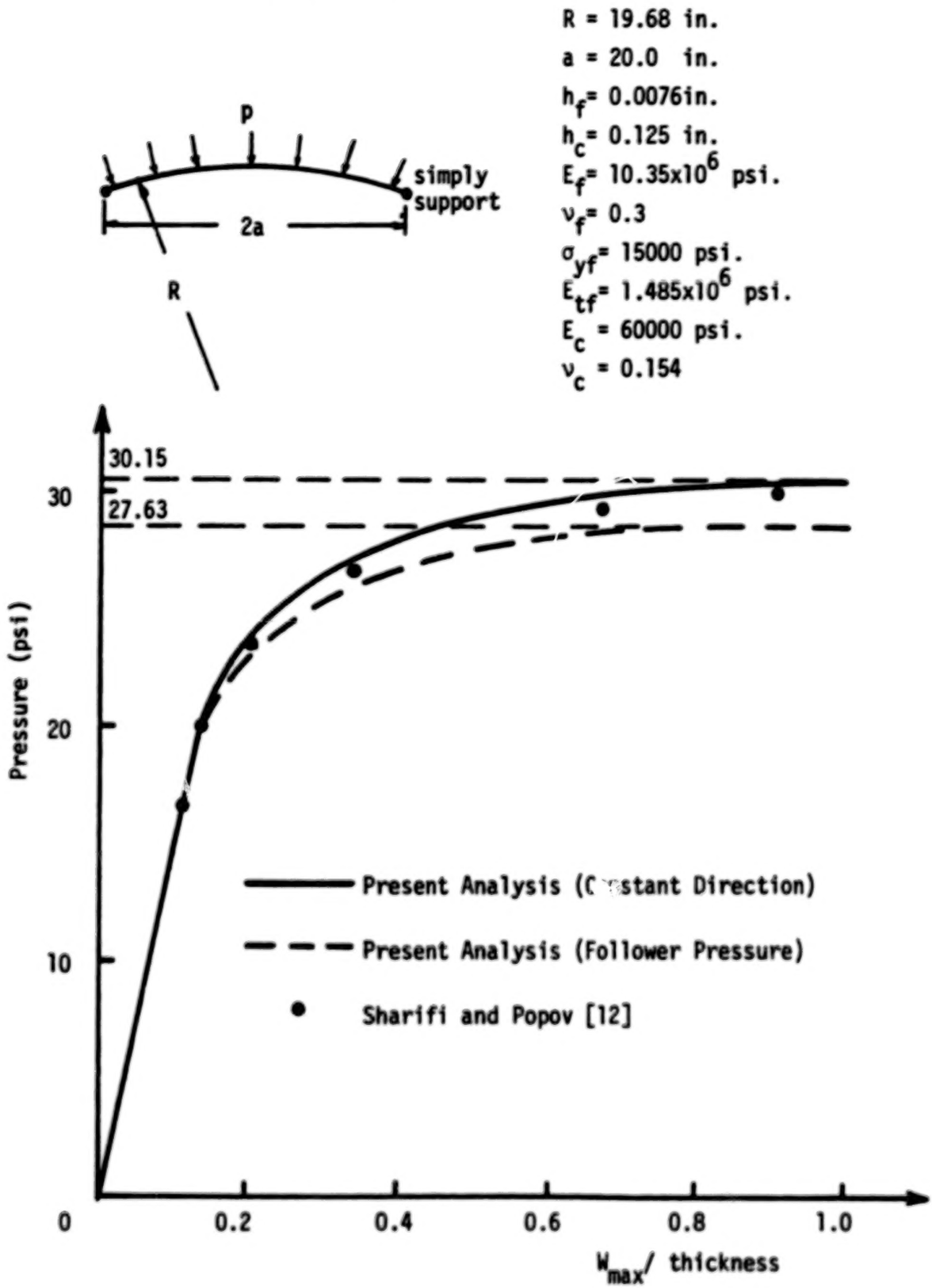


Fig. 3 Load-Deflection Response of an Elastic-Plastic Sandwich Spherical Cap

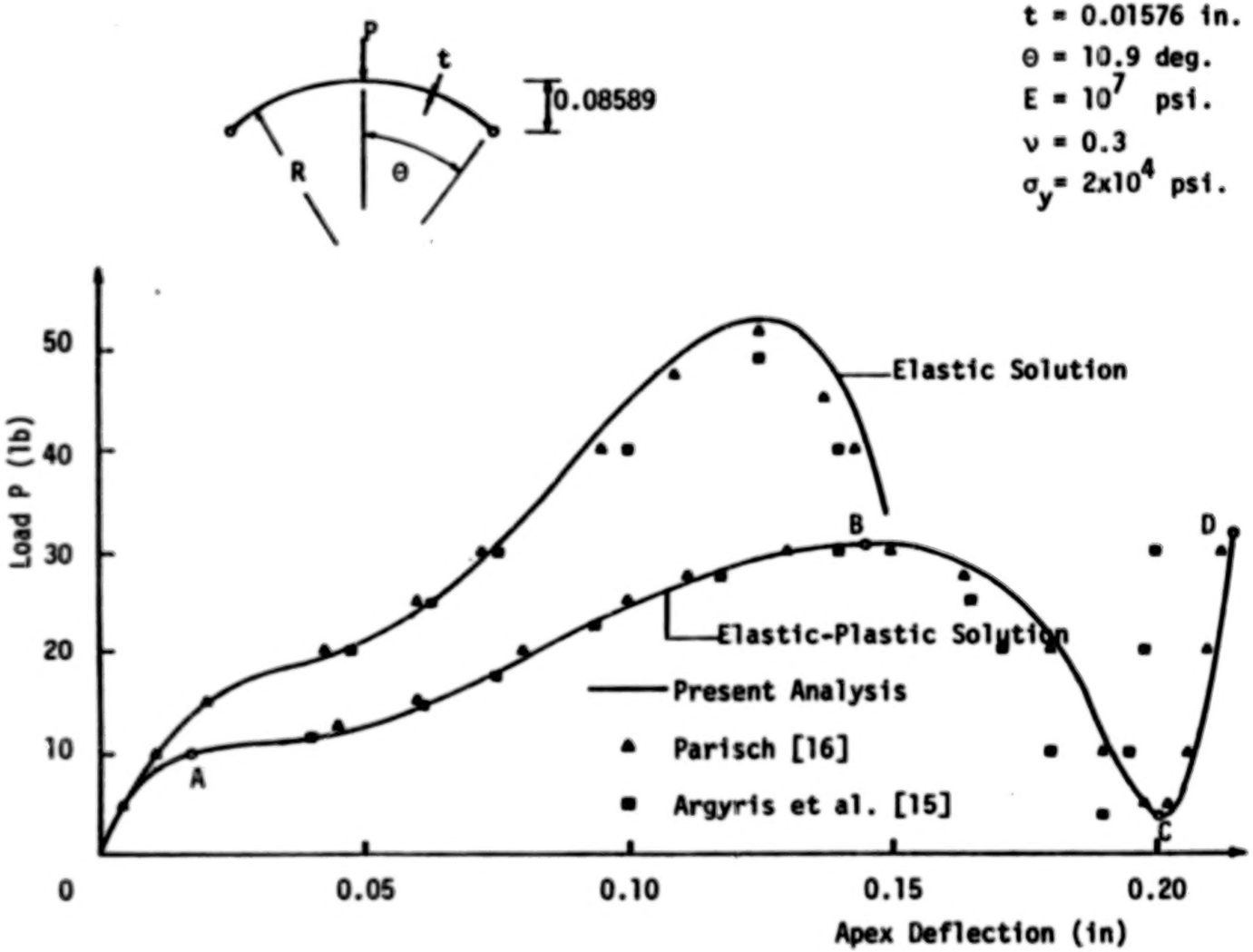


Fig. 4 Post-buckling Behavior of A Spherical Cap



ORIGINAL PAGE IS
OF POOR QUALITY

N84
31693

UNCLAS

N84 31693

D5

# SELF-ADAPTIVE SOLUTION STRATEGIES*

Joseph Padovan
University of Akron
Akron, Ohio 44325

## ABSTRACT

The paper briefly overviews progress on the development of enhancements to current generation nonlinear finite element algorithms of the incremental Newton-Raphson type. The main thrust of the work is to introduce work on new alternative formulations which lead to improved algorithms which avoid the need for global level updating and inversion. To quantify the enhanced Newton-Raphson scheme and the new alternative algorithm, the results of several benchmarks will be presented.

## INTRODUCTION

The main thrust of this work is to overview progress on the development and modification of algorithms which improve the efficiency and stability of solutions to nonlinear finite element (FE) simulations (ref. 1). The emphasis will be threefold namely, 1) To review briefly progress on the development of enhancements to current generation algorithms of the incremental Newton-Raphson (INR) type; 2) To introduce progress on the development of new alternative algorithmic schemes and; 3) To present the results of several benchmark problems.

## OVERVIEW OF PROGRESS ON ENHANCED INR TYPE ALGORITHMS

While numerous algorithms can be employed to solve the nonlinear algebraic equations arising from FE formulations, the most popular scheme is the NR type. This follows from the fact that it can handle kinematic and material nonlinearity say as in elastic-plastic-creep behavior. Regardless of its adaptability, the straight or modified INR suffer from several drawbacks namely:

1. Cannot handle turning points;
2. No direct control on successive iterates;
3. Difficult to ascertain zones of convergence as solution proceeds;
4. Requires global level updating and assembly;
5. Global level inversion/pseudo updating required;
6. Out of core blocking of solution awkward;
7. Control of individual degree of freedom excursions difficult;
8. Successive iterations occur on a global level hence control of individual degrees of freedom difficult.

To circumvent the more difficult of the foregoing shortcomings, constraint bounds were employed to:

*Supported by NASA Lewis Under Grant NAG3-54

1. Handle turning points;
2. Control successive iterates;
3. Introduce self-adaptive aspects to algorithm;
4. Expand regions of stable convergence properties and;
5. Facilitate evaluation of zones of convergence as solution proceeds.

In order to facilitate such properties the INR can be reinterpreted as the intersection of a tangent extrapolation of the solution curve and a constraint surface. For procedures such as the standard NR and those advocated by Wempner (ref. 2) and Riks (ref. 3), the constraint surfaces are open hence leading to potential nonintersection. In contrast, the use of closed constraint surfaces generally guarantees the intersection with the solution curve. While the circular constraint of Crisfield (ref. 4) satisfies the closedness criterion, it requires the use of limited step size increments. This follows from the manner in which the deflection and force excursions are interrelated in normed constraint space. In contrast, the elliptic and hyperbolic constraints developed by Padovan and Tovichakchaikul (refs. 5-7) provide for more flexible control of successive excursions.

The formal convergence properties of the constrained methology developed by Padovan and Tovichakchaikul has been considered in a very recent series of papers (refs. 8-10). This work illustrates various aspects of the formal properties of constrained INR schemes namely (refs. 8-10):

i) The existence of global sized safety zones wherein convergence can be guaranteed;

ii) The use of the various properties of the safety zones to establish self-adaptive attributes;

iii) The existence of quadratic-superlinear convergence rates.

Based on this work, the elliptically and hyperbolically constrained INR algorithm have been applied to a wide variety of benchmark problems. Specifically,

i) Elastic pre-postbuckling behavior of numerous structural configurations (ref. 5);

ii) Elastic-plastic-creep problems including kinematic nonlinearity and potential pre-postbuckling (ref. 5-7);

iii) Nonlinear heat conduction (ref.11,12) and;

iv) Rolling contact problems (ref. 13).

The results of this work (ref. 5-13) clearly illustrate the enhanced operating characteristics of constrained type INR schemes. In particular, the scheme:

1. Is inherently stable;
2. Yields significantly improved operating efficiency;
3. Can be applied to a wide variety of problem types;
4. Is completely compatible with current architectures of general purpose (GP) codes;
5. Handles turning points;

6. Controls successive iterates;
7. Introduces self-adaptive aspects to INR type algorithms;
8. Greatly expands regions of stable convergence, and;
9. Facilitates evaluation of zones of convergence as solution proceeds.

## ALTERNATIVE FORMULATIONS

The constrained INR approach greatly extends the capabilities to solve nonlinear problems. Regardless of this, the NR root of such a formulation still introduces difficulties namely

a) Global updating and assembly;
b) Global level inversion or pseudo-updating;
c) Awkward blocking and I/O for out of core problems;
d) Control of individual degree of freedom excursions is difficult; and
e) Iteration occurs on a global level hence contributing to difficulty of controlling individual degrees.

In the context of the foregoing, an alternative formulation will be sought. The main motivations of this work are

1. Solution scheme should have hierarchial application levels (degree of freedom, nodal, elemental, material group, substructural, global);
2. Bypass need of global level inversion;
3. Bypass need of global level updating;
4. Develop algorithmic structure enabling simplified I/O data flow for out of core problems;
5. Possess self adaptive attributes enabling hierarchial control (locally, globally) and;
6. Provide continuous hierarchial updating.

To establish an algorithm which satisfies the preceding requirements, an alternative starting point will be employed. Note, the Galerkin's and virtual work formulations typically yield algorithms requiring matrix inversion. The use of energy type formulations presents difficulties due to it's implicit form and can fluctuate in definiteness during anomalous iterative processes. In contrast, Rayleigh Ritz type expressions are positive definite, explicit in form and yield derivatives with a simplified structure.

Based on the standard virtual work principle, the governing FE field equations associated with large deformation (small strain large rotation) theory take the form (ref. 1).

$$\underset{\sim}{R}(\underset{\sim}{Y}) = \int_{V_0} [B^*(\underset{\sim}{Y})]^T \underset{\sim}{S}(\underset{\sim}{Y})\, dv = \underset{\sim}{F} \qquad (1)$$

where $\underset{\sim}{F}$ is the external load, $\underset{\sim}{S}$ the 2nd Piola-Kirchhoff stress tensor, and $\underset{\sim}{Y}$ the nodal deflections. Employing (1), the standard Rayleigh-Ritz (least square) expression takes the following form

$$E(\underset{\sim}{Y}) = \| \underset{\sim}{R}(\underset{\sim}{Y}) - \underset{\sim}{F} \|^2 \tag{2}$$

where $\|( )\|$ defines the usual Euclidean norm. To approximate (2), we can employ Taylor series. Furthermore, since (2) is positive definite, it has essentially quadratic properties about the minimizing solution $\underset{\sim}{Y}_M$. In this context we can recast (2) as (ref. 14)

i) Taylor approximation;

$$E^{I}(\underset{\sim}{Y}) = \| \underset{\sim}{R}(\underset{\sim}{Y}_M) - \underset{\sim}{F} + [K_T(\underset{\sim}{Y}_M)](\underset{\sim}{Y} - \underset{\sim}{Y}_M) \|^2 \tag{3}$$

ii) Quadratic approximation;

$$E^{II}(\underset{\sim}{Y}) = \gamma_M + (\underset{\sim}{Y} - \underset{\sim}{Y}_M)^T [\Gamma_M]^{-1} (\underset{\sim}{Y} - \underset{\sim}{Y}_M) \tag{4}$$

such that $\gamma_M$ defines the minimum value of $E(\underset{\sim}{Y})$ and $[K_T(\underset{\sim}{Y}_M)]$ is the tangent stiffness.

To establish a hierarchial algorithm wherein degree of freedom level updating is employed, $E^{I}(\underset{\sim}{Y})$ the quadratic approximation is recast in the form

$$E^{\theta I}_{i+1}(\underset{\sim}{Y}) =$$

$$(R_i(\underset{\sim}{Y}_i) - F_i + (\underset{\sim}{Y} - \underset{\sim}{Y}_i)^T \underset{\sim}{K}_{Ti}(\underset{\sim}{Y}_i))^2 + \theta_i E^{II}_i(\underset{\sim}{Y}) \tag{5}$$

where

$$E^{II}_i(\underset{\sim}{Y}) = \gamma_i + (\underset{\sim}{Y} - \underset{\sim}{Y}_i)^T [\Gamma_i]^{-1} (\underset{\sim}{Y} - \underset{\sim}{Y}_i) \tag{6}$$

such that $\underset{\sim}{K}_{Ti}$ is the $(i)^{th}$ column of $[K_T]$ and $\theta_i$ is a scaling factor which controls the amount of history of the $(i)^{th}$ degree of freedom admitted per any iteration.

Employing (5), the localized degree of freedom level algorithm is obtained by requiring that the Taylor and quadratic approximation satisfy higher order continuity requirements namely

$$E^{\theta I}_{i+1}(\underset{\sim}{Y}_i) = E^{II}_{i+1}(\underset{\sim}{Y}_i) \tag{7}$$

$$\frac{d}{d\underset{\sim}{Y}}(E^{\theta I}_{i+1}(\underset{\sim}{Y}_i)) = \frac{d}{d\underset{\sim}{Y}}(E^{II}_{i+1}(\underset{\sim}{Y}_i)) \tag{8}$$

$$\frac{d^2}{d\underset{\sim}{Y}^2}(E^{\theta I}_{i+1}(\underset{\sim}{Y}_i)) = \frac{d^2}{d\underset{\sim}{Y}^2}(E^{II}_{i+1}(\underset{\sim}{Y}_i)) \tag{9}$$

After extensive manipulations (7-9) yield the following expressions, that is

ORIGINAL PAGE IS
OF POOR QUALITY

$$\underset{\sim}{Y}_{i+1} = \underset{\sim}{Y}_i - \Psi_i \, (R_i(\underset{\sim}{Y}_i) - F_i)[\Gamma_i] \, \underset{\sim}{K}_{Ti} \tag{10}$$

$$[\Gamma_{i+1}] = \frac{1}{\theta} \left([\Gamma_i] - \Psi_i [\Gamma_i] (\underset{\sim}{K}_{Ti})^T \, (\underset{\sim}{K}_{Ti}) [\Gamma_i]^T \right) \tag{11}$$

where $\Psi_i$ is a scaling parameter controlling the modification of $[\Gamma_i]$.

The efficient architecture of (10 and 11) follows directly from the fact that partitioned matrix multiplication is employed to effect all necessary updating and iterating. For example, noting (10) it follows that only a narrow band of $[\Gamma_i]$ and $\underset{\sim}{K}_{Ti}$ is employed to update $\underset{\sim}{Y}_{i+1}$. Specifically

$[\Gamma_i] \, \underset{\sim}{K}_{Ti} =$

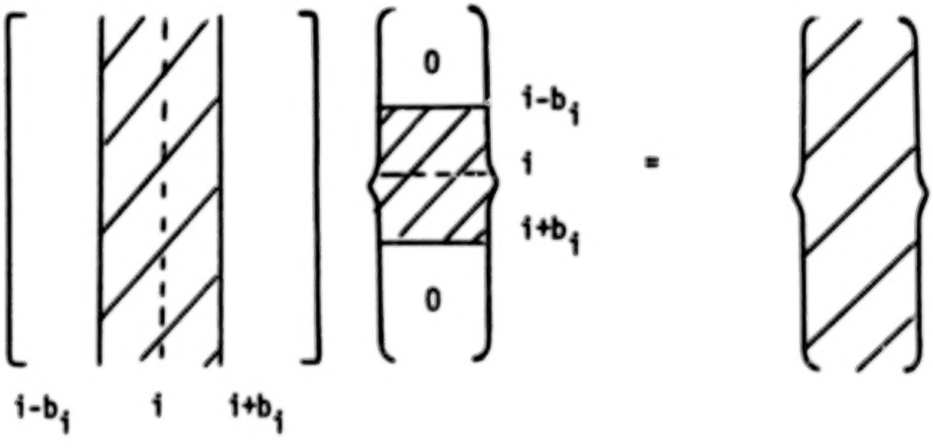


(12)

Similarly noting (11) we see that

$(\underset{\sim}{K}_{Ti})^T \, (\underset{\sim}{K}_{Ti}) =$

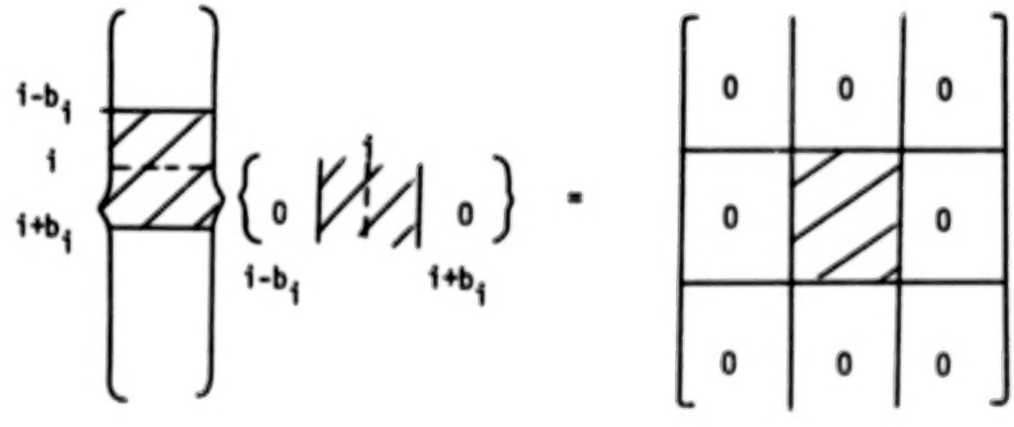


(13)

## BENCHMARKING

To benchmark the new algorithm, two highly nonlinear problems have been chosen to ascertain the operating characteristics. Figure 1 illustrates the geometry of a centrally loaded spherical cap modelled with 8 node quadralateral isoparametric axisymmetric elements. Figure 1 also illustrates the load deflection behavior solved via both the standard INR and (10,11). As can be seen, while the standard INR required 70 load increments and a total of some 233 iterations, (10,11) achieved a converged solution in one load increment involving 7 total cycles through all the degrees of freedom.

As a further demonstration of the use of (10,11), we consider the centrally loaded box truss structure given in Figure 2. This structure exhibits pre-postbuckling behavior. By imposing linear constraints on the choice of $\underline{F}$, the entire pre-postbuckling behavior is traced. This example illustrates the ability of (10,11) to handle both pre-postbuckling situations wherein transitions in definiteness are encountered.

## CONCLUSIONS AND FUTURE OBJECTIVES: ALTERNATIVE FORMULATION

Based on the foregoing development and benchmarking it follows that the alternative formulation defined by (10 and 11) is:

1. Stable;
2. Significantly improves solution efficiency (problem dependent);
3. Provides for hierarchial application levels;
4. Eliminates need of inverse;
5. Architecture of data flow stream-lined;
6. Can handle problems with turning points (through use of constraints); and;
7. Can handle general material properties.

The future objectives of work on the alternative algorithm will be severalfold namely:

1. Benchmark algorithm extensively;
2. Investigate such items as;
   - i) Hierarchial application levels;
   - ii) Use of localized/globalized constraints to enhance solution efficiency;
   - iii) Consider use with history dependent media and;
3. Establish convergence, stability characteristics on formal basis.

## ACKNOWLEDGMENT

The author is grateful to Dr. Chamis of NASA Lewis for the stimulation and encouragement.

## REFERENCES


1. Zienkiewicz, O.C., The Finite Element Method, McGraw-Hill, New York, 1977.
2. Wempner, G., Int. J. Solids Structure, 7, 1581, 1971.
3. Riks, E., Int. J. Solids Structure, 15, 529, 1979.
4. Crisfield, M.A., Computer Structures, 13, 55, 1981.
5. Padovan, J., and Tovichakchaikul, S., Computer Structures, 15, 365, 1982.
6. Padovan, J., and Tovichakchaikul, S. Computer Structures, 15, 379, 1982.
7. Padovan, J. and Tovichakchaikul, Computer Structures, 16, 199, 1983.
8. Padovan, J. and Arechaga, T., Int. J. Engineering Sci., 20, 1077, 1982.
9. Padovan, J. and Arechaga, T., J. Frank. Inst. 314, 143, 1982.
10. Padovan, J., Tovichakchaikul, S. and Arechaga, T., Jr. Frank. Inst. (in press).
11. Padovan, J., and Tovichakchaikul, S., Numerical Heat Transf. 5, 253, 1982.
12. Padovan, J., and Tovichakchaikul, S., AIAA Jr., (in press).
13. Padovan, J., and Tovichakchaikul, S., Computer Structures (in press).
14. Davidon, W.C., J. Optm. Theory Appl., 18, 187, 1976.

ORIGINAL PAGE IS
OF POOR QUALITY

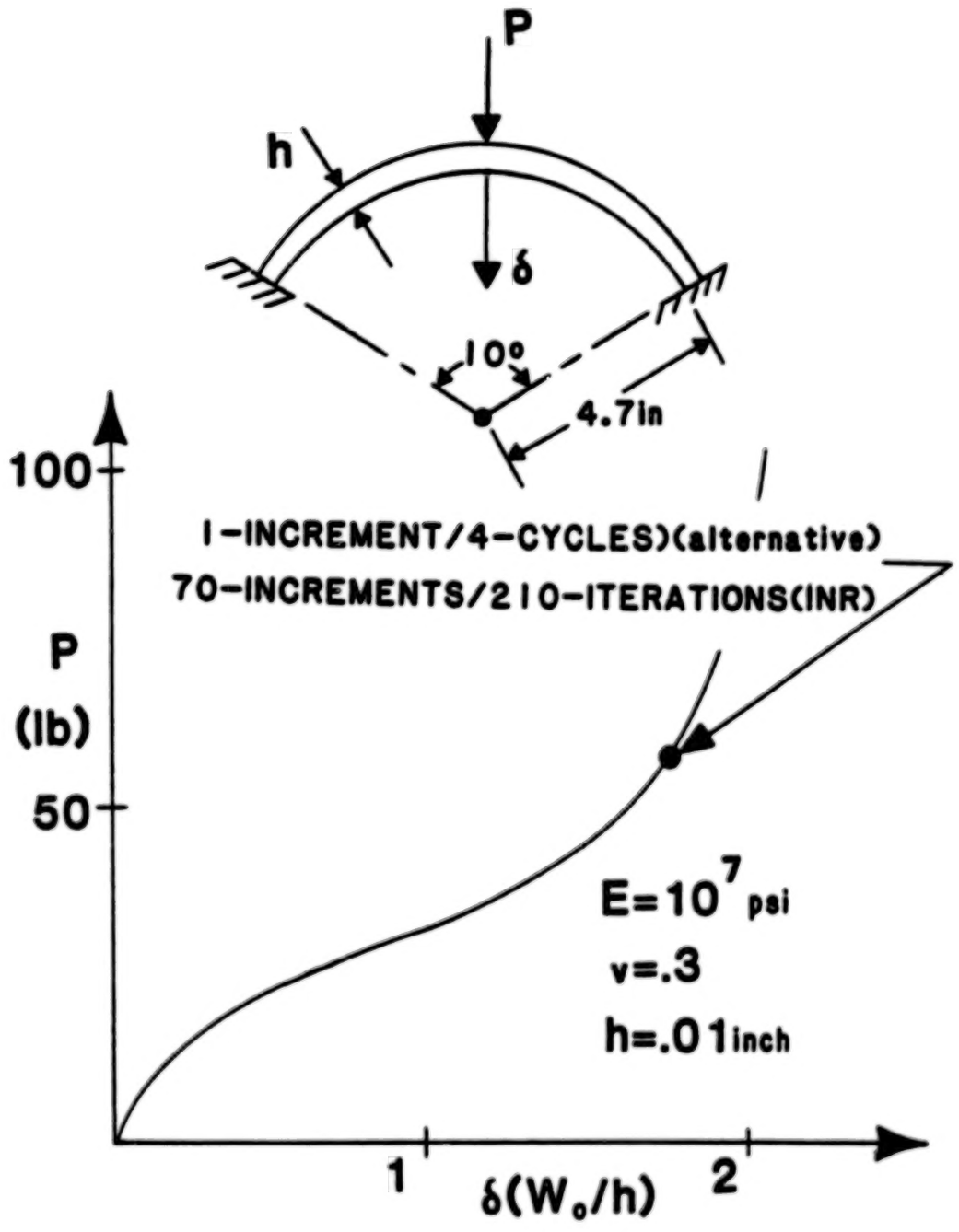


**FIG. 1** Load Deflection Characteristics of Spherical Cap

ORIGINAL PAGE IS
OF POOR QUALITY

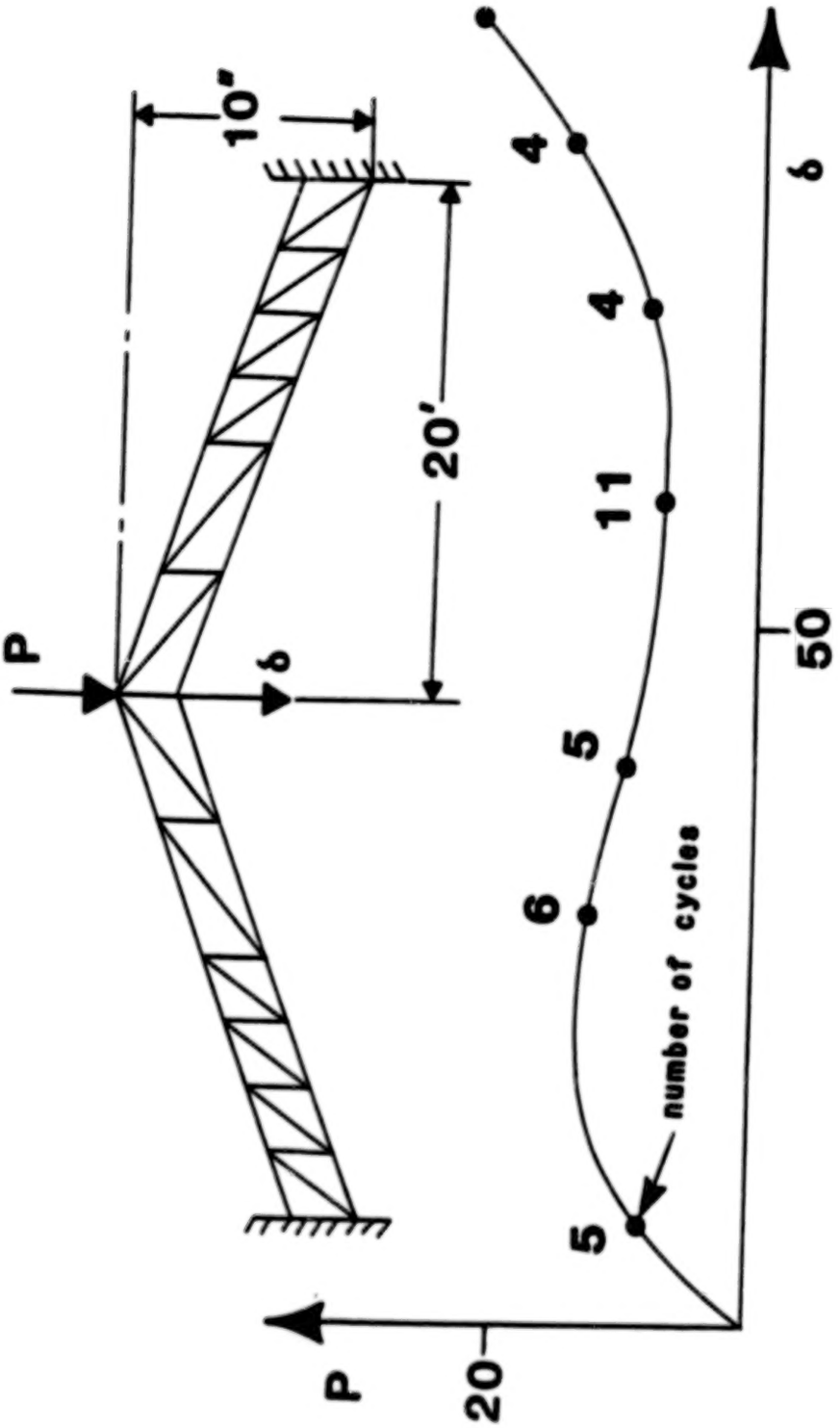


FIG. 2 Load Deflection Characteristics of Box Truss Structure

N84
31694

UNCLAS

N84 31694

# ELEMENT-BY-ELEMENT SOLUTION PROCEDURES FOR NONLINEAR STRUCTURAL ANALYSIS*

Thomas J.R. Hughes, James Winget and Itzhak Levit
Stanford University

## SUMMARY

Element-by-element approximate factorization procedures are proposed for solving the large finite element equation systems which arise in nonlinear structural mechanics. Architectural and data base advantages of the present algorithms over traditional direct elimination schemes are noted. Results of calculations suggest considerable potential for the methods described.

## INTRODUCTION

Despite the attainment of significant increases in computer storage and speed in recent years, many contemporary problems of engineering interest are simply too complex to be solved with existing numerical algorithms and presently-available hardware. In this paper we address the subject of solving the matrix equations arising from finite element spatial discretizations. In Appendix I a brief sketch is given of how finite element equation systems emanate from various classes of structural mechanics problems. The matrix equations, though sparsely populated, still entail enormous storage demands, especially in three-dimensional cases. This is the major drawback to matrix-based ("implicit") finite element procedures. The types of methods we have developed to deal with this circumvent the need to form and factorize large global arrays. These methods have their origins in procedures which pervade the numerical analysis literature. Basically, the idea is to replace a large, complicated array by a product of simpler arrays. The original concepts apparently emanate from the so-called "alternating direction (ADI) methods" (ref's. 6, 7, 10, 35). There is a large Russian literature on methods of this type which is summarized in the books of Marchuk and Yanenko (ref's. 31 and 38, resp.). In these works the terminologies used are the "method of fractional steps", the "splitting-up method", and the "method of weak approximation". In the field of computational aerodynamics these techniques are often described as "approximate factorization" methods (see e.g. Warming and Beam, ref. 37). The preceding references deal primarily with finite difference methods in which the splitting is usually performed by decomposing a multi-dimensional partial differential operator into one-dimensional operators. This, of course, places geometrical and topological limitations on the discretizations. Generally these methods are used most effectively in the context of rectangular domains, or domains which are at least topologically equivalent to rectangles. When circumstances like this prevail, very large problems can be efficiently solved. Progress has been made in developing analogous finite element

*Work performed under Grant No. NAG 3-319

 PRECEDING PAGE BLANK NOT FILMED

procedures (see ref's. 1, 5, 8, 9, 12-15). However, these procedures do not retain the full geometric and topological versatility of finite element discretizations.

The methods advocated herein derive many features from the preceding references. The approximate factorization aspect of the present approach is facilitated by what we feel are the most simple and natural constituents of the finite element process--the individual element arrays. No more than one element array needs to be formed and stored at one time and calculations proceed in an element-by-element (EBE) fashion. There is no geometric or topological restriction imposed by the method, and at the same time a remarkably concise computational architecture is achieved. It is pointed out herein that the present approach has significant advantages when implicit-explicit finite element mesh partitions are employed, and, what appears to be most significant for the future, the method is amenable to parallel calculations on multi-processor computers.

The idea of element-by-element factorizations was first proposed in Hughes, Levit and Winget (ref. 22) in which a transient algorithm for heat conduction was developed. Based upon this work, Ortiz, Pinsky and Taylor (ref. 34) constructed a novel time-stepping scheme for dynamics. However, our research revealed stringent accuracy requirements in certain circumstances, and we were led to reformulate the procedure as an iterative linear equation solver (see Hughes, Levit and Winget, ref. 23). In this way the usual accuracy and stability properties of standard finite element algorithms is attained. The problems that we have applied these procedures to are all time dependent and mostly nonlinear. Nour-Omid and Parlett (ref. 33) have applied similar procedures to static structures problems and also report encouraging results.

## ITERATIVE ALGORITHMS

A variety of algorithms may be employed in conjunction with approximately-factorized arrays. The following has been used in the numerical work presented herein.

### Parabolic Regularization

The derivation of this algorithm is based upon replacing the algebraic problem

$$\underset{\sim}{A}\,\underset{\sim}{x} = \underset{\sim}{b}$$

by a first-order ordinary differential equation whose asymptotic solution is $\underset{\sim}{x}$. The terminology "parabolic regularization" is used since the algebraic problem is replaced by what amounts to a spatially-discrete parabolic problem. The ordinary differential equation is discretized by backward differences and the implicit operator is approximately factorized. Quasi-Newton updates and line searches are employed to accelerate convergence. The flowchart summarizes the procedure for symmetric positive-definite arrays. Further details may be found in reference 23.

ORIGINAL PAGE IS
OF POOR QUALITY

**Flowchart of the parabolic regularization (PR) algorithm with line search and BFGS updates**

**Step 1.** Initialization:

$$m = 0 \quad , \quad \underset{\sim}{x}_0 = \underset{\sim}{0} \quad , \quad \underset{\sim}{r}_0 = \underset{\sim}{b}$$

$$\underset{\sim}{f}_k = \underset{\sim}{g}_k = \underset{\sim}{0} \quad \text{(loop: } k = 1 \text{ , } 2 \text{ ,..., } n_{BFGS})$$

$$\Delta\underset{\sim}{x} = \underset{\sim}{B}^{-1} \underset{\sim}{r}_0$$

**Step 2.** Line search:

$$s = \Delta\underset{\sim}{x}^T \underset{\sim}{r}_m / \Delta\underset{\sim}{x}^T \underset{\sim}{A} \Delta\underset{\sim}{x}$$

$$\underset{\sim}{x}_{m+1} = \underset{\sim}{x}_m + s \, \Delta\underset{\sim}{x}$$

**Step 3.** Convergence check:

$$||\underset{\sim}{r}_{m+1}|| < \delta$$

Yes: Return

No : Continue

**Step 4.** Relabel old BFGS vectors:

$$\underset{\sim}{f}_{k-1} = \underset{\sim}{f}_k \quad , \quad \underset{\sim}{g}_{k-1} = \underset{\sim}{g}_k \quad , \quad \text{(loop: } k = 2 \text{ , } 3 \text{ ,..., } n_{BFGS})$$

**Step 5.** Calculate new BFGS vectors:

$$\underset{\sim}{f}_{n_{BFGS}} = (\Delta\underset{\sim}{x}^T \underset{\sim}{r}_m)^{-1} \Delta\underset{\sim}{x}$$

$$\underset{\sim}{g}_{n_{BFGS}} = \underset{\sim}{r}_{m+1} - (1 - s^{\frac{1}{2}})\underset{\sim}{r}_m$$

**Step 6.** New search direction:

$$\underset{\sim}{z} = \underset{\sim}{r}_{m+1}$$

$$\underset{\sim}{z} \leftarrow \underset{\sim}{z} + (\underset{\sim}{f}_k^T \underset{\sim}{z})\underset{\sim}{g}_k \quad \text{(loop: } k = n_{BFGS} \text{ , } n_{BFGS} - 1 \text{ ,..., } 1)$$

$$\underset{\sim}{z} \leftarrow \underset{\sim}{B}^{-1} \underset{\sim}{z}$$

$$\underset{\sim}{z} \leftarrow \underset{\sim}{z} + (\underset{\sim}{g}_k^T \underset{\sim}{z})\underset{\sim}{f}_k \quad \text{(loop: } k = 1 \text{ , } 2 \text{ ,..., } n_{BFGS})$$

$$\Delta\underset{\sim}{x} = \underset{\sim}{z}$$

**Step 7.** $m \leftarrow m + 1$ , go to Step 2.

The notation in the flowchart is given as follows: $m$ is the iteration counter; the $f_k$'s and $g_k$'s are the BFGS vectors; $n_{BFGS}$ is the maximum number of BFGS vectors allowed; $B$ is a matrix which approximates $A$, but is more easily factorized; $s$ is the search parameter; $x_m$ is the $m^{th}$ approximation of $x$; $r_m = b - A x_m$ is the corresponding residual; $||r_m||$ is its Euclidean length; and $\delta$ is a preassigned error tolerance.

Remark 1. The search parameter in step 2 is determined by minimizing the potential energy

$$P(s) = - (x_m + s \Delta x)^T (b - \frac{1}{2} A(x_m + s \Delta x)) \qquad (1)$$

Remark 2. If we ignore the line search and BFGS update ingredients of the PR algorithm, then the classical Jacobi method is obtained when $B$ is taken to be the diagonal of $A$.

Remark 3. Our recent research has indicated that the preconditioned conjugate gradients method attains faster convergence than the PR algorithm (see ref. 28). In addition, conjugate gradients requires only a fixed number of vectors which makes it computationally more attractive than the PR algorithm with BFGS updates, because a considerable number of BFGS vectors typically need to be stored. For these reasons, conjugate gradients is currently our preferred procedure.

## APPROXIMATE FACTORIZATION

The convergence rate of the algorithm presented in the preceding section depends heavily upon the approximating matrix $B$. It may be noted that if $B = A$ then the exact solution $x$ is obtained immediately. Numerous choices for $B$ are possible. This subject is explored in reference 28. We limit the following discussion to the methods used in computing the results presented herein. To describe the procedures employed, we first consider matrices, $\tilde{A}$, written in the following form:

$$\tilde{A} = W^{\frac{1}{2}}(I + \varepsilon \bar{A})W^{\frac{1}{2}} \qquad (2)$$

where $I$ is the identity matrix, $W$ is a positive-definite diagonal matrix, $\varepsilon$ is a scalar, and $\bar{A}$ is a matrix which has the same sparsity pattern as $A$. $\tilde{A}$ is to be thought of as an approximation of $A$. Specific choices of $W$, $\varepsilon$ and $\bar{A}$ are considered later. The second and final stage of the approximation is to define

$$B = W^{\frac{1}{2}} C W^{\frac{1}{2}} \qquad (3)$$

where $C$ is an approximation of $I + \varepsilon \bar{A}$. Various choices are considered below:

ORIGINAL PAGE IS
OF POOR QUALITY

### Two-component Splitting

Let $\bar{\underset{\sim}{A}}$ be decomposed as follows:

$$\bar{\underset{\sim}{A}} = \bar{\underset{\sim}{A}}_1 + \bar{\underset{\sim}{A}}_2 \tag{4}$$

Then a possible definition of $\underset{\sim}{C}$ is

$$\underset{\sim}{C} = (\underset{\sim}{I} + \varepsilon \bar{\underset{\sim}{A}}_1)(\underset{\sim}{I} + \varepsilon \bar{\underset{\sim}{A}}_2) = \underset{\sim}{I} + \varepsilon \bar{\underset{\sim}{A}} + \varepsilon^2 \bar{\underset{\sim}{A}}_1 \bar{\underset{\sim}{A}}_2 = \underset{\sim}{I} + \varepsilon \bar{\underset{\sim}{A}} + O(\varepsilon^2) \tag{5}$$

The last part suggests the nature of the approximation. Computational simplicity is gained if $\bar{\underset{\sim}{A}}_1$ and $\bar{\underset{\sim}{A}}_2$ are very sparse and more easily factorized than $\bar{\underset{\sim}{A}}$.

### One-pass Multi-component Splitting

Consider a multi-component sum decomposition of $\bar{\underset{\sim}{A}}$:

$$\bar{\underset{\sim}{A}} = \sum_{i=1}^{n} \bar{\underset{\sim}{A}}_i \tag{6}$$

Let

$$\begin{aligned} \underset{\sim}{C} &= \prod_{i=1}^{n} (\underset{\sim}{I} + \varepsilon \bar{\underset{\sim}{A}}_i) \\ &= (\underset{\sim}{I} + \varepsilon \bar{\underset{\sim}{A}}_1)(\underset{\sim}{I} + \varepsilon \bar{\underset{\sim}{A}}_2) \ \ldots \ (\underset{\sim}{I} + \varepsilon \bar{\underset{\sim}{A}}_n) \\ &= \underset{\sim}{I} + \varepsilon \bar{\underset{\sim}{A}} + O(\varepsilon^2) \end{aligned} \tag{7}$$

Clearly, this is just a straightforward generalization of the two-component splitting.

### Two-pass Multi-component Splitting

This generalization of the preceding case has qualitative advantages under certain circumstances (Marchuk, ref. 31). Let

$$\underset{\sim}{C} = \prod_{i=1}^{n} (\underset{\sim}{I} + \frac{\varepsilon}{2} \bar{\underset{\sim}{A}}_i) \prod_{i=n}^{1} (\underset{\sim}{I} + \frac{\varepsilon}{2} \bar{\underset{\sim}{A}}_i)$$

(cont'd.)

$$= (\underset{\sim}{I} + \frac{\varepsilon}{2}\overline{\underset{\sim}{A}}_1)(\underset{\sim}{I} + \frac{\varepsilon}{2}\overline{\underset{\sim}{A}}_2) \ \ldots \ (\underset{\sim}{I} + \frac{\varepsilon}{2}\overline{\underset{\sim}{A}}_n) \ \times$$

$$\times \ (\underset{\sim}{I} + \frac{\varepsilon}{2}\overline{\underset{\sim}{A}}_n)(\underset{\sim}{I} + \frac{\varepsilon}{2}\overline{\underset{\sim}{A}}_{n-1}) \ \ldots \ (\underset{\sim}{I} + \frac{\varepsilon}{2}\overline{\underset{\sim}{A}}_1)$$

$$= \underset{\sim}{I} + \varepsilon\,\overline{\underset{\sim}{A}} + O(\varepsilon^2) \qquad (8)$$

If each $\overline{\underset{\sim}{A}}_i$ is symmetric and positive semi-definite, then $\underset{\sim}{C}$ is symmetric and positive-definite.

## Element-by-element (EBE) Approximate Factorizations

The EBE approximate factorization is simply a multi-component splitting in which the components are the finite element arrays themselves. That is we assume

$$\overline{\underset{\sim}{A}} = \sum_{i=1}^{n_{el}} \overline{\underset{\sim}{A}}^e \qquad (9)$$

where $\overline{\underset{\sim}{A}}^e$ is the $e^{th}$ element contribution to $\overline{\underset{\sim}{A}}$. Then $\underset{\sim}{C}$ may be defined by either the one-pass or two-pass formulae, viz.

$$\underset{\sim}{C} = \prod_{e=1}^{n_{el}} (\underset{\sim}{I} + \varepsilon\,\overline{\underset{\sim}{A}}^e) \qquad (10)$$

$$\underset{\sim}{C} = \prod_{i=1}^{n_{el}} (\underset{\sim}{I} + \frac{\varepsilon}{2}\overline{\underset{\sim}{A}}^e) \quad \prod_{e=n_{el}}^{1} (\underset{\sim}{I} + \frac{\varepsilon}{2}\overline{\underset{\sim}{A}}^e) \qquad \text{("Marchuk EBE")} \qquad (11)$$

Remark 1. We wish to use the term element in the generic sense of a "subdomain model", where an element could be an individual finite element or a subassembly of elements. Thus we allow limited assembly. Various equivalent terminologies have been used to define this concept, such as "substructures" and "superelements". Subdomain finite element models inherit the symmetry and definiteness properties of the global array. Consequently, the remark made after (8) applies.

Remark 2. Note that storage demands are vastly less in the EBE case. Only one element at a time need be stored and processed. Whether or not it is desirable to save factorized element arrays depends upon the availability of high speed RAM, and the trade-off between CPU and disk I/O costs.

Remark 3. If elements are segregated into non-contiguous subgroups then calculations are "parallelizable". For example, brick-like domains can be decomposed into eight non-contiguous element groups (see fig. 1). Because the elements in each subgroup have no common degrees-of-freedom, they can be processed in parallel. The eight groups, however, need to be processed sequentially. For analogous two-dimensional domains, four element groups need to be employed. This feature has significant

computational implications for vector and multi-processor machines.

Remark 4. It has been our computational experience that if $\underset{\sim}{A}$ is symmetric and positive-definite, then qualitatively faithful approximate factorizations which preserve these properties, such as (11), perform much better than those that do not. In the numerical examples presented herein we have employed (11) exclusively.

Remark 5. In Reference 28 we have explored the use of reordering the element factors and of approximately factorizing the individual element arrays. Preliminary results indicate that significant improvements over the basic scheme of (11) can be made.

## SELECTION OF $\underset{\sim}{W}$, $\epsilon$ AND $\overline{\underset{\sim}{A}}$

In the computations presented herein the following definitions were employed:

$$\underset{\sim}{W} = \text{diagonal entries of } \underset{\sim}{A} \tag{12}$$

$$\overline{\underset{\sim}{A}} = \frac{1}{\epsilon} \underset{\sim}{W}^{-\frac{1}{2}} \underset{\sim}{A} \underset{\sim}{W}^{-\frac{1}{2}} \tag{13}$$

Thus

$$\tilde{\underset{\sim}{A}} = \underset{\sim}{W} + \overline{\underset{\sim}{A}} \tag{14}$$

This choice is motivated by the derivation of the PR algorithm (see ref. 23).

Remark 1. A study performed by Nour-Omid and Parlett (ref. 33) indicates that the following procedure, suggested by Winget, is superior:

$$\overline{\underset{\sim}{A}} = \frac{1}{\epsilon} \underset{\sim}{W}^{-\frac{1}{2}} (\underset{\sim}{A} - \underset{\sim}{W}) \underset{\sim}{W}^{-\frac{1}{2}} \tag{15}$$

where $W$ is given by (12). This leads to

$$\tilde{\underset{\sim}{A}} = \underset{\sim}{A} \tag{16}$$

Remark 2. The implicit-explicit element concept (see ref's. 20, 21, 24-27) has a very simple and clean implementation within EBE approximate factorizations. Recall that an explicit element contributes only its diagonal mass matrix to the coefficient matrix $\underset{\sim}{A}$. Thus $\underset{\sim}{W}$, according to the preceding definition (i.e., eq. (12)), totally accounts for the explicit element contributions and the corresponding $\overline{\underset{\sim}{A}}^e$'s are identically zero. What this means is that explicit elements may be simply omitted from the formula for $\underset{\sim}{C}$. In nonlinear problems this opens the way to time-adaptive implicit-explicit element partitions. In calculating the element contributions to the residual (i.e. "$\underset{\sim}{b}$") a check can be made whether or not the critical time step is exceeded for the element. If it is not exceeded, a flag is set to indicate that element contributions to $\underset{\sim}{C}$ may be simply ignored. The potential savings in nonlinear transient analysis procedures incorporating these ideas is clearly considerable.

## SAMPLE PROBLEMS

The computed results were obtained on a VAX computer using single precision (32 bits per floating point word).

### Elastic Cantilever Beam

The configuration analyzed is shown in figure 2. It represents one-half of a plane strain beam modelled with 32 bilinear quadrilateral elements. A lumped mass matrix was employed. The loading and boundary conditions are set in accord with an exact, static linear elasticity solution (see pp. 35-39, ref. 36). However, here the problem is forced dynamically. The beam is assumed initially at rest and all loads are applied instantaneously at $t = 0+$. In formulating the problem, the Newmark algorithm is employed with $\beta = \frac{1}{4}$ and $\gamma = \frac{1}{2}$ (see Appendix I). With these parameters, unconditional stability is attained and no algorithmic damping is introduced (see ref's. 11, 17, 21).

The numerical solution is dominated by response in the fundamental mode. This is illustrated in figure 3. At a time step of $\Delta t = 2.5 \times 10^{-4}$, an essentially exact solution is obtained. At a larger step of $\Delta t = 2.5 \times 10^{-3}$, a very crude approximation of the response is obtained. It is interesting to relate the sizes of these steps to the critical time step for explicit integration, $\Delta t_{crit} = h_{min}/C_D = h_{min}/\sqrt{(\lambda + 2\mu)/\rho} = 1.336 \times 10^{-5}$, and the approximate period of the fundamental mode, $T_1 \cong .0122$ (see table 1). As may be seen, both time steps are far outside the range of explicit integration. The larger time step resolves the fundamental mode with only 5 steps, and thus is larger than the maximum feasible for this problem.

In comparing the results of the various methods it is important to keep in mind that all methods give identical solutions.* Consequently, the primary basis of comparison is the number of iterations needed to attain the solution. It was found that the number of iterations per time step did not vary significantly from one time step to another for a given method and specific step size. Results for the first time step are presented in table 2. The following observations may be made: In general the element-by-element results are superior to Jacobi. Use of line search and BFGS updates accelerate convergence. The best results are attained by the element-by-element procedure with line search and BFGS updates.

It is somewhat surprising that methods (v) and (vi) converge faster at the larger time step than at the smaller. At this point we have no explanation for this phenomenon.

### Elastic and Elastic-Perfectly Plastic Cantilever Beam

The geometrical definition of this problem is identical to the previous one except that the entire beam is discretized by a 64 element mesh (the lower part of the beam was added to the mesh of figure 2). The boundary conditions were changed to the following.

*The convergence tolerance, $\delta$ in step 3 of the flowchart, was taken to be $.01||\underline{b}||$.

ORIGINAL PAGE IS
OF POOR QUALITY

$$\left.\begin{aligned} u_1(0, x_2, t) &= u_2(0, 0, t) = 0 \\ t_2(L, x_2, t) &= Q\left(\frac{2t}{T}\right)\left(1 - \left(\frac{x_2}{c}\right)^2\right) \end{aligned}\right\} x_2 \in [-c, +c] \quad , \quad t \in [0, T]$$

$$Q = 1{,}000 \quad , \quad T = 0.04 \quad , \quad L = 16 \quad , \quad c = 2$$

The boundary tractions are zero on the remaining boundary segments. The tensile uniaxial yield stress was taken to be 3,000. Small deformations were assumed and the elastic stiffness matrix was used on the left-hand side throughout. The radial-return algorithm of reference 30 was employed to integrate the elastic-plastic constitutive equation.

Figures 4 and 5 compare the elastic and plastic stress distributions at t = .036. A fully developed plastic hinge is present at the root of the beam in the plastic case. The elastic critical time step of this problem is $\Delta t_{crit} = 1.336 \times 10^{-5}$ and the time step used was $\Delta t = 2.5 \times 10^{-3} = 187.1 \ \Delta t_{crit}$. The EBE method with BFGS updates and line searches was employed. The average number of iterations for both the elastic and plastic calculations was 4.

Elastic and Elastic-Perfectly Plastic Cantilever Beam with a Circular Hole

The geometric definition of the problem is shown in figure 6. The beam was discretized using a 500 element mesh. The following kinematic and stress boundary conditions were employed:

$$\left.\begin{aligned} u_1(0, x_2, t) &= u_2(0, 0, t) \\ t_2(L, x_2, t) &= Q\left(\frac{t}{T}\right)\left(1 - \left(\frac{x_2}{c}\right)^2\right) \end{aligned}\right\} x_2 \in [-c, +c] \quad , \quad t \in [0, T]$$

$$Q = 250 \quad , \quad T = 0.09 \quad , \quad L = 28 \quad , \quad c = 4$$

Where not specified to be nonzero, the tractions are zero. The uniaxial yield stress was taken to be 1000. A critical time step of $\Delta t_{crit} = 5.41 \times 10^{-6}$ was calculated on the basis of the smallest element edge length. (The critical time step based upon the shortest distance between opposite element edges, which may be a more meaningful distance, is less than half this number.) Two time steps were employed in the calculations: $\Delta t = 10 \times \Delta t_{crit}$ and $\Delta t = 50 \times \Delta t_{crit}$. The EBE algorithm with BFGS updates was also employed for this problem. Results for the smaller time step converged in 1 iteration, whereas for the latter, 7 iterations were required on average.

Figures 7 and 8 show the stress distributions at time t = 0.09 for the elastic and plastic solutions. A fully developed plastic hinge is present at the end of the

beam and a secondary plastic hinge has partially developed in the stress concentration zone (plastic regions are shown dashed in fig. 8c).

We wish to remark upon the contour-line routine used to obtain the results presented in this section. The finite element analyzer calculates the stresses at the integration points. The data is then extrapolated to the nodal points by means of a weighted average of all the integration points in the interior domains of all elements connected to the nodal point. The weights are taken as the inverse of the distance between the integration point and the nodal point. This type of data smoothing ensures that the values obtained at the nodal points will be bounded by the data calculated at the integration points which is an essential property when plastic stresses are present and ensures continuity of stress contours between element domains. However, this method has some drawbacks. For example, data which is anti-symmetric about the neutral axis of the beam, such as $\sigma_{11}$, will result in linear distribution of contour lines in all elements having the center line as part of their boundary even in the case where these elements have a uniform stress distribution (part of a plastic hinge). Data with symmetry with respect to the neutral axis, such as the von Mises stress, does not suffer from this type of smoothing.

## CONCLUDING REMARKS

In this paper EBE approximate factorization techniques have been proposed and compared on test problems. The PR algorithm with BFGS updates performed well, however, the need to store BFGS vectors is considered a significant disadvantage, and thus the fixed storage requirements and improved convergence characteristics of the conjugate gradients algorithm renders it preferable (ref. 28). Improved behavior has also been attained in reference 28 by employing reorderings of the element factors.

It should be kept in mind that the EBE concept has been explored herein as a finite element, linear equation solving procedure. Although initial attempts at directly using EBE ideas to develop time stepping algorithms had some deficiencies it may still ultimately prove profitable to couple EBE concepts with the time-stepping loop and even the nonlinear iterative loop. It is interesting to note that the multigrid method found its initial success as a linear equation solver, but in the most recent and successful variants the multigrid philosophy permeates all aspects of the methodology (see Brandt, ref. 4).

A step has been taken in the development of EBE solution of finite element equation systems. A considerable potential exists for the technique, but much research still remains to be done to bring the methods to fruition.

## APPENDIX I - DERIVATION OF LINEAR ALGEBRAIC SYSTEMS IN THE FINITE ELEMENT ANALYSIS OF NONLINEAR MECHANICS PROBLEMS

### Semi-discrete Equations of Nonlinear Mechanics

Consider the following semi-discrete system

$$\underset{\sim}{M}\,\underset{\sim}{a} = \underset{\sim}{F} \tag{I.1}$$

where $\underset{\sim}{M}$, $\underset{\sim}{a}$ and $\underset{\sim}{F}$ represent the (generalized) mass matrix, acceleration vector and force vector, respectively. Equation (I.1) may be thought of as arising from a finite element discretization of a solid, fluid, structure or combined system. In general, $\underset{\sim}{M}$, $\underset{\sim}{a}$ and $\underset{\sim}{F}$ each depend on time (t). Explicit characterization of $\underset{\sim}{M}$, $\underset{\sim}{a}$ and $\underset{\sim}{F}$ may be given for particular systems under consideration.

## Nonlinear Structural and Solid Mechanics

In nonlinear structural and solid mechanics the Lagrangian kinematical description is frequently adopted. In this case the important kinematical quantities are $\underset{\sim}{d}$, the material-particle displacement from a reference configuration; $\underset{\sim}{v} = \dot{\underset{\sim}{d}}$, the particle velocity; and $\underset{\sim}{a} = \dot{\underset{\sim}{v}} = \ddot{\underset{\sim}{d}}$, the particle acceleration. Dots indicate the Lagrangian time-derivative in which the material particle is held fixed. The forces are assumed to take the form

$$\underset{\sim}{F} = \underset{\sim}{F}^{ext} - \underset{\sim}{N} \tag{I.2}$$

where $\underset{\sim}{F}^{ext}$ is the vector of given external forces and $\underset{\sim}{N}$ denotes the vector of internal forces, which may depend upon $\underset{\sim}{d}$, $\dot{\underset{\sim}{d}}$ and their histories. To make the dependence precise, one need introduce equations which define the constitutive (i.e. stress-deformation) behavior of the materials in question. These equations vary widely in type and complexity. For example, they may be algebraic equations, differential equations or integro-differential equations. In addition, inequality constraints may be present, such as in plasticity theory.

## Time Discretization

To solve the semi-discrete problem, a time-discretization algorithm needs to be introduced. For purpose of illustration we shall employ the Newmark family of methods (ref. 32). Generalization to other time integrators, such as the Hilber-Hughes-Taylor algorithm (ref.'s. 16, 18, 19, 21) which possesses improved properties, may be easily facilitated without essential alteration to the following formulation.

The Newmark "predictors" are given by

$$\tilde{\underset{\sim}{d}}_{n+1} = \underset{\sim}{d}_n + \Delta t\, \underset{\sim}{v}_n + \frac{\Delta t^2}{2}(1 - 2\beta)\underset{\sim}{a}_n \tag{I.3}$$

$$\tilde{\underset{\sim}{v}}_{n+1} = \underset{\sim}{v}_n + \Delta t\,(1 - \gamma)\underset{\sim}{a}_n \tag{I.4}$$

where subscripts refer to the step number; $\Delta t$ is the time step; $\underset{\sim}{d}_n$, $\underset{\sim}{v}_n$ and $\underset{\sim}{a}_n$ are the approximations to $\underset{\sim}{d}(t_n)$, $\dot{\underset{\sim}{d}}(t_n)$ and $\ddot{\underset{\sim}{d}}(t_n)$, respectively; and $\beta$ and $\gamma$ are parameters which govern the accuracy and stability of the method (ref's. 11, 17, 29).

Calculations commence with the given initial data (i.e., $\underset{\sim}{d}_0$ and $\underset{\sim}{v}_0$) and $\underset{\sim}{a}_0$ which may be calculated from

$$\underset{\sim}{M}\,\underset{\sim}{a}_0 = \underset{\sim}{F}_0^{ext} - \underset{\sim}{N}_0 \tag{I.5}$$

if $\underset{\sim}{M}$ is diagonal, as is common in structural dynamics, the solution of (I.5) is rendered trivial. Otherwise, a factorization, forward reduction and back substitution are necessary to obtain $\underset{\sim}{a}_0$ .

In the sequel we are only interested in members of the Newmark family for which $\beta > 0$ .

In each time step a nonlinear algebraic problem arises which may be solved by Newton-Raphson and quasi-Newton-type iterative procedures. There are several ways of going about this. In the following implementation an algebraic problem is formulated in which acceleration increments are the unknowns. This form of the implementation is useful in that disparate field theories, such as fluid mechanics and heat conduction, may be formally considered as special cases.

## Acceleration Formulation

$$i = 0 \qquad \text{(i is the iteration counter)} \tag{I.6}$$

$$\left.\begin{aligned} \underset{\sim}{d}_{n+1}^{(i)} &= \tilde{\underset{\sim}{d}}_{n+1} \qquad (I.7)\\ \underset{\sim}{v}_{n+1}^{(i)} &= \tilde{\underset{\sim}{v}}_{n+1} \qquad (I.8)\\ \underset{\sim}{a}_{n+1}^{(i)} &= \underset{\sim}{0} \qquad (I.9) \end{aligned}\right\} \quad \text{(predictor phase)}$$

$$\underset{\sim}{R} = \underset{\sim}{F}_{n+1}^{ext} - \underset{\sim}{N}_{n+1}^{(i)} - \underset{\sim}{M}_{n+1}^{(i)}\,\underset{\sim}{a}_{n+1}^{(i)} \qquad \text{(residual, or out-of-balance, force)} \tag{I.10}$$

$$\underset{\sim}{M}^{*} = \underset{\sim}{M}_{n+1}^{(i)} + \gamma\Delta t\,\underset{\sim}{C}_{n+1}^{(i)} + \beta\Delta t^2\,\underset{\sim}{K}_{n+1}^{(i)} \qquad \text{(effective mass)} \tag{I.11}$$

$$\boxed{\underset{\sim}{M}^{*}\,\underset{\sim}{\Delta a} = \underset{\sim}{R}} \tag{I.12}$$

$$\left.\begin{aligned} \underset{\sim}{a}_{n+1}^{(i+1)} &= \underset{\sim}{a}_{n+1}^{(i)} + \underset{\sim}{\Delta a} \qquad (I.13)\\ \underset{\sim}{v}_{n+1}^{(i+1)} &= \underset{\sim}{v}_{n+1}^{(i)} + \gamma\Delta t\,\underset{\sim}{\Delta a} \qquad (I.14)\\ \underset{\sim}{d}_{n+1}^{(i+1)} &= \underset{\sim}{d}_{n+1}^{(i)} + \beta\Delta t^2\,\underset{\sim}{\Delta a} \qquad (I.15) \end{aligned}\right\} \quad \text{(corrector phase)}$$

If additional iterations are to be performed, $i$ is replaced by $i+1$, and calculations resume with (I.10). Either a fixed number of iterations may be performed, or iterating may be terminated when $\Delta\underset{\sim}{a}$ and/or $\underset{\sim}{R}$ satisfy preassigned convergence conditions. When the iterative phase is completed, the solution at step $n+1$ is defined by the last iterates (viz. $\underset{\sim}{d}_{n+1} = \underset{\sim}{d}_{n+1}^{(i+1)}$ ; $\underset{\sim}{v}_{n+1} = \underset{\sim}{v}_{n+1}^{(i+1)}$ ; and $\underset{\sim}{a}_{n+1} = \underset{\sim}{a}_{n+1}^{(i+1)}$ ). At this point, $n$ is replaced by $n+1$, and calculations for the next time step may begin.

In practice, $\underset{\sim}{d}_n$, $\underset{\sim}{v}_n$ and $\underset{\sim}{a}_n$ are generally saved during the iterative phase along with $\underset{\sim}{a}_{n+1}^{(i+1)}$ ; but $\underset{\sim}{v}_{n+1}^{(i+1)}$ and $\underset{\sim}{d}_{n+1}^{(i+1)}$ may be computed as needed, on the element level.

The matrices $\underset{\sim}{C}$ and $\underset{\sim}{K}$ are the tangent damping and tangent stiffness matrices, respectively. These are linearized operators associated with $\underset{\sim}{N}$. For example, if $\underset{\sim}{N}$ is an algebraic function of $\underset{\sim}{d}$ and $\dot{\underset{\sim}{d}}$, then

$$\underset{\sim}{K} = \partial \underset{\sim}{N} / \partial \underset{\sim}{d} \tag{I.16}$$

and

$$\underset{\sim}{C} = \partial \underset{\sim}{N} / \partial \dot{\underset{\sim}{d}} \tag{I.17}$$

Generally in structural and solid mechanics, $\underset{\sim}{M}$, $\underset{\sim}{K}$ and $\underset{\sim}{C}$ are symmetric, $\underset{\sim}{M}$ and $\underset{\sim}{K}$ are positive-definite, and $\underset{\sim}{C}$ is positive semi-definite.

So-called implicit-explicit mesh partitions (ref's. 2, 3, 20, 21, 24-27) may be encompassed by the above formulation simply by excluding explicit element/node contributions from the definitions of $\underset{\sim}{C}$ and $\underset{\sim}{K}$. A totally explicit formulation is attained by ignoring $\underset{\sim}{C}$ and $\underset{\sim}{K}$. In these cases it is necessary to employ a diagonal mass matrix in explicit regions to attain full computational efficiency.

It may be observed that the preceding algorithm may be specialized to nonlinear statics and linear dynamics and statics:

### Nonlinear Statics

In this case ignore $\underset{\sim}{M}$ and $\underset{\sim}{C}$ and set $\underset{\sim}{v}$ and $\underset{\sim}{a}$ to zero throughout.

### Linear Dynamics

In this case $\underset{\sim}{M}$, $\underset{\sim}{C}$ and $\underset{\sim}{K}$ are constant and

$$\underset{\sim}{N} = \underset{\sim}{C}\,\underset{\sim}{v} + \underset{\sim}{K}\,\underset{\sim}{d} \tag{I.18}$$

### Linear Statics

In this case ignore $\underset{\sim}{M}$ and $\underset{\sim}{C}$, set $\underset{\sim}{v}$ and $\underset{\sim}{a}$ to zero throughout, $\underset{\sim}{K}$ is constant and

$$\underset{\sim}{N} = \underset{\sim}{K}\,\underset{\sim}{d} \tag{I.19}$$

To simplify the writing in the body of this paper we adopt the following notations in place of (I.12):

$$\underset{\sim}{A}\,\underset{\sim}{x} = \underset{\sim}{b} \tag{I.20}$$

Thus during each step, at each iteration, we wish to solve (I.28) in which $\underset{\sim}{A}$ is assembled from element arrays, that is

$$\underset{\sim}{A} = \sum_{e=1}^{n_{el}} \underset{\sim}{A}^{e} \tag{I.21}$$

## REFERENCES


1. Baker, A. J., "Research on a Finite Element Algorithm for the Three-dimensional Navier-Stokes Equations," AFWAL-TR-82-3012, Wright-Patterson Air Force Base, Ohio, 1982.

2. Belytschko, T., and Mullen, R., "Mesh Partitions of Explicit-Implicit Time Integration," Formulations and Computational Algorithms in Finite Element Analysis, Eds. K. J. Bathe et al., M.I.T. Press, Cambridge, Massachusetts, 1977.

3. Belytschko, T., and Mullen, R., "Stability of Explicit-Implicit Mesh Partitions in Time Integration," International Journal for Numerical Methods in Engineering, Vol. 12, No. 10, 1575-1586 (1979).

4. Brandt, A., "Guide to Multigrid Development," in Multigrid Methods (W. Hackbusch and U. Trottenberg, eds.) Springer-Verlag, Berlin-Heidelberg-New York, 1982.

5. Dendy, J. E., and Fairweather, G., "Alternating-direction Galerkin Methods for Parabolic and Hyperbolic Problems on Rectangular Polygons," SIAM J. Numer. Anal., Vol. 2, 144-163 (1975).

6. Douglas, J., "On the Numerical Integration of $u_{xx} + u_{yy} = u_t$ by Implicit Methods," J. Soc. Indust. Appl. Math., Vol. 3, 42-65 (1965).

7. Douglas, J., "Alternating Direction Methods for Three Space Variables," Numer. Math., 4, 41-63 (1962).

8. Douglas, J., and Dupont, T., "Galerkin Methods for Parabolic Equations," SIAM J. Numer. Anal., Vol. 7, 575-626 (1970).

9. Douglas, J., and Dupont, T., "Alternating-direction Galerkin Methods on Rectangles," pp. 133-214 in Proceedings Symposium on Numerical Solution of Partial Differential Equations, II, B. Hubbard (ed.), Academic Press, New York, 1971.

10. Douglas, J., and Rachford, H. H., "On the Numerical Solution of Heat Conduction Problems in Two and Three Space Variables," Trans. Amer. Math. Soc., Vol. 82, 421-439 (1956).

11. Goudreau, G. L., and Taylor, R. L., "Evaluation of Numerical Integration Methods in Elastodynamics," Computer Methods in Applied Mechanics and Engineering, Vol. 2, 69-97 (1972).

12. Hayes, L. J., "A Comparison of Alternating-direction Collocation Methods for the Transport Equation," pp. 169-177 in New Concepts in Finite Element Analysis, AMD Vol. 44, (T.J.R. Hughes et al. eds.), ASME, New York, 1981.

13. Hayes, L. J., "Finite Element Patch Approximations and Alternating-Direction Methods," Mathematics and Computers in Simulation, Vol. XXII, 25-29 (1980).

14. Hayes, L. J., "Implementation of Finite Element Alternating-Direction Methods on Nonrectangular Regions," International Journal for Numerical Methods in Engineering, Vol. 16, 35-49 (1980).

15. Hayes, L. J., "Galerkin Alternating-Direction Methods for Nonrectangular Regions Using Patch Approximations," SIAM J. Numer. Anal., Vol. 18, No. 4, 627-643 (1981).

16. Hibbitt, H. D., and Karlsson, B. I., "Analysis of Pipe Whip," ASME Paper No. 79-PVP-122, presented at the Pressure Vessels and Piping Conference, San Francisco, California, June 25-29, 1979.

17. Hilber, H. M., Analysis and Design of Numerical Integration Methods in Structural Dynamics, Report No. EERC76-29, Earthquake Engineering Research Center, University of California, Berkeley, California, November 1976.

18. Hilber, H. M., and Hughes, T.J.R., "Collocation, Dissipation, and 'Overshoot' for Time Integration Schemes in Structural Dynamics," Earthquake Engineering and Structural Dynamics, Vol. 6, 99-118 (1978).

19. Hilber, H. M., Hughes, T.J.R., and Taylor, R. L., "Improved Numerical Dissipation for Time Integration Algorithms in Structural Dynamics: Earthquake Engineering and Structural Dynamics, Vol. 5, 283-292 (1977).

20. Hughes, T.J.R., "Implicit-explicit Finite Element Techniques for Symmetric and Non-symmetric Systems," pp. 255-267 in Recent Advances in Non-linear Computational Mechanics, (eds. E. Hinton, D.R.J. Owen and C. Taylor) Pineridge Press, Swansea, U.K., 1982.

21. Hughes, T.J.R., "Analysis of Transient Algorithms with Particular Reference to Stability Behavior," Computational Methods in Transient Analysis, (eds. T. Belytschko and T.J.R. Hughes), North-Holland Publishing Co., Amsterdam, 1983.

22. Hughes, T.J.R., Levit, I., and Winget, J., "Implicit, Unconditionally Stable, Element-by-element Algorithms for Heat Conduction Analysis," Journal of the Engineering Mechanics Division, ASCE, April 1983.

23. Hughes, T.J.R., Levit, I., and Winget, J., "An Element-by-element Solution Algorithm for Problems of Structural and Solid Mechanics," Computer Methods in Applied Mechanics and Engineering, 241-254, Vol. 36, No. 2 (1983).

24. Hughes, T.J.R., and Liu, W. K., "Implicit-Explicit Finite Elements in Transient Analysis: Stability Theory," Journal of Applied Mechanics, Vol. 45, 371-374 (1978).

25. Hughes, T.J.R., and Liu, W. K., "Implicit-Explicit Finite Elements in Transient Analysis: Implementation and Numerical Examples," Journal of Applied Mechanics, Vol. 45, 375-378 (1978).

26. Hughes, T.J.R., Pister, K. S., and Taylor, R. L., "Implicit-Explicit Finite Elements in Nonlinear Transient Analysis," Computer Methods in Applied Mechanics and Engineering, Vols. 17/18, 159-182 (1979).

27. Hughes, T.J.R., and Stephenson, R. A., "Convergence of Implicit-Explicit Algorithms in Nonlinear Transient Analysis," International Journal of Engineering Science, Vol. 19, No. 2, 295-302 (1981).

28. Hughes, T.J.R., Winget, J., Levit, I., and Tezduyar, T. E., "New Alternating Direction Procedures in Finite Element Analysis based upon EBE Approximate Factorizations," Proceedings of the Symposium on Recent Developments in Computer Methods for Nonlinear Solid and Structural Mechanics (eds. N. Perrone and S. Atluri) ASME AMD Volume, June 1983.

29. Krieg, R. D., and Key, S. W., "Transient Shell Response by Numerical Time Integration," International Journal for Numerical Methods in Engineering, Vol. 7, 273-286 (1973).

30. Krieg, R. D., and Krieg, D. B., "Accuracies of Numerical Solution Methods for the Elastic-Perfectly Plastic Model," Journal of Pressure Vessel Technology, 510-515, November 1977.

31. Marchuk, G. I., Methods of Numerical Mathematics, Springer-Verlag, New York-Heidelberg-Berlin, 1975.

32. Newmark, N. M., "A Method of Computation for Structural Dynamics," Journal of the Engineering Mechanics Division, ASCE, 67-94 (1959).

33. Nour-Omid, B., and Parlett, B. N., "Element Preconditioning," Report PAM-103, Center for Pure and Applied Mathematics, University of California, Berkeley, October 1982.

34. Ortiz, M., Pinsky, P. M., and Taylor, R. L., "Unconditionally Stable Element-by-element Algorithms for Dynamic Problems," Computer Methods in Applied Mechanics and Engineering, 223-239, Vol. 36, No. 2 (1983).

35. Peaceman, D. W., and Rachford, H. H., "The Numerical Solution of Parabolic and Elliptic Differential Equations," J. Soc. Indust. Appl. Math., Vol. 3, 28-41 (1955).

36. Timoshenko, S., and Goodier, J. N., Theory of Elasticity, Second Edition, McGraw-Hill, New York, 1951.

37. Warming, R. F., and Beam, R. M., "On the Construction and Application of Implicit Factored Schemes for Conservation Laws," SIAM-AMS PROCEEDINGS, Vol. 11, 85-129 (1978).

ORIGINAL PAGE IS
OF POOR QUALITY

38. Yanenko, N. N., The Method of Fractional Steps, Springer-Verlag, New York-Heidelberg-Berlin, 1971.

Table 1 Comparison of time steps used in calculations with characteristic time scales.

| $\Delta t$ | $2.5 \times 10^{-4}$ | $2.5 \times 10^{-3}$ |
|---|---|---|
| $\frac{\Delta t}{\Delta t_{crit}}$ | 18.71 | 187.1 |
| $\frac{T_1}{\Delta t}$ | 48.9 | 4.89 |

Table 2 Number of iterations required for convergence for the problem illustrated in Figure 2.

| Method \ $\Delta t$ | $2.5 \times 10^{-4}$ ($= 18.71\ \Delta t_{crit}$) | $2.5 \times 10^{-3}$ ($= 187.1\ \Delta t_{crit}$) |
|---|---|---|
| (i) Jacobi | 99 | $_{\infty}$(1) |
| (ii) Jacobi + LS | 38 | 75 |
| (iii) Jacobi + LS + BFGS | 15 | 21 |
| (iv) EBE | 14 | 16 |
| (v) EBE + LS | 9 | 6 |
| (vi) EBE + LS + BFGS | 5 | 4 |

Key: LS = line search
EBE = element-by-element

Note: (1) No convergence attained after 150 iterations.

ORIGINAL PAGE IS
OF POOR QUALITY

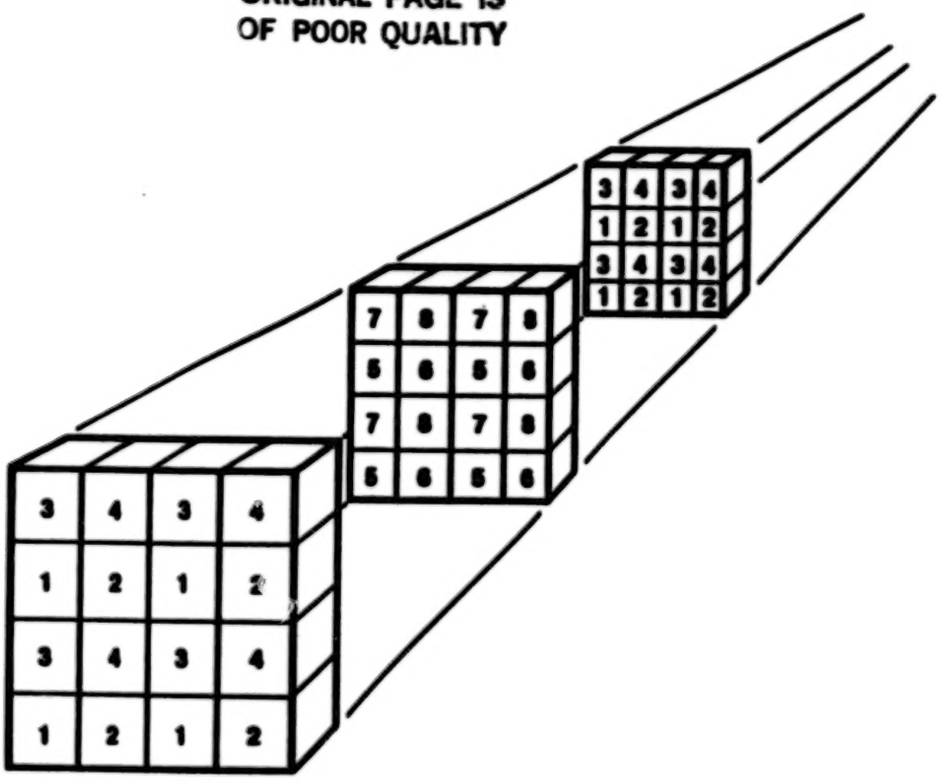


**Figure 1. Decompostion of three-dimensional domain into eight groups of brick elements for parallel processing.**

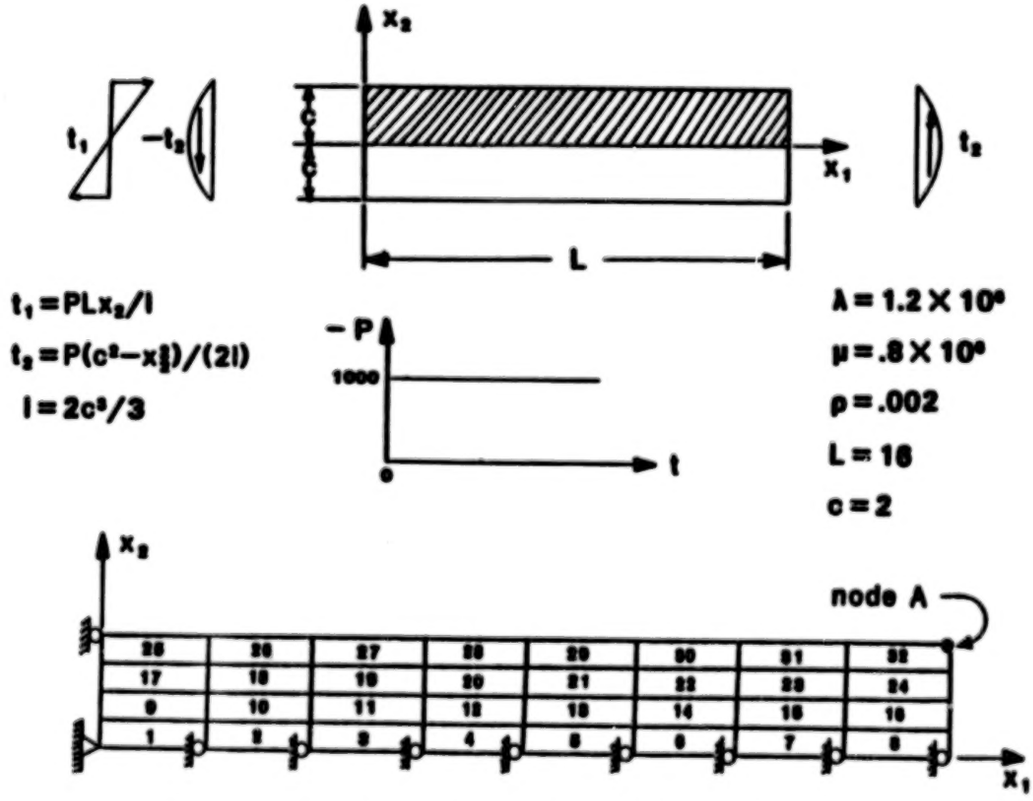


**Figure 2. Problem definition and finite element mesh**

ORIGINAL PAGE IS
OF POOR QUALITY

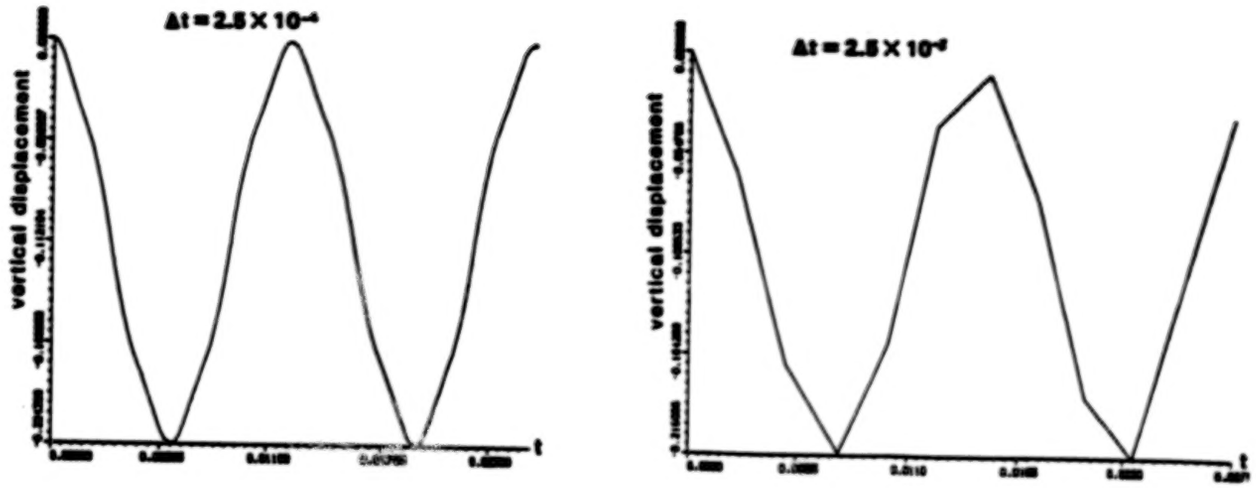


**Figure 3. Vertical displacement of node A**

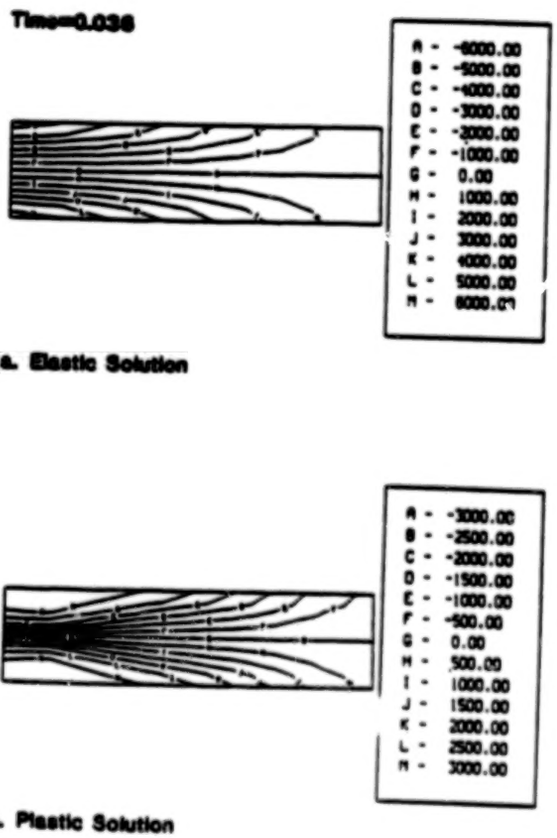


**Figure 4. Stress $\sigma_{11}$**

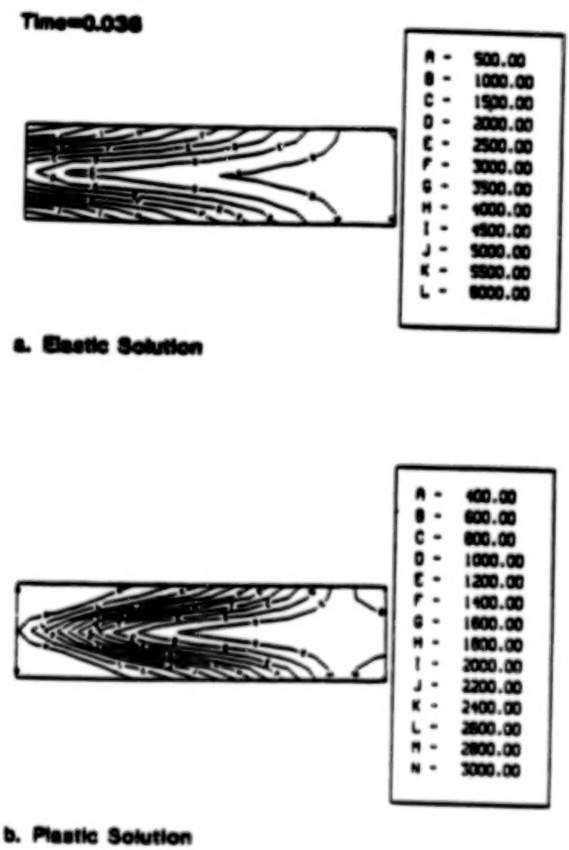


**Figure 5. Von Mises Stress**

ORIGINAL PAGE IS
OF POOR QUALITY

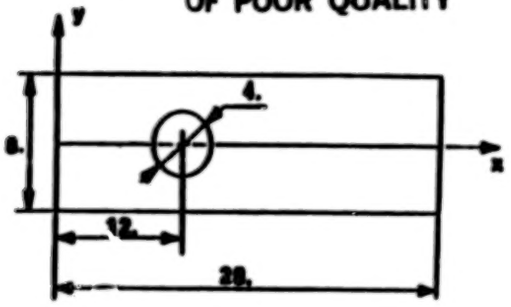


a. Geometry Definition

$\rho = 0.02$

$\lambda = 1200000.$

$\mu = 800000.$

$\sigma_y = 1000.$

b. Finite Element Mesh

**Figure 6.**

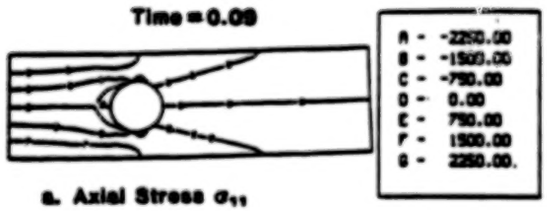


a. Axial Stress $\sigma_{11}$

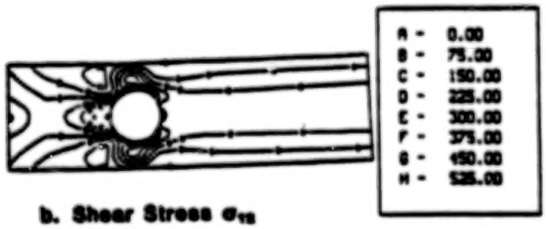


b. Shear Stress $\sigma_{12}$

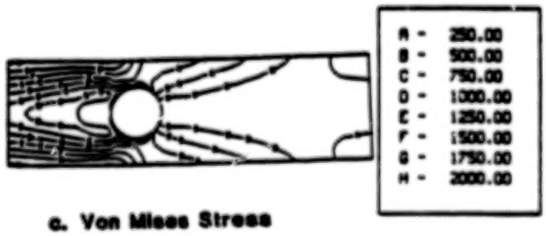


c. Von Mises Stress

**Figure 7. Stress Distribution (elastic solution)**

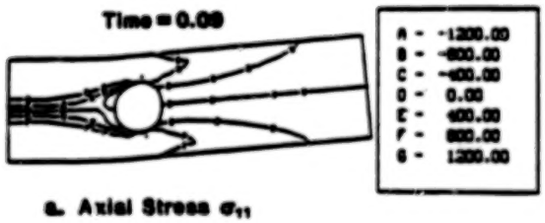


a. Axial Stress $\sigma_{11}$

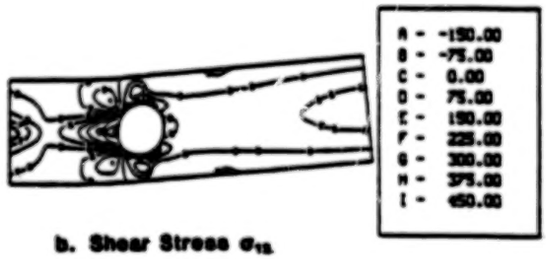


b. Shear Stress $\sigma_{12}$

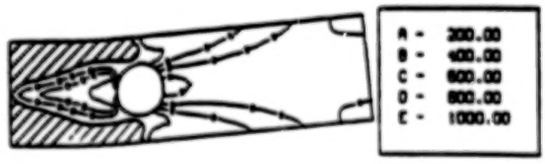


c. Von Mises Stress

**Figure 8. Stress Distribution (plastic solution)**

N84
31695

UNCLAS

N84 31695

# Automatic Finite Element Generators

Paul S. Wang*

Department of Mathematical Sciences
Kent State University
Kent, Ohio 44242

**ABSTRACT**

The design and implementation of a software system for generating finite elements and related computations are described. Exact symbolic computational techniques are employed to derive strain-displacement matrices and element stiffness matrices. Methods for dealing with the excessive growth of symbolic expressions are discussed. Automatic FORTRAN code generation is described with emphasis on improving the efficiency of the resultant code.

## 1. Introduction

Recent years have seen increasing interest in using computer-based symbolic and algebraic manipulation systems for computations in both linear and nonlinear finite element analysis. Application areas include the symbolic derivation of stiffness coefficients [ref. 1], [ref. 2], the reduction of tedium in algebraic manipulation, the generation of FORTRAN code from symbolic expressions [ref. 3], [ref. 4] etc. The benefits and usefulness of such an approach in engine structure research are evident. However, several problems need be solved before this approach can become widely accepted and practiced:

(i) the efficiency of the symbolic processor and its ability to handle the large expressions associated with practical problems,

(ii) the interface between a symbolic system and a finite element system on the same computer, and

(iii) the inefficiencies that are usually associated with automatically generated code.

The MACSYMA system [ref. 5] is a highly sophisticated computer system for performing exact symbolic mathematical computations. It

*Work reported herein has been supported in part by NASA under Grant NAG3-298.

provides many high-level commands for symbolic computation such as differentiation, matrix multiplication and matrix inverse. MACSYMA is developed at the Massachusetts Institute of Technology and has recently been made available on the VAX-11/780 computer which is an affordable high-performance minicomputer with a very large address space. The version of MACSYMA on the VAX under the UNIX operation system [ref. 6] is known as VAXIMA [ref. 7].

We describe our on-going research on the design and implementation of a finite element generator running under the VAXIMA system and our experience, so far, in dealing with the problems mentioned earlier.

## 2. Functional specifications and design

The finite element generator (Generator) as a software system should provide a set of predefined functionalities and be constructed in such a way as to exhibit prescribed characteristics. These functional specifications and design goals will then guide the detailed program design and implementation of the software system.

From a functional point of view, the Generator will perform the following:

(1) to assist the user in the symbolic derivation of finite elements;

(2) to provide routines for a variety of symbolic computations in finite element analysis, including linear and non-linear applications especially for shells [ref. 8];

(3) to provide easy to use interactive commands for most common operations;

(4) to allow the mode of operation to range from interactive manual control to fully automatic;

(5) to generate, based on symbolic computations, FORTRAN code in a form specified by the user;

(6) to automatically arrange for generated FORTRAN code to compile, link and run with FORTRAN-based finite element analysis packages such as the NFAP package [ref. 9];

(7) to provide for easy verification of computational results and testing of the code generated.

In providing the above functions attention must be paid to making the system easy to use, modify and extend. Our initial effort is focused on the isoparametric element family. Later the system can be extended to a wider range of finite elements.

## 3. Generation of element stiffness matrices

Symbolic processing can play a very important role in the generation of element matrices, especially for higher order elements. As an example, we shall describe the automatic processing leading to the derivation of the elment stiffness matrix [K] in the isoparametric formulation. From user supplied input information such as the element type, the number of nodes, the nodal degrees of freedom, the displacement field interpolation polynomial and the material properties matrix [D], the Generator will derive the shape functions, the strain-displacement matrix [B] and the element stiffness matrix [K].

The computation is divided into five logical phases (fig. I) each is implemented as a LISP program module running under the VAXIMA system. Aside from certain interface considerations, these modules are quite independent and can therefore be implemented and tested separately. This allows different people to work on different modules at the same time. After the modules are individually tested then they can be integrated and verified together. Any problems can be isolated to a module and fixed quickly. Detailed description of these phases follows.

### 3.1. Phase I : define input parameters

The task of this phase is to interact with the user to define all the input names, variables, and values that will be needed later. The basic input mode is interactive with the system prompting the user at the terminal for needed input information. While the basic input mode provides flexibility, the input phase can be tedious. Thus we also provide a menu-driven mode where well-known element types together with their usual parameter values are pre-defined for user selection. A fully user-friendly input phase is a goal of our system.

The input handling features planned include :

(1) free format for all input with interactive prompting showing the correct input form;

(2) editing capabilities for correcting typing errors;

(3) the capability of saving all or part of the input for use later;

(4) the flexibility of receiving input either interactively or from a text file.

### 3.2. Phase II : Jacobian and [B] matrix computation

The strain-displacement matrix [B] is derived from symbolically defined shape functions in this phase. Let n be the number of nodes then

$$H = (h_1, h_2, \ldots, h_n)$$

is the shape function vector whose components are the n shape functions $h_1$ through $h_n$. The value for the shape functions will be derived in a

later phase. Here we simply compute with the symbolic names. Let r,s and t be the natural coordinates in the isoparametric formulation and HP be a matrix

$$HP = \begin{bmatrix} H,r \\ H,s \\ H,t \end{bmatrix}$$

where H,r stands for the partial derivative of H with respect to r. The Jacobian J is then

$$J = HP \; . \; [x,y,z]$$

where x stands for the column vector $[x_1,\ldots, x_n]$ etc. Now the inverse, in full symbolic form, of J can be computed as

$$J^{-1} = \frac{invj}{det(J)}$$

By forming the matrix (invj . HP) we can then form the [B] matrix.

### 3.3. Phase III : shape function calculation

Based on the interpolation polynomials and nodal coordinates the shape function vector H is derived and expressed in terms of the natural coordinates r,s and t in the isoparametric formulation. Thus the explicit values for all $h_i$ and all their partial derivatives with respect to r,s and t, needed in HP are computed here.

### 3.4. Phase IV: FORTRAN code generation for [B]

A fortran subroutine for the numerical evaluation of the strain-displacement matrix [B] is generated for use with the NPAP package. This NPAP package is a large FORTRAN based system for linear and non-linear finite element analysis. It is developed and made available to us by P. Chang of the University of Akron. It has been modified and made to run in FORTRAN 77 under UNIX.

Assignment statements will be generated to define the components of the shape function vector H and the various partial derivatives. These variables are then used in assigning values to the FORTRAN array corresponding to [B]. FORTRAN code generation is controlled by a "template" file which is a skeleton FORTRAN program with special instructions for code generation.

Details of the FORTRAN code generator will be discussed later.

### 3.5. Phase V : compute and generate FORTRAN code for [K]

The inverse of the Jacobian, J, appears in [B]. By keeping the inverse of J as INVJ/det(J), the quantity det(J) can be factored from [B] and, denoting by [BJ] the matrix [B] thus reduced, we have

$$[K] = \int \frac{[BJ]^T \; . \; [D] \; . \; [BJ]}{det(J)} \; dr \; ds \; dt$$

The determinant of the Jacobian involves the natural coordinates which makes the exact integration in the above formula quite difficult. We elect to evaluate det(J) at r=s=t=0 and factor it out of the integral. The resulting integrand involves only polynomials in r,s and t which are readily integrated. We believe this approximation is reasonable and the resulting symbolic expression for [K] will still be more accurate than results obtainable from numerical quadrature.

To avoid accumulating large amounts of symbolic expressions, we generate the stiffness matrix [K] one entry at a time. Namely, the integrand matrix is not formed all at once, instead each entry is computed and integrated individually. Furthermore, the FORTRAN code of each [K] entry is output after it is computed. Usually [K] is symmetric and only the upper triangular part need be computed. Although there is a general purpose integration package routine available in VAXIMA, we use a specially designed integration program to gain speed and efficiency. The integration is organized in such a way as to combine common subexpressions and produce FORTRAN code which is faster and more compact. Details on this later.

## 4. The FORTRAN code generator

A set of LISP programs have been written for generating FORTRAN code based on symbolic mathematical expressions derived in VAXIMA. This code generator runs under VAXIMA and generates FORTRAN code by following a given "template" file (fig. II). A template file contains FORTRAN statements any of which may contain an "active part" which is one or several correct VAXIMA statements enclosed in "{" and "}". A typical template may look like the following.

```
      SUBROUTINE STIFF2(ST,B,YZ,C,THICK,R,S,ND,KKK)
      IMPLICIT REAL*8 (A-H,O-Z)
      DIMENSION ST(1),B(4,1),YZ(2,1),C(4,1),SK(18,18)
C
C          KKK = 1 STIFFNESS CALCULATION
C          KKK = 2 STRAIN-DISPACEMENT MATRIX CALCULATION
C
      IF ( KKK .EQ. 1 ) GO TO 500
C Here are some active statements enclosed in {}
{ f77(det=detj), bfortran() }
      RETURN
 500  CONTINUE
C kfortran generates code for [K]
{ kfortran(b,dx,[r,s]) }
      DO 510 I = 1 , ND
        DO 510 J = 1 , ND
          KL = KL+1
          ST(KL) = SK(I,J)*THICK
 510  CONTINUE
      RETURN
      END
```

C-2

To invoke the FORTRAN generator the following VAXIMA command is used.

GENFORTRAN(template-file-name,output-file-name)

GENFORTRAN reads the given template file and passes all characters into the output file without modification except for the active parts contained in "{" and "}". The VAXIMA commands in the active part will be executed by the Generator in the order given and any resultant output will be directed to the output file as well. Thus, in the above example, we can see where the strain-displacement matrix [B] and the stiffness matrix [K] are being generated. The output file will be the template with all active parts replaced by generated code. This output file will therefore be a syntactically correct FORTRAN file ready to compile.

Comment lines are copied into the output file without checking for any active parts. This allows the use of {, } inside comment lines. Recursive invocation of GENFORTRAN from within a template is allowed. This makes it easy to generate a set of related subroutines under the control of GENFORTRAN. This arrangement is very flexible and works quite well for our purposes.

When the code generator is fully developed, it will have the ability to generate code in separate sessions rather than all at once. This means partially generated code can be completed later without regenerating what's already been done. When substantial amount of code is generated automatically, this feature will become important. To help organize the code generated, multiple output files can be automatically used to contain groupings of subroutines.

## 5. Expression growth and Efficiency of FORTRAN code

Previous work in using systems such as VAXIMA for finite element computation uses user-level programs which does not allow much control over the exact manner in which computations are carried out. As a result, the ability of handling realistic cases in practice is very restricted because of expression growth, a phenomenon in symbolic computation when intermediate expressions become too large for efficient manipulation.

We use LISP level programs with direct access to internal data structures. Thus it is possible to construct programs which will carry out computations in such a way as to avoid expression growth as much as possible. Therefore, our programs will be able to handle practical problems with efficiency. Let us illustrate the control of expression growth by the [K] matrix computation.

First of all, the [B] matrix in the integrand is computed with "unevaluated" symbols to keep things small. Thus a typical non-zero entry of [B] looks like

$$hr_2\ hs\ .\ y - hr\ .\ y\ hs_2$$

where $hr_2$ = the second component of H,r and $y = [y_1,\ldots,y_n]$. But these

symbols remain un-evaluated at this point. As stated before, we proceed to generate the entries of [K] one at a time to keep expressions small. In doing this, we apply the formula

$$[K] = \sum_i \sum_j \int [B]_i^T [D]_{ij} [B]_j \, dV$$

to collect terms with respect to $[D]_{ij}$. Coefficients thus obtained are kept in un-expanded form on a list which is consulted for duplicates whenever a new coefficient is generated. This identifies common (duplicate) subexpressions in different entries of [K] and keep the resulting FORTRAN code compact and more efficient. When a new coefficient is formed then it is evaluated and expressed as a polynomial involving the natural coordinates r,s and t. Now a special-purpose integration routine is used. The integration result for each coefficient is converted into FORTRAN code and assigned to a temporary FORTRAN variable. Thus a typical section of the code for [K] may look like the following.

```
      t30 = -((16*y3-4*y2-12*y1)*y4+(-12*y2-4*y1)*y3
     1   +4*y2**2+8*y1*y2+4*y1**2)/3.0
      t31 = ((16*x3-4*x2-12*x1)*y4+(-12*x3+4*x2+8*x1)*y2
     1   +(-4*x3+4*x1)*y1)/3.0
      t32 = ((16*x4-12*x2-4*x1)*y3+(-4*x4+4*x2)*y2
     1   +(-12*x4+8*x2+4*x1)*y1)/3.0
      t33 = -((16*x3-4*x2-12*x1)*x4+(-12*x2-4*x1)*x3
     1   +4*x2**2+8*x1*x2+4*x1**2)/3.0
      k(5,7) = 4*(d6*t33+d3*(t32+t31)+d1*t30)/detk
      k(5,8) = 4*(d5*t33+d6*t32+m2*t31+d3*t30)/detk
```

In the above, t30 etc. are the temporary variables and d1,d2 etc. are entries of the material properties matrix [D]. Without the techniques mentioned here, the code for each single [K] entry will require 5 to 8 continuation cards (for a plane 4-node element).

Experiments on the VAX-11/780 with the NFAP package together with code for the [B] and [K] matrices generated show that there is a 10% CPU time savings with the above described simplification for the 4-node plane element. The savings will be much greater for larger problems. Among other things. we are currently studying ways to further simplify the expressions for the t's.

## 6. References


[1] Cecchi, M. M. and Lami, C. [1977], "Automatic generation of stiffness matrices for finite element analysis", Int. J. Num. Meth. Engng 11, pp. 396-400.

[2] Korncoff, A. R. and Fenves, S. J. [1979], "Symbolic generation of finite element stiffness matrices", Comput. Structures, 10, pp. 119-124.

[3] Noor, A. K. and Andersen C. M. [1981] "Computerized Symbolic Manipulation in Nonlinear Finite Element Analysis", Comput. Structures 13, pp. 379-403.

[4] Noor, A. K. and Andersen C. M., [1979], "Computerized symbolic Manipulation in structural mechanics-progress and potential", Comput. Structures 10, pp. 95-118.

[5] MACSYMA Reference Manual [1977], version nine, the MATHLAB Group, Laboratory for Computer Science, M.I.T., Cambridge, Mass.

[6] UNIX programmer's manual [1979], Vol. I and II, Seventh Edition, Bell Telephone Laboratories, Inc., Murray Hill, New Jersey.

[7] Foderaro, J. K. and Fateman, R. J. [1981], "Characterization of VAX Macsyma", Proceedings, ACM SYMSAC'81 Conference, Aug. 5-8, Snowbird, Utah, pp. 14-19.

[8] Chang, T. Y. and Sawamiphakdi, K. [1981], "Large Deformation Analysis of Laminated Shells by Finite Element Method", Comput. Structures, Vol. 13.

[9] Chang, T. Y. [1980], "NFAP - A Nonlinear Finite Element Analysis Program Vol. 2 - User's Manual", Technical Report, College of Engineering, University of Akron.

AUTOMATIC GENERATION OF [B] AND [K]

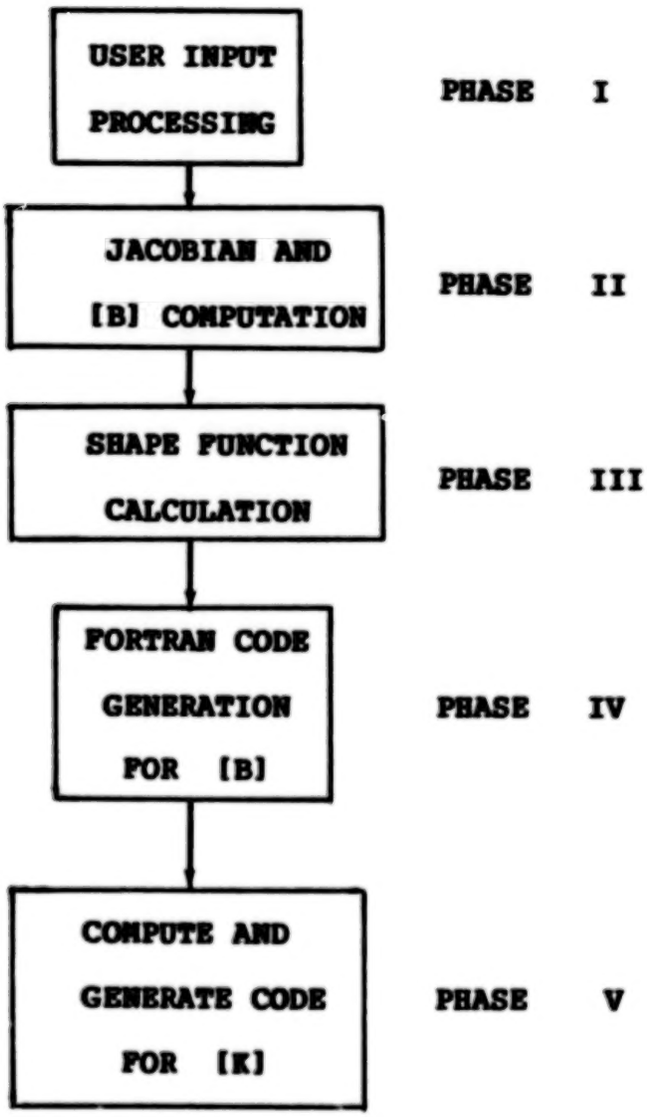


Figure I

FORTRAN CODE GENERATION

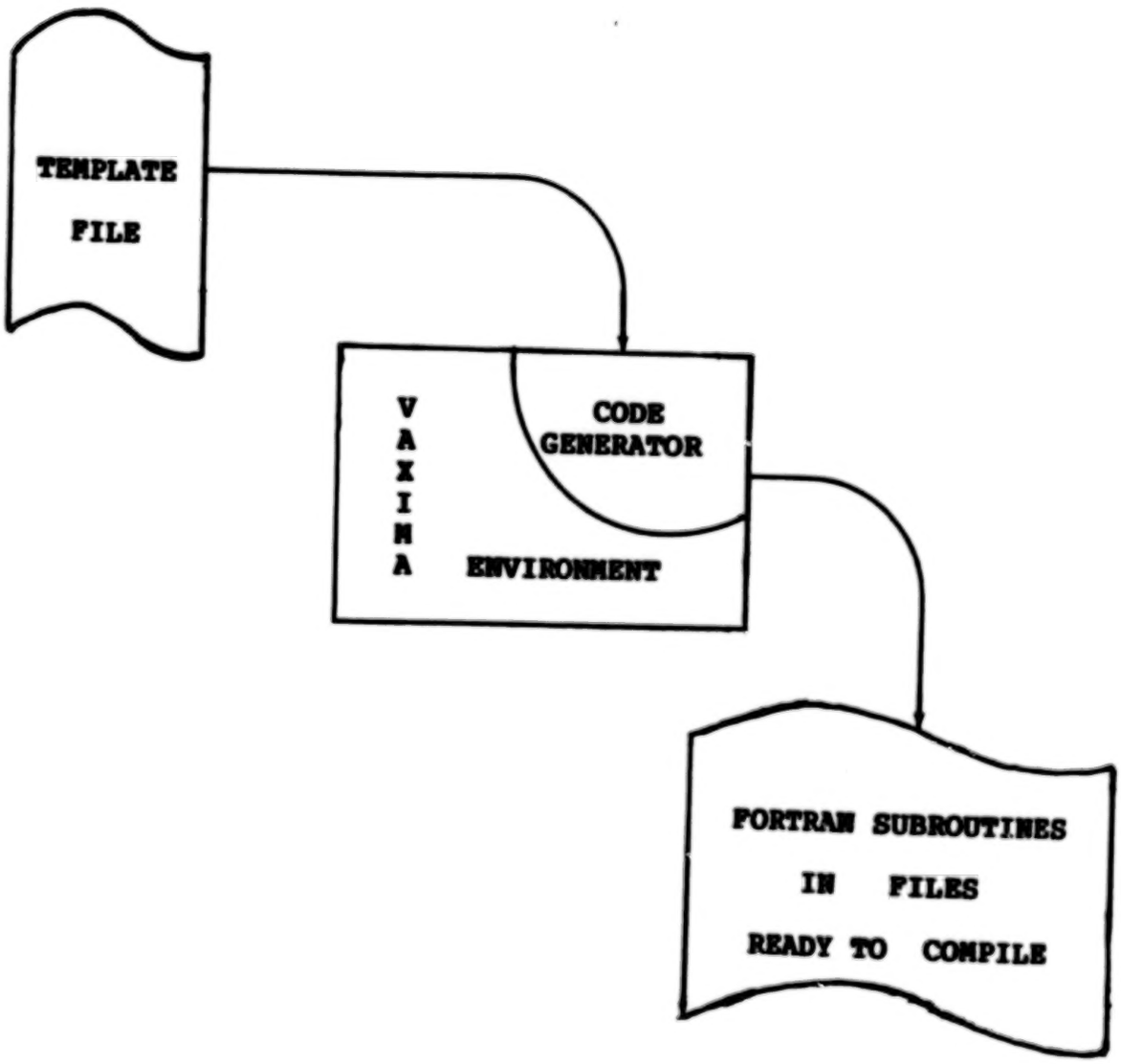


Figure II

N84
31696

UNCLAS

N84 31696

# STABILITY AND CONVERGENCE OF UNDERINTEGRATED FINITE ELEMENT APPROXIMATIONS*

J. Tinsley Oden
The University of Texas

## SUMMARY

An analysis of the effects of underintegration on the numerical stability and convergence characteristics of certain classes of finite element approximations is given. Particular attention is given to so-called hourglassing instabilities that arise from underintegrating the stiffness matrix entries and checkerboard-instabilities that arise from underintegrating constraint terms such as those arising from incompressibility conditions. A fundamental result reported here is the proof that the fully integrated stiffness can be restored in some cases through a post-processing operation.

## INTRODUCTION

In virtually all finite element codes, numerical quadrature is used to evaluate integrals defining various matrices in the equations governing the discrete model. In recent years, many practitioners underintegrate various entries in the stiffness, constraint, or mass matrices so as to either reduce the computational effort required to solve a problem or in attempts to improve convergence characteristics of certain methods. By "underintegration" we mean the use of quadrature rules of an order lower than that required to produce exact integrals of the polynomials appearing in various finite element matrices.

Unfortunately, the use of underintegration frequently leads to serious numerical instabilities. Underintegration of the stiffness matrices, for example, may produce spurious patterns in the displacement fields which are referred to as "hourglass," "chickenwire," or "keystone" modes, whereas underintegration of constraint terms such as those arising from incompressibility conditions may lead to spurious oscillations in stress or pressures known as "checkerboard" modes. An example of a checkerboard pattern in a stress field in a highly-deformed hyperelastic cylinder under axial compression, computed using eight-node isoparametric elements and reduced integration of an incompressibility constraint, is shown in Fig. 1. The hourglass-instability phenomena has been discussed by Flannagan and Belytschko (ref. 1) in recent times, whereas instabilities due to underintegration of penalized constraints have been studied by Oden, Kikuchi, and Song (ref. 2), Oden and Kikuchi (ref. 3), and Oden and Jacquotte (refs. 3 and 4).

In the present paper, particular attention is given to the issue of hourglass instabilities in the well-known four-node isoparametric element.

*This work was supported by NASA Lewis Research Center under Grant NAG3-329.

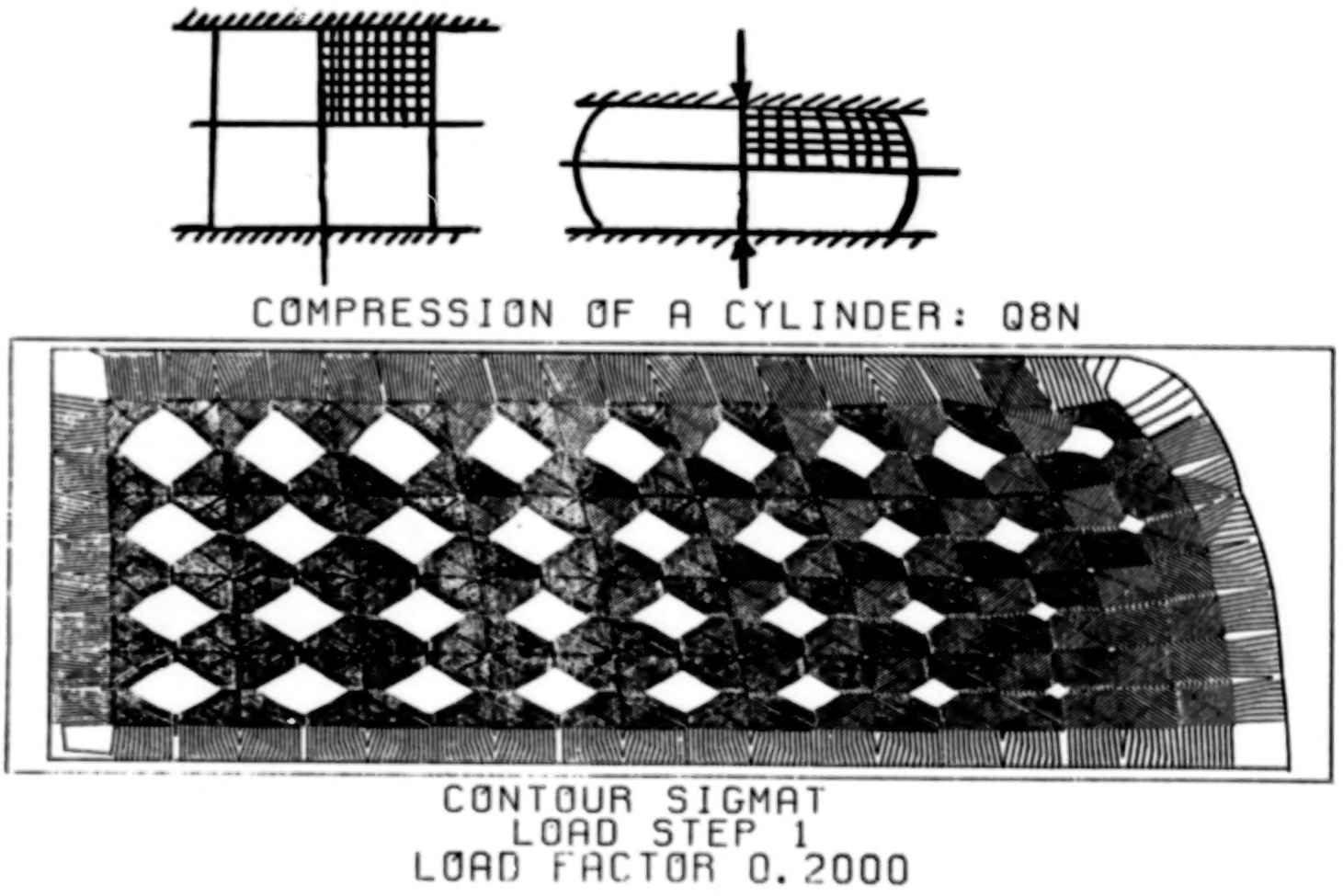


ORIGINAL PAGE IS
OF POOR QUALITY



Figure 1. Computed stress profiles in a compressed incompressible hyperelastic cylinder showing actual spurious checkerboard modes.

ORIGINAL PAGE IS
OF POOR QUALITY

## STUDY OF A MODEL PROBLEM

To focus on some key features of hourglass instabilities, it suffices to consider a model boundary-value problem defined as follows:

$$\left.\begin{aligned} &\text{Find a function } u \in H^1(\Omega) \text{ such that} \\ &\quad a(u,v) = (f,v) \quad \text{for all } v \text{ in } H^1(\Omega) \end{aligned}\right\} \tag{1}$$

where

$$\left.\begin{aligned} a(u,v) &= \int_\Omega \nabla u \cdot \nabla v \, dxdy \\ (f,v) &= \int_\Omega fv \, dxdy \end{aligned}\right\} \tag{2}$$

Here $\Omega$ is a smooth bounded domain in the x,y-plane, $f$ is a smooth function defined on $\Omega$, $a(\cdot,\cdot)$ is a continuous bilinear form defined on the usual space $H^1(\Omega)$ of functions with $L^2$-first derivatives, and $(\cdot,\cdot)$ denotes the $L^2$-inner product. For simplicity, $\Omega$ will generally be taken as rectangular. Problem (1), of course, is a variational statement of the Neumann problem,

$$-\Delta u = f \text{ in } \Omega, \qquad \frac{\partial u}{\partial n} = 0 \text{ on } \partial\Omega$$

We next construct a standard, conforming, finite element approximation of (1) on a uniform mesh of $Q_1$-elements-(four node elements with bilinear shape functions), the length of the sides of each element being $h$. The approximate problem is then

$$\left.\begin{aligned} &\text{Find } u_h \in H^h \subset H^1(\Omega) \text{ such that} \\ &\quad a(u_h, v_h) = (f,v_h) \quad \text{for all } v_h \text{ in } H^h \end{aligned}\right\} \tag{3}$$

where

$$H^h = \{v_h \in C^0(\bar{\Omega}) \,|\, v_h|_{\Omega_e} \in Q_1(\Omega_e)\} \tag{4}$$

To evaluate $a(u_h,v_h)$ in (3), we use a Gaussian quadrature rule of the type,

$$a(u_h,v_h) = \sum_{e=1}^{E} \sum_{j=1}^{G} w_j^e u_h(\xi_j^e) v_h(\xi_j^e) \tag{5}$$

where

E = the total number of elements in the mesh

G = the number of Gauss points ($G \geq 4$)

$w_j^e$ = quadrature weights of element $e$ $(1 \leq j \leq 4)$

$\xi_j^e$ = Gaussian quadrature points for element $e$ $(1 \leq j \leq 4)$

Similarly, $(f,v_h)$ may also be computed by Gaussian quadrature -- exactly whenever $f$ is a polynomial. In this way, we are led to the usual discrete system,

$$\underset{\sim}{K}\underset{\sim}{U} = \underset{\sim}{F} \tag{6}$$

where $\underset{\sim}{K}$ is the stiffness matrix, $\underset{\sim}{U}$ the vector of unknown nodal displacements, and $\underset{\sim}{F}$ is the load vector.

Now instead of using (3), we wish to employ an underintegrated bilinear form

$$a_h(u_h,v_h) = \sum_e w_e u_h(\hat{\xi}_e) v_h(\hat{\xi}_e) \tag{7}$$

with $\hat{\xi}_e$ the centroid of element $e$, corresponding to the use of only one integration point. Then we consider the problem

$$\left.\begin{array}{l} \text{Find } \bar{u}_h \in H^h \text{ such that} \\ a_h(u_h,v_h) = (f_h,v_h) \text{ for all } v_h \text{ in } H^h \end{array}\right\} \tag{8}$$

where $f_h$ is an approximation of $f$ to be defined later. This leads to the new discrete problem

$$\underset{\sim}{\bar{K}}\underset{\sim}{\bar{U}} = \underset{\sim}{\bar{F}} \tag{9}$$

where $\underset{\sim}{\bar{F}}$ is a modification of $\underset{\sim}{F}$ (defined below) designed so as to belong to the range of the new underintegrated stiffness matrix $\underset{\sim}{\bar{K}}$.

The major questions are:

1. What is the relationship between $\underset{\sim}{U}$ and $\underset{\sim}{\bar{U}}$ (if any)?
2. Will $\bar{u}_h$ converge to $u$ as $h$ tends to zero? If not, what can be done to enhance the quality of the underintegrated approximation $\bar{u}_h$?

We shall provide an explicit answer to (1) and, while $\bar{u}_h$ may not converge, we shall show that $u_h$ can be obtained from $\bar{u}_h$ by a simple post-processing operation!

## HOURGLASS MODES

We note that (for smooth enough $u$ and $v$)

$$a(\underset{\sim}{u},\underset{\sim}{v}) = -\int_\Omega \Delta u v \, dxdy + \oint_{\partial\Omega} \frac{\partial u}{\partial n} v \, ds \equiv \langle Au, v \rangle \tag{10}$$

ORIGINAL PAGE IS
OF POOR QUALITY

and ker A = {1} (i.e., the solution to the model problem can be determined only to within an arbitrary constant). Likewise, ker $\bar{K}$ = {(1,1,...,1)}. However, the underintegration of $a(\cdot,\cdot)$ enlarges the kernel of A . Indeed,

$$\ker \underset{\sim}{\bar{K}} = \{\underset{\sim}{H},\underset{\sim}{1}\} \tag{11}$$

where $\underset{\sim}{1} = (1,1,\ldots,1)$ and $\underset{\sim}{H}$ is an *hourglass mode*. In particular, for a typical element e ,

$$\left.\begin{aligned} \underset{\sim e}{\bar{K}}\underset{\sim}{h} = \underset{\sim}{0},\ \underset{\sim e}{\bar{K}}\underset{\sim}{1} = \underset{\sim}{0},\ \underset{\sim}{h}^T = \{1,\ -1,\ 1,\ -1),\\ \underset{\sim}{1}^T = \{1,1,1,1)\end{aligned}\right\} \tag{12}$$

Thus, *the presence of hourglassing modes arises from the failure of the underintegrated stiffness to adequately model the kernel of the operator defining the given boundary-value problem.*

Our first result in the direction of studying the hourglass mode is recorded as follows:

Lemma 1. Let $a'(\cdot,\cdot)$ denote the bilinear form

$$a' = a - a_h \tag{13}$$

where $a(\cdot,\cdot)$ is defined in (2) and $a_h(\cdot,\cdot)$ is the underintegrated bilinear form appearing in (7). Let $H \in \ker A$ be a (global) hourglass mode, i.e.

$$a_h(H,v_h) = 0 \quad \text{for all } v_h \text{ in } H^h \tag{14}$$

Then

$$a'(H,w_h) = 0 \quad \text{for all } w_h \text{ in } (\ker A_h)^{\perp} \tag{15}$$

where $(\ker A_h)^{\perp}$ is the orthogonal complement of those functions $v_h$ such that $a_h(v_h,\tilde{v}_h) = 0$ for all $\tilde{v}_h \in H^h$ . □

Details of the proof of this and several related results shall be the subject of a later paper. It is sufficient to note here that for any $v_h$ we may take the projection into $\ker A_h$ as

$$(H,v_h)\ \frac{H}{(H,H)}\ , \qquad H \in \ker A_h$$

Thus, a typical function $w_h \in (\ker A_h)^{\perp}$ is of the form

$$w_h = v_h - \frac{(H,v_h)}{(H,H)}\ H \tag{16}$$

and one can show from this that (15) holds.

ORIGINAL PAGE IS
OF POOR QUALITY

It is clear from (16) that every $v_h \in H^h$ is of the form

$$v_h = w_h + \lambda H \,, \quad w_h \in (\ker A_h)^{\perp}, \ \lambda \in \mathbb{R}$$

Hence,

$$a(u_h,v_h) = a_h(u_h,w_h) + \lambda a'(u_h,H)$$

$$= \lambda(f,H) + (f,w_h)$$

so that

$$a'(u_h,H) = (f,H) \qquad H = \text{hourglass mode} \tag{17}$$

$$a\,(u_h,w_h) = (f,w_h) \qquad \text{for all } w_h \in (\ker A_h) \tag{18}$$

Since $w_h$ can be given by (16),

$$(f,w_h) = (f - \frac{(f,H)}{(H,H)}\, H,\ v_h)$$

and, therefore,

$$a_h(\bar{u}_h,v_h) = (f,v_h) - \frac{(f,H)}{(H,H)}\,(H,v_h)$$

$$\text{for all } v_h \in H^h \tag{19}$$

Hence, in (8) we take as $f_h$ the projection,

$$f_h = f - \frac{(f,H)}{(H,H)}\, H \tag{20}$$

From (18), we have

$$a_h(u_h,w_h) = (f,w_h) - a'(u_h,w_h)$$

$$a_h(u_h,v_h) = (f_h,v_h) - a'(u_h,w_h)$$

$$= a_h(\bar{u}_h,v_h) - a'(u_h,w_h)$$

Thus,

ORIGINAL PAGE IS
OF POOR QUALITY

$$a_h(u_h - \bar{u}_h, v_h) = -a'(u_h, w_h)$$

$$= -a'(u_h, v_h) + \frac{(v_h, H)}{(H,H)}\, a'(u_h, H) \tag{21}$$

This result seems to imply that $u_h$ and $\bar{u}_h$ *do not differ by an hourglassing mode*, else the right hand side of (21) would be zero. Thus, the procedures usually used to correct underintegrated solutions (by adding multiples of H) may not improve solutions. This issue is currently being explored and requires much further study.

## CALCULATION OF STIFFNESS MATRICES

Confining our attention to a unit $Q_1$ element, we introduce the matrices

$$\left.\begin{aligned}
&\underset{\sim}{s}^T = \{1,-1,-1,1\}\ ,\ \underset{\sim}{s}'^T = \{1,1,-1,-1\} \\
&\underset{\sim}{h}^T = \{1,-1,1,-1\}\ ,\ \underset{\sim}{1}^T = \{1,1,1,1\} \\
&\underset{\sim}{x}^T = \{x^1,x^2,x^3,x^4\}\ ,\ \underset{\sim}{y}^T = \{y^1,y^2,y^3,y^4\} \\
&\underset{\sim}{b}_1^T = \tfrac{1}{2}\{y_2-y_4,\ y_3-y_1,\ y_4-y_2,\ y_1-y_3\} \\
&\underset{\sim}{b}_2^T = \tfrac{1}{2}\{x_4-x_1,\ x_1-x_3,\ x_2-x_4,\ x_3-x_1\}
\end{aligned}\right\} \tag{22}$$

where $x_i, y_i$ = coordinates of node $i$, $i = 1,2,3,4$. We no longer confine ourselves to a uniform rectangular mesh. If $(\xi,\eta)$ denote coordinates of a unit master $Q_1$-element, then the stiffness matrix $\underset{\sim}{K}_e$ of a typical finite element can be shown to be given by

$$\underset{\sim}{K}_e = \int_{\hat{\Omega}} \left( \frac{\underset{\sim\sim\sim}{A}\underset{\sim}{x}\underset{\sim}{x}^T\underset{\sim}{A}^T}{\underset{\sim}{y}^T\underset{\sim\sim}{A}\underset{\sim}{x}} + \frac{\underset{\sim\sim\sim}{A}\underset{\sim}{y}\underset{\sim}{y}^T\underset{\sim}{A}^T}{\underset{\sim}{y}^T\underset{\sim\sim}{A}\underset{\sim}{x}} \right) d\xi d\eta \tag{23}$$

($\hat{\Omega}$ = unit square)

$$\underset{\sim\sim}{A} = \frac{1}{4}(\underset{\sim}{s}'\underset{\sim}{s}^T - \underset{\sim\sim}{s}\underset{\sim}{s}'^T) + \frac{\xi}{2}(\underset{\sim\sim}{s}\underset{\sim}{h}^T - \underset{\sim}{h}\underset{\sim}{s}^T) + \frac{\eta}{2}(\underset{\sim\sim}{h}\underset{\sim}{s}'^T - \underset{\sim}{s}'\underset{\sim}{h}^T) \tag{24}$$

whereas the underintegrated (one-point) stiffness matrix is

$$\underset{\sim}{K}_e^{(1)} = \frac{1}{|\Omega_e|}\ (\underset{\sim}{b}_1\underset{\sim}{b}_1^T + \underset{\sim}{b}_2\underset{\sim}{b}_2^T) \tag{25}$$

ORIGINAL PAGE IS
OF POOR QUALITY

and $|\Omega_e|$ denotes the area of the element. The rank deficiency of $\underset{\sim}{K}_e^{(1)}$ follows immediately from the fact that

$$\underset{\sim}{b}_i^T\underset{\sim}{h} = \underset{\sim}{0}\ , \quad \underset{\sim}{b}_i^T\underset{\sim}{1} = \underset{\sim}{0}\ , \quad i = 1,2 \tag{26}$$

*Our goal here is to compute exactly* $\underset{\sim}{K}$ *(or* $\underset{\sim}{K}_e$*) from* $\underset{\sim}{K}^{(1)}$ *(or* $\underset{\sim}{K}_e^{(1)}$*) by a simple post-processing operation.* That this is possible follows from the fact that

$$\underset{\sim}{h}^T\underset{\sim}{K}_e\underset{\sim}{h} = 16\,\bar{\varepsilon} \tag{27}$$

$$\underset{\sim}{K}_e = \underset{\sim}{K}_e^{(1)} + \bar{\varepsilon}\,\underset{\sim}{\gamma}\underset{\sim}{\gamma}^T \tag{28}$$

where

$$\underset{\sim}{\gamma} = \underset{\sim}{h} - \frac{1}{|\Omega_e|}\,(\underset{\sim}{h}^T\underset{\sim}{x}\,\underset{\sim}{b}_1 - \underset{\sim}{h}^T\underset{\sim}{y}\,\underset{\sim}{b}_2) \tag{29}$$

$$\bar{\varepsilon} = \frac{1}{4}\int_{\hat{\Omega}} \frac{(\xi\,\underset{\sim}{s}^T\underset{\sim}{x} - \eta\underset{\sim}{s}'^T\underset{\sim}{x})^2 + (\xi(\underset{\sim}{s}^T\underset{\sim}{y} - \eta(\underset{\sim}{s}'^T\underset{\sim}{y}))^2}{|\Omega_e| + \xi A_o + \eta B_o}\,d\xi d\eta \tag{30}$$

and

$$A_o = (y_4-y_3)(x_1-x_2) + (y_1-y_2)(x_3-x_4)$$

$$B_o = (y_3-y_2)(x_1-x_4) + (y_1-y_4)(x_2-x_3)$$

Note that for parallelograms, $\bar{\varepsilon} = [(x_1-x_3)^2 + (x_2-x_4)^2 + (y_1-y_3)^2 + (y_2-y_4)^2]/24|\Omega_e|$ whereas for rectangular elements of diameter $h_e$, $\bar{\varepsilon} = h_e^2/12|\Omega_e|$.

The difference matrix,

$$\underset{\sim}{K}_e^1 = \underset{\sim}{K}_e - \underset{\sim}{K}_e^{(1)} \tag{31}$$

can be written

$$K_e^1 = \frac{1}{3}\,\frac{\underset{\sim}{h}\,\underset{\sim}{h}^T}{\|\underset{\sim}{h}\|^2} \tag{32}$$

Upon assembly, we obtain systems

ORIGINAL PAGE IS
OF POOR QUALITY

$$\underset{\sim}{K}\underset{\sim}{U} = \underset{\sim}{F}, \quad \underset{\sim}{K}^{(1)}\underset{\sim}{U} = \overline{\underset{\sim}{F}} \tag{33}$$

$$\overline{\underset{\sim}{F}} = \underset{\sim}{F} - \underset{\sim}{F}^{T}\hat{\underset{\sim}{H}}\hat{\underset{\sim}{H}} \tag{34}$$

in analogy with (3) and (8), respectively. In analogy with (21),

$$\underset{\sim}{K}^{(1)}(\underset{\sim}{U}-\overline{\underset{\sim}{U}}) = \frac{1}{3}\sum_{e} \underset{\sim e}{u}(\underset{\sim e}{h}^{T}\hat{\underset{\sim}{H}}\hat{\underset{\sim}{H}} - \underset{\sim e}{h}/\|\underset{\sim}{H}\|) \tag{35}$$

where $\underset{\sim e}{u} = \underset{\sim e}{h}^{T}\underset{\sim}{U}/\|\underset{\sim}{h}^{e}\|$ and $\hat{\underset{\sim}{H}} = \underset{\sim}{H}/\|\underset{\sim}{H}\|$. We can use this result to show that

$$\|\underset{\sim}{K}^{(1)}(\underset{\sim}{U}-\overline{\underset{\sim}{U}})\| \leq \|\underset{\sim}{K}'\underset{\sim}{U}\| \tag{36}$$

Thus, the success of the underintegration method will again depend upon how small one can make the norm $\|K'U\|$. This issue is to be the subject of a forthcoming paper.

## CONCLUSIONS

1) The fully integrated and underintegrated finite element approximations apparently do not differ by an hourglassing mode. Thus, the introducing of orthogonal hourglassing corrections may not be sufficient to produce acceptable solutions from underintegrated solutions. This subject requires further study.

2) On the other hand, it is possible to generate exactly the fully integrated stiffness matrix from the underintegrated stiffness matrix using fairly simple post-processing operations. An exact formula for such calculations has been presented in equation (30).

## REFERENCES

1. Flannagan, D.P. and Belytschko, T., "A Uniform Strain Hexahedron and Quadrilateral with Orthogonal Hourglass Control," International Journal of Numerical Methods in Engineering, Vol. 17, 1981, 679-706.

2. Oden, J.T., Kikuchi, N., and Song, Y.J., "Penalty-Finite Element Methods for the Analysis of Stokesian Flows," Computer Methods in Applied Mechanics and Engineering, Vol. 31, 1982, 297-329.

3. Oden, J.T. and Kikuchi, N., "Finite Element Methods for Constrained Problems in Elasticity," International Journal of Numerical Methods in Engineering, Vol. 18, 1982, 701-725.

4. Oden, J.T. and Jacquotte, O., "Stable Second-Order Accurate Finite Element Scheme for the Analysis of the Two-Dimensional Incompressible Viscous Flows," Finite Elements in Fluids, Vol. V, edited by J.T. Oden et al., John Wiley & Sons, Ltd., London (to appear).

5. Oden, J.T. and Jacquotte, O., "Stability of Some RIP Finite Element Methods for Stokesian Flows," TICOM Report 82-8, Austin, 1982.

N84
31697

UNCLAS

N84 31697

# INELASTIC AND DYNAMIC FRACTURE, AND STRESS ANALYSES*

Satya N. Atluri
Georgia Institute of Technology

## SUMMARY

The current work of the author and his students in the areas of (*i*) large deformation inelastic stress analysis, (*ii*) inelastic and dynamic crack propagation, is summarized. The salient topics of interest in engine structure analysis that are discussed herein include: (a) a new path-independent integral ($\dot{T}$) in inelastic fracture mechanics, (b) analysis of dynamic crack propagation, (c) generalization of constitutive relations of inelasticity for finite deformations, (d) complementary energy approaches in inelastic analyses, and (e) objectivity of time integration schemes in inelastic stress analysis.

## INELASTIC FRACTURE MECHANICS

The most widely researched topic in elastic-plastic fracture mechanics, in the past decade or so, and one that has made certain impressive advances in ductile fracture mechanics, has been the now well-known J integral (refs. 1,2). It is also well known that J is in fact the component along the crack-line of a vector integral, and its significance is in the context of incipient self-similar growth of a crack in a (nonlinear) *elastic* material. In this case, J has the meaning of the rate of energy-release per unit of crack extension. In deformation theory of plasticity, which precludes unloading and which is mathematically equivalent to a nonlinear theory of elasticity, J still characterizes the crack-tip field and is still a path-independent integral. However, in this case, J does not have the meaning of energy-release rate; it is simply the total potential-energy difference between two identical and identically loaded cracked bodies which differ in crack lengths by a differential amount. However, in a flow theory of plasticity, even under monotonic loading, the path-independence of J cannot be theoretically established. Also, under *arbitrary load histories*, which may include loading and unloading, J is not only not path independent, but also it does not have any physical meaning.

Also, a significant amount of crack growth in a ductile material is necessarily accompanied by a significant non-proportional plastic deformation which invalidates the deformation-theory of plasticity. Thus, theoretically the validity of J is questionable under these circumstances. However, for *limited amounts* of crack-growth, it has been argued (ref. 3) that the strain field undergoes a proportional increment due to an increment in applied loading and that J is still a controlling parameter. For such situations of J-controlled growth, the concepts of a tearing modulus and J-resistance curves have been introduced (ref. 4) to analyze the stability of such growth. Using the above concepts, and the related concept of CTOA, engineering approaches to elastic-plastic fracture analyses were elaborated upon in references 5 and 6.

*Some results of research supported under NASA grant NAG3-346.



PRECEDING PAGE BLANK NOT FILMED

Thus, further research is necessary to understand the mechanics of growth initiation of cracks in elastic-plastic materials subject to arbitrary loading/unloading histories. Also, more-theoretically-valid parameters/criteria are necessary to analyze situations wherein there may be substantial amounts of stable crack-growth which are no longer within the limits of J-controlled growth.

Turning to the problem of crack growth in structures operating at elevated temperatures — the so-called problem of creep crack-growth, numerous experiments have recently been undertaken (refs. 7,8 for example) with the purpose of finding a parameter which may correlate with the creep crack-propagation rate. Most of these investigators considered as candidate parameters, $K_I$, some form of net section stress, or in more recent studies, $C^*$. The parameter $C^*$ has been introduced in reference 9 and is valid only in pure steady-state creep ($\dot{\varepsilon} \sim \sigma^n$). This situation is characterized by: (*i*) the body being essentially at steady-state creep conditions which implies very slow crack propagation and (*ii*) the creep-damage process zone being local to and therefore controlled by the crack-tip field. However, suppose a particular material and geometry result in a crack-propagation rate such that elastic strains are not negligible compared to creep rates (ie., non-steady creep) and that at the same time, creep strains are no longer localized to the crack-tip region. While $C^*$ is not a valid parameter for this case, it appears reasonable to expect that crack growth rate is still determined by the local crack-tip field since the creep damage process zone is still assumed to be local to the crack-tip. Further, even though $C^*$ is a path-independent integral at steady-state creep conditions, it does not seem to have any physical meaning even under such conditions. These and other difficulties with $C^*$ have been noted in recent literature (refs. 7, 8). Thus, there is a need to explore alternatives to $C^*$ which remain valid even under non-steady creep conditions, which are path-independent integrals and which have a well-defined physical meaning so that they may be measured in laboratory specimens in an unambiguous manner.

With the above objectives, the author has studied (ref. 10) certain path-independent integrals, of relevance in the presence of cracks, in nonlinear elastic and inelastic solids. The hypothesized material properties included: (*i*) finite and infinitesimal elasticity, (*ii*) rate-independent incremental flow theory of plasticity, and (*iii*) rate-sensitive behavior including viscoplasticity and creep. In each case, finite deformations were considered, along with the effects of body forces, material acceleration, and arbitrary traction/displacement conditions on the crack front. Also, the physical interpretations of each of the integrals either in terms of crack-tip energy release rates or simply the energy-rate differences in two comparison cracked bodies were explored. Several differences between the presently obtained results and those considered well established in literature were pointed out and discussed.

We omit the mathematical details of the development but present here the end results for incremental, path-independent, vector integrals which are of relevance in ductile fracture mechanics under arbitrary load histories. Further, for simplicity, we consider: (*i*) quasi-static crack growth initiation and stable crack growth and (*ii*) the deformations to be small, so that the distinctions between various stress measures disappear. Consider a generic increment of external load (load-control) from an initial state with stresses $\underline{\underline{T}}$ and initial displacements $\underline{u}$. Let the incremental stresses be $\Delta\underline{\underline{T}}$ and the incremental displacements be $\Delta\underline{u}$. We consider two paths $\Gamma_1$ and $\Gamma_2$ surrounding the crack-tip. We allow the incremental potential $\Delta U$ for $\Delta\underline{\underline{T}}$ to be an explicit function of the location of the material particle through parameters $\alpha$ (which can be 1 for plastic loading and 0 for elastic unloading) and

ORIGINAL PAGE IS
OF POOR QUALITY

g (the strain-hardening parameter). Thus, there can be plastic loading/or elastic unloading from a plastic state/or pure elastic-loading taking place arbitrarily near the crack-tip as well as elsewhere in the body. Then it has been shown (refs. 10,11) that the following path-independent integrals prevail:

$$(\Delta \underline{T})_p = \int_{\Gamma_1+\Gamma_c} [\underline{\tau}:\Delta \underline{e} + \Delta U)\underline{N} - \underline{N}\cdot\underline{\tau}\cdot\Delta \underline{e} - \underline{N}\cdot\Delta\underline{\tau}\cdot\underline{e}]ds$$

$$+ \int_{V_t-V_1} [\underline{\nabla\tau} + \tfrac{1}{2}\underline{\nabla}\Delta\underline{\tau}):\Delta\underline{\varepsilon} - (\underline{\nabla\varepsilon} + \tfrac{1}{2}\underline{\nabla}\Delta\underline{\varepsilon}):\Delta\underline{\tau}]dv$$

$$= \int_{\Gamma_2+\Gamma_c} [(\underline{\tau}:\Delta \underline{e} + \Delta U)\underline{N} - \underline{N}\cdot\underline{\tau}\cdot\Delta \underline{e} - \underline{N}\cdot\Delta\underline{\tau}\cdot\underline{e}]ds$$

$$+ \int_{V_t-V_2} [(\underline{\nabla\tau} + \tfrac{1}{2}\underline{\nabla}\Delta\underline{\tau}):\Delta\underline{\varepsilon} - (\underline{\nabla\varepsilon} + \tfrac{1}{2}\underline{\nabla}\Delta\underline{\varepsilon}):\Delta\underline{\tau}]dv \qquad (1)$$

$$\text{and } (\Delta \underline{T}^*)_p = \int_{\Gamma_\varepsilon} [(\underline{\tau}:\Delta \underline{e} + \Delta U)\underline{N} - \underline{N}\cdot\underline{\tau}\cdot\Delta \underline{e} - \underline{N}\cdot\Delta\underline{\tau}\cdot\underline{e}]ds$$

$$= \int_{\Gamma} [(\underline{\tau}:\Delta \underline{e} + \Delta U)\underline{N} - \underline{N}\cdot\underline{\tau}\cdot\Delta \underline{e} - \underline{N}\cdot\Delta\underline{\tau}\cdot\underline{e}]ds$$

$$+ \int_{V-V_\varepsilon} [\Delta\underline{\tau}:(\underline{\nabla\varepsilon} + \tfrac{1}{2}\underline{\nabla}\Delta\underline{\varepsilon}) - \Delta\underline{\varepsilon}:(\underline{\nabla\tau} + \tfrac{1}{2}\underline{\nabla}\Delta\underline{\tau})]dv \qquad (2)$$

In the above $V_t$ is the total volume of the cracked body, $V_1$ and $V_2$ are the volumes enclosed by $\Gamma_1$ and $\Gamma_2$, $\Gamma_\varepsilon$ is a path arbitrarily close to the crack-tip, and $V_\varepsilon$ is the volume enclosed by $\Gamma_\varepsilon$. It can be shown (ref. 11) that path-independence in the sense of equations (1,2) prevails even when there is arbitrary loading/unloading occuring in $V_1$ and $V_2$ and thus between $V_2$ and $V_1$. In the above, $(\underline{\ })\cdot(\underline{\ })$ implies a tensor inner product and $(\underline{\ }):(\underline{\ })$ implies a trace (see ref. 10 for details). It has been shown (ref. 11) that in Mode I, $(\Delta T_1)_p$ has the meaning: (*i*) it is the incremental area corresponding to an incremental load between the load-deflection curves of two identical and identically loaded cracked bodies with crack lengths differing by a differential amount, (*ii*) this physical meaning remains valid in loading as well as unloading, and (*iii*) under monotonic loading when near-proportionality prevails near the crack-tip, $\Sigma\Delta T_p = J$ (the summation is for all increments of loading, using rate theory of plasticity). In reference 11, a numerical experiment was also discussed wherein a compact tension specimen was loaded to a certain load level, unloaded to a compressive load, and reloaded again. The observations are: (*i*) during loading $\Sigma(\Delta T_1)_p = J$ and (*ii*) $(\Delta T_1)_p$ remains strictly path-independent even for subsequent unloading and reloading, whereas, J not only has no meaning during unloading, but its numerical value varies widely (±50%) over different paths.

Thus, while much further work remains to be done, it is evident that the integrals in equations (1,2) provide a theoretical basis for elastic-plastic fracture

mechanics under arbitrary loading and when the material behavior is characterized by realistic rate theories as opposed to a simple deformation theory. Analogous derivations of path-independent incremental vector integral $(\Delta \underline{T})_c$ valid in *general unsteady creep*, and a discussion of its merits as compared to the $C^*$ integral, have been presented elaborately by Stonesifer and Atluri (refs. 12-14).

## DYNAMIC FRACTURE MECHANICS

We first consider linear elastodynamic crack propagation in a self-similar fashion. Consider, for instance, a two-dimensional problem. Let the velocity of crack propagation be denoted by the vector $\underline{C}$, with modulus C. Consider a small loop $\Gamma_\varepsilon$, of radius $\varepsilon$, centered around the crack-tip at time t, and assume that the crack-tip moves by an amount $(dt\underline{C})$ into $\Gamma_\varepsilon$ at time t+dt, ie., $\varepsilon > Cdt$ without loss of generality. Let the unit outward normal to $\Gamma_\varepsilon$ be $\underline{N}$, and let the kinetic energy density be $T(= \frac{1}{2}\rho \underline{v}\cdot\underline{v}$, where $\underline{v}$ is the absolute velocity of a material particle and $\rho$ the mass density). Note that $\underline{v}$ is singular near the propagating crack-tip. From studies in reference 10, it is seen that the rate of energy release rate G per unit of elastodynamic crack growth is given by:

$$G = (1/C) \lim_{\varepsilon \to 0} \underline{C}\cdot\int_{\Gamma_\varepsilon} [(W+T)\underline{N} - \underline{t}\cdot\underline{e}]d\Gamma = (1/C)\underline{C}\cdot\underline{G} \qquad (3)$$

Now we consider the problem of analyzing crack-propagation in an arbitrary body, the shape of which and the loading on which, we suppose, preclude any possibility of an analytical solution. Suppose that we have to use a numerical solution. Such a numerical solution may be based on a "propagating singular element" within which the asymptotic mixed mode solution is embedded; and hence the K-factors can be evaluated directly, as demonstrated by the author's group (refs. 15-18). However, in order to use a simple numerical procedure, say using distorted (singular) isoparametric finite elements or non-singular isoparametric elements, it is convenient to have available path-independent integrals which have the same meaning as the energy release rate G of equation (3). If so, the integral can be evaluated on a path that is far removed from the crack-tip and hence is insensitive to the details of modeling of crack-tip stress-strain fields.

Such a path-independent integral has been derived based on general conservation laws, as shown in references 10 and 19, and is given below:

$$\underline{J}' = \int_\Gamma [(W+T)\underline{N} - \underline{t}\cdot\underline{e}]d\Gamma + \int_{V-V_\varepsilon} [\rho(\underline{a}-\underline{\bar{F}})\cdot\underline{e} - \underline{\nabla}T]dv$$

$$+ \int_{\Gamma_c} [(W^+-W^-)\underline{N}^+ + (T^+-T^-)\underline{N}^+ - \underline{\bar{t}}\cdot\underline{e}]d\Gamma = \underline{G} \qquad (4)$$

where (+) and (-) refer, arbitrarily, to the "upper" and "lower" crack faces; $\underline{N}^+ = -\underline{N}^-$ is the unit normal to $\Gamma_c^+$; and $\underline{\bar{t}}$ are prescribed tractions on the crack face.

The practical application of the above new path-independent integral has been demonstrated in references 20 and 21.

## GENERALIZATION OF CONSTITUTIVE RELATIONS TO FINITE DEFORMATIONS

At a symposium on finite strain plasticity held at Stanford University in 1981, Nagtegaal and de Jong (ref. 22) presented some interesting results for stresses generated by simple shear of elastic-plastic and rigid-plastic materials which exhibit anisotropic hardening. In the equation for the rate of change of the shift tensor $\underset{\sim}{\alpha}$, they used the Zaremba-Jaumann-Noll rigid body rate of $\underset{\sim}{\alpha}$. They found the rather spurious result that the shear stress is oscillatory in time.

The above 'anamoly' has prompted a series of investigations by Lee and his associates (refs. 23,24). As a 'remedy', Lee et al. (refs. 23,24) suggest the use of a 'modified' Jaumann derivative of $\underset{\sim}{\alpha}$ in the evolution equation for $\underset{\sim}{\alpha}$. While the use of such a modified derivative in the specific problem of simple shear has been illustrated in references 23 and 24, its generalization to three-dimensional, non-homogeneous cases is not yet fully developed. It has been suggested in reference 23 that "a complete investigation of the micro-mechanics and the structures of possible macroscopic constitutive relations will no doubt be needed to fully understand this phenomenon and to generate a fully-tested theory".

Recently the author has shown (ref. 25) that the anamolies as described above are not peculiar to the anisotropic plasticity alone; similar behaviour in finite shear may result even in the case of hypo-elasticity and classical isotropic-hardening plasticity theory. Thus, in reference 25, the central problem of 'generalizing' to the finite deformation case, of the constitutive relations of infinitesimal strain theories of elasticity (hypoelasticity), and of classical plasticity with isotropic or kinematic hardening was discussed in detail. It has been shown in reference 25 that the current controversies surrounding the choice of stress rate in the finite-strain generalizations of the constitutive relations and the anamolies surrounding the kinematic hardening plasticity theory are easily resolvable.

Here we briefly illustrate the case of kinematic hardening plasticity. In this case, considering a simple $J_2$ theory, the current yield surface can be represented by:

$$f = (\underset{\sim}{\sigma}' - \underset{\sim}{\alpha}'):(\underset{\sim}{\sigma}' - \underset{\sim}{\alpha}') - \frac{2}{3}\bar{\sigma}^2 = 0 \tag{5}$$

where $(_)'$ denotes the deviator of a tensor, $\underset{\sim}{\sigma}$ is the Kirchhoff stress tensor, and $\underset{\sim}{\alpha}$ is the back stress. The normality condition is:

$$\underset{\sim}{\varepsilon}^P = \lambda(\partial f/\partial \underset{\sim}{\sigma}) \tag{6}$$

We define, as in reference 25, generalized 'objective' rates, $\overset{*}{\underset{\sim}{\sigma}}$ and $\overset{*}{\underset{\sim}{\alpha}}$ of $\underset{\sim}{\sigma}$ and $\underset{\sim}{\alpha}$ respectively, as follows:

$$\dot{\underline{\sigma}}^{*} = \dot{\underline{\sigma}}^{0} - \gamma_7(\underline{\sigma}\cdot\underline{\varepsilon}) - \gamma_8(\underline{\varepsilon}\cdot\underline{\sigma}) \tag{7}$$

and $$\dot{\underline{\alpha}}^{*} = \dot{\underline{\alpha}}^{0} - \gamma_7(\underline{\alpha}\cdot\underline{\varepsilon}) - \gamma_8(\underline{\varepsilon}\cdot\underline{\alpha}) \tag{8}$$

where $\dot{\underline{\sigma}}^{0}$ can be any one of the currently-used stress-rates. For instance,

$$\dot{\underline{\sigma}}^{0} = \dot{\underline{\sigma}}^{m} - \underline{e}\cdot\underline{\sigma} - \underline{\sigma}\cdot\underline{e}^{T} \qquad \text{(Oldroyd)} \tag{9}$$

$$\dot{\underline{\sigma}}^{0} = \dot{\underline{\sigma}}^{m} + \underline{e}^{T}\cdot\underline{\sigma} + \underline{\sigma}\cdot\underline{e} \qquad \text{(Cotter-Rivlin)} \tag{10}$$

$$\dot{\underline{\sigma}}^{0} = \dot{\underline{\sigma}}^{m} - \underline{e}\cdot\underline{\sigma} + \underline{\sigma}\cdot\underline{e} \qquad \text{(mixed-1)} \tag{11}$$

$$\dot{\underline{\sigma}}^{0} = \dot{\underline{\sigma}}^{m} + \underline{e}^{T}\cdot\underline{\sigma} - \underline{\sigma}\cdot\underline{e}^{T} \qquad \text{(mixed-2)} \tag{12}$$

$$\dot{\underline{\sigma}}^{0} = \dot{\underline{\sigma}}^{m} + \underline{\sigma}\cdot\underline{\omega} - \underline{\omega}\cdot\underline{\sigma} \qquad \text{(Zaremba-Jaumann-Noll)} \tag{13}$$

In equations (7-13), $\underline{e}$ is the velocity gradient, $\underline{\varepsilon}$ the strain-rate, $\underline{\omega}$ is the spin, and $\dot{\underline{\sigma}}^{m}$ is the non-objective material rate. Since, for a classical continuum without body couples, the material rate $\dot{\underline{\sigma}}^{m}$ should be symmetric, the generalized stress rates $\dot{\underline{\sigma}}^{*}$ and $\dot{\underline{\alpha}}^{*}$ are defined in reference 25, such that:

$$\mu_7 = \gamma_7 = \gamma_8 \qquad \text{if } \dot{\underline{\sigma}}^{0} \text{ is that of Zaremba-Jaumann-Noll} \tag{14}$$

$$\mu_7 = (\gamma_7+1) = (\gamma_8+1) \qquad \text{if } \dot{\underline{\sigma}}^{0} \text{ is that of Oldroyd} \tag{15}$$

$$\mu_7 = (\gamma_7-1) = (\gamma_8-1) \qquad \text{if } \dot{\underline{\sigma}}^{0} \text{ is that of Cotter-Rivlin} \tag{16}$$

$$\mu_7 = (\gamma_7-1) = (\gamma_8+1) \qquad \text{if } \dot{\underline{\sigma}}^{0} \text{ is that of mixed-1} \tag{17}$$

$$\mu_7 = (\gamma_8-1) = (\gamma_7+1) \qquad \text{if } \dot{\sigma}^{0} \text{ is that of mixed-2} \tag{18}$$

The linear kinematic hardening theory of Prager, as generalized to finite deformations, states that:

$$\dot{\underline{\alpha}}^{*} = c\underline{\varepsilon}^{P} \tag{19}$$

where c is a constant of proportionality. It can be shown (ref. 25) that the plastic strain-rate can be written, for the yield function given in equation (5), as:

$$\underset{\sim}{\varepsilon}^{P} = \frac{3}{2c\bar{\sigma}^2} [(\underset{\sim}{\sigma}'-\underset{\sim}{\alpha}'):\dot{\underset{\sim}{\sigma}}^{*}](\underset{\sim}{\sigma}'-\underset{\sim}{\alpha}') \tag{20}$$

Using equations (7,8), (14-18), and (20), the material rates $\dot{\underset{\sim}{\sigma}}^{m}$ and $\dot{\underset{\sim}{\alpha}}^{m}$ can be written as:

$$\dot{\underset{\sim}{\alpha}}^{m} = c\underset{\sim}{\varepsilon}^{P} + \underset{\sim}{\omega}\cdot\underset{\sim}{\alpha} - \underset{\sim}{\alpha}\cdot\underset{\sim}{\omega} + \mu_7(\underset{\sim}{\alpha}\cdot\underset{\sim}{\varepsilon} + \underset{\sim}{\varepsilon}\cdot\underset{\sim}{\alpha}) \tag{21}$$

$$\dot{\underset{\sim}{\sigma}}^{m} = 2\mu\underset{\sim}{\varepsilon} + \lambda(\underset{\sim}{\varepsilon}:\underset{\sim}{I})\underset{\sim}{I} - 2\mu\left[\frac{3\mu}{(c+2\mu)\bar{\sigma}^2} [\underset{\sim}{\varepsilon}:(\underset{\sim}{\sigma}'-\underset{\sim}{\alpha}')](\underset{\sim}{\sigma}'-\underset{\sim}{\alpha}')\right]$$

$$+ \underset{\sim}{\omega}\cdot\underset{\sim}{\sigma} - \underset{\sim}{\sigma}\cdot\underset{\sim}{\omega} + \mu_7(\underset{\sim}{\sigma}\cdot\underset{\sim}{\varepsilon} + \underset{\sim}{\varepsilon}\cdot\underset{\sim}{\sigma}) \tag{22}$$

In a finite shear problem, we may prescribe velocities:

$$v_1 = 2\omega x_2 \qquad v_2 = 0 \tag{23}$$

such that the strain-rate $\underset{\sim}{\varepsilon}$ and the spin $\underset{\sim}{\omega}$ are, respectively:

$$\underset{\sim}{\varepsilon} = \begin{bmatrix} 0 & \omega & 0 \\ \omega & 0 & 0 \\ 0 & 0 & 0 \end{bmatrix} \quad \text{and} \quad \underset{\sim}{\omega} = \begin{bmatrix} 0 & \omega & 0 \\ -\omega & 0 & 0 \\ 0 & 0 & 0 \end{bmatrix} \tag{24}$$

Lee et al. (refs. 23,24) consider the case when: (*i*) $\gamma_7$ and $\gamma_8$ are zero in equations (7) and (8); (*ii*) $\mu_7 = 0$ in equations (14,21,22) ie., they consider the case when $\dot{\underset{\sim}{\sigma}}^{0}$ is the Zaremba-Jaumann-Noll rate. The obtained solutions are oscillatory in references (23,24). Thus, the generalization of Lee et al. (ref. 23,24) *is improper.* On the other hand, it has been shown by the author (ref. 25)that if $\mu_7$ is ±1 in equations (21,22), the *obtained solutions for stresses are non-oscillatory.* Furthermore, it is seen that the condition $\mu_7 = \pm 1$ can be satisfied even when any one of the stress-rates as in equations (9-13) are used. The way to do this is *to use the generalized stress-rates* $\dot{\underset{\sim}{\sigma}}^{*}$ *and* $\dot{\underset{\sim}{\alpha}}^{*}$ *as in equations (7,8) and to choose* $\gamma_7$ *and* $\gamma_8$ *as in equations (14-18).*

## COMPLEMENTARY ENERGY APPROACHES IN INELASTIC ANALYSIS

Recently Reed and Atluri (refs. 26-31) presented comprehensive studies of a new hybrid-stress finite element algorithm, suitable for analyses of large, quasistatic,

inelastic deformations. The algorithm is based on a new complementary energy principle for rate type materials given earlier by Atluri (ref. 32). The principal variables in this formulation are the nominal stress-rate and spin, and the resulting finite element equations are discrete versions of the equations of compatibility and angular momentum balance.

The algorithm produces true rates, time derivatives, as opposed to 'increments'. There results a complete separation of the boundary value problem (for stress-rate and velocity) and the initial value problem (for total stress and deformation); hence, their numerical treatments are essentially independent. In references 30-31, a comprehensive discussion of the numerical treatment of the boundary value problem and detailed examination of the initial value problem covering the topics of efficiency, stability, and objectivity were presented. Several problems dealing with homogeneous as well as inhomogeneous large deformations of inelastic materials were solved, and the solutions discussed in detail. In the following, we present a brief outline of the methodology.

The boundary-value problem for the rates of stress and spin is governed by a variational principle corresponding to the stationarity of the functional:

$$\Pi_c(\underline{\omega},\dot{\underline{t}}) = \int_V \{-R(\dot{\underline{t}},\underline{\omega}) - \tfrac{1}{2}\underline{\tau}:(\underline{\omega}\cdot\underline{\omega}) + \dot{\underline{t}}:\underline{\omega}\}dV + \int_{S_v} \underline{n}\cdot\dot{\underline{t}}\cdot\bar{\underline{v}}\ dS \tag{25}$$

where $\underline{\omega}$ is the spin, and $\dot{\underline{t}}$ is the rate of the first-Piola stress as referred to the current configuration. In the above, R is the rate of complementary energy density, $\underline{\tau}$ is the current Cauchy stress, $\bar{\underline{v}}$ are prescribed velocities at the boundary-segment $S_v$ of the solid, $\underline{n}$ is a unit outward normal to $S_v$, and V is the volume of the solid. In equation (25), the following definitions and a priori constraints apply:

$$\underline{\nabla}\cdot\dot{\underline{t}} + \rho\dot{\underline{b}} = 0 \quad \text{in V} \qquad \text{or } \dot{\underline{t}} = \underline{\nabla}\times\underline{\phi} + \dot{\underline{t}}^b \tag{26}$$

$$\underline{n}\cdot\dot{\underline{t}} = \dot{\bar{\underline{T}}} \quad \text{at } S_\sigma \tag{27}$$

$$\frac{\partial R}{\partial \dot{\underline{\tau}}} = \underline{\varepsilon} \tag{28}$$

$$\dot{\underline{\tau}} = \tfrac{1}{2}(\dot{\underline{t}} + \underline{\tau}\cdot\underline{\omega} + \underline{\omega}^T\cdot\underline{\tau} + \dot{\underline{t}}^T) \tag{29}$$

In the above, $\underline{\nabla}$ is the gradient operator in the current configuration of the body, and $\underline{b}$ are prescribed body forces; $\underline{\phi}$ is a first-order (once-differentiable) stress-function, $\dot{\underline{t}}^b$ is a particular solution for $\dot{\underline{t}}$; and $\underline{\varepsilon}$ is the strain rate. The Euler-Lagrange equations that follow from $\delta\Pi_c = 0$ are:

$$(\underline{\varepsilon}+\underline{\omega})\cdot\underline{\tau} + \dot{\underline{t}} = \dot{\underline{t}}^T + \underline{\tau}\cdot(\underline{\varepsilon}+\underline{\omega}^T) \tag{30}$$

ORIGINAL PAGE IS
OF POOR QUALITY

$$\underline{v} = \bar{\underline{v}} \quad \text{at } S_v \tag{31}$$

$$\underline{\nabla v} = (\underline{\varepsilon}+\underline{\omega})^T \tag{32}$$

Equation (30) is the angular momentum balance condition, equation (31) is the velocity boundary condition, and (32) is the kinematic compatibility condition for the rate problem.

In the finite element formulation, we assume for each element:

$$\underline{v} = \sum_{i=1}^{NQ} \underline{N}_i q_N^i \; ; \quad \underline{N} = \text{isoparametric shape functions} \tag{33}$$

$$\underline{\omega} = \sum_{i=1}^{NW} \underline{QW}_i \alpha_N^i \qquad \text{where } \underline{QW}_i + \underline{QW}_i^T = 0 \tag{34}$$

$$\dot{\underline{t}} = \sum_{i=1}^{NT} \underline{QT}_i \beta_N^i + \dot{\underline{t}}^b \qquad \text{where } \underline{QT}_i = \underline{\nabla} \times \underline{\phi}_i \text{ and } \underline{\nabla}\cdot\dot{\underline{t}}^b = -\rho\dot{\underline{b}} \tag{35}$$

where NQ is the number of velocity parameters, NW is the number of spin parameters, and NT is the number of stress parameters.

Use of equations (33-35) in (25) can be shown to lead (ref. 30) to the algebraic system:

$$\underline{\underline{K}}\underline{v}^* = \underline{f} \tag{36}$$

where $\underline{v}^*$ is the vector of global nodal velocities. Solution of (36) leads to global velocities, from which the rate $\dot{\underline{t}}$ and the spin $\underline{\omega}$ in each element can be computed. We are thus led to initial value problem to integrate $\underline{v}$, $\dot{\underline{t}}$, and $\underline{\omega}$ in time to find the solution for displacement, total stress, and rotation at each material point.

In references (30-31) an elaborate study of various time-stepping schemes for integration of the above initial value problem as to their efficiency, stability, and objectivity was presented. In the following, we limit ourselves to a brief description of an important and interesting aspect of this time integration--which pertains to the question of maintaining "objectivity" of numerical integration.

## OBJECTIVITY OF NUMERICAL INTEGRATION

In order to be called *objective*, a numerical approximation for a physical entity must transform between two observer frames according to the same rule as the entity itself. An algorithm which produces an objective approximation will itself be called objective.

Suppose that as an objective rate one were to consider the Zaremba-Jaumann-Noll rate, ie.,

$$\underset{\sim}{\dot{\sigma}}^{0} = \frac{D\underset{\sim}{\sigma}}{Dt} + \underset{\sim}{\sigma}\cdot\underset{\sim}{\omega} - \underset{\sim}{\omega}\cdot\underset{\sim}{\sigma} \tag{37}$$

Suppose also that the solution at time $t = \tau$ is known, ie., $\underset{\sim}{\sigma}(\tau) = \underset{\sim}{\sigma}$ at $t = \tau$. If the usual Euler integration approximation were used, ie.,

$$\underset{\sim}{\sigma}(\tau+\Delta t) = \underset{\sim}{\sigma}(\tau) + (\underset{\sim}{\dot{\sigma}}^{0} - \underset{\sim}{\sigma}\cdot\underset{\sim}{\omega} + \underset{\sim}{\omega}\cdot\underset{\sim}{\sigma})\Delta t \tag{38}$$

the result will be in error, since $(\underset{\sim}{I} + \underset{\sim}{\omega}\Delta t)$ is not an orthogonal tensor.

Recently two algorithms were presented (refs. 33-34) which preserve the stress-integration and give a proper expression that is different from equation (38). In reference 30, Reed and Atluri presented an approach that is slightly different from that of references 33-34 in that numerical objectivity is treated as a general question without specific reference to stress-integration. This approach involves the concept of the so-called Jaumann integral (ref. 35) using which objectivity can be preserved in any numerical integration. Here, we present the use of the Jaumann integral in stress-integration.

The Jaumann stress-integral, which can be viewed as operation inverse to the Jaumann-differential of equation (37), can be written (ref. 30) as:

$$\underset{\sim}{\tau}(t) = \underset{\sim}{J}_{\tau}^{-1}(t)\underset{\sim}{Q}(t)\cdot\underset{\sim}{\tau}(\tau)\cdot\underset{\sim}{Q}^{T}(t) + \int_{\tau}^{t} [\underset{\sim}{J}_{\xi}(\zeta)\underset{\sim}{Q}(t)\cdot\underset{\sim}{Q}^{T}(\zeta)\cdot\underset{\sim}{\dot{\delta}}^{0}(\zeta)\cdot\underset{\sim}{Q}(\zeta)\cdot\underset{\sim}{Q}^{T}(t)]\,d\zeta \tag{39}$$

where $\underset{\sim}{\tau}$ is the true stress, and $\underset{\sim}{Q}(t)$ is the solution of the differential equation:

$$\dot{\underset{\sim}{Q}}(t) = \underset{\sim}{\omega}(t)\cdot\underset{\sim}{Q}(t) \;;\quad \underset{\sim}{Q}(\tau) = \underset{\sim}{I} \tag{40}$$

Now let $t_{\theta}$ be the time such that

$$t_{\theta} = \tau + \theta\Delta t \qquad 0 < \theta < 1 \tag{41}$$

we replace equation (40) by an *approximate* differential equation:

ORIGINAL PAGE IS
OF POOR QUALITY

$$\dot{\underset{\sim}{Q}}(t) \simeq \underset{\sim}{\omega}_\theta \cdot \underset{\sim}{Q}(t) \; ; \quad \underset{\sim}{\omega}_\theta = \underset{\sim}{\omega}(\tau + \theta\Delta t) \tag{42}$$

and treat $\underset{\sim}{\omega}_\theta$ as a constant in equation (42). The *exact* solution of equation (42) would be:

$$\underset{\sim}{Q}_\theta = \underset{\sim}{Q}(t_\theta) = (\exp. \underset{\sim}{\omega}_\theta t_\theta) \cdot \underset{\sim}{I}$$

$$= \underset{\sim}{I} + \frac{\sin\omega_\theta t_\theta}{\omega_\theta} \underset{\sim}{\omega}_\theta + \frac{(1 - \cos\omega_\theta t_\theta)}{\omega_\theta} \underset{\sim}{\omega}_\theta^2 \tag{43}$$

where $$\omega_\theta = \sqrt{\tfrac{1}{2}\underset{\sim}{\omega}_\theta : \underset{\sim}{\omega}_\theta} \tag{44}$$

Now let $$\underset{\sim}{Q}_1 = \underset{\sim}{Q}(t_1) = \underset{\sim}{Q}(\tau + \Delta t) \tag{45}$$

Then, an *approximation* to the Jaumann integral, equation (39), can be written as:

$$\underset{\sim}{\tau}(\tau + \Delta t) = \underset{\tau}{J^{-1}}(t_1) \cdot \underset{\sim}{Q}_1 \cdot \underset{\sim}{\tau} \cdot \underset{\sim}{Q}_1^T + [(\Delta t) J_1(t_\theta) \underset{\sim}{Q}_1 \cdot \underset{\sim}{Q}_\theta^T \cdot \dot{\underset{\sim}{\sigma}}_\theta^0 \cdot \underset{\sim}{Q}_\theta \cdot \underset{\sim}{Q}_1^T] \; ; \quad 0 < \theta < 1 \tag{46}$$

where $t_1 = \tau + \Delta t$. For $\theta = \frac{1}{2}$ we obtain the so-called "generalized midpoint rule", which agrees with that presented earlier in reference 34. The formula of reference 33 cannot be recovered since they use a midpoint constitutive evaluation but fail to properly rotate the resulting stress increment. The present concept of "objective integration" has the advantage that it provides a general framework for any time-integration.

## REFERENCES

1. Eshelby, J. D., "The Continuum Theory of Lattice Defects", Solid State Physics, Vol. III, Academic Press, 1956, pp. 79-144.

2. Rice, J. R., "A Path Independent Integral and the Approximate Analysis of Strain Concentration by Notches and Cracks", Journal of Applied Mechanics, Vol. 35, 1968, pp. 379-386.

3. Hutchinson, J. W. and Paris, P. C., "Stability Analysis of J-Controlled Crack Growth", Elastic-Plastic Fracture, ASTM STP 668, 1979, pp. 37-64.

4. Paris, P. C., Tada, H., Zahoor, A., and Ernst, H., "The Theory of Instability of the Tearing Mode of Elastic-Plastic Crack Growth", Elastic-Plastic Fracture, ASTM STP 668, 1979, pp. 5-36.

5. Kanninen, M. F. et al., "Development of a Plastic Fracture Methodology", EPRI NP-1734, Project 601-1, Final Report, March 1981.

6. Kumar, V., German, M. D., and Shih, C. F., "An Engineering Approach for Elastic-Plastic Fracture Analysis", EPRI NP-1931, Electric Power Research Institute Report, July 1981.

7. Saxena, A., Ernst, H. A., and Landes, J. D., "Creep Crack Growth Behavior in 316 Stainless Steel at 594°C (1100°F)", Sci. Paper No. 82-1D7-REACT-P1, Westinghouse R & D Center, August 1982.

8. Elfer, N. C., "Constant Displacement Compliance and Crack Growth in PMMA", Dept. Fracture Mechanics and Mechanical Properties, DFVLR, Cologne, April 1982.

9. Goldman, N. L. and Hutchinson, J. W., "Fully Plastic Crack Problems: The Center Cracked Strip Under Plane Strain", Int. Jnl. Solids & Structures, Vol. 11, 1975, pp. 575-595.

10. Atluri, S. N. "Path-Independent Integrals in Finite Elasticity and Inelasticity, with Body Forces, Inertia, and Arbitrary Crack Face Conditions", Engineering Fracture Mechanics, Vol. 16, No. 3, 1982, pp. 341-364.

11. Nakagaki, M. and Atluri, S. N., "Use of ($\dot{\underline{T}}$) Integral in Elastic-Plastic Fracture Mechanics", Proceedings of Workshop on Mechanics of Damage and Fracture, Stone Mountain, GA, November 1982 (In Press).

12. Stonesifer, R. B. and Atluri, S. N., "On a Study of the $(\Delta\underline{T})_c$ and $C^*$ Integrals for Fracture Analysis Under Non-Steady Creep", Engineering Fracture Mechanics, Vol. 16, No. 5, 1982, pp. 625-643.

13. Stonesifer, R. B. and Atluri, S. N., "Moving Singularity Creep Crack Growth Analysis with the $(\dot{\underline{T}})_c$ and $C^*$ Integrals", Engineering Fracture Mechanics, Vol. 16, No. 6, 1982, pp. 769-782.

14. Stonesifer, R. B. and Atluri, S. N., "A New Path-Independent Integral $(\dot{\underline{T}})_c$, and Computational Studies", NASA Contractor Report, NASA Lewis Research Center, March 1982.

15. Atluri, S. N., Nishioka, T., and Nakagaki, M., "Numerical Modeling of Dynamic and Nonlinear Crack Propagation in Finite Bodies by Moving Singular Elements", Nonlinear and Dynamic Fracture Mechanics, (Eds. N. Perrone and S. N. Atluri), ASME AMD Vol. 35, 1979, pp. 37-66.

16. Nishioka, T. and Atluri, S. N., "Numerical Modeling of Dynamic Crack Propagation in Finite Bodies by Moving Singular Elements, Part I: Formulation and Part II: Results", Journal of Applied Mechanics, Vol. 47, No. 3, 1980, pp. 570-576 and pp. 576-583.

17. Nishioka, T. and Atluri, S. N., "Numerical Analysis of Dynamic Crack Propagation: Generation and Prediction Studies", Engineering Fracture Mechanics, Vol. 16, No. 3, 1982, pp. 303-332.

18. Nishioka, T. and Atluri, S. N., "Finite Element Simulation of Fast Fracture in Steel DCB Specimen", Engineering Fracture Mechanics, Vol. 16, No. 2, 1982, pp. 157-175.

19. Nishioka, T. and Atluri, S. N., "Path-Independent Integrals, Energy Release Rates, and General Solutions of Near-Tip Fields in Mixed Mode Dynamic Fracture Mechanics", Engineering Fracture Mechanics, Vol. 17, 1983 (In Press).

20. Nishioka, T. and Atluri, S. N., "A Numerical Study of the Use of Path-Independent Integrals in Dynamic Crack Propagation", Engineering Fracture Mechanics, Vol. 17, 1983 (In Press).

21. Nishioka, T. and Atluri, S. N., "Dynamic Crack Propagation Analysis Using a New Path-Independent Integral and Moving Nonsingular Isoparametric Elements", Proceedings AIAA/ASME/ASCE Structures, Structural Dynamics, and Materials Conf., Lake Tahoe, May 1983.

22. Nagtegaal, J. C. and de Jong, J. E., "Some Aspects of Non-Isotropic Workhardening in Finite Strain Plasticity", Plasticity of Metals at Finite Strain: Theory, Experiment, and Computation, (Eds. E. H. Lee and R. L. Mallett), Dvn. Appl. Mech., Stanford Univ. and Dept. Mech. Engg., RPI, pp. 65-102, 1982.

23. Lee, E. H. Mallett, R. L., and Wertheimer, T. B., "Stress Analysis for Anisotropic Hardening in Finite Deformation Plasticity", RPI Report, Received October-November 1982.

24. Lee, E. H., "Finite Deformation Effects in Plasticity Theory", Developments in Theoretical and Applied Mechanics, Published by the University of Alabama in Huntsville, 1982, pp. 75-90.

25. Atluri, S. N., "On Constitutive Relations at Finite Strain: Elasto-Plasticity with Isotropic or Kinematic Hardening", Report GIT-CACM-SNA-83-16, Georgia Tech, February 1983.

26. Reed, K. W. and Atluri, S. N., "Visco-Plasticity and Creep: A Finite Deformation Analysis Using Stress-Based Finite Elements", Advances in Aerospace Structures and Materials, (Eds. S. S. Wang and J. Renton), ASME AD-01, 1982, pp. 211-219.

27. Reed, K. W., Stonesifer, R. B., and Atluri, S. N., "Stress and Fracture Analyses Under Elasto-Plastic and Creep Conditions", Proceedings Symposium on Nonlinear Constitutive Relations for High Temperature Applications, Univ. of Akron, Akron, Ohio, May 1982.

28. Reed, K. W. and Atluri, S. N., "Hybrid Stess Finite Elements for Large Deformations of Inelastic Solids", Jnl. Computers and Structures (K. Washizu Memorial Issue), 1983 (In Press).

29. Reed, K. W. and Atluri, S. N., "On the Generalization of Certain Rate-Type Constitutive Equations for Very Large Strains", Proceedings Int. Conf. on Constitutive Laws for Engineering Materials Theory and Application (Eds. C. S. Desai and R. H. Gallagher), 1983, pp. 71-77.

30. Reed, K. W. and Atluri, S. N., "Analysis of Large Quasistatic Deformations of Inelastic Bodies by a New Hybrid-Stress Finite Element Algorithm", Computer Methods in Applied Mechanics and Engineering, 1983 (In Press).

31. Reed, K. W. and Atluri, S. N., "Analysis of Large Quasistatic Deformations of Inelastic Bodies by a New Hybrid-Stress Finite Element Algorithm: Applications", Computer Methods in Applied Mechanics and Engineering, 1983 (In Press).

32. Atluri, S. N., "On Some New General and Complementary Energy Theorems for the Rate Problems of Finite Strain, Classical Elasto-Plasticity", Jnl. of Structural Mechanics, Vol. 8, No. 1, 1980, pp. 61-92.

33. Hughes, T. J. R. and Winget, J., "Finite Rotation Effects in Numerical Integration of Rate Constitutive Equations Arising in Large-Deformation Analysis", Int. Jnl. Num. Meth. in Engg., Vol. 15, 1980, pp. 1862-1867.

34. Rubinstein, R. and Atluri, S.N., "Objectivity of Incremental Constitutive Relations Over Finite Time Steps in Computational Finite Deformation Analysis", Computer Methods in Applied Mechanics and Engineering, 1983 (In Press).

35. Goddard, J. D. and Miller, C., "An Inverse for the Jaumann Derivative and Some Applications to the Rheology of Viscous Fluids", Rheologica Acta, Vol. 5, 1966, pp. 177-184.

N84
31698

UNCLAS

N84 31698 D/0

# INTERACTIVE FINITE ELEMENTS

# FOR GENERAL ENGINE DYNAMICS ANALYSIS*

Maurice L. Adams
Case Western Reserve University

Joseph Podovan and Demeter G. Fertis
The University of Akron

## SUMMARY

The major objective of this work has been to adapt general nonlinear finite-element codes for the purpose of analyzing the dynamics of gas turbine engines. In particular, this adaptation required the development of a squeeze-film damper element software package and its implantation into a representative current generation code. The ADINA code was selected because of our prior use of it and familiarity with its internal structure and logic. This objective has been met and our results indicate that such use of general purpose codes is a viable alternative to specialized codes for general dynamics analysis of engines.

## INTRODUCTION

There is currently a considerable interest and level of activity in developing computational schemes to predict general engine dynamic behavior. The general feeling among researchers working on engine vibration problems is that various modes of operation, such as blade-loss events, require a high level of analysis sophistication to realistically model the engine. Proper account of system nonlinearities (particularly at the bearings, dampers and rubs) appears to be necessary if analytical predictions are to be realistic. The approach described in this paper seeks to make use of already proven general finite-element nonlinear time-transient computer codes which are available on the open market.

Present-day jet engine configurations have evolved to a substantial degree through a trial-and-error process involving extensive testing. There are many fundamental dynamic phenomena which take place within these engines for which basic description and understanding have yet to be generated. Nonetheless, they work well. Modern aircraft engines are typical of current high-technology products in which the recently acquired computing capabilities of today are being used to better understand and improve what is already designed, built and operating.

A better understanding of the basic dynamic characteristics of existing and new engine configurations is a prerequisite for producing acceptable engine efficiencies on advanced configurations (i.e., smaller rotor/stator running clearances). Also,

*This work is sponsored by NASA Lewis Research Center under grant NSG-3283; NASA Technical Monitor, C.C. Chamis.

a better definition of engine dynamic response would more than likely provide valuable information and insights leading to reduced maintenance and overhaul costs on existing configurations. Furthermore, application of advanced engine dynamic simulation methods could potentially provide a considerable cost reduction in the development of new engine configurations by eliminating some of the trial-and-error process done with engine hardware development.

The emergence of advanced finite element codes, such as NASTRAN, NONSAP, MARC, ADINA, ANSYS and ABAQUS and related algorithmic advances, have placed comprehensive engine system dynamic analyses within reasonable reach. What remains to be done is to develop new component element software to properly model engine rotor/stator interactive components, such as the squeeze-film damper, within the algorithmic logic of already proven finite-element codes. This is the major mission of this work.

For good reasons, aircraft gas turbine engines use rolling element bearings exclusively. This design philosophy has, until recent years, deprived engines of beneficial damping inherent in many other types of rotating machinery where fluid-film journal bearings are used. The implementation of squeeze-film dampers in recent engine designs has now provided engine designers with an effective means of vibration energy dissipation. The net result is that engines with squeeze-film dampers are less sensitive to residual rotor imbalance and better able to control vibration and transmitted force levels resulting from various excitation sources within the engine.

The field of rotor dynamics has evolved to its present state primarily through the solution to problems in classes of machinery older than aircraft engines. In most other types of rotating machinery (e.g., steam turbines, centrifugal pumps and compressors, fans, generators, motors, etc.) the rotor can be adequately modeled as an Euler or Timoshenko beam [1]. In addition, the support structure holding each bearing can often be adequately modeled as a separate mass-damping-stiffness path to ground (i.e., to the inertial frame). Also, for most purposes, bearing dynamic properties are characterized as stiffness and damping elements, linearized for small vibration amplitudes about some static equilibrium state. With few exceptions (e.g., Hibner [2]), it is this level of sophistication that has been utilized for the most part in rotor-dynamics analyses of aircraft engines.

Present day aircraft engines are structurally far more complex than most other types of rotating machinery. The multi-shaft configuration, plus the fact that the shafts are thin rotating shells, creates unique but significant complicating differences between aircraft engines and other machinery. Also, the stator structural support at each rotor bearing represents anything but a separate mass-damper-stiffness path to an inertial frame. In fact, setting the inertial frame for the engine is not a simple matter when the full range of in-service maneuvers is realized. Dynamic paths between different bearings exist not only through the rotor but through several other paths within the nonrotating engine structure, i.e., a "multi-level," "multi-branch" system. As many as eight significant "levels" have been identified.

Adams [3] demonstrated the use of a free-free modal vector space for the rotor in the numerical integration of the motion equation with nonlinear journal bearings and base-motion inputs. The resulting computer code (ROTNL) has been applied to large steam turbine blade-out unbalance, instability limit cycles and base-motion excitation of nuclear machinery (earthquake and underwater explosive shock). This same approach was later applied by Gallardo et al., [4] in developing the TETRA code for double-spool shaft gas turbine engines. The approach used in references [3] and

[4] uses a standard code (i.e., NASTRAN) to generate the free-free undamped normal modes and natural frequencies for rotor and stator configurations. Nonlinear forces and connections between substructures are carried on the right hand side of the equations of motion, and updated at each time step of the particular numerical integration scheme. In this approach, a special purpose code is used to perform the integration of the motion equations, and handle input and output processing. Considerable flexibility and continual program advancement is therefore convenient. Also, this provides easier control of the basic mathematical model.

On the other hand, the major advantage of the approach summarized in our work is that full advantage can be taken of the multiplicity of computational and modeling advancements typical of the capability in current generation nonlinear general purpose finite-element codes. The disadvantage is that the general purpose code is more of a "black box" than one's own special purpose code.

## TIME-TRANSIENT NONLINEAR DYNAMIC ANALYSES

In recent years it has become evident that an important class of engine dynamic phenomena can not be studied without accounting for the highly nonlinear forces produced at bearings/dampers, labyrinths and other close-running rotor/stator clearances under large amplitude vibrations. In such cases, linear theory typically predicts vibration amplitudes larger than the actual running clearances. Furthermore, important vibratory phenomena, such as subharmonic resonance and motion limit cycles, are "filtered" out of the problem with a linear model, giving grossly erroneous predictions, qualitatively as well as quantitatively [3].

With few exceptions, nonlinear dynamics problems must be solved numerically as time-transient responses, whether the sought answer is a steady-state periodic motion or is strictly a transient phenomenon. The problem is mathematically categorized as an initial value problem in which the displacements and velocities of the complete system must all be specified at the beginning of the transient. From that point forward in time, the equations of motion are numerically integrated (known as "marching) as far in time as one wishes to study the system motions and forces. If the system is dynamically stable, the transient motion dies out yielding the steady state response which in a system with a periodic force excitation will be periodic motion. In a stable system with no time-varying force excitation, the transient will die out as the system comes to rest at one of its stable static equilibrium positions. If the system is unstable, the transient does not die out but continues to grow in time unless or until some nonlinear mechanism in the system limits the motion to what is frequently called a "limit cycle" [3].

In order to study the general dynamical characteristics of aircraft engines, nonlinear dynamics computational schemes are required. The approach taken is to develop software packages to model engine components which are not typically found on dynamical structures and therefore are not already built into existing nonlinear finite element structural dynamics computer codes. The initial effort has concentrated on developing such a software package for squeeze-film bearing dampers.

## OVERALL APPROACH-INTERACTIVE ELEMENTS

Considering the typical engine structural complexities, an improved computational approach is necessary if a proper transient/steady-state model is to be developed for gas turbine engines. In this approach, it appears that the finite-element method is one of the attractive modeling techniques for such problems. Its inherent capabilities include features essential to modern engines: 1) automatically handles multi-branch, multi-level structures in a more direct and efficient manner than flexibilities approaches, 2) well-suited to handle nonlinearities associated with structural kinematic and kinetic effects [7], 3) easily accommodates various types of boundary and constraint conditions, and 4) easily accommodates material nonisotropy and nonlinearity [7,8]. A body of established and proven algorithms are available which can handle these various important effects [7,9] as well as geometric complexities (e.g., beam, plate, 2-D and 3-D elements [10].

The required features which are presently not available with general purpose finite-element codes are provisions to handle rotor/stator interactive forces originating from squeeze-film dampers, seals and rub/impact events. Presented herein are the results of an effort to develop a squeeze-film damper computer software package which can be "plugged" into existing finite-element codes. This work is detailed in references [5] and [6].

## DEVELOPMENT AND IMPLANTATION OF SQUEEZE-FILM DAMPER ELEMENT

The basic implant approach is quite simple as shown in Figure 1. In addition to the standard structural element input provided for the particular general purpose code (i.e., host program) being used, an additional small block of fixed inputs is provided for each damper in the model. In the computational stream for numerical integration of the motion equations, the damper software routine is called at each time step of the marching scheme, and provides the total instantaneous interactive force generated in the fluid film of the squeeze-film damper. This instantaneous force is then applied to the structures as an "external" force. The damper also provides an option to compute the instantaneous tangent stiffness and damping matrices for the damper if such is needed for improvement to the numerical integration scheme of the host program. Details of the formulation and solution technique used in the squeeze film software package are detailed in reference [5].

To "experiment" with the damper element independent of a general purpose code, a small four degree-of-freedom host program was written which treated the rotor and stator each as point masses with two degrees of freedom apiece, "joined" to each other only by the squeeze-film damper (see Figure 2). Sample runs are shown in Figures 3, 4, 5 and 6.

As detailed in reference [6], the damper element was successfully "implanted" into the ADINA code and several case studies were made. These are summarized here in Figures 7, 8 and 9 for a multi-bearing simple rotor and different types of transient loading.

## EXPERIMENTAL CONFIRMATION

A two-bearing two-damper test rig was designed and fabricated. The rotor consists of a slender constant diameter shaft with a concentrated disk mast at the center of the bearing span (see Figure 10). Extensive testing was performed with this set up and rotor vibrational orbits were measured using Bently proximity probes and signal conditioning instrumentation. We are currently completing this work by making runs for this configuration using the ADINA program with squeeze-film software package implanted. We anticipate completing our correlations of experimental and computational results in the immediate future.

## REFERENCES


1. Fertis, D. G.: Dynamics and Vibrations of Structures. Wiley, New York, 1973.

2. Hibner, D. H.: Dynamic Response of Viscous-Damped Multi-Shaft Jet Engines. AIAA Journal of Aircraft, Vol. 12, 1975, pp. 305-312.

3. Adams, M. L.: Nonlinear Dynamics of Flexible Multi-Bearing Rotors. Journal of Sound and Vibration, Vol. 71(1), 1980, pp. 129-144.

4. Gallardo, V. C. et al.: Blade Loss Transient Dynamics Analysis. Volumes I, II and III, Contractor's final reports and program documentation for the TETRA program developed for NASA Lewis Research Center (Contract NAS3-22053) June 1981.

5. Adams, M. L.; Padovan, J.; and Fertis, D. G.: Engine Dynamic Analysis with General Nonlinear Finite-Element Codes, Part 1. Trans. ASME Journal of Engineering for Power, Vol. 104(3), July 1982, pp. 586-593.

6. Padovan, J.; Adams, M. L.; Fertis, D. G.: Zeid, I.; and Lam P.: Engine Dynamic Analysis with General Nonlinear Finite Element Codes, Part 2. ASME Paper No. 82-GT-292, 1982, 9 p.

7. Belytschko, T.: Nonlinear Analyses - Descriptions and Numerical Stability. In Computer Programs in Shock and Vibrations, ed. W. Pilkey and B. Pilkey, Shock and Vibration Information Center, Washington, D.C., 1975, p. 537.

8. Zienkiewicz, O.D.: The Finite Element Method. McGraw-Hill, London, 1977.

9. Felippa, C. A.; and Park, K. C.: Direct Time Integration Methods in Nonlinear Structural Dynamics. Presented at FENOMECH, University of Stutgart, 1978.

10. Structural Mechanics Computer Programs. Ed. W. Pilkey, K. Saczalski and H. Schaeffer, University Press of Virginia, Charlottesville, 1975.

ORIGINAL PAGE IS
OF POOR QUALITY

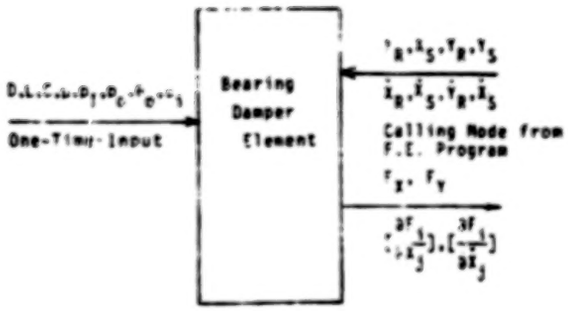


Figure 1 Input/Output of Damper Code.

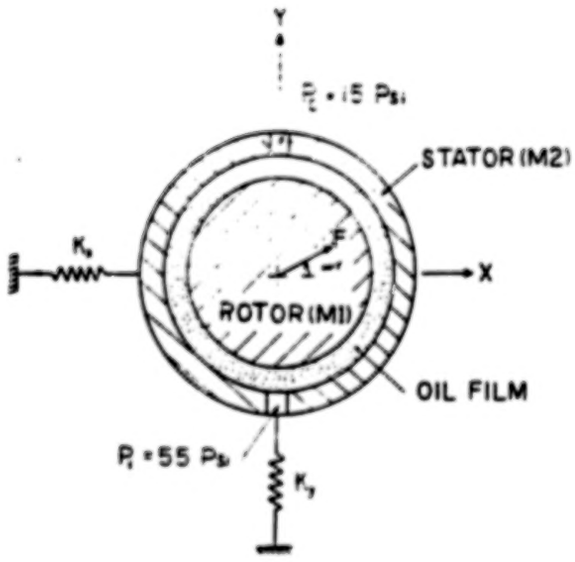


Figure 2 Simple 2-Mass 4-Degree of Freedom Test Model.

ORIGINAL PAGE IS
OF POOR QUALITY

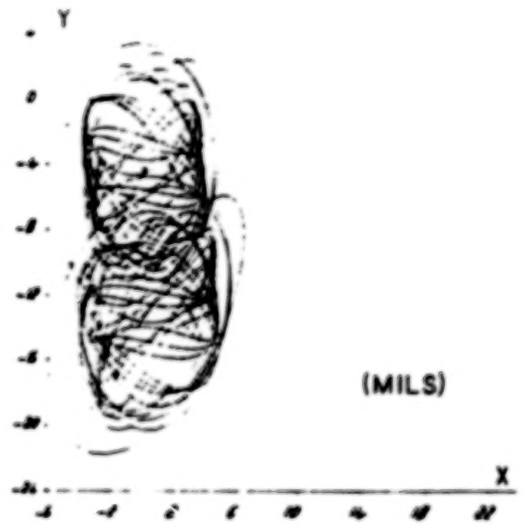


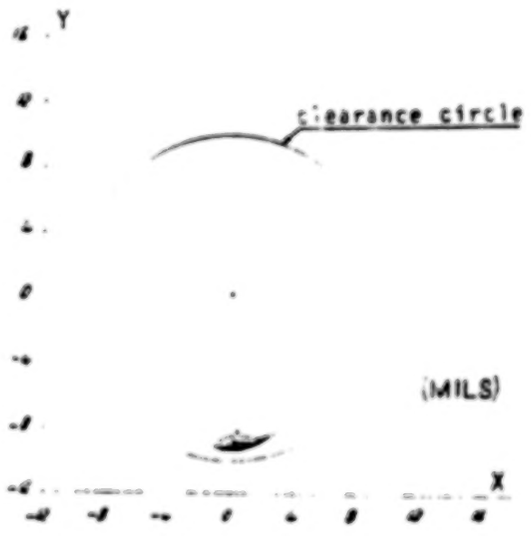


Fig. 3 Nonlinear Dynamic Transient of Simple 4 DOF System (see Fig. 8)
|F| = 300 lbs, ω = 150 rad/sec,
M1 = M2 = 500 lbs, Kx = Ky = 116000 lbs/in

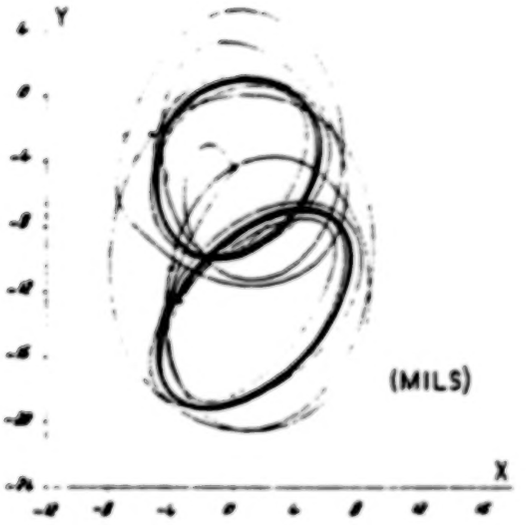


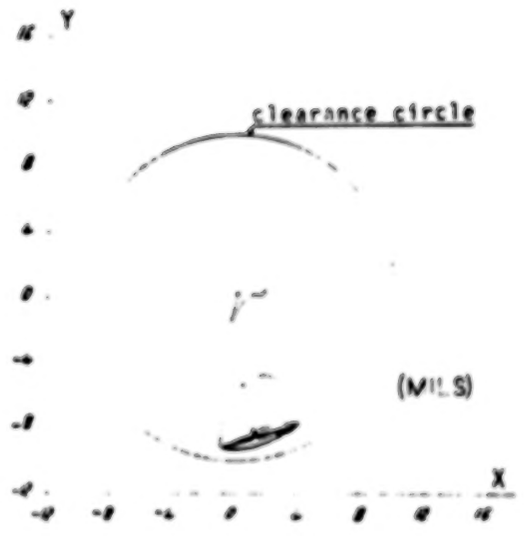


Fig. 4 Nonlinear Dynamic Transient of Simple 4 DOF System (see Fig. 8)
|F| = 300 lbs, ω = 150 rad/sec,
M1 = M2 = 500 lbs, Kx = Ky = 116000 lbs/in.

ORIGINAL PAGE IS
OF POOR QUALITY

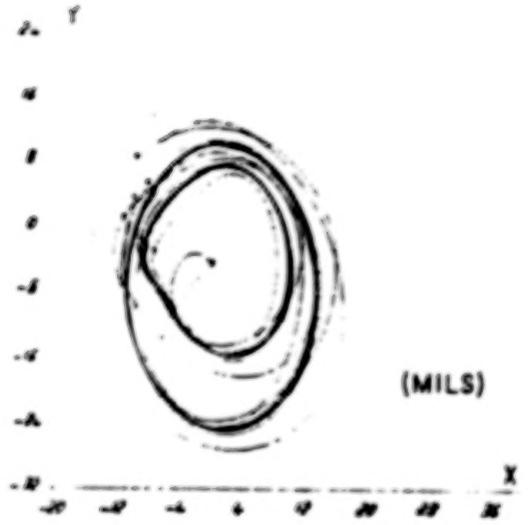


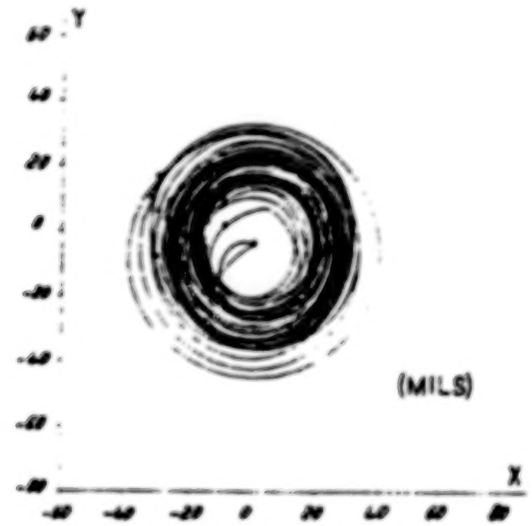


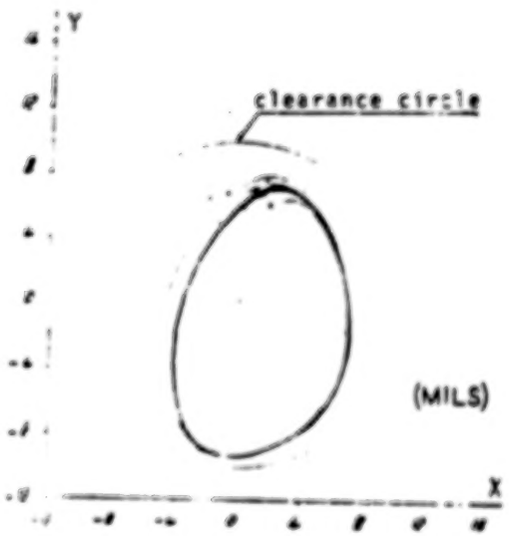


Fig. 5 Nonlinear Dynamic Transient of Simple 4 DOE System (see Fig. 8)
F = 500 lbs, ω = 150 rad/sec,
M1 = M2 = 500 lbs, Kx = Ky = 6000 lbs/in.

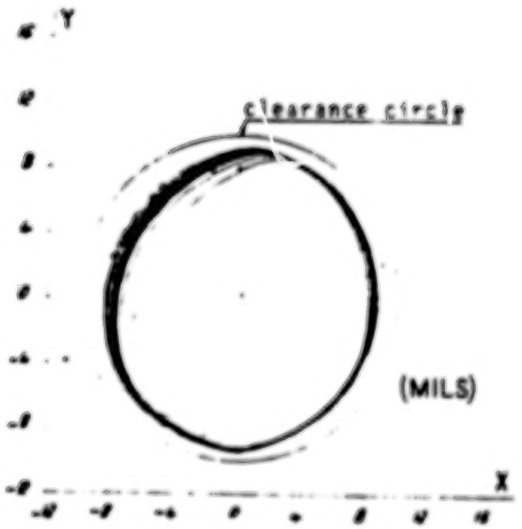


Fig. 6 Nonlinear Dynamic Transient of Simple 4 DOE System (see Fig. 8)
F = 1000 lbs, ω = 150 rad/sec,
M1 = M2 = 500 lbs, Kx = Ky = 6000 lbs/in.

ORIGINAL PAGE IS
OF POOR QUALITY

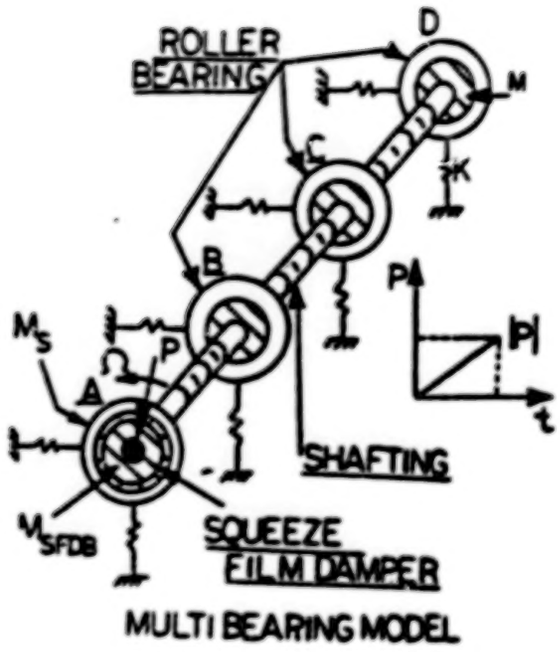


MULTI BEARING MODEL

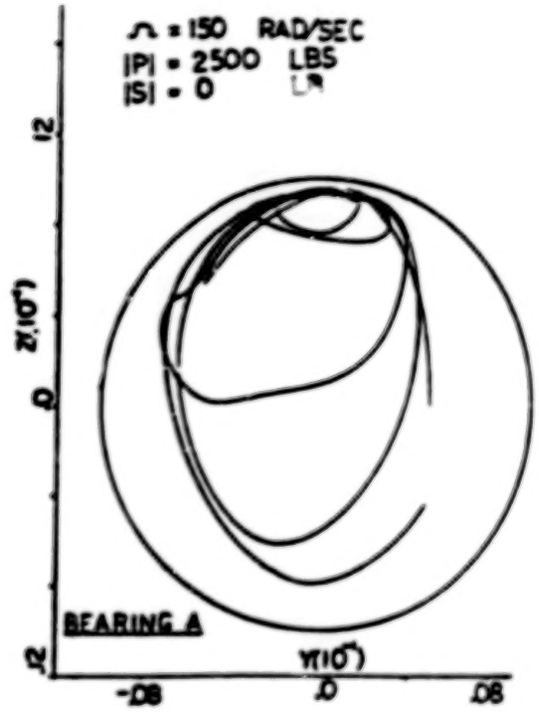


ROTOR OPBIT

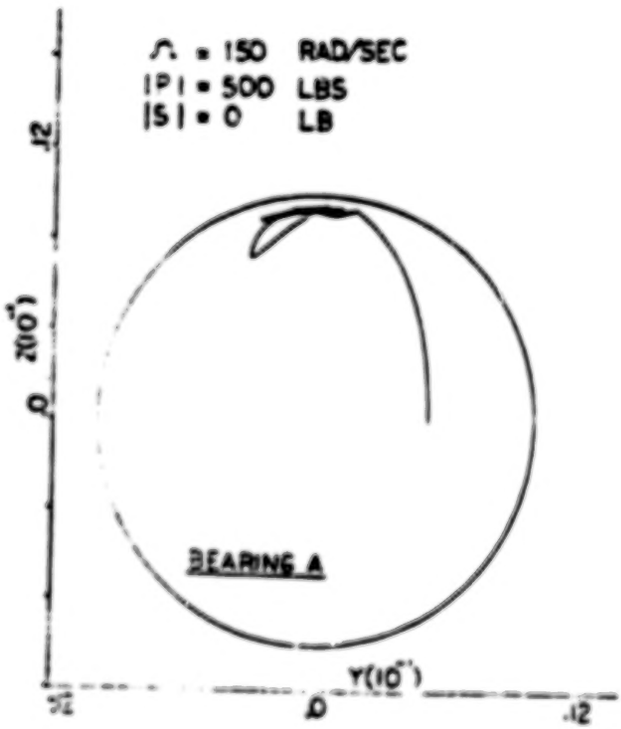


ROTOR ORBIT

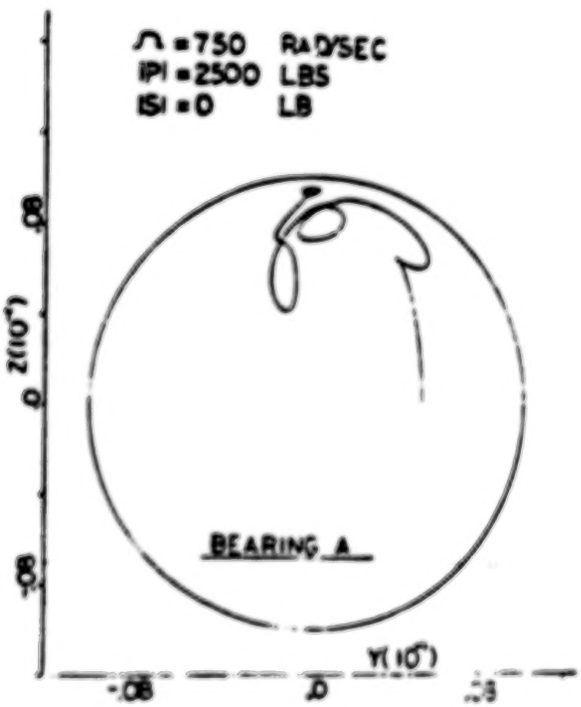


ROTOR ORBIT

Figure 7 Multi-bearing Example Computation.

ORIGINAL PAGE IS
OF POOR QUALITY

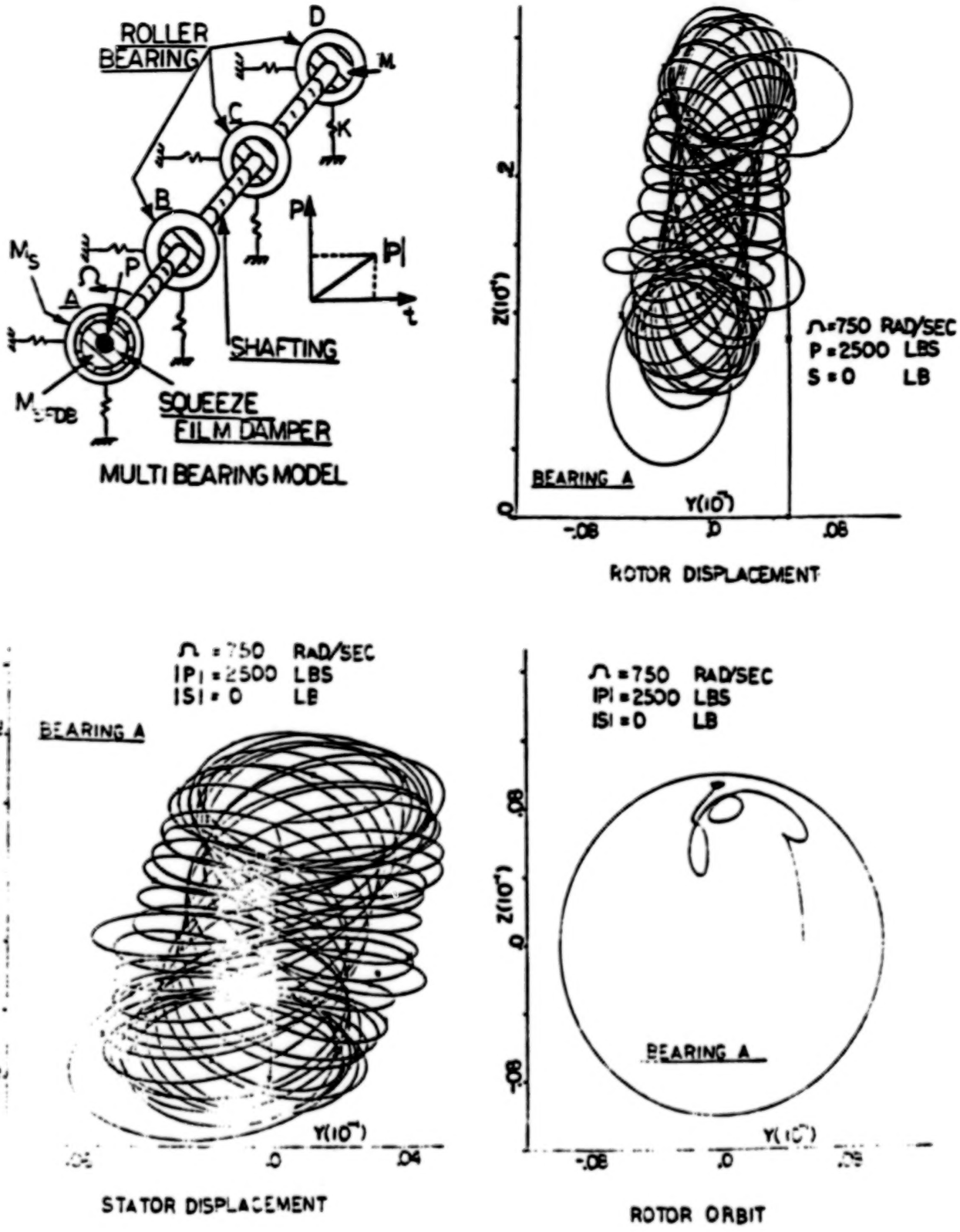


Figure 8 Multi-bearing Example Computation

ORIGINAL PAGE IS
OF POOR QUALITY

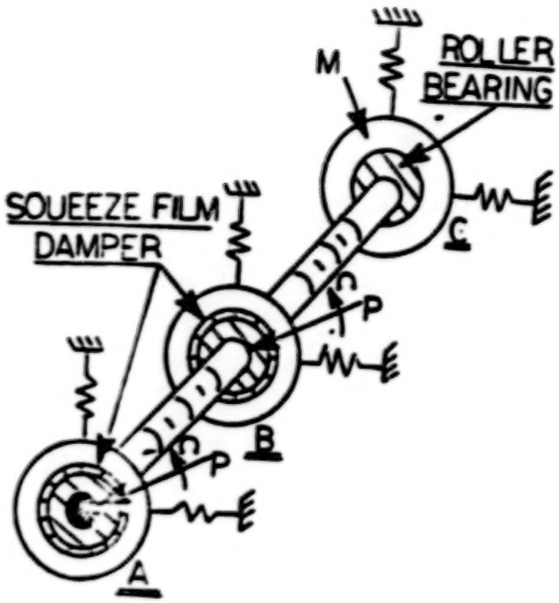


MULTI BEARING MODEL

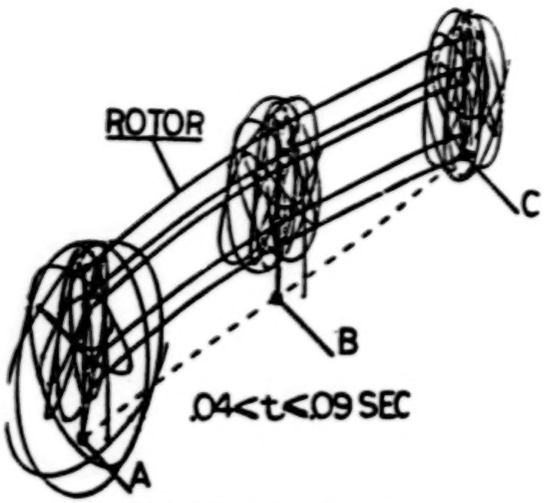


ROTOR TRAJECTORY

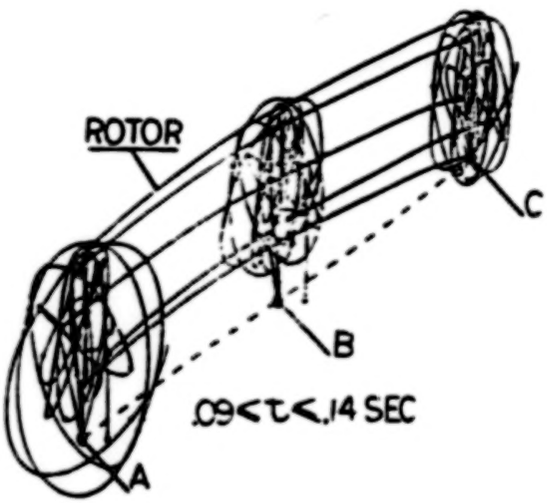


ROTOR TRAJECTORY

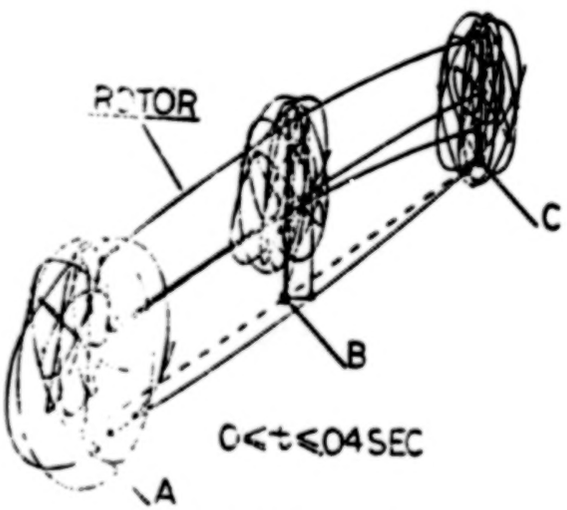


ROTOR TRAJECTORY

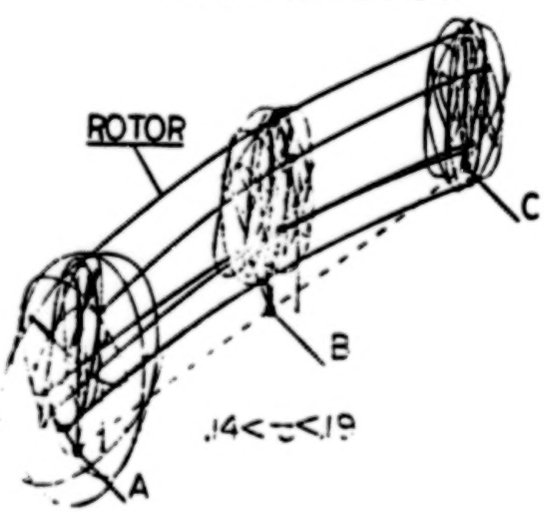


ROTOR TRAJECTORY

**Figure 9 Multi-bearing Example Computation**

ORIGINAL PAGE IS
OF POOR QUALITY

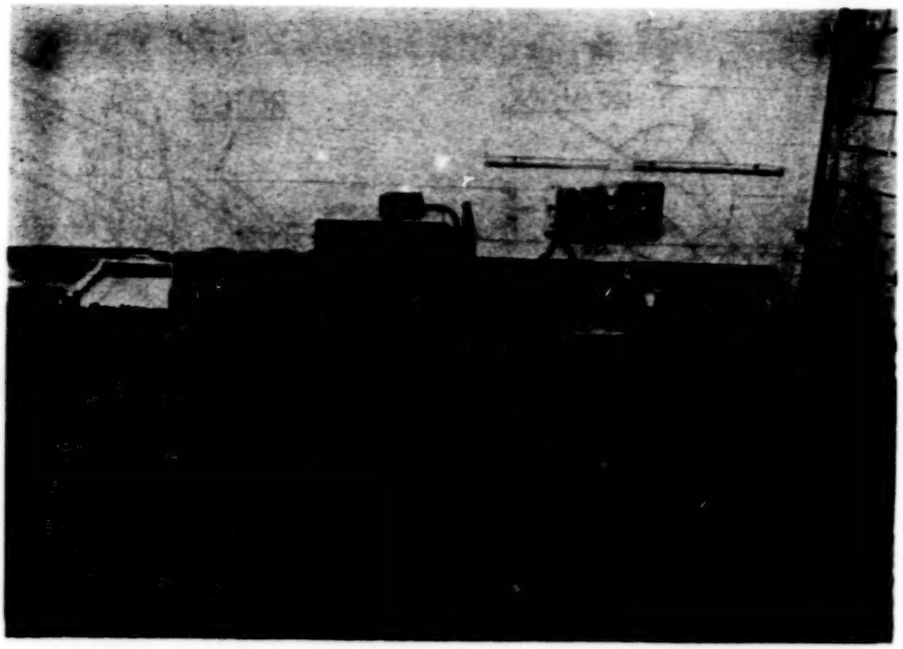

(a) Complete Test Coop With Instrumentation

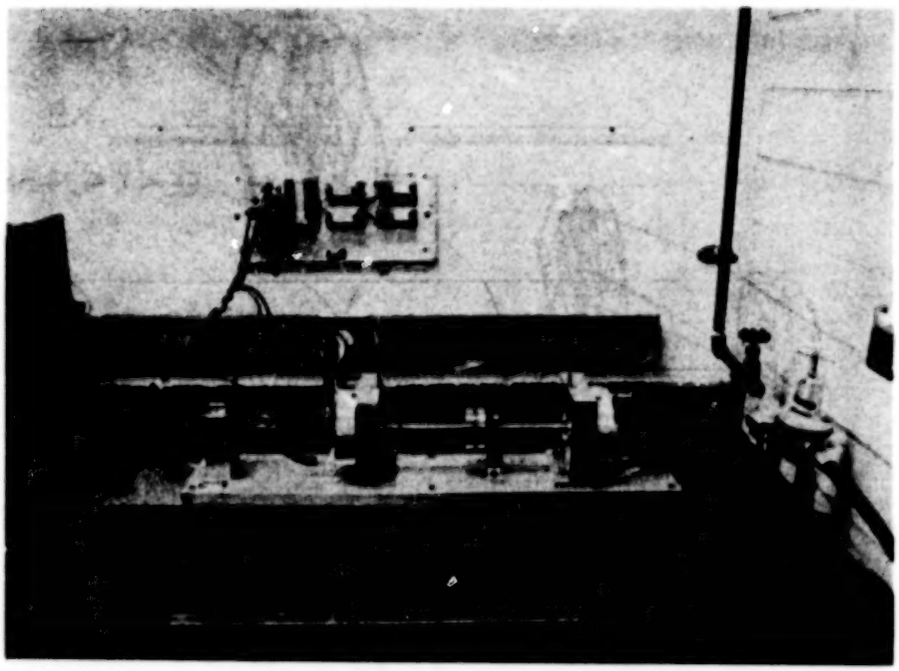

(b) Rotor Test Bed With Squeeze-Film Dampers

Figure 10 Existing Experimental Test Facility Rotor Dynamical Studies With Squeeze-Film Dampers.

N84
31699

UNCLAS

N84 31699 D11

# NONLINEAR ANALYSIS FOR HIGH-TEMPERATURE COMPOSITES - TURBINE BLADES/VANES

Dale A. Hopkins and Christos C. Chamis
NASA Lewis Research Center

## SUMMARY

An integrated approach to nonlinear analysis of high-temperature composites in turbine blade/vane applications is presented. The overall strategy of this approach and the key elements comprising this approach are summarized. Preliminary results for a tungsten-fiber-reinforced superalloy (TFRS) composite are discussed.

## INTRODUCTION

A major thrust of current aeropropulsion research is directed at improving the performance/efficiency of aircraft gas turbine engines. One area of research where efforts have been focused concerns the potential use of advanced and high-temperature composite materials for critical engine hot-section applications such as high-pressure turbine (HPT) blade/vane components. The temperature-limited capability of the conventional materials (mostly nickel- and cobalt-based monolithic superalloys) used in HPT blades/vanes is a key factor affecting the ability to augment engine performance/efficiency.

The ability to increase the maximum engine operating cycle temperature and, thus, improve engine performance/efficiency would be greatly enhanced by improving the elevated temperature capability of turbine blade/vane materials. For this reason a particular family of the refractory-fiber metal-matrix category of high-temperature composites, namely the tungsten-fiber-reinforced superalloys (TFRS), are being investigated (refs. 1-2) as a potential alternative to conventional monolithic superalloys for use in HPT blade/vane components. Moreover, a specific TFRS composite has been identified (ref. 3) as having an excellent combination of complementary properties to make it a viable candidate as a first-generation composite turbine blade/vane material.

From a qualitative viewpoint, the potential benefit of using high-temperature composite materials in engine hot-section applications, such as TFRS for HPT blades/vanes, is evident. Despite the promising outlook, a dilemma exists regarding the lack of adequate methods available to quantitatively assess a high-temperature composite in an engine hot-section application. For example, any present attempt to analyze the behavior of TFRS in a HPT blade/vane application would be forced to rely on experimental evaluations which are economically impractical. A definite need exists for an analytical capability with which to make a quantitative assessment of the mechanical performance and structural integrity of high-temperature composites, such as TFRS, in engine applications, such as HPT blades/vanes.

In view of the above discussion, a formal program was initiated at the NASA Lewis Research Center to develop a structural/stress analysis capability specifically tailored for the nonlinear analysis of TFRS composite HPT blades/vanes. Although the capability has been tailored for a specific application, the overall approach of this analytical capability is general and as such is applicable to the analysis of practically any composite structure where material nonlinearity is a concern.

The emphasis throughout the development of this structural/stress analysis capability for TFRS composite HPT blade/vane components has been to incorporate the physics governing this application into the analytical formulation of the problem. The blade/vane components of the HPT section operate in severe environments which subjects them to complex and cyclic thermomechanical loading conditions. These loads give rise to highly nonlinear material behavior which, for the case of TFRS composites, is assumed to be attributable to a stress-temperature-time dependency of the constituent (fiber/matrix/interphase) material properties. Furthermore, in the extended service elevated temperature environment of a HPT blade/vane, TFRS composites are subject to a metallurgical phenomenon known as fiber degradation which involves a chemical interaction at the fiber-matrix interface and results in the generation of an interphase of material.

To develop a nonlinear structural/stress analysis capability for TFRS composite HPT blade/vane components, the COBSTRAN computer code was used as a foundation. COBSTRAN is a software package developed as an in-house research tool at the NASA Lewis Research Center to perform linear-elastic structural analyses of composite blade structures. The resulting nonlinear version of COBSTRAN incorporates the appropriate nonlinear thermoviscoplastic (TVP) material relationships, fiber degradation expression, composite micromechanics equations, laminate theory, and global structural analysis to relate the global nonlinear structural response of a HPT blade/vane component to the behavior of the TFRS composite constituent materials.

Development of a nonlinear version of COBSTRAN was undertaken as an evolutionary task. The intent is to "fine-tune" nonlinear COBSTRAN through an iterative process of empirical investigation and analytical methodolgy refinement. During this iterative process, nonlinear COBSTRAN will be used as a tool to conduct parametric/sensitivity studies to isolate the critical factors affecting the behavior of TFRS composites in HPT blade/vane applications. Information from the parametric studies will be used to identify appropriate experimental investigations to further examine the critical factors that warrant accountability in a structural analysis.

## ANALYTICAL APPROACH

The overall approach taken here for the nonlinear structural analysis of a TFRS composite HPT blade/vane component is illustrated in the schematic in Figure 1. This schematic is representative of the general solution strategy of nonlinear COBSTRAN. This approach is referred to as an upward-integrated top-down-structured analysis. Figure 1 illustrates the levels of heirarchy involved in this approach and summarizes the key elements comprising this approach.

The circular arrangement of Figure 1 is intended to illustrate the incremental nature of a nonlinear structural analysis and the iterative process involved in the solution of such a problem. The cycle corresponds to the analysis of each distinct load increment. The solution process for a nonlinear analysis by this approach involves iteration at two levels. A primary iteration occurs for the load increments of the total solution range. For each increment, a secondary iteration occurs to establish equilibrium, in the integrated sense, of the global structural response.

## Nonlinear Thermoviscoplastic Relationships

As pointed out earlier, material nonlinearity for a TFRS composite HPT blade/vane is attributed to a stress-temperature-time dependency of the constituent material properties. To account for or model the material nonlinearity in a structural analysis, the nonlinear TVP relationships shown in Figure 2 have been implemented into nonlinear COBSTRAN for the purpose of updating the constituent material properties at each iteration during the analysis solution process.

As shown in Figure 2 the nonlinear TVP expressions provide a relationship between the current value (P) and reference value ($P_o$) of a material property according to the current and reference state of the constituent material as described by the indicated field variables. The properties being modified include; normal moduli ($E_{11}$, $E_{22}$), average heat capacity (C), thermal conductivities ($K_{11}$, $K_{22}$), thermal expansion coefficients ($\alpha_{11}$, $\alpha_{22}$), and remaining strengths ($S_{11}$, $S_{22}$, $S_{12}$).

These particular nonlinear TVP relationships are presented with the realization that they do not represent an exact or complete mathematical model for describing the nonlinear material behavior for a composite structure. The expressions in Figure 2 represent an attempt to account for the material nonlinearity involved in the application of TFRS composites in a HPT blade/vane compenents by treating the problem at the fundamental level.

## Composite Micromechanics

In short, composite micromechanics is the branch of composite mechanics which provides the formal structure to relate the behavior of a composite lamina to the behavior of the constituents. Composite micromechanics equations have been derived to predict; the material properties (mechanical, thermal, and uniaxial strength) of a unidirectional fiber-reinforced lamina based on the corresponding properties of the constituent materials, and, the distribution of microstresses in the constituent materials resulting from the stress state occurring in a lamina.

In the lamina transverse directions (2- and 3-directions, see Figure 3), the distribution of constituent microstresses ($\sigma_{22}$, $\sigma_{12}$, $\sigma_{23}$) is non-uniform through the thickness of the ply. By virtue of the nonlinear TVP relationships discussed earlier, this intralaminar non-uniformity of transverse microstresses results in a non-uniformity of transverse material properties for the constituents. This intrlaminar non-uniformity is illustrated in Figure 3 in terms of the

regions or zones used to characterize the non-uniformity. Figure 3 also lists the equations used to calculate average constituent transverse properties.

The composite micromechanics equations for predicting lamina mechanical properties are shown in Figure 4 together with a schematic defining the material property coordinate axis system. Similar equations exist for predicting lamina thermal properties and uniaxial strengths as well as for predicting the distribution of constituent microstresses from the corresponding lamina stresses.

In a sense, the composite micromechanics equations presented here can be thought of as a first level of approximation for idealizing an inhomogeneous laminated TFRS composite HPT blade/vane component as a pseudo-homogeneous structure.

## Laminate Theory

In short, laminate theory (laminated plate theory) provides the formal structure to describe the behavior of a laminated composite structure in terms of the individual laminae comprising the laminate. A cursory summary of the governing equations of classical laminated plate theory is given in Figure 5. Just as the composite micromechanics equations were considered as a first level of approximation, laminate theory can be thought of as a second level of approximation in idealizing an inhomogeneous TFRS composite HPT blade/vane component as a pseudo-homogeneous structure.

## Global Structural Analysis

The global finite element formulation of a general linear structural analysis problem is summarized by the equations shown in Figure 6. Although this collection of equations presents a superficial view of the finite element method of structural analysis, these equations are representative of the governing equations of structural analysis as implemented in a general purpose finite element code such as NASTRAN.

The basis of the integrated approach presented here for the nonlinear analysis of a TFRS composite HPT blade/vane component involves the application of the linear finite element formulation summarized in Figure 6 in an incremental manner.

## PRELIMINARY RESULTS AND DISCUSSION

Results were obtained from the analysis of a single unidirectional TFRS composite lamina using the integrated approach just presented as implemented into nonlinear COBSTRAN. Details of the analysis are left out here as the purpose of presenting these results is merely to: illustrate the capabilities of this integrated analytical approach by showing the types of information obtainable; identify trends of material behavior being accounted for and traced in a nonlinear analysis by this integrated

approach, and; point out the possible significance of a fabrication process in conducting a nonlinear analysis of a composite engine structure such as a turbine blade/vane.

The results in Figure 7 were obtained from the analysis of a single unidirectional TFRS composite lamina subjected to a temperature load representative of the cooling portion of a typical fabrication process. The first plot illustrates the large longitudinal normal residual stresses ($\sigma_{11}$) existing in the constituents at the end of this fabrication process. These stresses are the result of the difference in thermal expansion coefficients between the constituents. The second plot shows the variation of longitudinal normal modulus ($E_{11}$) for the constituents and ply during the fabrication process. Note that the modulus for the matrix initially increases but then decreases continuously for the duration of cooling. This reflects the relative influence or effect of the individual dependency terms in the nonlinear TVP relationships presented earlier. At first, the temperature-dependency dominates and, as might be expected, the modulus increases to a point where the residual stress becomes large enough such that the stress-dependency becomes dominant. The results for the fiber and interphase (degraded zone) can be explained in a similar manner. The result for the ply, as determined from the corresponding micromechanics equation, reflects the behavior of the fiber and matrix as the volume fraction of interphase was nominal in this case.

The third plot in Figure 7 illustrates the variation of remaining strength available in the ply and constituents during the fabrication process. The results are consistent with the corresponding nonlinear TVP relationship for strength. Finally, the last plot shows the build-up of transverse normal residual microstress ($\sigma_{22}$) in the constituents similar to that shown for $\sigma_{11}$. The point to be noted here is the difference in microstress from region to region for the matrix and interphase (degraded zone). This reflects the intra-laminar non-uniformity discussed earlier.

The conclusion to be drawn from these results is that perhaps the fabrication process for individual laminae, laminate panels, and a composite component itself should not be neglected.

## REFERENCES


1. D. W. Petrasek and R. A. Signorelli, "Tungsten Fiber Reinforced Superalloys - A Status Review," NASA TM-82590, 1981.

2. E. A. Winsa, "Tungsten Fiber Reinforced Superalloy Composite High Temperature Component Design Considerations," NASA TM-82811, 1982.

3. D. W. petrasek, E. A. Winsa, L. J. Westfall and R. A. Signorelli, "Tungsten Fiber Reinforced FeCrAlY - A First Generation Composite Turbine Blade Material," NASA TM-79094, 1979.

## SYMBOLS

| | |
|---|---|
| $k$ | volume fraction |
| $n, m, l$ | exponential constants (equations, Figure 2) |
| $t$ | total time |
| $z$ | distance to lamina (equations, Figure 5) |
| $A$ | laminate membrane stiffness matrix |
| $C$ | heat capacity, laminate coupled membrane-bendind stiffness matrix, or global structural damping matrix |
| $C_1, C_2, C_3$ | constants (equations, Figure 2) |
| $D_o, D$ | initial fiber diameter and current fiber diameter or laminate bending stiffness matrix |
| $E$ | normal modulus or material property matrix |
| $G$ | shear modulus |
| $K$ | thermal conductivity or global structural stiffness matrix |
| $M$ | laminate moment resultants or global structural mass matrix |
| $N$ | laminate stress resultants |
| $N_T, N_m$ | thermal and mechanical load cycles (equations, Figure 2) |
| $P_o, P$ | initial and current value for a property (equations, Figure 2) |
| $R$ | lamina transformation matrix |
| $S_o, S, S_c, S_F$ | initial, current remaining, cumulative, and fracture strengths (equations, Figure 2) |
| $T_o, T, T_m$ | initial, current, and melting temperatures (equations, Figure 2) |
| $\alpha$ | thermal expansion coefficients |
| $\varepsilon, \varepsilon^o$ | strain, and laminate midplane strains |
| $\kappa$ | laminate curvatures |
| $\nu$ | Poisson's ratio |

| | |
|---|---|
| $\sigma_o$, $\sigma$ | initial, and current stress |
| $\dot{\sigma}_o$, $\dot{\sigma}$, $\dot{\sigma}_H$ | initial, current, and reference maximum stress rates (equations, Figure 2) |
| $\omega$ | vibration frequency |

subscripts:

| | |
|---|---|
| c | composite or laminate |
| F, M, D, L | fiber, matrix, interphase, and lamina |
| 1, 2, 3 | lamina material property coordinate axes |
| x, y, z | global structural axes |

ORIGINAL PAGE IS
OF POOR QUALITY

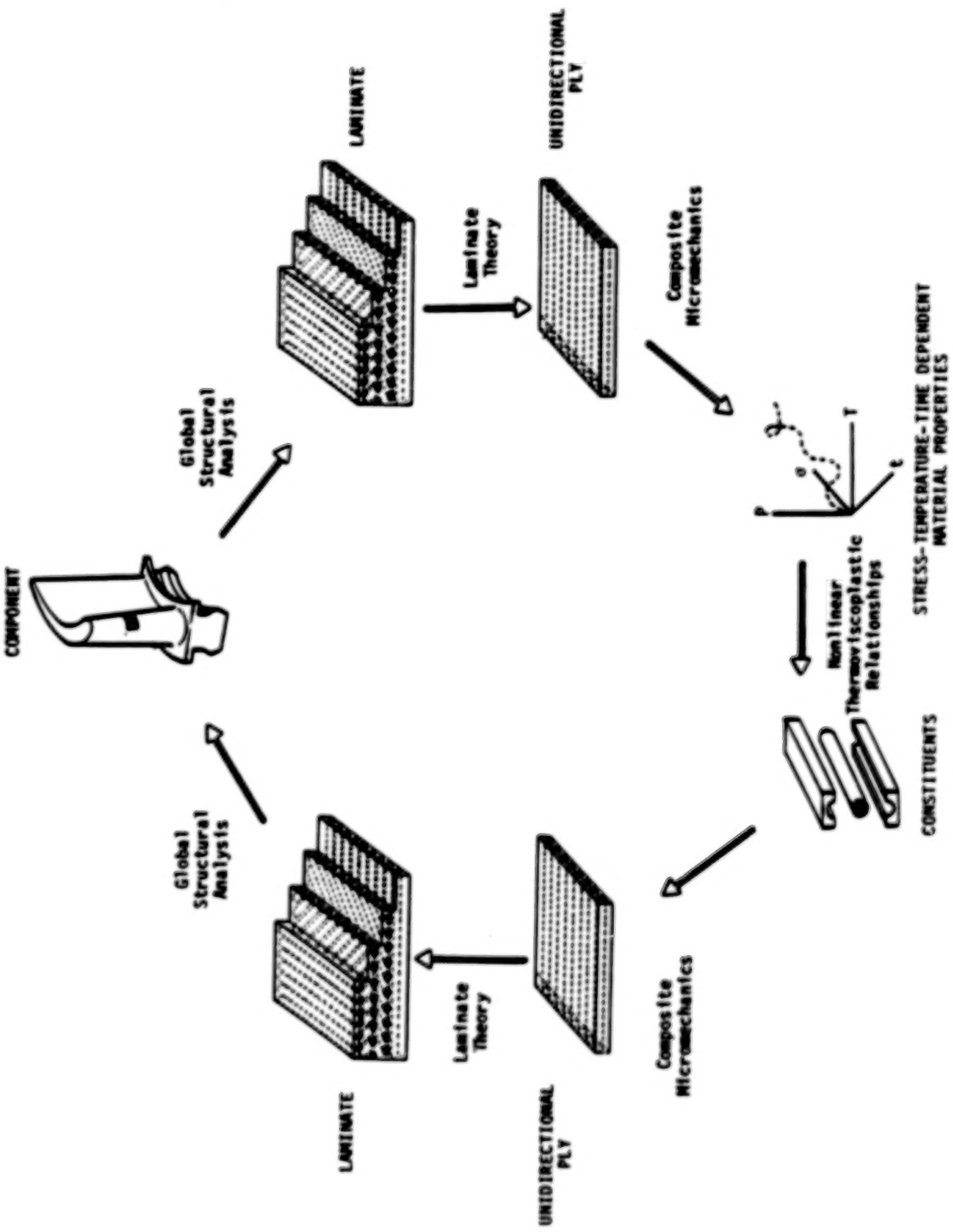


Figure 1 - Upward-integrated top-down-structured approach for nonlinear analysis of a composite engine structure

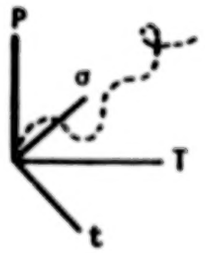


MECHANICAL PROPERTIES (E): $$P = \left[\frac{T_M - T}{T_M - T_o}\right]^n \left[\frac{S_F - \sigma}{S_F - \sigma_o}\right]^m \left[\frac{\dot{\sigma}_M - \dot{\sigma}_o}{\dot{\sigma}_M - \dot{\sigma}}\right]^k (P_o)$$

THERMAL PROPERTIES (C, K, α): $$\left[\frac{T_M - T_o}{T_M - T}\right]^n \left[\frac{S_F - \sigma_o}{S_F - \sigma}\right]^m \left[\frac{\dot{\sigma}_M - \dot{\sigma}}{\dot{\sigma}_M - \dot{\sigma}_o}\right]^k (P_o)$$

REMAINING STRENGTH (S): $$S = \left\{\left[\frac{T_M - T}{T_M - T_o}\right]^n - C_1 \log_{10} N_T - C_2 \log_{10} N_m - C_3 \log_{10} t\right\} (S_o) - S_c$$

Figure 2 - Nonlinear thermoviscoplastic (TVP) relationships to characterize composite material nonlinearity in terms of stress-temperature-time dependant constituent properties



ORIGINAL PAGE IS
OF POOR QUALITY

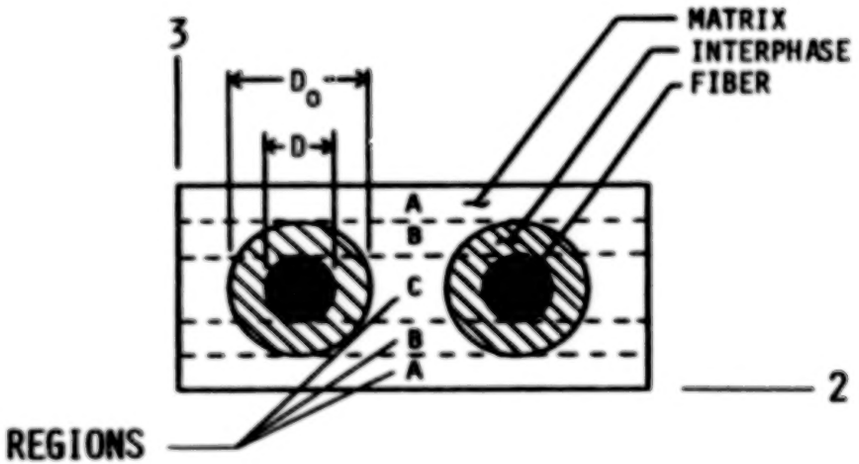


AVERAGE TRANSVERSE PROPERTIES ($E_{22}$, $G_{12}$, $G_{23}$, $K_{22}$, $\alpha_{22}$)

MATRIX : $$P_m = \frac{1}{1+\sqrt{k_f}} \left[ P_m^{(A)} + \left(1 - \frac{D}{D_o}\right) P_m^{(B)} + \sqrt{k_f}\left(\frac{D}{D_o}\right) P_m^{(C)} \right]$$

INTERPHASE : $$P_i = \frac{1}{1+\frac{D}{D_o}} \left[ P_i^{(B)} + \left(\frac{D}{D_o}\right) P_i^{(C)} \right]$$

Figure 3 - Various regions used to characterize intralaminar non-uniformity of transverse constituent properties and microstresses



ORIGINAL PAGE IS
OF POOR QUALITY

NORMAL MODULI: $$E_{L11} = k_M E_{M11} + k_F \left\{ \left[ 1 - \left( \frac{D}{D_o} \right)^2 \right] E_{D11} + \left( \frac{D}{D_o} \right)^2 E_{F11} \right\}$$

$$E_{L22} = E_{M22} \left\{ (1 - \sqrt{k_F}) + \frac{\sqrt{k_F}\left(1 - \frac{D}{D_o}\right)}{1 - \sqrt{k_F}\left(1 - \frac{E_{M22}}{E_{D22}}\right)} + \frac{\sqrt{k_F}\left(\frac{D}{D_o}\right)}{1 - \sqrt{k_F}\left[1 - \left(1 - \frac{D}{D_o}\right)\frac{E_{M22}}{E_{D22}} - \left(\frac{D}{D_o}\right)\frac{E_{M22}}{E_{F22}}\right]} \right\}$$

SIMILARLY FOR $E_{L33}$

SHEAR MODULI: $$G_{L12} = G_{M12} \left\{ (1 - \sqrt{k_F}) + \frac{\sqrt{k_F}\left(1 - \frac{D}{D_o}\right)}{1 - \sqrt{k_F}\left(1 - \frac{G_{M12}}{G_{D12}}\right)} + \frac{\sqrt{k_F}\left(\frac{D}{D_o}\right)}{1 - \sqrt{k_F}\left[1 - \left(1 - \frac{D}{D_o}\right)\frac{G_{M12}}{G_{D12}} - \left(\frac{D}{D_o}\right)\frac{G_{M12}}{G_{F12}}\right]} \right\}$$

SIMILARLY FOR $G_{L23}$ AND $G_{L13}$

POISSON'S RATIOS: $$\nu_{L12} = k_M \nu_{M12} + k_F \left\{ \left[ 1 - \left( \frac{D}{D_o} \right)^2 \right] \nu_{D12} + \left( \frac{D}{D_o} \right)^2 \nu_{F12} \right\}$$

SIMILARLY FOR $\nu_{L13}$

$$\nu_{L23} = \frac{E_{L22}}{2 G_{L23}} - 1$$

(F) FIBER
(M) MATRIX
(D) INTERPHASE
(L) PLY

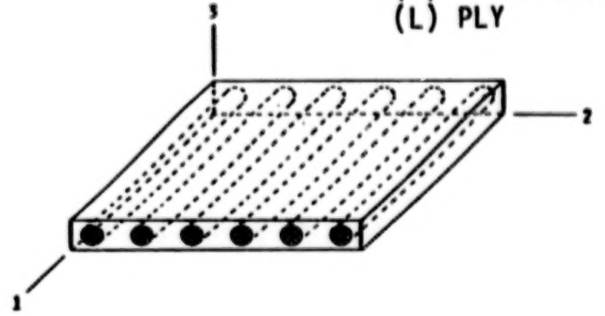


Figure 4 - Composite micromechanics equations for predicting average mechanical properties of a unidirectional fiber-reinforced ply

ORIGINAL PAGE IS
OF POOR QUALITY

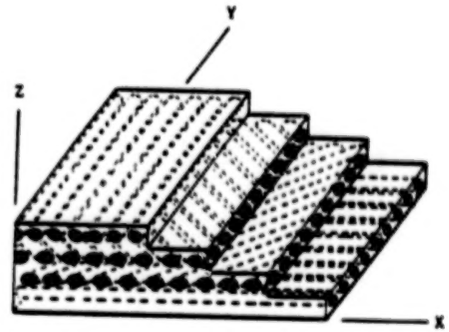


PLY CONSTITUTIVE RELATIONSHIP: $\{\epsilon\}_L = [E]_L^{-1}\{\sigma\}_L + \Delta T_L \{\alpha\}_L$

PLY STRAIN: $\{\epsilon\}_L = [R]_L \left\langle \{\epsilon^0\}_c + z_L \{\kappa\}_c \right\rangle$

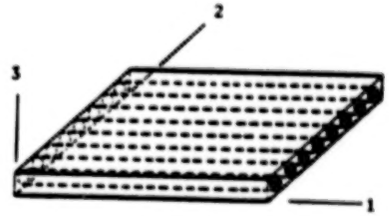


PLY STRESS: $\{\sigma\}_L = [E]_L \left\langle \{\epsilon\}_L + \Delta T_L \{\alpha\}_L \right\rangle$

LAMINATE CONSTITUTIVE RELATIONSHIP: $\left\{\begin{matrix} N \\ M \end{matrix}\right\}_c = \left[\begin{array}{c|c} A & C \\ \hline C & D \end{array}\right]_c \left\{\begin{matrix} \epsilon^0 \\ \kappa \end{matrix}\right\}_c + \left\{\begin{matrix} N_T \\ M_T \end{matrix}\right\}_c$

$$\{N_T, M_T\}_c = \sum_{L=1}^{n} [R]_L^T [E]_L [R]_L \, \Delta T_L \{\alpha\}_L \left\langle (z_L - z_{L-1}),\ \tfrac{1}{2}(z_L^2 - z_{L-1}^2) \right\rangle$$

LAMINATE STIFFNESS: $[A, C, D]_c = \sum_{L=1}^{n} [R]_L^T [E]_L [R]_L \left\langle (z_L - z_{L-1}),\ \tfrac{1}{2}(z_L^2 - z_{L-1}^2),\ \tfrac{1}{3}(z_L^3 - z_{L-1}^3) \right\rangle$

Figure 5 - Summary of the governing equations of laminate theory



ORIGINAL PAGE IS
OF POOR QUALITY

$$[M]\{\ddot{u}\} + [C]\{\dot{u}\} + [K]\{u\} = \{F(t)\}$$

$$\langle [K] - \lambda[I] \rangle \{u\} = \{0\} \rightarrow \{S_c\}$$

$$\langle [K] - \lambda[M] \rangle \{u\} = \{0\} \rightarrow \{\omega_n\}$$

$$\{u\} \leq \{u_a\}$$

$$\{\sigma\} = [E][B]\{u\} \leq \{S_a\}$$

$$\{\omega\} \leq \{\omega_a\}$$

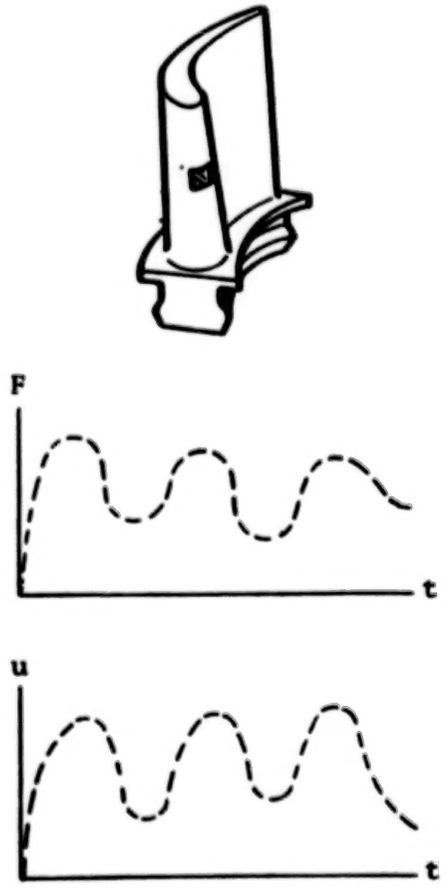


ORIGINAL PAGE IS
OF POOR QUALITY



Figure 6 - Summary of the global finite element formulation of a general linear structural analysis problem

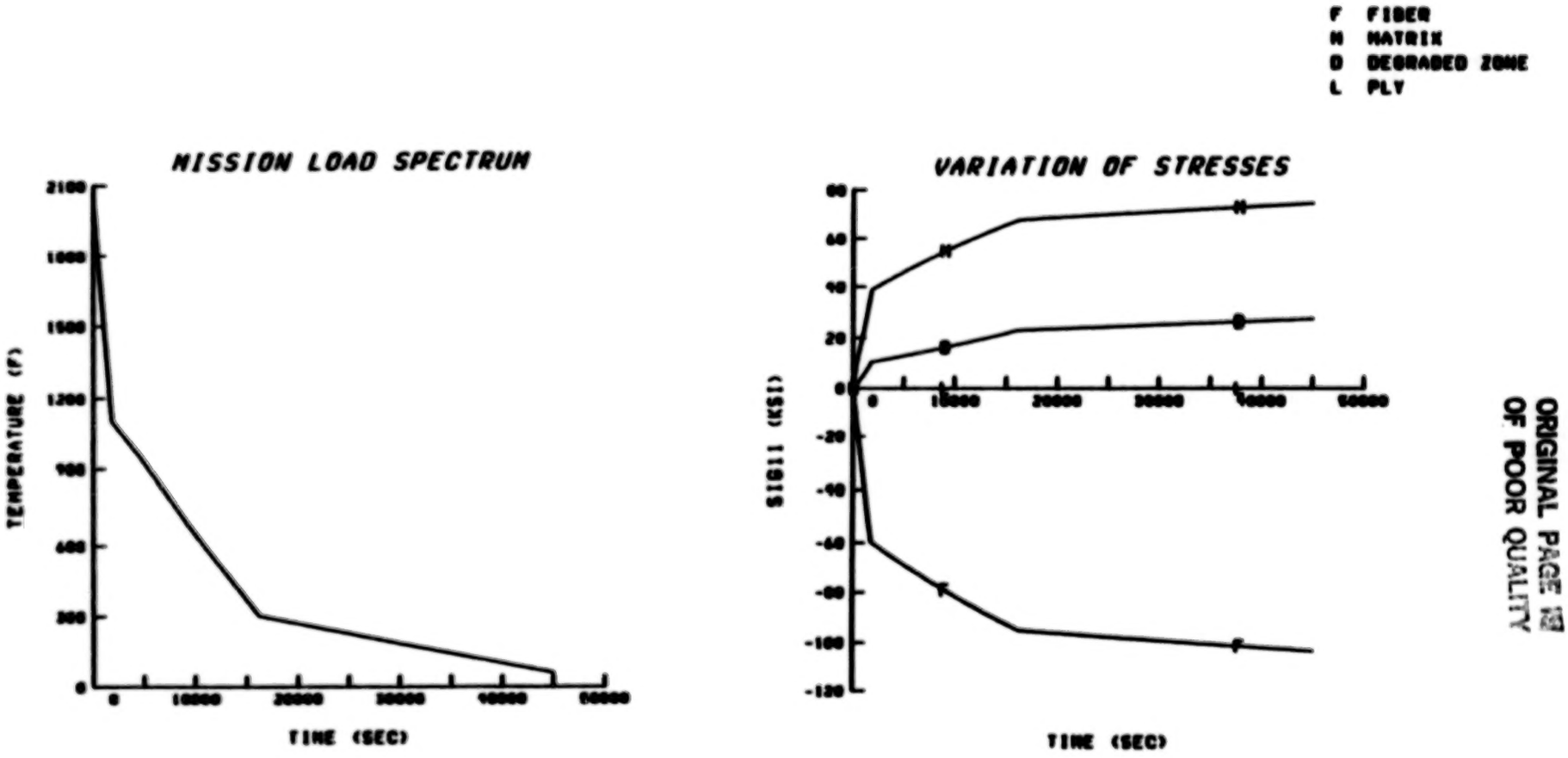


Figure 7 - Preliminary results of an analysis of a single unidirectional lamina subjected to the cooling half of an hypothetical fabrication process; variation of longitudinal normal stress ($\sigma_{11}$)

ORIGINAL PAGE IS
OF POOR QUALITY

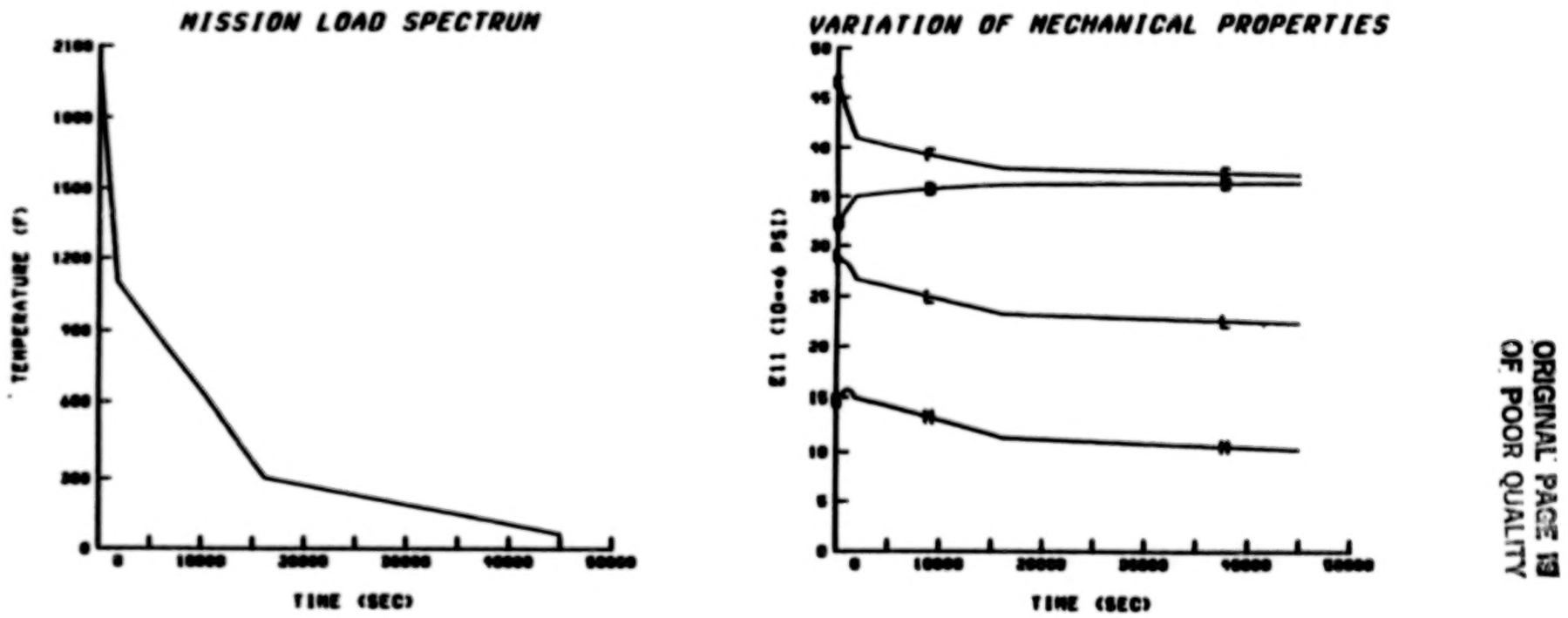


ORIGINAL PAGE IS
OF POOR QUALITY

Figure 7 - continued; variation of longitudinal normal modulus ($E_{11}$)

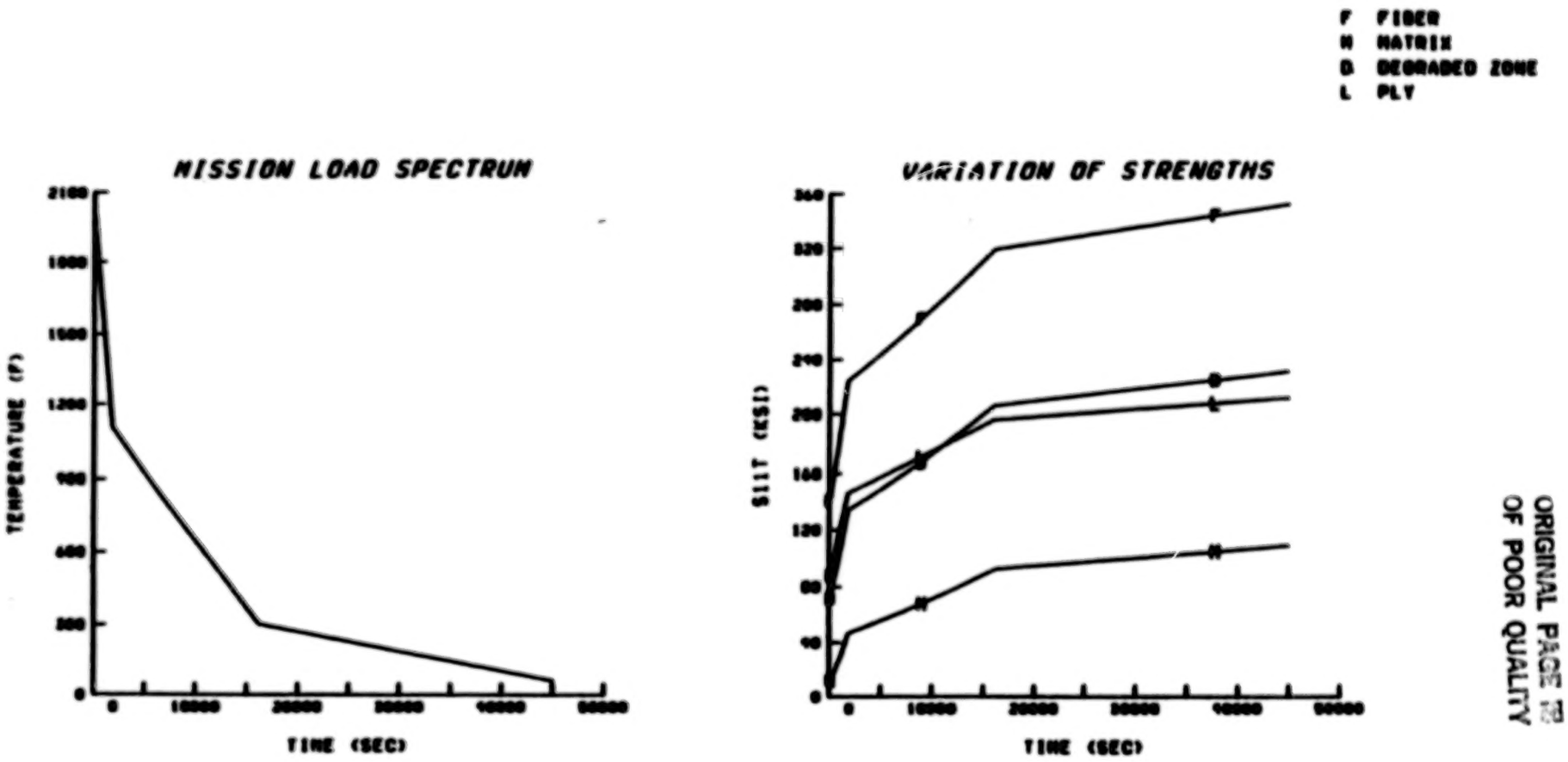


ORIGINAL PAGE IS
OF POOR QUALITY



Figure 7 - continued; variation of longitudinal tensile strength ($S_{11T}$)

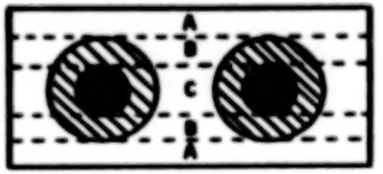


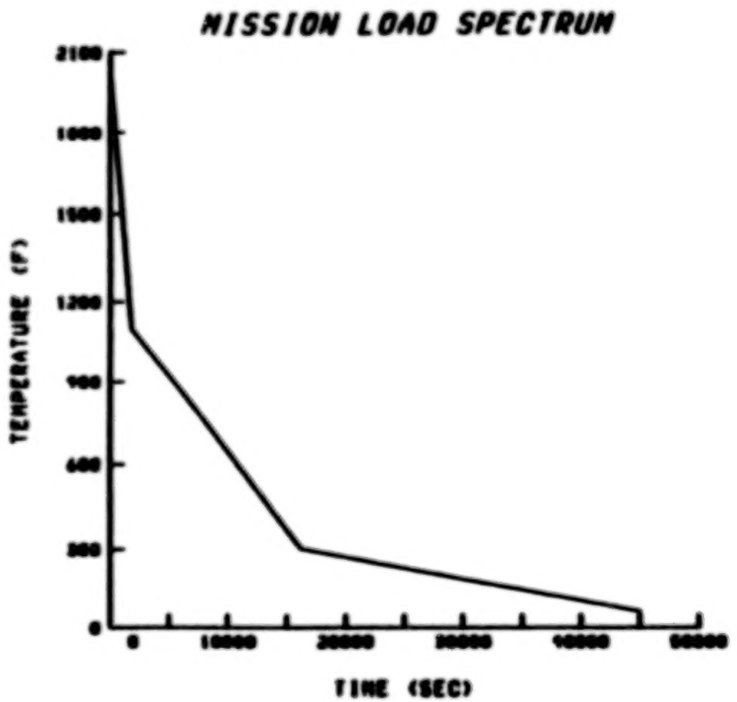


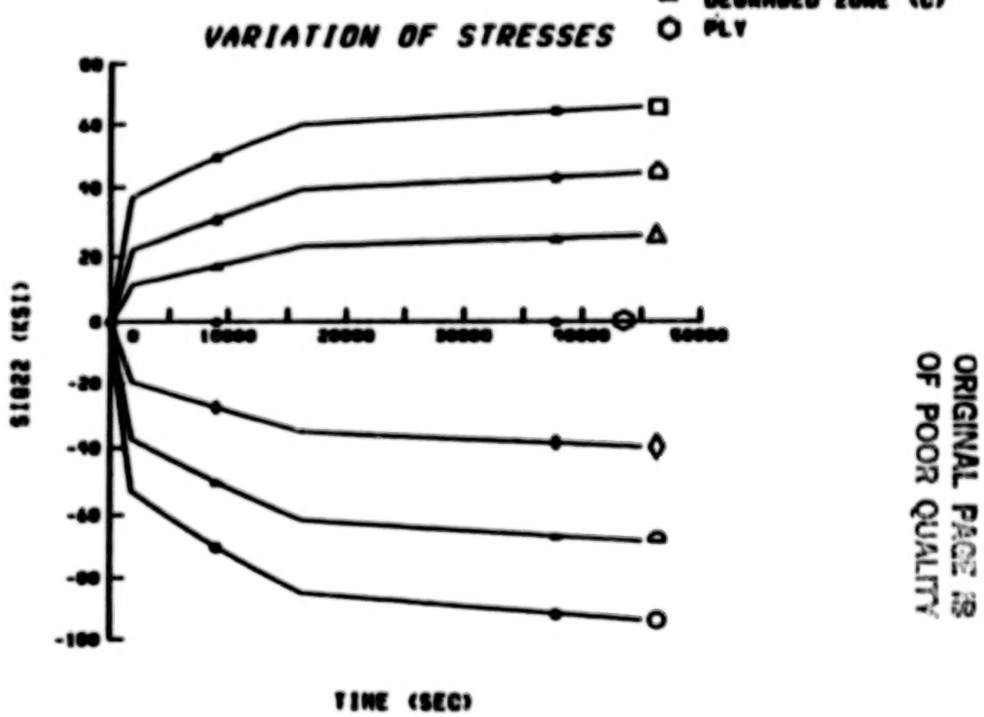


ORIGINAL PAGE IS
OF POOR QUALITY



Figure 7 - continued; variation of transverse normal stress ($\sigma_{22}$)

N84
31700

UNCLAS

N84 31700 D12

# THREE-DIMENSIONAL STRESS ANALYSIS USING THE BOUNDARY ELEMENT METHOD*

Raymond B. Wilson
Pratt & Whitney Aircraft

Prasanta K. Banerjee
State Universuty of New York - Buffalo

## SUMMARY

The boundary element method will be extended (as part of the NASA Inelastic Analysis Methods program) to the three-dimensional stress analysis of gas turbine engine hot section components. This paper outlines the analytical basis of the method (as developed in elasticity), summarizes its numerical implementation and indicates the approaches to be followed in extending the method to include inelastic material response.

## NOTATION

| | |
|---|---|
| $V$ | interior of three-dimensional body |
| $S$ | surface of three-dimensional body |
| $u_i$ | displacement vector |
| $\epsilon_{ij}$ | strain tensor |
| $\sigma_{ij}$ | stress tensor |
| $n_i$ | unit normal vector |
| $t_i$ | traction vector |
| $f_i$ | body force distribution |
| $\delta_{ij}$ | Kronecker delta |
| $e_j$ | arbitrary unit vector |
| $E$ | Young's modulus |
| $\upsilon$ | Poisson's ratio |
| $\mu$ | shear modulus |
| $\alpha$ | coefficient of thermal expansion |
| $\theta$ | temperature |

PRECEDING PAGE BLANK NOT FILMED

*Work done in support of NASA contract NAS3-23697.

## INTRODUCTION

It has been established that the durability of hot section components is a major driver of gas turbine engine costs, in design, manufacture and maintenance. Major savings will be realized if the lives of these components can be extended and their cost reduced. The NASA HOST (Hot Section Structural Technology) program is supporting a variety of approaches to these problems. As part of the HOST program a need has been identified for an improved inelastic three-dimensional stress analysis capability which is efficient enough for use in the design cycle. NASA Contract NAS3-23697 (3-D Inelastic Analysis Methods for Hot Section Components), recently awarded to the Commercial Engineering Division of Pratt & Whitney Aircraft, is directed at the development of analysis tools to meet this need.

The analysis requirements are severe. Hot section components, and the related stress analyses, are characterized by:

1. Extreme geometrical complexity. The components typically include surfaces of very general shape. Small structural details must be accurately represented, since these are frequently life limiting locations. The components usually contain holes of various sizes to allow for air and fuel flow and these can both weaken the overall structure and act as local stress risers. It may also be necessary to account for the presence of single or multiple cracks within the structure.

2. Loading complexity. Loads typically include gas path and cooling air pressures, mechanical loads due to other components, thermal loads (derived from unsteady temperature distributions) and, in some cases, extremely significant centrifugal loads. Durability analysis for hot section components requires consideration of the stress-strain history throughout a flight cycle, and thus all of the boundary conditions and other loads are potentially time dependent.

3. Complex material response. In all cases the elastic material response in hot section components is inhomogeneous due to the high temperatures involved and the temperature dependence of elastic modulus. In some cases the materials are anisotropic. Inelastic response usually occurs, at least in local regions, over some part of the flight cycle. In some cases global inelastic response (plasticity, creep or both) of the component is encountered.

The requirements of the design process cannot readily be met using a single analysis tool. The early phases of the design process require rapid and inexpensive analyses of a variety of designs. In the final phase of design analysis a very accurate determination of the stress-strain state is required for final life prediction, but greater analysis time and cost are acceptable.

Much of the work in the present program will be devoted to the development of simplified (beam, shell) analysis methods for use in early design and to the development of special purpose finite element modules for the efficient analysis of hot section components. Significant effort will also be devoted to the extension of the boundary element method to the three-dimensional stress analysis of hot section components. This will provide a complementary method which can be used as an alternative to finite element analysis. It is expected that, for some problem classes, accuracy and efficiency will be improved relative to the use of finite element analysis.

The remainder of this paper reviews the analytical development of the elastic boundary element method, briefly discusses its numerical implementation, gives an example of its use for a rather complex structure and indicates the approach to be adopted in extending the method to inelastic analysis.

## ELASTIC ANALYTICAL FORMULATION

The boundary element method is a numerical method applicable to the solution of problems in homogeneous elasticity. It is similar to the finite element method in utilizing piecewise approximations to geometry and field quantities. These approximations allow the effective treatment of complex structures such as those encountered in gas turbine engines. The boundary element method is based on an entirely different mathematical development than is the finite element method, and this leads to profound differences in the numerical implementation. The key feature of this development is the use of classical results in mechanics and potential theory to reduce the dimensionality of the problem. Thus a three-dimensional elasticity problem is solved solely in terms of the surface of the body. The mathematical development is discussed below. Further details may be found in reference 1.

The starting point for the development is the Reciprocal Theorem (ref. 2)

$$\int_V \sigma^*_{ij} \; \epsilon_{ij} \, dV = \int_V \sigma_{ij} \; \epsilon^*_{ij} \, dV \tag{1}$$

where $(\sigma_{ij}, \epsilon_{ij})$ and $(\sigma^*_{ij}, \epsilon^*_{ij})$ are the stresses and strains derived from any two displacement fields satisfying the equilibrium and compatibility equations. Use of the strain displacement equations and the divergence theorem allows the recasting of the Reciprocal Theorem in an alternate form involving surface integrals of the displacement and traction fields, and volume integrals of the displacement fields and body force distributions.

$$\int_S t^*_i \; u_i \, dS + \int_V f^*_i \; u_i \, dV = \int_S t_i \; u^*_i \, dS + \int_V f_i \; u^*_i \, dV \tag{2}$$

The displacement states chosen are completely arbitrary, except for the requirement that equilibrium be satisfied. For isotropic, homogeneous materials one can identify the (*) solution with the displacement field due to a unit force applied in the direction $e^*_j$ at the point $y_i$ (the Kelvin solution, ref. 1). Formally this is the displacement field satisfying

$$\frac{\partial \sigma^*_{ij}}{\partial x_j} + \delta_{ij} \; \delta(x,y) \; e^*_j + f^*_i \tag{3}$$

and it can be represented in the form

$$u_i^* (x) = G_{ij} (x,y)\, e_j^* (y) \tag{4}$$

where

$$G_{ij} = \frac{1}{16\pi\mu\ (1-\nu) r}\left[(3 - 4\nu)\ \delta_{ij} + \frac{(x_i - y_i)(x_j - y_j)}{r^2}\right] \tag{5}$$

$$(r = |x - y|)$$

The strains, stresses and (on the surface, S) the tractions can be represented in similar forms,

$$\begin{aligned} \epsilon_{ij}^* &= B_{ijk}\, e_k^* \\ \sigma_{ij}^* &= T_{ijk}\, e_k^* \\ t_i^* &= \sigma_{ij}\, n_j = T_{ijk}\, n_j\, e_k^* = F_{ik}\, e_k^* \end{aligned} \tag{6}$$

where the tensors $B_{ijk}$, $T_{ijk}$ and $F_{ik}$ are derived from the displacement tensor, $G_{ij}$, by appropriate differentiation and use of Hooke's Law. A similar approach is available for anisotropic materials, although closed form representations are not generally available.

By substituting $u_i^*$, $t_i^*$ and $f_i^*$ in the Reciprocal Work Theorem and utilizing the formal definition of $f_i^*$, an identity (Somigliana's identity) can be derived which expresses displacements at an arbitrary interior point in terms of the displacements and tractions on the surface. Appropriate differentiation and use of Hooke's Law allow derivation of similar results for stresses and strains, solely in terms of boundary data.

$$u_j(y) = \int_S [t_i(x)\, G_{ij}(x,y) - F_{ij}(x,y)\, u_i(x)]\ dS(x) + \int_V f_i(x)\, G_{ij}(x,y) dV(x) \tag{7}$$

It then becomes possible to carry out a limiting operation in which the interior point y approaches a specific point $x_o$ on the surface of the body. The functions $G_{ij}$ and $F_{ij}$ both become singular, and the integral involving $F_{ij}$ must be evaluated as the sum of a principal value integral and a separately calculated jump term. After the required manipulations have been carried out, the boundary integral (constraint) equation

$$\begin{aligned} [1 - \alpha_{ij}(x)]\, u_j(x_o) = &\int_S [t_i(x)\, G_{ij}(x,x_o) - F_{ij}(x,x_o)\, u_i(x)]\ dS(x) \\ &+ \int_V f_i(x)\, G_{ij}(x,x_o)\ dV(x) \end{aligned} \tag{8}$$

is obtained. The tensor $\alpha_{ij}$ is due to the jump term in the integral of $F_{ij}$. At any point at which the surface is smooth, $\alpha_{ij} = 1/2\ \delta_{ij}$. At other points its behavior is more complex.

The basic content of this equation is that a well posed three-dimensional elasticity problem can be solved solely in terms of surface displacements and tractions. The equations represent constraints on the unknown boundary data which ensure that they will be in equilibrium with the prescribed boundary data.

## ELASTIC NUMERICAL IMPLEMENTATION

While the analytical form of the boundary integral equation is of considerable theoretical interest, there are almost no geometry and loading combinations of any practical interest for which an exact solution exists. Classical forms of approximation, such as series solutions, are cumbersome and, often, of questionable accuracy. Practical exploitation of the equation thus requires a technique for reducing it to a linear algebraic system.

Since the boundary integral equation is written in terms of the displacements and tractions on the surface of the body, it is necessary to define a convenient geometric approximation to the true surface and to define approximations to the displacement and traction variation over this surface. This allows the evaluation of the required integrals in terms of the algebraic parameters defining the displacement and traction variation and, thus, reduction of the overall system to a set of linear algebraic equations. If nonzero body forces are involved, then an appropriate interior approximation may also be required. It need not be related to, or consistent with the surface approximation. The solution is still carried out solely in terms of boundary data.

Two major approaches have been taken to the three-dimensional numerical implementation:

1. The surface is modeled as an assembly of plane triangular patches. Displacement and traction are taken to be either constant (ref. 3) or linearly varying (ref. 4) over each such patch. Using these approximations it is possible to evaluate all required integrals over each surface patch in closed form. This leads to an efficient and highly accurate calculation of the coefficients in the resulting algebraic system. However, the representation of complex geometry requires the use of a large number of elements, and the limitation to linear variation of surface data tends to reduce accuracy in cases where significant bending or large surface element aspect ratios are involved.

2. The surface is modeled using quadratic isoparametric (fig. 1) surface patches (either quadrilateral or triangular). These are derived from the use of similar elements in finite element analysis. Surface data is then modeled, over each element, using the linear, quadratic or cubic isoparametric shape functions (ref. 5). Experience with this form of representation has shown that complex geometries can be modeled using a reasonable number of elements. The use of quadratic surface data variation yields a significant improvement in accuracy, so that a geometrically satisfactory model normally possesses sufficient refinement to give sufficient definition of stresses and strains. The use of cubic variation

has not been found necessary in modeling gas turbine engine components. The use of these more general approximations requires the (at least partial) use of numerical integration in evaluating the coefficients of the linear equation system.

Using either form of approximation, it is possible to develop algebraic representations for interior quantities.

While both the boundary element and finite element methods are numerical stress analysis techniques, significant differences exist between them. In particular:

1. In the finite element method displacements are approximated throughout the body. Stress and strain are always derived quantities. In the boundary element method only the surface variations of both displacement and traction are modeled. Interior results are calculated only at points where they are desired. These interior quantities satisfy the exact equations of elasticity.

2. A single finite element is a structure. That is, an elasticity problem can be posed and solved for a single element. A single patch used in boundary element method modeling is not a structure. It requires an assembly of patches enclosing a volume before an elasticity problem can be solved.

3. The structure of a finite element system matrix and a boundary element system matrix differ. A finite element matrix is typically large (since the entire volume must be modeled) but is banded and symmetric. The boundary element method matrix is significantly smaller but is typically full (because of the surface integrals) and nonsymmetric.

## TURBINE RIM COOLING HOLE

The boundary element method has been applied (using both the forms of approximation discussed above) to the calculation of stresses and strains at turbine cooling hole exits, which are possible life limiting locations for turbine disks (ref. 6). A test program was carried out, using a large scale model (fig. 2), to determine the strain variation around the exit of a radially oriented hole intended to feed cooling air to the blade (fig. 3). The program was designed to study the effect of different strategies for blending the sharp corner of the hole exit.

An initial attempt was made to analyze the structure using a three-dimensional finite element code. It did not prove possible to resolve the strain concentration at the hole exit at a reasonable cost (for either model generation or computer time). In order to resolve the local behavior a boundary element analysis, using plane triangular elements (the BINTEQ code), was carried out. The quarter section shown in figure 3 was modeled, as shown in figure 4, using 436 surface patches. Boundary conditions were taken from the finite element analysis, based on the assumption that the overall load transfer in the finite element analysis was correct. Results from the analysis showed good agreement with the strain gage data from the model tests (fig. 5).

The boundary element method analysis was later redone using isoparametric elements (the BASQUE code). The model (fig. 6) required only 97 patches, a reduction factor of 4.5. This reduction is directly related to the use of curved elements, particularly in the doubly curved region at the hole exit. The results of this analysis showed even better agreement with the data than did those of the original analysis using plane triangles (fig. 7). The cost was significantly less, although computing system changes make an exact comparison impossible.

The results of these analyses suggest that the boundary element method is particularly effective in resolving rapid stress and strain variations, especially when accurate geometrical modeling is also required. This observation is consistent with results obtained in other analyses as well (ref. 6, 7). It is not yet clear whether the boundary element method will be competitive with finite elements for the solution of general three-dimensional load transfer problems not involving high gradients. In general, the methods should be viewed as complementary, not as competitors, of which only one will eventually be used.

## INHOMOGENEOUS AND INELASTIC ANALYSIS

It was noted above that the analysis of hot section components typically involves centrifugal and nonsteady thermal loads, as well as both inhomogeneous and inelastic material response. Both the centrifugal and thermal loads can be incorporated directly as body forces. For the centrifugal loads (where R is the distance from the axis of rotation)

$$f_i \propto \rho\omega^2 R \tag{9}$$

while for the thermal loads

$$f_i = \frac{-\alpha E}{(1-2\upsilon)}\theta,i \tag{10}$$

It should be noted that these representations are not unique. The use of the divergence theorem allows transformations of the body force terms to be carried out. While the resulting representations are analytically equivalent the choice made can have significant numerical effects.

The introduction of inhomogeneous and inelastic response is more complex. The homogeneous, elastic boundary integral equation can be written, in operator notation, as

$$L(v) = F \tag{11}$$

where L is a linear operator, v is the unknown surface data and F is derived from all known loads and surface data. Other linear operators exist for the calculation of any desired interior results:

$$\begin{aligned} u &= I_u(V) + F_u \\ \epsilon &= I_\epsilon(V) + F_\epsilon \\ \sigma &= I_\sigma(V) + F_\sigma \end{aligned} \tag{12}$$

The stresses and strains obtained using the operators $I_\epsilon$ and $I_\sigma$ will satisfy Hooke's Law using the assumed homogeneous elastic modulus. If either inhomogeneity or inelastic response occurs, then the interior stresses and strains will not satisfy the true stress strain relation. This imbalance can be represented in terms of modified body forces and surface tractions or as volume distributions of initial stress or initial strain. If, for example, the body force representation is chosen, then the imbalance can be cycled back to the boundary integral equation

$$[\,1 - \alpha_{ij}]\, u_j^1 = \int_S [t_i^1\, G_{ij} - F_{ij}\, u_i^1\,]\, dS + \int_V [f_i + f_i^1\,]\, G_{ij}\, dV \tag{13}$$

where $f_i^1$ is derived from the interior imbalance evaluation. The new boundary solution $u_i^1$, $t_i^1$ will produce interior results which reduce the interior imbalance due to the inhomogeneous and inelastic behavior. In matrix form the system equation becomes

$$[T]\, \underline{u}^1 + [U]\, \underline{t}^1 = \underline{f} + \underline{f}^1 \tag{14}$$

It is particularly important to note that the kernel functions and the matrices [T] and [U] remain unchanged during the iteration process. Thus the calculation of these matrices and the decomposition of the system matrices need be done only once for the entire analysis. The overall solution sequence, written in operator form is then

```
calculate L
calculate N                 } single elastic calculations
calculate L^-1              }                                        (15)

→ calculate F
    f^o = 0
  → v^i = L^-1 (F + f^i)    } inelastic/inhomogeneous iteration }  time/load
  ↳ f^i+1 = N (v^i)         }                                   }  stepping
    t = t + Δt
```

The sequence presented above is valid for a single time or load increment. The quantities u, t and F must, for an inelastic analysis, be regarded as either increments or rates depending on the type of inelastic material model used. In either case a number of time steps or load increments will be required for the complete solution. The key point to be noted is that the surface and volume problems have been uncoupled. In a sense the overall structural analysis problem is solved on the surface while the complex material response is evaluated in the interior. It remains unnecessary to have compatibility between the surface and volume discretizations.

Significant progress has been made in the application of these techniques in two-dimensional analysis (ref. 8, 9). It is to be expected that, with careful attention to the details of the numerical implementation, the inelastic three-dimensional boundary element method will prove to be highly effective for many problems of practical importance.

## REFERENCES


1. Banerjee, P. K. and Butterfield, R.: Boundary Element Methods in Engineering Science. McGraw-Hill (UK), 1981.

2. Sokolnikoff, I. S.: Mathematical Theory of Elasticity. McGraw-Hill, 1956.

3. Cruse, T. A.: Application of the Boundary Integral Equation Method to Three Dimensional Stress Analysis. Computer and Structs, 3, 509-527 (1973).

4. Cruse, T. A.: An Improved Boundary Integral Equation Method for Three Dimensional Elastic Stress Analysis. Computer and Structs, 4, 741-754 (1974).

5. Lachat, J. C. and Watson, J. O.: Effective Numerical Treatment of Boundary Integral Equations: A Formulation for Three-Dimensional Elasto-Statics. Int. J. Num. Meth. in Engng., 10, 991-1005 (1976).

6. Wilson, R. B., Potter, R. G. and Wong, J. K.: Boundary Integral Equation Analysis of an Advanced Turbine Disk Rim-Slot. Paper No. 14, Proc AGARD Cont. (1978).

7. Wilson, R. B., Potter, R. G. and Cruse, T. A.: Calculations of Three-Dimensional Concentrated Stress Fields by Boundary Integral Method. Symposium on the Unification of Finite Elements, Finite Differences and Boundary Integral Equations, University of Connecticut, 1978.

8. Banerjee, P. K., Cathie, D. N. and Davies, T. G.: Two and Three-Dimensional Problems of Elasto-Plasticity. Developments in Boundary Element Methods, Banerjee, P. K. and Butterfield, R. (ed), Applied Science Publishers, 1979.

9. Marjaria, M. and Mukherjee, S.: Improved Boundary Integral Equation Method for Time Dependent Inelastic Deformation in Metals. Int. J. Num. Meth. in Engrg., 15, 97-111, 1979.

ORIGINAL PAGE IS
OF POOR QUALITY

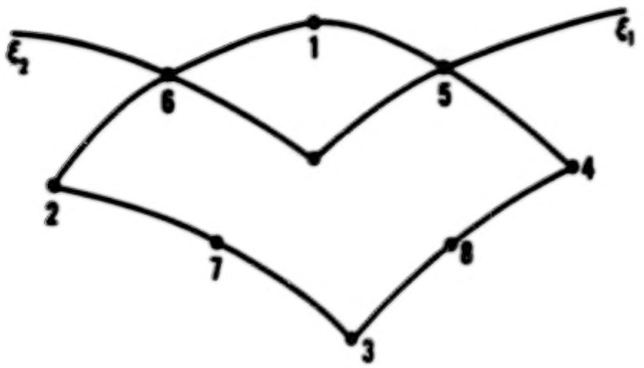


$$X_i(\xi) = M^{\alpha}(\xi)\, X_i^{\alpha} \quad \alpha = 1,2,\cdots,8$$

$$M^1(\xi) = \tfrac{1}{4}(\xi_1+1)(\xi_2+1)(\xi_1+\xi_2-1)$$

$$\vdots$$

$$M^5(\xi) = \tfrac{1}{2}(\xi_1+1)(1-\xi_2^2)$$

$$\vdots$$

Figure 1 Quadratic Isoparametric Shape Functions

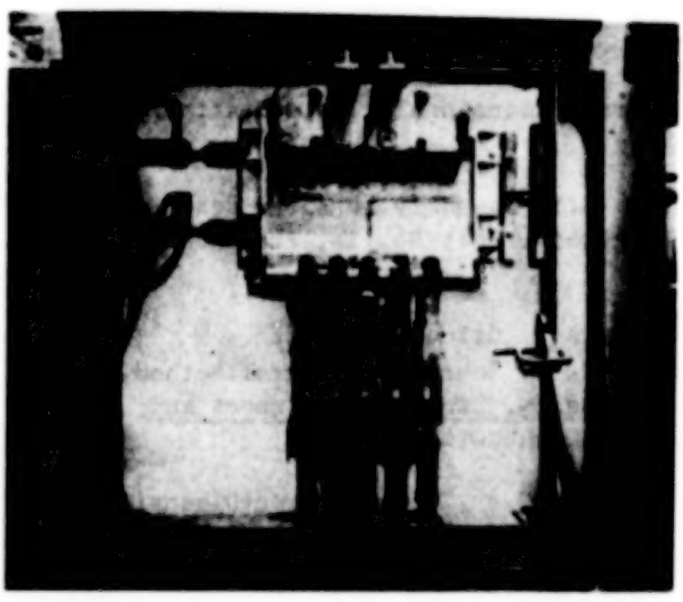

Figure 2 Disk Rim Model in Test Rig

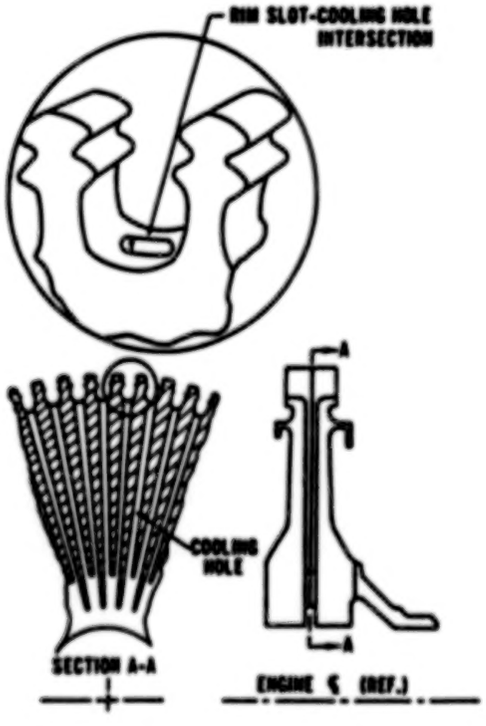


Figure 3 Rim Slot-Cooling Hole Intersection

ORIGINAL PAGE IS
OF POOR QUALITY

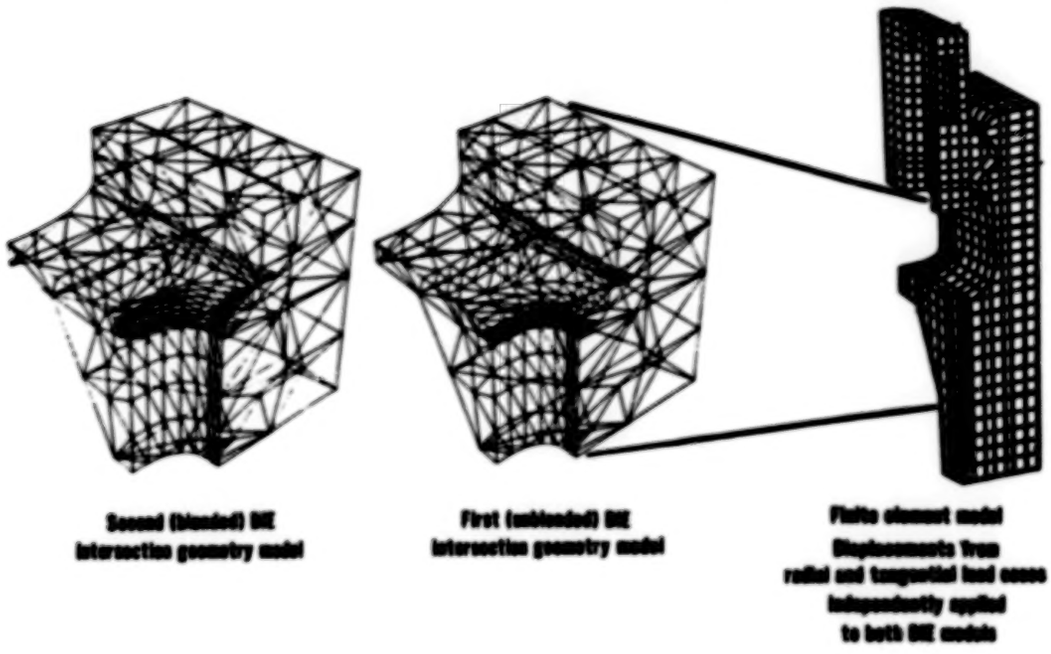


Figure 4 Piecewise Linear Three-Dimensional Boundary Integral Equation Models for Analysis of Turbine Disk Rim Slot-Cooling Hole Intersection

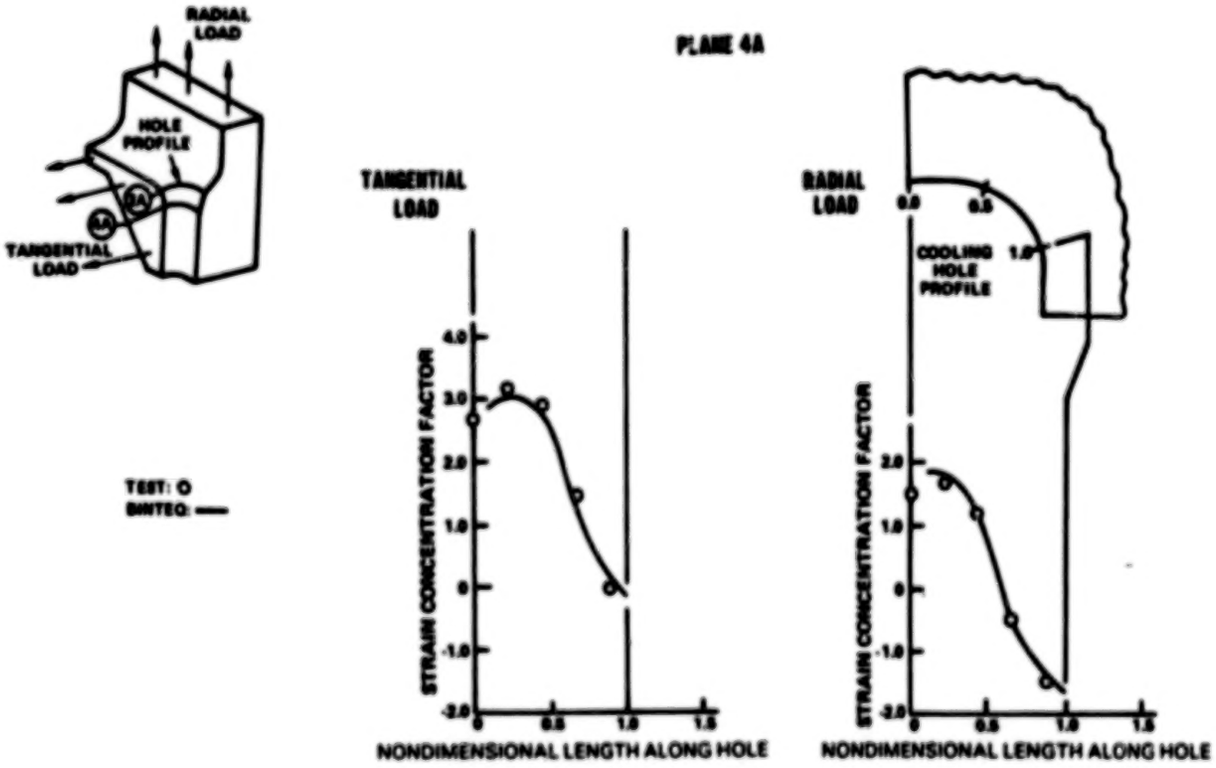


Figure 5 Correlation of Test and Boundary Integral Equation Results-Second Intersection Geometry, Planes 2A and 4A

ORIGINAL PAGE IS
OF POOR QUALITY

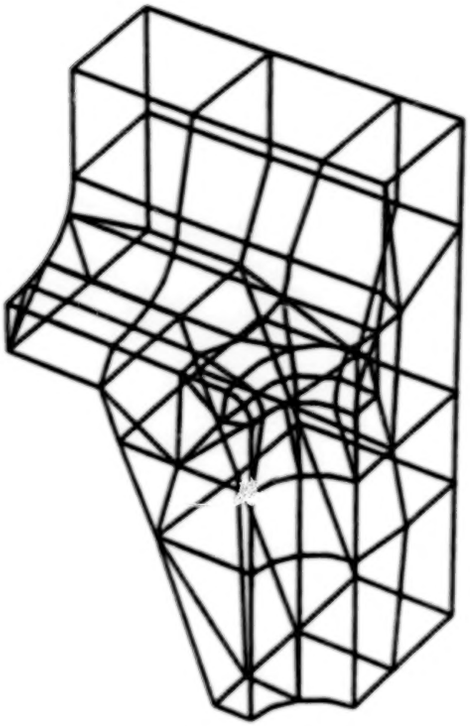

MODEL USING 97 QUADRATIC
ISOPARAMETRIC ELEMENTS

Figure 6 Quadratic Isoparametric Boundary Integral Equation Map for Analysis of Turbine Disk Rim Slot-Cooling Hole Intersection

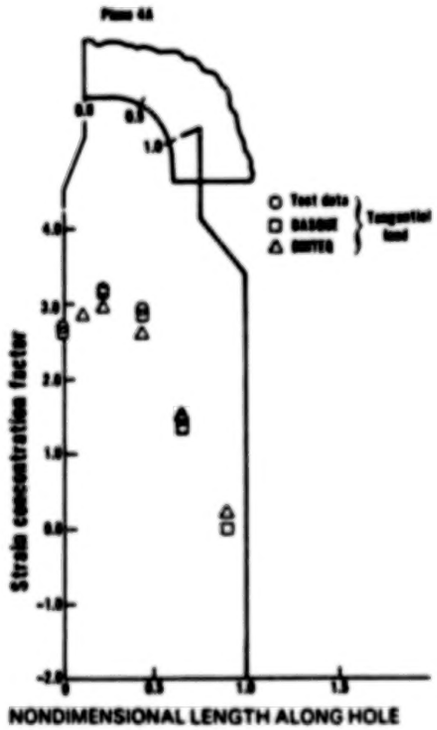


Figure 7 Improvement Due to Higher Order Boundary Integral Equation Modeling

OMIT TO END

## SUMMARY

Christos C. Chamis

National Aeronautics and Space Administration
Lewis Research Center
Cleveland, Ohio 44135

Significant results, conclusions, and issues addressed at the Lewis/Industry/University Workshop on Nonlinear Structural Analysis are summarized below by discipline: New Concepts/Formulations, Algorithms/Convergence, and Inelastic Analysis and Interactive elements.

New concepts/formulations. - (1) The slave finite element approach to nonlinear analysis is viable. The large number of degrees of freedom (DOF) associated with this approach, however, would require innovative computational algorithms to obtain computational effectiveness compared with traditional approaches. The ease in changing increment steps, the increased detailed information available within the subinterval, and accuracy demonstrated to date for elastic problems are promising. (2) A new variational principle has been developed. This principle is based on the combined Hellinger-Reissner and Hu-Washizu principles with additional internal displacement DOF. Hybrid stress elements based on this new principle have invariant properties and are less sensitive to geometric distortions. This new variational principle is considered to represent a significant advance in finite element development. (3) The three-dimensional degenerated elements offer modeling and computational efficiency for the analysis of general shells with layered structure, undergoing large deformations (in-plane, bending, and shear) and transient motions. As expected, these elements take more computational time for special shell problems compared with finite elements based on deformable shell theories. (4) A nine-node Lagrange shell finite element proved effective in the buckling, postbuckling, and elastic-plastic analyses of shells. This element did not exhibit "shear locking" even in very large aspect ratio shells (up to $10^8$). Application of the element to other nonlinear problems such as dynamic, creep buckling, and ratcheting requires additional research. The magnitude of the effort required to develop the element formulation for these other nonlinear problems may be substantially reduced using symbolic language manipulators.

Algorithms/convergence. - (1) The new computational algorithm developed for self-adaptive solution strategies proved to be very effective in the solution of two highly nonlinear problems (snap-through load-deformation history of a spherical cap and a box-truss). This new algorithm is stable, eliminates the need for global inverse, and handles problems with turning points and general material properties. Formal establishment of convergence and stability characteristics of the algorithm requires additional research. (2) Element-by-element (EBE) approximate factorization techniques were compared to test problems for elastic and elastic-perfectly plastic cantilever beams with and without a circular hole. The EBE solution method converged with seven iterations (with the hole) and four iterations (without the hole). EBE is a linear equation-solving procedure. Direct use to develop EBE time stepping-solution algorithms requires additonal research. (3) Finite element generators using symbolic manipulator languages (VAXIMA) are viable. Initial

results show that the lines of program required to generate the strain-displacement and stiffness element matrices can be reduced substantially. (4) The stability convergence of underintegrated finite element approximations can be improved by simple post-processing operations. These operations can be described by an exact formula in some cases. Additional research is needed for more general cases.

Inelastic analysis and interactive elements. - (1) Elastic-plastic fracture under arbitrary loading and material behavior, characterized by realistic crack-growth rates, can be described by two integral equations. A new path-independent integral has been derived to describe dynamic crack propagation. A set of equations/conditions has been developed which generalizes the constitutive relations for inelasticity and finite deformations. Variational principles were used to derive a hybrid finite element for describing dynamic crack propagation. (2) Interactive finite elements can be used to describe the dynamic interaction of rotating squeeze film bearings, shafts, and supports. This type of analysis is the only one available to date which describes the dynamic interaction in an integrated manner and which can be used as a "plug-in" in general purpose finite element codes. The interactive finite element approach is presently being confirmed experimentally using a two-bearing, two-damper test rig. (3) An upward-integrated and "top-down traced" computerized capability has been developed for the nonlinear analysis of high-temperature composites applicable to turbine blades and vanes. This theory accounts for the complex thermoviscoplastic behavior of composites in turbine environments and includes effects of the fabrication process. Initial results indicate that the fabrication process induces a substantial thermoviscoplastic stress state in the composite. (4) Boundary element methods have proven computationally effective for two-dimensional linear problems. Extensions to three-dimensional, nonlinear and time-dependent problems is the subject of current focused research. It is anticipated that boundary elements will provide a complementary analysis methodology to finite element methods.

Collectively, the summary points out the multidisciplinary approach necessary to develop methods for complex nonlinear structural analysis problems. This multidisciplinary approach encompasses new formulations and concepts, invention of more general variational principles, finite element generators, development of interactive elements, innovative solution algorithms, adaptive solution strategies, and formal criteria for a priori assessing solution stability and convergence. The contributors to these proceedings describe what can be done, future potential, and direction in each discipline.

The goal of the highly focused research described in these proceedings is to develop methodologies which lead to designs of more cost-effective and reliable engine structures and components. It is hoped that, in addition, these proceedings will provide a valuable source of information of on-going research and future direction in nonlinear structural analysis in general.

INDEX


Acceleration, secant, 48
Admissible, 3
Admissible, 3
Ahmad, 45, 49
Algorithm,
  Hierarchial, 58
  Hybrid-stress finite element, 111
  Incremental Newton-Raphson, 55
  Newmark, 72
  Newton-Raphson, 46, 49
  Parabolic regularization, 66, 67
Analysis
  Boundary element method, 154
  Global 132
  Postbuckling, 46
  Thin plate, 47
  Thin shell, 47
  Top-down-structured 132
  Upward-integrated 132
Application levels, hierarchial, 57
Arc length, constrained, 46, 49
Aspect ratio, Large, iii
Attributes, self-adaptive, 56, 57

Beam, cantilever, 71
Bearing dampers, squeeze-film, 121
Bearings
  Fluid-film journal, 120
  Rolling element, 120
Behavior
  Inelastic, 156
  Inhomogeneous, 156
  Pre-postbuckling, 60
  Rate sensitive, 106
Bending
  Modes, inextensional, 20
  Static, 35
Bilinear, 97
Blade/vane components, high-pressure turbine (HPT), 131, 132
Boundary element, 154, 155, 162
Boundary element method, 149
Boundary integral, iii

Cap
  Sandwich spherical, 48
  Spherical, 36, 60
Closedness criterion, 56
Composites
  Constituent materials, 132 - 134
  Fiber reinforced, 31
  High-temperature materials, 131, 162
Composites (cont.)
  Inhomogeneous TFRS, 134
  Intralaminar
  Microstresses, 133
  Non-uniformity, 134
  Lamina, 133
  Mechanical strength, 133
  Mechanics, 133
  Micromechanics, 133, 134
  Refractory-fiber metal-matrix, 131
  Thermal strength, 133
  Unidirectional TFRS, 134, 135
  see Tungsten-fiber-reinforced superalloys
Computer code
  ADINA, 122
  COBSTRAN, 132, 133, 134
  FORTRAN, 85, 86
  FORTRAN 77, 88, 89
  Interactive prompting, 87
  LISP, 87, 89, 90
  MACSYMA, iii, 85, 86
  Menu driven, 87
  NASTRAN, 120, 121, 134
  TETRA, 120
  User-level programs, 90
  VAXIMA, 86, 87, 89
Computer operating system, UNIX, 86, 88
Computers, VAX-11/780, 86, 91
Concave shape, 49
Configuration, multi-shaft, 120
Conservation laws, 108
Constitutive laws, 3
Constitutive relation, 105
Constraint
  Circular, 56
  Hyperbolic, 56
  Surface of, 56
Contour line, 74
Convergence, 162
  Criteria, iii
  Rates, superlinear, 56
  Stable, 57
Convex shape, 49
Coordinates, curvilinear, 33
Cowper, 22
Crack propagation
  Dynamic, 105, 162
  Elastodynamic, 108
  Self-similar, 1052, 108
  See also creep
Creep
  Behavior, elastic-plastic, 55, 56

Creep (cont.)
Crack-growth, 106
Damage process, 106
Steady-state 106
Cycle, limit, 121

Dampers, squeeze-film, 120, 122, 123
Dams, 22
Deflection, large, 48
Deformation
Elastic-plastic, 48
Inelastic, 112
Large, 46, 47
Theory of, 105
Determinant ratio, 49
Derivative
Spatial, 3
Temporal, 3
Discretizations, 65
Non-prismatic, 10
Semi-prismatic, 10
Displacements
Constrained, 48
Internal, 20
Statically condensed, 18
Distortions, geometric, 20
Dynamics, nonlinear, 121

Eight-node, 20
Elastic-plastic material, Bilinear, 48
Elastic-plastic, 46
Elasticity
Finite, 106
Infinitesimal, 106
Element-by-element, iii
Elements
Bilinear quadrilateral, 72
Boundary, 151
Cylindrical shell, 22
Degenerated, 161
Higher order, 87
Hybrid, 17
Hybrid semi-Loof, 21
Implicit-explicit, 71
Invariant,17, 20
Isoparametric, 155
Lagrange, 46
Nine-node, 47
Quadralateral isoparametric, 60
Semi-loof, 17,20-22
Thin shell, 20, 21
Three-dimensional degenerated, 31, 32, 40
Time-adaptive implicit-explicit partition of, 71
Two-dimensional, 40

Elliptic, 56
Energy, complementary, iii, 112
Equation
Boundary integral, 153
Euler-Lagrange, 112
Micromechanics, 132
Euclidean norm, 58
Euler-Lagrange, 112
Factorization, 76
Alternating direction method, 65
Element-by element, 65, 66, 70, 71, 161
Fractional steps method, 65
Methods of discretization, 65, 66
Splitting-up method, 65
Weak approximation method, 65
Finite elements, 33, 85, 86, 111
Analysis, 45, 55
Conforming, approximation, 97
Generators of, 161
Global, 134
Hybrid stress, iii
Interactive, iii, 162
Nonlinear simulation, 55
Slave, iii, 161
Flow theory, rate-independent, 106
Force excitation, periodic, 121
Formulation
Galerkin, 57
Rayleigh-Ritz, 57
Virtual work, 57
Fracture
Dynamic, iii
Mechanics, 105, 107
Elastic-plastic, 107, 162
Frequencies, natural, 121
Function, bilinear, 7, 8
Functional, 112

Global inversion, 57
Global updating, 57
Green-Lagrange, 32, 33
Growth, self-similar, 105

Hamilton's law, 1, 2
Hardening, anisotropic, 109
Heat conduction, nonlinear, 56
Heirarchy, 132
Hellinger-Reissner, 17, 18
Higher order, 46
Hinge, plastic, 48
Hu-Washizu, 17
Hybrid elements, 17
Hypo-elasticity, 109

Incompressibility, 95

ORIGINAL PAGE IS
OF POOR QUALITY

Inelastic analysis, iii, 149
Instabilities, hourglass, 97
Instantaneous, 122
Integral
  Path-independent, 105, 106, 108, 109, 162
  Principal value, 152
Integration
  Reduced, 45
  direct, Newmark, 35
Interphase, 132, 135
Invariant, 18
Iron, 45, 49
Isoparametric, 18
Instabilities, numerical, 95
Iteration, Newton-Raphson, 48
J integral, 105
Jaumann integral, 115
Jump term, 152, 153

Labyrinths, 121
Lagrange, 46
Lagrange element
  Higher order, 47
  Nine-node, 48
Lagrangian
  Kinematical, 75
  Total, 32
Lamina transverse directions, 133
Laminate theory, 132, 134
Large global arrays, factorizing, 65
Limit cycle, 121
Load, temperature, 135
Loading/unloading histories, 106

Manipulation, algebraic, 85
Marguerre, 22
Material
  Elastic, 48
  Elastic-plastic, 48, 109
  Elastic-perfectly plastic, 48, 72, 73
  Rigid-plastic, 109
Matrix
  Lumped mass, 72
  Tangent damping, 77
  Tangent stiffness, 77
Membrane
  Action, 49
  Quadrilateral, 18
  Stresses, momentless, 22
Mesh partitions, implicit-explicit, 66
Micro-mechanics, 109
Mindlin, 46
Modes
  Checkerboard, 95
  Chickenwire, 95
Modes (cont.)
  Free-free unclamped normal, 121
  Hourglass, 95, 98, 99
  Keystone, 95
  Rigid body, 20
Morley, 22
Motion, geometrically nonlinear, 32
Multi-branch, multi-level system, 120, 122
Multi-component splitting formulae
  Two-pass, 69, 70
  One-pass, 70
Multiprocessor computer, 66

NFAP, 88, 91
Newmark, 35, 75
Newton-Raphson, 46
Nonlinear, 85
Nonlinearity
  Kinematic, 55
  Material, 55
Noor, 36
Normality condition, 109

Objectivity, 113, 105, 114

Panel, circular cylindrical, 35
Parallelizable, 70
Partitions, implicit-explicit mesh, 77
Patch test, 18
Patches
  Quadratic isoparametric surface, 153
  Triangular, 153
Path-independent, iii
Patterns, spurious, 95
Phenomenon, transient, 121
Piola-Kirchoff. 32, 58
Plastic deformation, non-proportional, 105
Plastic zone, 49
Plasticity theory
  Linear kinematic hardening, 110
  Isotropic-hardening, 109
Plates, twisted, 36
Polynomials
  Bilinear, 18
  Interpolation, 88
  Quadratic, 46
Positive definite, 71, 77
Positive semi-definite, 77
Postbuckling, 48, 49
  Algorithm, 48
  Analysis, artificial spring method, 46
Prebuckling, 49
Pre-postbuckling, elastic, 56
Pressure, 48
  Follower, 48

Pressure (cont.)
Constant-direction, 48
Principle, variational, iii, 18, 161
Prismatic, 2
Propagating singular element, 108

Quadrature
Gaussian, 98
Numerical, 95
Quadrilateral planform, 21

Ramberg-Osgood, 7
Ramm, 46, 50
Rank, 18
Rate
Objective, 109, 110
Strain, 111
Stress, 110, 112
Zaremba-Jaumann-Noll, 111
Rayleigh-Ritz, 58
Relations, macroscopic constitutive, 109
Resonance, subharmonic, 121
Response, transient, 35, 36
Riks, 46, 50
Rolling contact, 56
Rotor-stator
As interactive components, 120
Clearances, 121
Interactive forces, 122
Rub/impact, 122

Safety zones, 56
Seals, 122
Secant accelerated, 46
Self-adaptive, iii
Semi-discrete, 75
SemiLoof, see Elements
Sensitivity studies, 132
Serendipity, 46
Shape function, 87
Shear
Locking, 45, 47
Finite, 111
Shell
Angle-ply, 36, 40
Cross-ply, 36, 40
Cylindrical, 36, 40
Degenerated, 45, 47
Elements, 47
Laminated anisotropic, 31
Large aspect ratio, 161
Shear-deformed, iii
Spherical, 36
Spherical shallow, 48
Theory, 22
Thin rotating, 120
Shell theory
Cylindrical, 22
Deep shallow, 22
Shallow, 22
Solid element, degenerated, 22
Solution
Curve, 56
Self-adaptive, 161
Somigliana's identity, 152
Space-time, 3
Splitting, two-component, 69
Stationarity, 112
Stiffness, incremental tangent, 46
Strain
Green-Lagrangian, 33
Momentless membrane, 20
Rate, 111
Stress
Dependency, 135
Hybrid, 19
Incremental, 33
Large deformation inelastic analysis, 105
Tensor, Piola-Kirchhoff, 32, 58
Stress-strain field, Crack-tip, 108
Stricklin, 36
Structural analysis, 134
Structure, box truss, 60
Subdomain model, 70
Subgroups, Non-contiguous, 70
Substructures, 70
Superelements, 70
Swept panel, 20
Symbolic, 85, 86
Expressions, 89
Processing, 87
TFRS, see Tungsten-fiber-reinforced superalloys
Tangent stiffness, singularity of, 46
Taylor series, 58
Temperature dependency, 135
Temporal, 3
Test rig, 123
Theory
Deformation, 105
Four-dimensional unified, 10
Laminate, 132
Thermoviscoplastic (TVP), nonlinear, iii, 132, 133, 135
Thin plate analysis, 47
Thin shell analysis, 47
Top-down traced, 162
Transient, geometrically nonlinear, 31
Triangular elements, 21, 22
Tungsten-fiber-reinforced superalloys (TFRS), 131, 132, 134
Blades/vanes, 133
Fiber degradation of, 132

Tungsten-fiber-reinforced superalloys (cont.)
Fiber-matrix interface of, 132
Nonlinear analysis of, 132
Turning points, 56

Underintegration, 95
Bilinear, 98
Unstable, 48
Upward-integrated, 162

Vibration, natural, 35, 36
Viscoplasticity, 106

Work theorem, reciprocal, 152

Zienkiewicz, 45, 49
Zone, degraded, 135

END

DATE

FILMED

OCT 30 1984